



HAL
open science

Simulation and optimization of solar domestic hot water production systems

Saïf Ed-Dîn Fertahi

► **To cite this version:**

Saïf Ed-Dîn Fertahi. Simulation and optimization of solar domestic hot water production systems. Chemical and Process Engineering. Université de Pau et des Pays de l'Adour; Université Sidi Mohamed ben Abdellah (Fès, Maroc). Faculté des Sciences et Techniques, 2019. English. NNT: 2019PAUU3034 . tel-02528278

HAL Id: tel-02528278

<https://theses.hal.science/tel-02528278>

Submitted on 1 Apr 2020

HAL is a multi-disciplinary open access archive for the deposit and dissemination of scientific research documents, whether they are published or not. The documents may come from teaching and research institutions in France or abroad, or from public or private research centers.

L'archive ouverte pluridisciplinaire **HAL**, est destinée au dépôt et à la diffusion de documents scientifiques de niveau recherche, publiés ou non, émanant des établissements d'enseignement et de recherche français ou étrangers, des laboratoires publics ou privés.

THÈSE

UNIVERSITE DE PAU ET DES PAYS DE L'ADOUR

École Doctorale Sciences Exactes Et Leurs Applications - ED 211

Présentée et soutenue le 14 décembre 2019

par Saïf ed-Dîn FERTAH

pour obtenir le grade de docteur

de l'Université de Pau et des Pays de l'Adour

**Spécialité : Mécanique des fluides, Energétique, Thermique, Combustion,
Acoustique**

SIMULATION ET OPTIMISATION DES SYSTEMES DE PRODUCTION DE L'EAU CHAUDE SANITAIRE SOLAIRE

RAPPORTEURS

- Zeghmati Belkacem
- Royon Laurent

PR / Université de Perpignan Via Domitia (UPVD-France)

PR / Université Paris Diderot (UPD-France)

EXAMINATEURS

- Rachid Saadani

PES / Université Moulay Ismail (UMI-Maroc)

DIRECTEURS

- Ali BENBASSOU
- Abdelmajid JAMIL
- Tarik KOUSKSOU

PES / Université Sidi Mohamed Ben Abdellah (USMBA-Maroc)

PES / Université Sidi Mohamed Ben Abdellah (USMBA-Maroc)

HDR / Université de Pau et des Pays de l'Adour (UPPA-France)

Contents

1 Acknowledgment	I
2 Nomenclature	II
3 General introduction	VIII
4 Part I: Technological challenge of solar water heaters (<i>SWHs</i>) in Morocco and a focused insight on hot water stratified storage tanks	1
4.1 Chapter I: A synthesis on the technology transfer of solar water heaters and inclusion as solar energy policy in Morocco	2
4.2 Introduction	2
4.2.1 Background and state of the art	2
4.2.2 Aim and motivations	4
4.3 Global market of <i>SWHs</i>	4
4.3.1 Installed capacity of solar thermal collectors	4
4.3.2 Classification of the world's <i>SWH</i> market	7
4.4 Market situation of <i>SWHs</i> in Morocco	8
4.4.1 History of <i>SWH's</i> market development	8
4.4.2 Socio-economic situation and energy context	8
4.4.3 Current state of the market data	9
4.4.4 Assessment of <i>SWH's</i> installation cost	10
4.4.5 Main industrial actors of <i>SWH</i> in Morocco	10
4.5 <i>SOL'R SHEMSY</i> project	11
4.5.1 Main purposes and general overview	11
4.5.2 <i>SHEMSY's</i> experimental platform	12
4.6 Solar energy profile in Morocco	17
4.6.1 Geography of Morocco	17
4.6.2 Extraterrestrial solar radiation equations	19
4.6.3 Incident solar radiations (G_{on})	19
4.6.4 Daily radiation's amount (H_0)	23
4.7 Conclusion and policy implications	25
4.7.1 Conclusions	25
4.7.2 Policy implications	25
4.8 Chapter II: Review on solar thermal stratified storage tanks: insight on stratification studies and efficiency indicators	27
4.9 Introduction	27
4.10 State of the art	28
4.10.1 Solar water heaters (<i>SWHs</i>)	28
4.10.2 Storage tank components: heat exchangers and auxiliary systems	30
4.10.3 Investigations on stratified storage tanks	31
4.10.4 Experimental studies	31
4.10.5 Numerical studies	33
4.10.6 Overwhelming <i>PCMs</i> inside storage tanks	34

4.10.7 Thermal stratification assessment	37
4.11 Mathematical modeling of thermal stratification	40
4.11.1 Three dimensional <i>CFD</i> approach	40
4.11.2 Continuity equation	41
4.11.3 Momentum conservation equations	41
4.11.4 Heat transport equation	42
4.11.5 Two dimensional formulation based on vorticity stream function equation	43
4.11.6 Continuity equation	43
4.11.7 Momentum equation	44
4.11.8 Heat transport equation	44
4.11.9 Vorticity stream function formulation of the momentum equation	44
4.12 Thermal stratification assessment through performance indicators	46
4.12.1 Dimensional and non-dimensional graphical methods	46
4.12.2 Indicators based on temperature distribution and temperature measurements	47
4.12.3 Stratification number	47
4.12.4 <i>MIX</i> number	49
4.12.5 Richardson number	51
4.12.6 Charging efficiency	52
4.12.7 Storage efficiency	53
4.12.8 Cumulative Charge Fraction (CCF)	53
4.12.9 Exergy efficiency	54
4.13 Conclusion	55
5 Part II: Thermomechanical efficiency enhancement of individual <i>SWHs</i> integrating <i>ETC</i> with submerged heat pipes using numerical simulations	56
5.1 Chapter III: Performance optimization of a two-phase closed thermosyphon through <i>CFD</i> numerical simulations	57
5.2 Introduction	57
5.3 Mathematical model	59
5.3.1 Physical model and basic equations	59
5.3.2 Continuity equation for <i>VOF</i> model (volume fraction equation)	61
5.3.3 Momentum equation for <i>VOF</i> model	61
5.3.4 Energy equation for <i>VOF</i> model	62
5.3.5 Heat transfer model in the metal wall	62
5.4 Validation methodology of the numerical <i>VOF</i> model	63
5.4.1 Description of the experimental device	63
5.4.2 Description of the experimental procedure of Fadhl et al. [1]	63
5.4.3 Solution strategy and convergence criteria	64
5.4.4 Simulation model	65
5.4.5 Uncertainty analysis	65
5.4.6 Validation results	66
5.5 Assessed geometries and computational mesh	68
5.6 Boundary conditions and <i>CFD</i> solution procedure	68
5.7 Flow visualization of <i>CFD</i> simulation results	69
5.8 Conclusion	76

5.9 Chapter IV: Thermo-mechanical strength analysis for energy storage improvement of horizontal storage tanks integrating evacuated tube collectors	78
5.10 Introduction	78
5.11 Material selection	80
5.12 Thermo-mechanical coupling solving method	83
5.12.1 Thermo-mechanical coupling equations	83
5.12.2 Simplifications and assumptions	84
5.12.3 Heat transfer model	84
5.12.4 Thermal conduction equation	84
5.12.5 Stress model	84
5.13 Thermo-mechanical coupling models	85
5.13.1 Calculation models building: Geometry, Mesh	85
5.13.2 Pre-sizing	85
5.13.3 Simulations methods and Setting the boundary conditions	88
5.13.4 Thermal boundary conditions	88
5.14 Results of the simulation	89
5.14.1 Strength failure desing code	90
5.14.2 Study 1: Geometrical optimization	90
5.14.3 Study 2: Material selection effect	92
5.14.4 Study 3: Thickness effect	93
5.15 Conclusion	94
5.16 Chapter V: Experimental study and CFD thermal assessment of horizontal hot water storage tank integrating Evacuated Tube Collectors with heat pipes	96
5.17 Introduction	96
5.17.1 Background	96
5.17.2 Literature CFD studies on thermal storage enhancement	97
5.17.3 Aim of the present study	100
5.18 Description of the case study	100
5.18.1 Parametric study	101
5.19 Governing equations	102
5.19.1 Continuity and conservation of mass	102
5.19.2 Balance equation for momentum	102
5.19.3 Energy equation	102
5.19.4 Assumptions of the physical models	103
5.20 Storage efficiency and performance indicators	103
5.20.1 Thermal efficiency assessment	103
5.20.2 Discharging efficiency	104
5.21 Research methodology	104
5.22 Experimental study	105
5.22.1 Description of the experimental setup	105
5.22.2 Uncertainty analysis	105
5.22.3 Experimental results	106
5.22.4 Temperature map	106

5.23	CFD code validation	107
5.23.1	Experimental and numerical study of Zachar et al. [2]	108
5.24	Mesh independence test and Boundary conditions	110
5.24.1	Mesh independence test	110
5.24.2	Boundary conditions	111
5.25	Solution strategy and convergence criteria	112
5.26	Results and discussion	112
5.26.1	Effect of heat pipe's number on <i>HTC</i>	112
5.26.2	Effect of heat pipe's number on the temperature and streamlines contours	114
5.26.3	Effect of heat pipe's number on the median temperature	118
5.26.4	Effect of heat pipe's number on the tank's average temperature and the discharging efficiency	118
5.27	Conclusion	119
6	Part III: Thermal efficiency optimization and enhancement of collective <i>SWHs</i> through dynamic simulations	121
6.1	Chapter VI: Design and thermal performance optimization of a forced collective solar hot water production system in Morocco for energy saving in residential buildings	122
6.2	Introduction	122
6.3	Collective system description	124
6.4	Weather data and Load profile	126
6.4.1	Weather data	126
6.4.2	Load profile	126
6.5	Physical modeling of solar hot water components	128
6.5.1	Solar collector panel	128
6.5.2	Storage tank	129
6.5.3	Flow streams	129
6.5.4	Energy flows	130
6.5.5	Solar fraction	130
6.6	Results and Discussion	131
6.6.1	First study: Effect of the collector's field area and arrangement	131
6.6.2	Second study: Effect of storage tank's volume	134
6.6.3	Third study: Effect of the collector's characteristics from various manufacturers	136
6.6.4	Fourth study: Effect of collectors arrangement	138
6.7	Conclusion	139
6.8	Chapter VII: Energy performance enhancement of a collective hot water production process equipped with a centralized storage tank	141
6.9	Introduction	141
6.10	Description of the studied case	143
6.10.1	Collective system description	144
6.10.2	Weather data and load profile	146
6.11	Equation setting	149
6.11.1	Thermal collector	149
6.11.2	Storage tank	151

6.11.3 Solar fraction of the collective process	152
6.12 Results and discussion	153
6.12.1 First parametric study: effect of the storage tank volume	153
6.12.2 Second parametric study: Collector effect on the annual solar fraction . . .	161
6.13 Conclusion	164
7 General conclusion and perspectives	166
7.1 General conclusion	166
7.2 Perspectives	168

List of Figures

1	History of thermal collector development on a worldwide scale [3].	4
2	Share of total installed capacity in operation (end of 2013) [3].	5
3	Distribution of the total installed capacity by collector's type in 2013 [3].	5
4	(a), (b)- Distribution of the total installed capacity by collector's type in 2013. (c)- Installed capacity per 1000 kWh in some considered countries of the world. [3]	6
5	Growth in the market for thermal collectors 2012/2013. (a)- Thermosyphon system, (b)- Forced circulation system.	6
6	New installed capacity per 1000 kWh in some countries of the world.	7
7	Market classification by <i>SWH's</i> type [4], [5].	7
8	Main aims of <i>SOL'R SHEMSY</i> project [6].	12
9	Data acquisition, their processing and recording in " <i>SHEMSY Cloud connector</i> ".	13
10	Location of the controllers to be installed in several Moroccan cities.	13
11	<i>SHEMSY's</i> experimental platform. (a)-Basic configuration of forced circulation <i>SWH</i> system. (b)-Experimental platform of forced circulation <i>SWH</i> system de- veloped in our laboratory.	14
12	High pressure <i>SHEMSY SWH</i> integrating <i>ETC</i> with heat pipes [7].	15
13	Temperature map of several devices integrated in the experimental <i>SOL'R SHEMSY</i> platform.	16
14	Solar collector field of the experimental <i>SHEMSY</i> platform, constituted from <i>ETC</i> and <i>FPC</i> technologies.	16
15	Temperature map of the inlet/outlet of the solar thermal <i>ETC</i> and <i>FPC</i> connected to the forced circulation <i>SWH</i>	17
16	Various solar radiation intensities in Morocco [8].	18
17	Annual average solar radiation (G_{on}).	20
18	Daily incident solar radiations (G_{on}) for 50 stations in Morocco.	22
19	Annual average radiation's amount (H_0).	23
20	Daily incident solar radiations (H_0) for 50 stations in Morocco.	24
21	(a)- Scheme of reverse flow in <i>SWHs</i> [9]. (b)- Experimental solar water heating system [10]. (c)- Scheme of <i>CSHPSS</i> [11].	28
22	Different configurations of hot water storage tanks. (a)- Storage tank with dual heat sink and heat source mass flow loops [12]. (b)- Storage tank with mantle heat exchanger in contact with the tank's wall [12]. (c)- Storage tank with an internal heat exchanger (IHX) coil [12]. (d)- Schematic of storage tank and IHX [12]. (e)- 3D design of the tank geometry including the heat exchangers [13]. (f)- Schematic cut view of the designed thermal storage tank [14].	30
23	Vertical storage tanks. (a)- with top heat exchanger for boiler backup. (b)- Electrical heating element.	31
24	(a)- Thermosyphon <i>SWH</i> in situ and its schematic [15]. (b)- Different cases of hot water inlet to the tank (right) and the cold water outlet (left) [15]. (c)- Different cases of the location of cold fluid at the outlet [15]. (d)- Different cases of the location of the hot water inlet [15].	31

25	(a)- Experiment setup. (b)- Detail description of conical collector assembly design [16]. 1- data logger, 2- Tank, 3- Pump, 4- Valve, 5- Flow meter, 6- Dual axis tracking system, 7- Sun sensor, 8- Pyranometer, 9- Double tube absorber, 10- Conical concentrator, 11- P/T sensor [16].	32
26	(a)- Schematic diagram of the experimental apparatus [17]. (b)- Schematic of thermocouple locations used in experimental data collection [18]. (c)- Location of Thermocouples and diffuser inside the tank [19]. (d)- Schematic diagram for the experimental setup [20]. (e)- Picture and schematic diagram of test tank made from polymer with an inlet stratifier connected to a heat storage test facility and 15 temperature sensors were located inside de tank [21]. (f)- Flow visualization for an inlet flow nozzle at $T_i = 49.0^\circ\text{C}$ and $\dot{V} = 5.7 \text{ ml/s}$ ($\text{Re} = 500$ and $\text{Ri} = 9087.3$) [22]. . .	33
27	(a)- Schematic view of solar collector connected to the storage tank [9]. (b)- Experimental assessment of thermal storage tank [9]. (c)- Installation in Planta Experimental de Energía Solar, Arganda del Rey (CSIC) [9]. (d)- Experimental setup at the Department of Civil Engineering of the University of Nebraska-Lincoln [23]. . .	33
28	(a)- Development of sucking effects in the fluid mechanical charge systems (Sucking of warmer water) [24]. (b)- Velocity field in the charge system A and the storage tank computed with CFD [24]. (c)- Examined charge designs [24].	34
29	(a)- Upper and front views of the tank. [25]. (b)- Schematic representation of the heat transfer process between the HTF inside the storage tank and the PCM [12]. (c)- 3D cross section view of the PCM storage tank [26]. (d)- 3D representation of the computational field [26]. (e)- Temperature distribution along different cross sections of the tank for a HTF flow rate of 11 g/s after 2 h of charging operating mode [26].	35
30	(a)- Schematic illustration of the experimental setup and the HTF path in the heat charging and discharging process [27]. (b)- Schematic illustration of the LTES unit [27]. (c)- Liquid fraction distributions on the cross sections of the LTES unit at different recorded instants during the heat charging process (inlet temperature: 80°C , inlet flow velocity: 0.1 m/s). Liquid fraction distribution at $t = 2500 \text{ s}$ [27].	36
31	(a)- Charging experiments with full mixing at the top [28]. (b)- Discharging experiments with full mixing at the bottom [28].	37
32	(a)- Different stratification's degrees inside the vertical storage tank with the same amount of the stored energy: Highly stratified, (b)- moderately stratified (c)- unstratified storage (fully mixed) [28].	38
33	(a)- The physical system and the corresponding numerical model with mesh distribution [29]. (b)- Evolution of the temperature contours of the 3D model from 250 s to 2750 s with 500 s increment (from left to right): top row (three-dimensional), and bottom row (sectioned two-dimensional) [29] [29]. (c)- Schematic view of the center plane of the thermal storage tank design. (d)- Aspect ratio effect at different diameters on the temperature contours ($L = 1194 \text{ mm}$ at $t = 500 \text{ s}$) [30].	38
34	(a)- Schematic view of the vertical mantled hot water tank. (b)- Obstacle location inside the storage tank [31]. (c)- Schematic diagram of the SWH [32]. (d)- Mechanical design for hot water thermal storage tank [33].	39

35	(a)- Vertical thermal storage tank with internal heat exchanger located at the bottom. (b)- The grid applied for the calculations [34].(c)- The effect of injecting cold water at 20°C on the evolution of the static temperature contours at t=120s [35].	40
36	(a)- Vertical storage tank with submerged heat exchanger designed by Gomez et al.[36]. (b)- Temperature contours for CM01, (c)- Temperature contours for CM02 and (d)- Temperature contours for CM03 [36].	42
37	(a)- The considered storage tanks designed and described in [37]. (b)- Temperature fields at $\tau_{ch}=3600$ s [37].	45
38	(a)- Geometries of the hot water storage tank designed and evaluated in the released study of Kursun et al. [38]. (b)- Temperature contours of the storage tank for two configurations of the insulation evaluated by Kursen et al. [38]: cylindrical and conical.	46
39	Miscellaneous methods to assess thermal stratification inside water storage tanks.	47
40	(a)- Vertical storage tank connected to ETC panel [35]. (b)- Temperature map of the storage tank with different configurations of the enhancing stratified plates [35].	48
41	(a)- Temperature contours and (b)- velocity vectors for Grashof number (Gr) below 5×10^{10} at $t^*=1$ [14].	49
42	(a)- Schematic layout of the experimental setup designed by Kumar et al. [39]. (b)- Dimensions of the TES tank with the selected location of the sensors [39].	52
43	(a)- Thermal storage tank with an integrated equalizer [40]. (b)- Temperature contours evolution for a constant flow rate of 1 liter/min [40].	54
44	Energy transfer mechanism by a series of wickless heat pipes inserted into a cylindrical exchanger.	60
45	Experimental setup of Alizadehdakheel et al. [41].	63
46	The thermocouples positions on the thermosyphon and the reviewed cases for validation.	65
47	Comparison of temperatures evolution for different positions.	67
48	Case 1 - The vapor fraction contours evolution as a function of time.	68
49	Thermosyphon new design. (a): Smooth condenser. (b): Condenser with fins. (c): Structured mesh grid of the condenser section of the studied configurations (smooth and with fins).	68
50	Nusselt number for both configurations. On the left: Smooth condenser. On the right: Condenser with fins.	70
51	Evolution of the heat transfer coefficient for both configurations as a function of time.	70
52	Evolution of the heat flux transferred by the condenser section according to time.	71
53	Evolution of mass transfer rate at the condenser section as a function of time. On the left: both configurations are presented. On the right: Scale enlargement of the MTR variation in the smooth condenser.	72
54	Evolution of the static temperature contours (K) over a period of 30 s - Smooth condenser.	73
55	Evolution of the static temperature contours (K) over a period of 30 s - Condenser with fins.	73
56	Evolution of vapor fraction contours over a period of 30 s - Smooth condenser.	74
57	Evolution of vapor fraction contours over a period of 30 s - Condenser with fins.	75
58	Evolution of the vertical velocity contours (m/s) over a period of 30 s - Smooth condenser.	76

59	Evolution of the vertical velocity contours (m/s) over a period of 25 s - condenser with fins.	76
60	Three-dimensional model of the studied storage tank integrating a series of 10 evacuated tubes with heat pipes.	80
61	(1)-3D model of the tank. (2),(3)- 2D axisymmetric FE model of the tank.	86
62	(1)- The tank shell discretization, (2)- the refinement grid structure,(3)- Axisymmetric three-dimensional mesh.	87
63	(1)- Mesh convergence test, (2)- Location of point (A) where the local stress was measured.	87
64	Thermo mechanical boundary conditions applied on the 2D-axisymmetric tank model.	89
65	Curvature radius variation of the junction connecting the cylindrical part to the flat dished bottoms to avoid the appearance of the stress concentration zones.	90
66	(1)-strain, (2)-Displacement and (3)-stress values along the path (1-2).	91
67	Stress contours (1)-config.(a), (2)-config.(e). (3)-Thermal strain resulting from applying the stagnation temperature on the tank inner walls.	92
68	Displacement values measured along the path (1 – 2) for four different materials.	93
69	The effect of five different thicknesses on the tank’s shell displacement over the center line (path (1-2)).	94
70	Solar water heater prototype ”SOL’R SHEMSY” [6]. The thermal performances of the storage tank are under assessment and improvement stage [42].	100
71	(a)- Inner shell of the horizontal storage tank which includes a series of ETCs where the head of the heat pipes is integrated. (b)-Parameterization of the horizontal storage tank which includes four heat pipes inserted on its internal lateral surface. (c)- Internal shell of the horizontal storage tank integrating heat pipe head made from copper [43].	101
72	Schematic view of four configurations of the horizontal storage tank integrating different numbers of heat pipes, $n = 4$, $n = 6$, $n = 8$ and $n = 10$	102
73	(a)- Experimental setup for measuring the temperature at the head of the heat pipe using a thermal camera. (b)- The total radiation on the ETC absorber measured on the first day of November 2017. (c)- The ambient temperature measured at Fez on the first day of November 2017.	105
74	Thermal camera view of the head of the heat pipe. (a)- Measured temperatures at the heat pipe’s head below 100°C. (b)- Measured temperature at the heat pipe’s head above 100°C.	107
75	(a)- Picture of the experimental set-up achieved by Zachar et al. [2]. (b)- Representative diagrams of a two-dimensional section of the vertical storage tank that includes a plate for the improvement of thermal stratification.	107
76	(a)- Effect of the vertical position on the dimensionless temperature (validation curve). (b)- Instantaneous contours of temperature that are corresponding to CFD numerical simulations, and which describe the development of thermal stratification inside the vertical storage tank.	109
77	(a)- Symmetrical modeling of the storage tank. (b)- Structured quadrilateral mesh of the fluid field, in addition to the refinement of the meshing elements constituting the different surfaces of the heat pipe’s walls.	110

78	(a)- Line measurement of the average temperature inside the storage tank. (b)- Mesh independence test results.	111
79	(a)- Locations where the boundary conditions are applied. (b)- Constant heat flux applied at the heat pipes, while the surfaces Σ_1 , Σ_2 and Σ_3 are maintained adiabatic.	112
80	Effect of heat pipe's number on the heat transfer coefficient (HTC) evolution.	113
81	Dynamic evolution of the temperature contours for four configurations, namely n=4, n=6, n=8 and n=10.	116
82	Dynamic evolution of the streamline contours for the fourth considered configurations.	117
83	Temperature measurements according to the horizontal and vertical lines for the configurations n=4, n=6, n=8 and n=10.	118
84	(a)- Evolution of the mean temperature according to the studied configurations. (b)- Discharging efficiency assessed for n=4, n=6, n=8 and n=10.	119
85	Typical residential building for collective hot water generation [44].	125
86	Simplified model of solar hot water collective system [44].	126
87	Fez's Weather data which are considered for simulations.	126
88	Hot water load profile.	127
89	Daily hot water flow rate.	127
90	Configuration of a stratified fluid storage tank with a representative flow streams scheme between segments.	129
91	Incident solar radiation for different solar collector's arrangement.	132
92	Useful energy gain for different solar collector's arrangement.	132
93	Performance of solar collective system for different solar collector's arrangement.	133
94	Annual and seasonal solar fraction of the collective system for different solar collector configurations.	134
95	Seasonal solar fraction for different storage tank volumes.	135
96	Hydraulic booster consumption for different storage tank volumes.	135
97	Solar energy contribution for different storage tank volumes.	136
98	Incident solar radiation for various industrial manufacturers.	137
99	Thermal performance of collective system for various industrial manufacturers.	138
100	Serial and parallel connection of the collective system's collectors [44].	138
101	Thermal performance of the collective system for various connections.	139
102	Thermal performance of the collective system for various row's number of solar collectors.	139
103	Simplified scheme of the collective hot water process [44].	144
104	(a)- Centralized storage tank equipped with internal coil heat exchanger. (b)- Centralized storage tank equipped with external plate heat exchanger. (c)- Decentralized storage tank equipped with internal heat exchanger.	144
105	Various solar radiation intensities in Morocco [8].	147
106	(a)- Fez weather data [44]. (b)- The total radiation on the collector's horizontal [44].	147
107	Typical hot water loading profiles used during the dynamic simulations (daily profiles/single monthly profile) [44].	148
108	DHW consumption flow rate corresponding to each load profile for the first five days of January [44].	149
109	Combined series and parallel flow through a collector array.	150
110	Schematic of the thermal storage tank's energy balance.	152

111	Effect of load profiles and storage tank volumes on the energy recovered by the solar collector.	154
112	Outlet temperature evolution from collector over the first five days of January.	155
113	Solar top tank temperature evolution for three different centralized storage tank volumes and for five load profiles on a range of the first 15 cold days of January.	155
114	Effect of the load profile on the consumption of the auxiliary booster for different storage tank volumes.	157
115	Effect of different storage tank volume on the solar fraction for the considered loading profiles.	157
116	Effect of the <i>ETC</i> collectors designed from different manufacturers on the annual solar fraction of the collective system for a storage tank volume of 3000 liters.	158
117	Effect of the collector field arrangement on the solar fraction for different load profiles.	160
118	Effect of different collector technologies designed from different manufacturers on the incident energy on the solar collector plane for $V = 2000$ l (Diario-DTIE load profile). (a)- <i>ETC</i> technologies. (b)- <i>FPC</i> technologies.	161
119	Effect of the <i>ETC</i> technology on the useful energy gain from collector for $V=2000$ l (Diario-DTIE load profile).	162
120	Effect of the <i>ETC</i> technology on the solar fraction gains for $V=3000$ l (Diario-DTIE load profile). (a)-Comparison between the annual solar fractions of the Viessmann brand (<i>ETC</i>) and four different <i>FPC</i> brands. (b)-Comparison between the annual solar fractions of the Viessmann brand (<i>ETC</i>) and Chaffotoux brand (<i>FPC</i>).	163

List of Tables

1	Prospects for the development of the low-temperature thermal solar sector in Morocco [45].	8
2	Brands of <i>SWH</i> systems marketed in Morocco.	10
3	National Energy Outlook Horizon perceived in Morocco towards 2030 [46].	11
4	Active actors in the solar thermal field in Morocco.	11
5	Local geographical coordinates of the considered 50 stations.	18
6	Average, minimal and maximal values of (G_{on}) recorded for 50 Moroccan stations.	20
7	Monthly solar irradiation (G_{on}) incident on 50 stations of Morocco in (W/m^2).	21
8	Average annual radiation's amount (H_0) assessed for 50 stations in Morocco.	23
9	Richardson number effect on thermal stratification.	51
10	Experimental conditions used for the numerical study.	64
11	Validation of case 1 - Comparison of the numerical temperatures and the relative errors assesment.	66
12	Validation of case 1 - Comparison of the average temperature error on the level of the adiabatic section and the condenser section.	66
13	Validation of case 2 - Comparison of the numerical temperatures and the relative errors assesment.	67
14	Thermomechanical properties of the tank materials.	93
15	Summary of the studies performed on stratified thermal storage tanks	99
16	Values of the length of the heat pipe's head (a) and the spacing (b) between each heat pipe corresponding to their number (n) inside the horizontal tank.	101
17	Used methods to assess thermal efficiency storage.	104
18	Technical specifications of <i>FLIR</i> T1020 thermal imaging camera [47].	106
19	Technical characteristics of the Evacuated Tube Collector integrating the heat pipe used during the experimental study [6], [43].	106
20	Comparison between the numerical dimensionless temperatures and the relative error's evaluation.	110
21	Collectors field connexion and arrangement.	131
22	Performance of collective system for different arrangement of solar collector.	131
23	Intrinsic characteristics of solar collector for various industrial manufacturers [44].	136
24	Database of the solar collector panel [44].	145
25	Technical characteristics of the solar collectors panel [44].	146
26	Characteristics of the solar collectors field [44].	146
27	Dimensions of the centralized tank for each storage capacity [44].	151
28	Location of water injection nozzles (Solar and hot water circuits)	151
29	Technical features of the auxiliary booster [44].	156
30	<i>ETC</i> s collectors technologies effect on the annual solar fraction (%) for the considered load profiles.	159
31	Effect of <i>ETC</i> arrangement on the collective process solar fraction during the cold season.	159
32	Incident energy on the solar collector plane for the cold period of the year.	161
33	Useful energy gain from the collector for Jingsu Sunrain Solar Energy product.	162

34	The solar fraction of the collective process during the cold periode of the year and	
	the relative gains in terms of energy if <i>ETC</i> collectors (<i>Viessmann Werke GmbH &</i>	
	<i>Co</i>) are used.	164

1. Acknowledgment

First of all, I would like to express my gratitude to my two PhD supervisors, Mr. Ali Benbassou and Mr. Abdelmajid Jamil from Université Sidi Mohamed Ben Abdellah (USMBA-Maroc), and my supervisor Mr. Tarik Kousksou from Université de Pau et des Pays de l'Adour (UPPA-France) for suggesting an original research topic that has allowed me to flourish both of my academic and intellectual levels. I would like to warmly thank all of them for the time they gave to me during these four years of scientific research and for the good atmosphere that has always prevailed.

Moreover, I thank Mr. Ahmed Arid, Mr. Tarik El Rhafiki and Mr. Tarik Kousksou infinitely for having strongly encouraged me to do scientific research and to subscribe in a thesis topic since the defense of my graduation project at ENSAM-Meknès in 2015, because they believed in my skills and my ambitions, which I had a lot of pleasure to develop with them.

I also thank the prestigious Institut de Recherche en Energie Solaire et Energie Nouvelle (IRESEN-Morocco) to have funded my thesis subject and to have offered me all the favorable conditions to carry out my scientific research.

This thesis would never have succeeded without the kind presence of many people who encouraged me and to whom I am faithful and grateful. I would like to use this opportunity to extend very warm thanks to my parents for all the things they did throughout the last three years to guide me in this research field. My brother Saâd to have inspired me, and my sister Yassamine for providing her unlimited affection. Tarik Bouhal (brother in arms), for his dedication, his time and his encouragement. Zehra, for her love, her joy of living and the good memories to look back on in the future. Jihad, for her genius, to whom I have a lot of esteem and admiration from a very young age. Douae, for her love, her infinite sweetness and her special soul. Zohra, for her friendship, her generosity and for taking care of me during the last two years wherever we were together on a mission. Anass for the good atmosphere and moments of relaxation and joy. Finally, Omar Rajad (son of people) for the goodness of his heart.

Saïf ed-Dîn FERTAHI

2. Nomenclature

a	length of the heat pipe [m]	H_{tank}	tank height [m]
A	surface of the heat pipe head [m ²]	I_{rad}	the total horizontal radiation [W/m ²]
b	spacing between two heat pipes [m]	j^{th}	position of the tank layer
D	diameter of the tank [m]	k_1	first order heat loss coefficient [W/K.m ²]
e	energy [J]	k_2	first order heat loss coefficient [W/K ² .m ²]
E	Young module [Gpa]	k_l	liquid conductivity [W/K.m]
f	solar fraction [-]	k_v	vapor conductivity [W/K.m]
g	gravity [m/s ²]	L_c	characteristic length [m]
Gr	Grashof number	m_{store}	stored mass [kg]
h	heat transfer coefficient [W/K.m ²]	m_T	storage tank's mass [kg]
H	maximum storage tank height [m]	n_i	normal vector
h	heat transfer coefficient [W/K.m ²]	n_j	normal vector at the surface
h	height [m]	P_e	applied internal pressure [Mpa]
I	the total solar irradiance on the titeld surfaces of the collectors [W/m ²]	Q_{aux}	auxiliary energy of the booster system [W]
j	index	$Q_{auxiliary}$	energy of the booster system [W]
k	conductivity [W/K.m]	Q_{evap}	heat flux at the evaporator section [W]
L	height of the tank [m]	Q_{in}	inlet mass flow rate [kg/s]
MIX	mix number	Q_{load}	hot water energy to load [W]
n	the day year	Q_{loss}	convection losses to the surrounding environment [W]
N	surface force vector	Q_{out}	outlet mass flow rate [kg/s]
n	number of used heat pipes	Q_t	the flow module into the test circuit [l/h.m ²]
N	number of fully mixed [uniform temperature] tank layers [N 15]	Q_{tank}	stored energy inside the tank [W]
Nu	Nusselt number	Q_u	useful energy [W/m ²]
P	pressure [Pa]	r_l	relaxation time
r	thermosyphon radius [m]	r_v	relaxation time
Re	Reynolds number	Ri	Richardson number
Re	external radius [mm]	S_E	energy source terme [W/m ³]
Ri	internal radius [mm]	T^*	non-dimension temperature
s	safety factor	T_∞	temperature far from the heated walls of the heat pipes [K]
Str	Stratification number	T_0	initial tank temperature [K]
T	temperature [K]	T_a	temperature of the adiabatic section [K]
t	time [s]	T_a, T_{amb}	ambient temperature [K]
T	temperature [K]	$T_{avg}[t]$	average temperature [K]
t	thickness [mm]	$T_{c,avg}$	average temperature of the condenser [K]
T	temperature [K]	$T_{c,i}$	condenser temperature at i the position [K]
T	liquid temperature [K]	$T_{e,avg}$	average temperature of the evaporator [K]
u	displacement vector [mm]	T_{env}	temperature of the environment surrounding the tank [K]
V	storage tank volume [l]	T_h	temperature of the fluid entering the storage tank from the heat [K]

y	height of vertical storage tank [m]	T_{hpi}	applied temperature at heat pipe [i] [K]
Q_c	heat flux transferred from the condenser [W]	T_i	inlet temperature [K]
Q_{in}	incident heat flux on the evaporator section [W]	T_i	temperature of the i^{th} tank segment [K]
R_{exp}	experimental thermal resistance [K/W]	T_{in}	inlet temperature [K]
ΔE	internal energy change of the tank	T_{ini}	initial temperature [K]
ΔT	temperature difference [K]	T_j	temperature in node j [K]
Δx	the space steps discretization [m]	T_j	temperature of the node j
\dot{m}	inlet mass flow rate [kg/s]	T_L	liquidus temperature [K]
\dot{m}_L	fluid mass flow rate to the load and/or of the makeup fluid [kg/s]	T_L	temperature of the fluid replacing that extracted to supply the load [K]
\dot{m}_{load}	mass flow rate to load [kg/s]	T_l	temperature [K]
\dot{m}_{lv}	mass evaporated [kg/s/m ³]	T_m	average temperature [K]
\dot{m}_{vl}	mass condensed [kg/s/m ³]	T_{max}	maximal temperature [K]
\dot{Q}_i	rate of energy input by the heating element to the i^{th} segment	T_{min}	minimum temperature [K]
\dot{Q}_s	rate at which sensible energy is removed from the tank to supply the load	T_o	outlet temperature [K]
\dot{Q}_u	useful mass flow rate [kg/s]	$T_o(t)$	instantaneous outlet temperature [K]
\vec{U}	velocity vector [m/s]	T_{out}	outlet temperature [K]
\vec{u}	velocity vector [m/s]	T_p	wall temperature [K]
\vec{u}_v	vapor phase velocity [m/s]	T_{ref}	reference temperature [K]
a_0	zero loss efficiency [-]	T_S	solidus temperature [K]
a_1	first order heat loss coefficients [W/K.m ²]	T_{SAT}	saturation temperature [K]
a_2	second order heat loss coefficients [W/K ² .m ²]	$T_{stagnation}$	stagnation temperature [K]
A_c	collector area [m ²]	T_u	useful temperature [K]
A_i	surface area of the i^{th} tank layer [m ²]	U_i	loss coefficient between the tank and its environment [per unit area] [W/K.m ²]
A_j	lateral surface of the tank [m ²]	U_T	heat exchange coefficient [W/K.m ²]
$C_{p,l}$	liquid specific heat capacity [J/K.kg]	U_x	mechanical displacement according to x direction [mm]
$C_{p,v}$	vapor specific heat capacity [J/K.kg]	u_x, u_y	velocity components according to x and y [m/s]
C_p	heat capacity [J/K.kg]	U_y	mechanical displacement according to y direction [mm]
C_{pf}	specific heat of the tank fluid [J/K.kg]	v_c	characteristic velocity [m/s]
C_v	surface curvative	V_j	volume contained inside j^{th} layer
C_w	metal wall specific heat capacity [J/K.kg]	V_t	tank volume [l]
e_l	liquid energy [J]	y^*	dimensionless height [m]
e_v	vapor energy [J]	$[C^t]$	specific heat matrix [J/K kg]
F_{CSF}	continuum surface force [N]	[K]	stifness matrix [N/m]
G_{on}	solar radiation on a horizontal plane outside the Earth's atmosphere [W/m ²]	$[K^t]$	total conductivity matrix [W/k m]
G_{sc}	Solar constant [W/mm ²]	[M]	mass matrix [kg]
H_0	amount of daily radiation [J/m ² /day]	F	structural load [N]
h_1	length of the outlet nozzle [m]	Q	thermal load [W]
h_2	length of the inlt nozzle [m]	Q	heat flux vector [J/K kg]
h_c	HTC at the condenser section [W/K.m ²]	T	temperature vector [K]

<i>Greek symbols</i>			
η	the efficiency of the thermosyphon	μ_l	liquid dynamic viscosity [Pa.s]
α	thermal expansion coefficient [$1/^\circ\text{C}$]	μ_v	vapor dynamic viscosity [Pa.s]
α	thermal diffusivity [m^2/s]	ω	vorticity function of the velocity field in the tank
α_l	control function defined by $\alpha_i = 1$ if $i = S_h$; 0 otherwise	ω, ω_s	location's latitude of the considered stations
α_l	liquid fraction	ϕ	tilt angle
α_v	vapor fraction	ϕ_{in}	internal diameter [mm]
β	thermal expansion coefficient [K^{-1}]	ϕ_{tank}	tank diameter [m]
β_i	control function defined by $\beta_i = 1$ if $i = S_L$; 0 otherwise	ψ	stream-function of the velocity field in the tank
χ_j	control function [kg/s]	ρ	density [kg/m^3]
ΔT	temperature difference [K]	ρ_f	fluid density
Δt	time step [s]	ρ_l	liquid density [kg/m^3]
ΔT_χ	temperature difference [K]	ρ_v	vapor density [kg/m^3]
$\Delta x, \Delta y$	space discretization following x and y [m]	ρ_w	metal wall density [kg/m^3]
Δy	the space steps discretization [m]	σ	normal stress [Mpa]
δ	zenith angle	$\sigma_{\theta\theta}$	circumferential stress [Mpa]
δ_k	control function [-]	$\sigma_1, \sigma_2, \sigma_{VM}$	principal stress [Mpa]
ϵ	normal strain	σ_e	yield stress [Mpa]
ϵ_k	control function [-]	Σ_i	tank surface [i]
η	exergy efficiency	σ_{ij}	stress tensor [Mpa]
η	efficiency [-]	σ_{lv}	surface tension [N/m]
η_0	zero loss efficiency [-]	σ_{max}	maximal constraint [Mpa]
$\eta_{ch}[t]$	charging efficiency	σ_{min}	minimal constraint [Mpa]
$\eta_{storage}[t]$	storage efficiency	σ_{rr}	radial stress [Mpa]
γ	distortion strain	σ_{total}	total surface area of the collector field [m^2]
γ_f	control function that defines if the auxiliary heater is off or on. 1 is off, 0 is on	σ_{VM}	Von-Mises stress [Mpa]
λ	thermal conductivity [W/k m]	τ	stress tensor [Pa]
μ	dynamic viscosity [Pa.s]	θ_z	hour angle
μ	second coefficient of Lamé [Gpa]	T_χ	Temperature [K]
		V_θ	orthoradial velocity [m/s]

<i>Abbreviations</i>			
AC	Arab Contries	HTC	Heat Transfer Coefficient
ACI	Anode to Current Imposed	HTF	Heat Transfer Fluid
AMEE	Agence Marocaine pour l'Efficacité Energétique	IAM	Incident Angle Modifier
APA	Electronic Protection Anode	IPP	Independent Power Projects
CAD	Computer-Aided Design	IRESEN	Institut de Recherche en Energie Solaire et Energies Nouvelles
CCF	Cumulative Charge Fraction	ISFH	Institute for Solar Energy Research
CDRE	Center for the Development of Renewable Energies	MEM	Moroccan Ministry of Energy
CFD	Computational Fluid Dynamic	MENA	Middle East and North Africa Region
CPC	Compound Parabolic Collector	MTR	Mass Transfer Rate
CSP	Concentrating Solar Power	NCGs	Non Condensable Gases
CSTB	Centre Scientifique et Technique du Bâtiment	NEOH	National Energy Outlook Horizon
CSWH	Conical Solar Water Heater	NES	National Energy Strategy
CU	Control Unit	PCM	Phase Change Material
DHW	Domestic Hot Water	RE	Renewable Energy
DSHW	Domestic Solar Water Heating	SBCD	Sintered Bronze Conical Diffuser
EE	Energy Efficiency	SWH	Solar Water Heater
EST	Energy Storage System	TES	Thermal Energy Storage
ETC	Evacuated Tube Collector	TPCT	Two Phase Closed Thermosyphon
FEM	Finite Element Method	TPCT	Two Phase Closed Thermosyphon
FPC	Flat Plate Collector	VOF	Volume Of Fluid
HCP	High Commission for Planning		

Abstract

The world market for solar water heaters (*SWH*) is in great expansion. In fact, *SWHs* have become a challenging alternative system to gas and electric heating devices, because of their low CO_2 emissions and their explicit involvement in the reduction of the building's electric bills. L'institut de recherche en énergie solaire et énergies nouvelles (*IRESEN-Morocco*) is actually providing the necessary funding support to promote research and development field of *SWHs* in Morocco. Hence, in February 2016, *SOL'R SHEMSY* project has been defined in order to design and commercialize the first *SWH* integrating Evacuated Tube Collectors (*ETC*) with heat pipes, under the constraints of being accessible to the Moroccan public users. For the time being, several technologies of solar collectors with different brands are commercialized in Morocco such as flat plat collectors (*FPC*) and Evacuated Tube Collectors (*ETC*), besides to thermosyphon and forced circulation *SWHs* to convert solar energy to thermal energy, in order to produce hot water with the temperature required in several applications (individual, collective, industrial and the tertiary applications). However, a serious challenge of adjustment, integration and technology transfer should be considered before importing *SWHs* with *ETC* into the Moroccan market from supplier countries such as China, Spain, Germany and Turkey described as the leading manufacturer of *SWH* in the world. Indeed, the imported *SWHs* in Morocco presented thermo-mechanical failure modes after a short period of use such as the limestone deposited inside the storage tanks, corrosion and cracking of their inner shell...

Taking into account the challenge of adjustment, integration and technology transfer of *SWHs* in Morocco is necessary, because the conditions of use differ from one country to another in terms of climatic conditions, which can be summarized in solar radiations, ambient temperature, wind velocity and the percentage of humidity in the air. In addition, the consumer's random consumption profile usually affects the thermal efficiency of the collector field and the overall solar fraction of *SWHs*.

The main aim of this thesis is to carry out numerical simulations and optimizations of *SWHs* taking into account the techno-economic context of Morocco and its intrinsic weather conditions. Two simulation approaches were used to achieve this purpose. The first approach was based on unsteady Computational Fluid Dynamics (*CFD*) numerical simulation in order to enhance the efficiency of the heat pipes integrated inside *ETCs* and to increase the thermal stratification indicators of horizontal thermal storage tanks with submerged heat pipes. Finally, improve the storage tank's structure using thermo-mechanical coupling simulations. The second approach is based on dynamic simulations, which have been performed to assess and optimize the energy performance of a collective hot water process intended to produce domestic hot water (*DHW*) under the climatic conditions of Fez city located in Morocco. Indeed, several parameters have been considered, in particular the effect of the storage tank volume, the brands of collectors and their technology from different manufacturers, the connection between the solar panel and the overall surface of the *ETC* and *FPC* which constitute the collector field etc.

Key words: Solar water heaters (*SWHs*); *SOL'R SHEMSY*; Evacuated Tube Collectors (*ETC*); Heat pipes; Adjustment and integration; Technology transfer; Morocco; Computational Fluid Dynamics (*CFD*); Dynamic simulations; Solar fraction; Optimization.

Résumé

Le marché mondial des chauffe-eau solaires (*CES*) est en essor. En effet, les *CES* sont devenus des systèmes compétitifs aux appareils de chauffage par gaz naturel et énergie électrique, en raison de leurs faibles émissions de CO_2 et de leur participation explicite à la réduction des factures d'électricité du consommateur marocain. Actuellement, l'Institut de Recherche en Energie Solaire et Energies Nouvelles (*IRESEN-Maroc*) pourvoit le soutien financier nécessaire pour promouvoir la recherche et le développement dans le domaine des *CES* au Maroc. Ainsi, en février 2016, le projet *SOL'R SHEMSY* a été défini pour concevoir et commercialiser le premier *CES* intégrant la technologie des capteurs à tubes sous vide (*ETC*) avec des caloducs, en rendant son acquisition accessible au sociale marocain.

Il paraît qu'à l'heure actuelle, plusieurs technologies de capteurs solaires de marques différentes sont commercialisées au Maroc tels que les capteurs plan (*FPC*) et les capteurs à tube sous vide (*ETC*), outre le thermosiphon et les *CES* à circulation forcée pour convertir l'énergie solaire en une énergie thermique, afin de produire de l'eau chaude avec la température requise dans plusieurs applications individuelles, collectives, industrielles et tertiaires. Cependant, une sérieuse problématique d'ajustement, d'intégration et de transfert technologique devrait être envisagée avant d'importer les *CES* à capteur *ETC* munis de caloduc sur le marché marocain auprès de pays fournisseurs tels que la Chine, l'Espagne, l'Allemagne et la Turquie considérés comme des leaders internationaux dans le domaine des *CES*. Car en effet, les *CES* importés au Maroc ont présenté des modes de défaillances thermomécaniques après une courte période d'utilisation, comme le dépôt de calcaire à l'intérieur des ballons de stockage, la corrosion et la fissuration de leur coque interne...

Prendre en considération la problématique d'ajustement, de l'intégration et du transfert technologique des *CES* au marché marocain est nécessaire, étant donné que les conditions d'utilisation diffèrent d'un pays à un autre en termes de conditions climatiques, qui peuvent être résumées par l'amplitude de l'irradiation solaire, la température ambiante, la vitesse du vent et le pourcentage de l'humidité dans l'air. Par ailleurs, le profil de consommation aléatoire du consommateur affecte à son tour l'efficacité thermique du champ de capteurs et la fraction solaire globale des *CES*.

L'objectif principal de cette thèse est de mener des simulations numériques et des optimisations qui portent sur les *CES*, en prenant en compte le contexte technico-économique du Maroc et ses conditions climatiques intrinsèques. Deux approches de simulation ont été utilisées pour atteindre cet objectif. La première approche s'est basée sur des simulations numériques *CFD* (Computational Fluid Dynamics) instationnaires pour améliorer l'efficacité énergétique des caloducs intégrés dans les *ETC* et d'augmenter les indicateurs de stratification thermique des ballons horizontaux dans lesquels les caloducs sont immergés. Enfin, d'améliorer la structure du réservoir du *CES* en utilisant des simulations qui permettent de modéliser un couplage thermomécanique. La deuxième approche est basée sur des simulations dynamiques, qui ont été menées pour évaluer et optimiser la performance énergétique d'un système collectif destiné à produire de l'eau chaude sanitaire (*ECS*) sous les conditions climatiques de la ville de Fès-Maroc. En effet, plusieurs paramètres ont été considérés, en particulier l'effet du volume du réservoir de stockage, les marques des capteurs, leurs rendements et leurs technologies issues de différents fabricants, et finalement l'effet de la connexion série/parallèle et mixte entre les panneaux solaires (*ETC* et *FPC*) qui constituent le champ capteur, etc.

Mots-clés: Chauffe-eau solaire (*CES*); *SOL'R SHEMSY*; Capteur à tube sous vide (*ETC*); Caloducs; Adaptation et intégration; Transfert technologique; Maroc; Computational Fluid Dynamics (*CFD*); Simulations dynamiques; Fraction solaire; Optimisation.

3. General introduction

The chapters presented in this thesis manuscript are part of *SOL'R SHEMSY* project, which is a research and development project funded by *IRESEN-Morocco*. *SOL'R SHEMSY* aims to ensure the technological transfer of *SWHs* to Morocco. In addition, it is intended to realize and commercialize the first *SWH* in Morocco that is integrating *ETCs* with heat pipes, and to make it available to the Moroccan public users. To enlighten our studies and our developments, we have structured the manuscript in three parts. The first part is constituted from two chapters, the second part from three chapters, while the third part is composed of two chapters.

The first chapter entitled “*A synthesis on the technology transfer of solar water heaters and inclusion as solar energy policy in Morocco*” aims to describe the global market of *SWH* besides to the global overview on their installed capacity in the world. In addition, it provides an assessment of the world’s market growth of solar thermal collectors. The general market overview of solar thermal collectors in the world has also been presented and the *SWH* market situation in Morocco according to socio-economic frame and energy context was described in details. Finally, an energy feasibility study regarding the integration, adjustment and generalization of *SWH* through the assessment of the daily horizontal radiation incident on 50 stations in Morocco has been carried out.

The second chapter is a review on solar thermal stratified storage tanks, which provides an insight on stratification studies and efficiency indicators. In fact, this chapter was written in three parts. The first part provided a recent insight regarding the studies that investigated solar storage tanks of different technologies of *SWHs* such as thermosyphons and forced systems. Also, the auxiliary systems integrated inside the storage tanks to meet the requirements of the produced hot water were presented. Moreover, innovation, experimental and numerical studies performed on stratified storage tanks were also discussed in this first section of the review. The second section presents the equation setting to be established to ensure the physical modeling of thermal stratification inside the designed storage tanks. Indeed, two approaches have been detailed: the three-dimensional *CFD* approach and the two-dimensional formulation based on the introduction of the vorticity stream function equation. Finally, the third section of this review highlighted a set of thermal performance indicators commonly used by the scientific community to assess the thermal efficiency of hot water storage tanks connected to *SWHs*.

The third chapter entitled “*Performance optimization of a two-phase closed thermosyphon through CFD numerical simulations*” aims to investigate numerically the phase change in a closed thermosyphon subjected to specific terms and conditions related to the field of solar thermal applications, more precisely an application to *SWHs*. The fourth chapter is a thermo-mechanical strength analysis for energy storage improvement of horizontal storage tanks integrating *ETC*. This study aims to determine the factors to improve in the tank design model in order to extend its life span, because it is an important device ensuring solar energy storage. Three studies were performed. The first study is a geometrical optimization. In fact, the shape of the storage tank’s dished bottoms was maintained as flat and the curvative radius (R_i) and (R_e) were varied to avoid the appearance of the stress concentration zones. The second study was conducted to predict the material effect and hence to facilitate its choice. Indeed, four different materials were assigned to the tank’s shell, namely standard steel, stainless steel, aluminum alloy and the copper alloy. Last but not least, the third study presented a set of simulations to investigate the tank shell thickness on which the thermo-mechanical constraints were applied with regard to the studied operating conditions.

The fifth chapter is an experimental study and *CFD* thermal assessment of horizontal hot water storage tank integrating *ETC* with heat pipes. The aim of the present study is to measure experimentally the temperature in stagnation of the heat pipe head using a thermal camera, and to turn the achieved findings to perform *CFD* calculations intended to assess the thermal efficiency of the solar horizontal storage tank which integrates *ETC*. Indeed, the experimental achieved temperature will be applied as a thermal boundary condition, during the two-dimensional numerical modeling, on the tubular device where the head of the heat pipes is located. The validation of the physical models of "*Fluent*" calculation code that controls the physical phenomena of heat transfer and flow has been ensured by reproducing the experimental study of Zachar et al. [2], which describes in detail the thermal stratification in a vertical tank that pre-stores hot water subjected to charging and discharging cycles. Four configurations of the horizontal storage tank were considered, namely $n=4$, $n=6$, $n=8$ and $n=10$. Besides, several results were presented to describe and analyze the effect of the heat pipe number on the heat transfer by convection and conduction inside the considered solar storage tank.

Chapter six is a design and thermal performance optimization of a forced collective solar hot water production system in Morocco for energy saving in residential buildings. In this way, the current work aims to derive a knowledgeable data base for the energetic performance parameters concerning the use and implementation of dynamic solar collective systems in Morocco, because in general, the majority of the research works focuses on hot water individual systems and uses simplified model in the simulations of the collective systems [48] and [49]. Accordingly, four parametric studies were presented in this paper to design the collective solar water heater system and to ensure its optimization during the dynamic mode operation. The combined effects of collector's area and its characteristics, climatic conditions and hot water load profile on the performance of the solar collective system were carried out. In addition to this, simulations were conducted for the currently wide-spread solar collector *ETC* and four different types of manufacturers were considered to provide useful guidelines about the operation of the hot water collective system under a realistic load profile. In this sense, an energy analysis and performance assessment of this system was achieved, and the system's optimal design was reported.

The last chapter is a forced hot water collective systems optimization for low energy consumption in Morocco. According to the best of our knowledge, up to now, there is no study treating the assessment of solar collective systems under Moroccan conditions. In this vision, the aim of this paper is to take profit from the recent climatic zoning in Morocco to assess the thermal performance of a dynamic solar collective system applied to a residency in Fez. The chapter maps out the collective domestic hot water consumption throughout one state of Morocco and hints at the benefit of using solar collective heating devices as energy saver in domestic building, respectively. Two different solar devices were compared towards their thermal efficiency throughout the whole year. Individual personal preferences/habits regarding hot water usage were taken into account as well. This study highlights the influence of the parameters cited above on the annual solar fraction saving of the collective residential domestic *SWH*. Several performance indicators were defined to carry out this work on the basis of recent search [50] and [51]. Heating water for various domestic applications is performed by using electric or gas devices, and this work opens up a new perspective of water heating using solar energy, an abundant resource in Morocco throughout the year.

4. **Part I: Technological challenge of solar water heaters (*SWHs*) in Morocco and a focused insight on hot water stratified storage tanks**

4.1. *Chapter I: A synthesis on the technology transfer of solar water heaters and inclusion as solar energy policy in Morocco*

4.2. *Introduction*

This chapter highlights the technology transfer of solar water heaters (*SWH*), their adjustment and integration as energy policy in Morocco. First of all, the global market of *SWH* besides to the global overview on their installed capacity in the world has been described. Secondly, the world's market growth of thermal collectors has been assessed, and the general market overview regarding their total installed capacity in the world has been reported. Thirdly, the market situation of *SWH* in Morocco has been described according to socio-economic frame and energy context, taking into consideration several parameters, such as the current state of the market data, the installation cost and the main local industrial actors. Moreover, the amount of minimum, maximum and average values of the daily horizontal radiation have been assessed for 50 stations in Morocco to investigate the feasibility of using solar energy to integrate, adjust and generalize *SWH* technologies in Morocco. The achieved results showed that the Kingdom of Morocco benefits from a significant annual solar radiation that would promote the adjustment of *SWH*, as well as the transfer of their technology to Morocco. *SOL'R SHEMA* project was presented. Indeed, it consists of installing *SWH* prototypes in 30 cities of Morocco to assess their performance under different climatic conditions. The measured physical quantities are recorded in a centralized cloud system, which is located in Fez city to carry out the necessary post-treatment, subsequently to conclude on the technological transfer of *SWH* in Morocco. Last but not least, a modular experimental platform has been installed in Fez to conduct the necessary experimental studies that will help suggesting the technological adaptation to be made on the *SWHs*, in order to ensure their generalization in Morocco.

4.2.1. *Background and state of the art*

Renewable energy has become a target for the Middle East and North Africa (MENA) countries. Hence, several energy collaborations and strategies were made in Morocco, Algeria, Tunisia, and Egypt [52], such as the integration of renewable power within the electricity systems [53] and the integration of concentrating solar power (CSP) technologies for the MENA electricity system [54], because their penalty cost is considered minor compared to southern Europe due to notable difference in the incident solar radiations values [55]. A regional perspective study regarding the development of renewable energy in Arab countries (AC) has been carried out by Chedid et al. [56]. They shed light on the current status of renewable-energy (RE) in AC, because it is considered as a lever for the sustainable socio-economic developments of these countries, which are already widely known by gas and oil resources [57]. Recently, national roadmaps describing the implementation details of those strategies and collaborations were backed by master plan documents and miscellaneous renewable energy ambitious goals towards 2020 and 2030 were defined by MENA countries.

According to Griffiths et al. [58] a significant regional and international transformation have been recorded regarding the development of the actual energy policies in the MENA region that are illustrated through involving new renewable energy technologies [35], economic and political trend, besides increasing diversification of energy sources and remaining seriously concerned by climate change issues. As presented in the review released on the energy policy assessment by Griffiths et al. [58], MENA region is actually in the midst of an energy transition. However, it has uncertain outcomes that could have long lasting impacts on the energy system.

It is noted that Eberhard et al. [59] focused on the Independent Power Projects (IPP) funded by China in Sub-Saharan Africa and presented the new adopted investment trends and derived policy lessons. Indeed, they showed that additional work and power are needed in Sub-Saharan Africa and the contribution of the private sector's investment would be a major key to achieve a socio-economic development. Moreover, they relied on renewable energy, because it promotes the emergence of serious environmental, economic and social issues.

Several strategic studies and acceleration plans of socio-economic and energy emergence have been defined and established recently in Morocco to demonstrate the interest towards renewable energies more particularly the solar thermal energy [60], and the wind energy [61]. According to Belakhdar et al. [62] and Alhamwi et al. [63] the Moroccan National Energy Strategy (NES) launched in 2008 is expecting that the total of energy mix coming from renewable energy sources towards 2020 such as hydroelectric generation, solar and wind capacities are expected to be 2000 MW each. In other words, the purpose is to establish 42% of total installed capacity by combining the contribution of several types of renewable energies. Moreover, Moroccan NES highlights the importance of the meteorological factors for the strategic consideration of future energy systems such as individual or collective solar water heaters systems that are the aim of this study.

Bennouna et al. [64] defined a new frame regarding energy needs for Morocco towards 2030, using both GDP-energy and GDP-energy intensity correlations. Their main findings related to our study can be presented as follows: butane subsidies have widened the gap with other fuels. Hence, they have to be removed as soon as possible in order to decrease the growth of its consumption and energy intensity. In addition, the continuation of the electric equipment program after 2020 have to be clarified further and any implementation delays must be avoided. Furthermore, Omri et al. [65] used simultaneous-equations models coupled with panel data of 14 MENA countries which includes Morocco, for 21 years since 1990, to predict and examine the nexus between CO₂ emissions, energy consumption and economic growth. They showed through their empirical results that the dissimilarities in the nexus between economic growth and energy consumption should be recognized by the considered energy policies in order to achieve and maintain sustainable economic growth for the countries of MENA region.

It has been affirmed through our state of the art synthesis that few studies were conducted recently on SWHs in Morocco. For instance, Bouhal et al. [50] investigated the effect of load profile that describes the consumption pattern of hot water and solar collector technologies namely flat plate collector (FPC) and compound parabolic collectors (CPC) on the fractional savings achieved by solar domestic water heaters evaluated under different weather conditions in Morocco. They found that the solar energy contribution would cover 80% of energy requirements needed to heat water according to a well-defined consumption profile, especially in cities with high solar energy potential. Moreover, the thermal optimization and the Design of a forced collective solar hot water production system in Morocco has been studied by Fertahi et al. [66] to achieve energy saving in residential buildings. Besides, The thermal performance of solar water heater flat plate collector has been analyzed and optimized by considering the weather conditions of Tetouan city located in the north of Morocco by Dagdougui et al. [67]. The main goal of their study is to support the designers of SWH in the definition of the optimal water flow and of the optimal collector flat area of the collector, so as to achieve a compromise between the solar fraction of the solar collector panel efficiency and the loaded hot water intended for consumption.

4.2.2. Aim and motivations

This chapter aims to describe the global market of *SWH* besides to the global overview on their installed capacity in the world. In addition, it provides an assessment of the world's market growth of solar thermal collectors. Moreover, the general market overview of solar thermal collectors in the world has also been presented and the *SWH* market situation in Morocco according to socio-economic frame and energy context was described in details. Finally, an energy feasibility study regarding the integration, adjustment and generalization of *SWHs* through the assessment of the daily horizontal radiation incident on 50 stations in Morocco has been carried out.

4.3. Global market of *SWHs*

4.3.1. Installed capacity of solar thermal collectors

Fig. 1(a) presents the history of thermal collector development on a worldwide scale, while Fig. 1(b) shows the annual installed of thermal collectors capacity in China, Europe and rest of the world. The world market for thermal manifolds has been characterized by a steady upward trend between 2000 and 2011 and has shown stability since 2012. Moreover, the annual installed capacity has increased from around 9.8 GWth in 2002 to around 53.3 GWth in 2013. Compared with 2012, the growth rate fell from 6.8% to 1.7% in 2013.

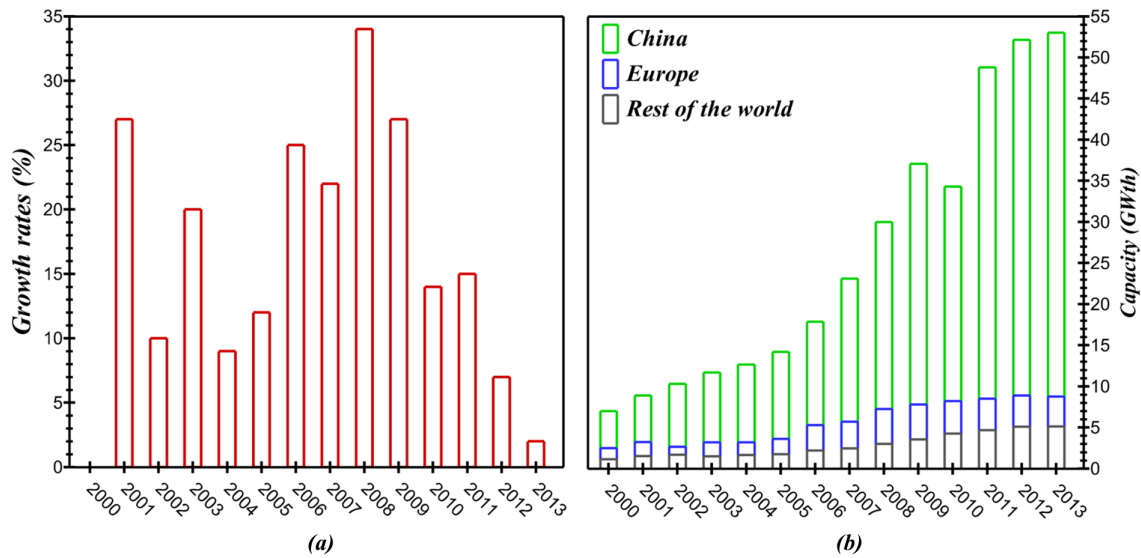


Figure 1: History of thermal collector development on a worldwide scale [3].

World overview on the installed capacity of *SWH*

At the end of 2013, an installed capacity of 374.7 GWth corresponding to a total capacity of 535.2 million square meters of in-service manifolds was identified. The majority of the total capacity in service was installed in China 262.3 GWth and Europe with 44.1 GWth, which together accounted for 82% of the total installed capacity of *SWH*. The remaining installed capacity was shared between the United States and Canada with 17.7 GWth, Asia (excluding China) with 10.0 GWth, Latin America with 8.7 GWth, MENA region composed of Jordan, Lebanon, Morocco, the Palestinian Territories and Tunisia with 6.1 GWth, Australia and New Zealand with 5.9 GWth, and countries in sub-Saharan Africa such as Mauritius, Mozambique, Namibia, South Africa and

Zimbabwe with 2 GWth. It is noted that the remaining "other countries" market is estimated at 5% of total installations with 18.7 GWth (Fig. 2).

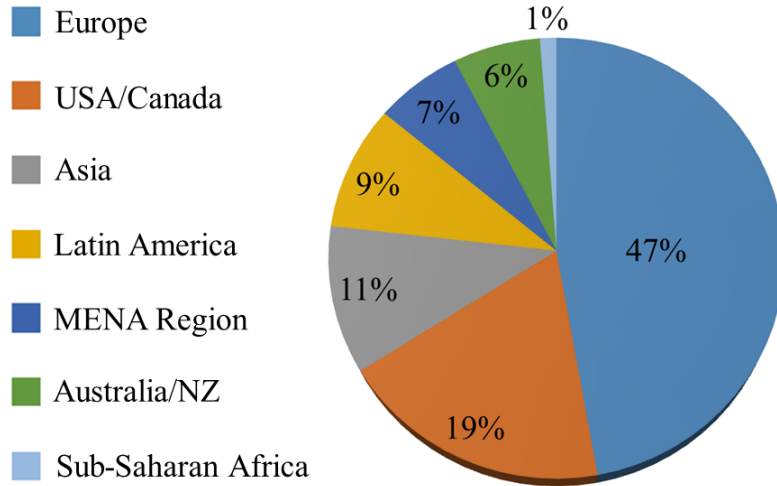


Figure 2: Share of total installed capacity in operation (end of 2013) [3].

The total capacity of the installations in service until the end of 2013 is divided technically into flat glazed collectors with 83.9 GWth (119.9 million square meters), evacuated tube collectors with 264.1 GWth (377.3 million square meters), unglazed flat collectors with 25.0 GWth (35.7 million square meters), and glazed and unglazed air collectors with 1.7 GWth (2.4 million square meters). Moreover, with a share of 70.5%, *ETC* are the predominant technology of solar thermal collectors worldwide, followed by 22.4% flat glass collectors and non-glazed flat collectors with 6.7%. In fact, air collectors play only a minor role in the total number of installations currently in service (Fig. 3(a)). On the other hand, in Europe, flat collectors are much more widespread. Indeed, their market share is of the order of 83.3% against 10.5% for *ETC* (Fig. 3(b)).

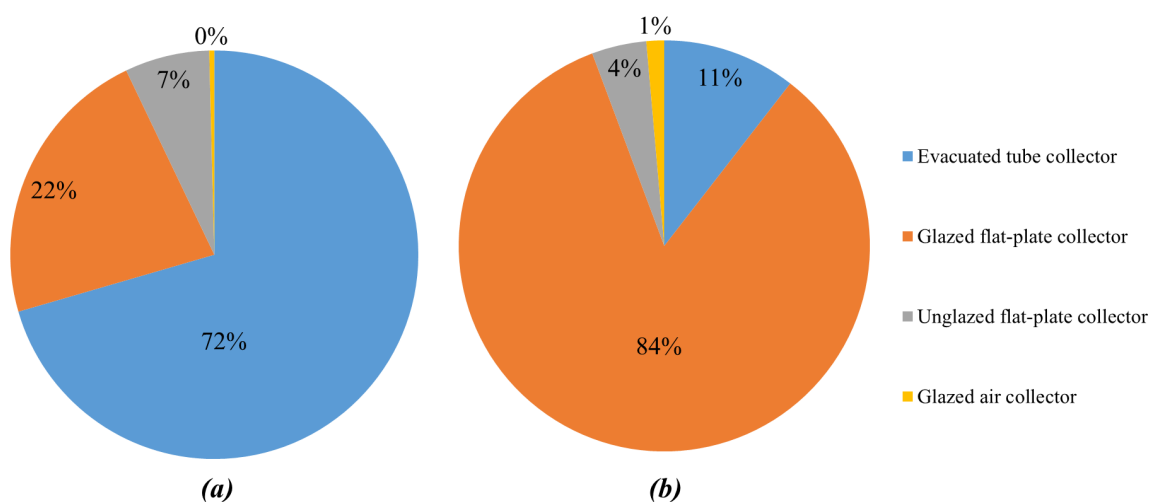


Figure 3: Distribution of the total installed capacity by collector's type in 2013 [3].

A ratio of the total installed capacity per 1000 inhabitants was introduced as indicator (Fig. 4), in order to situate the current situation of Morocco in relation with the other countries regarding the development of glazed thermal collectors.

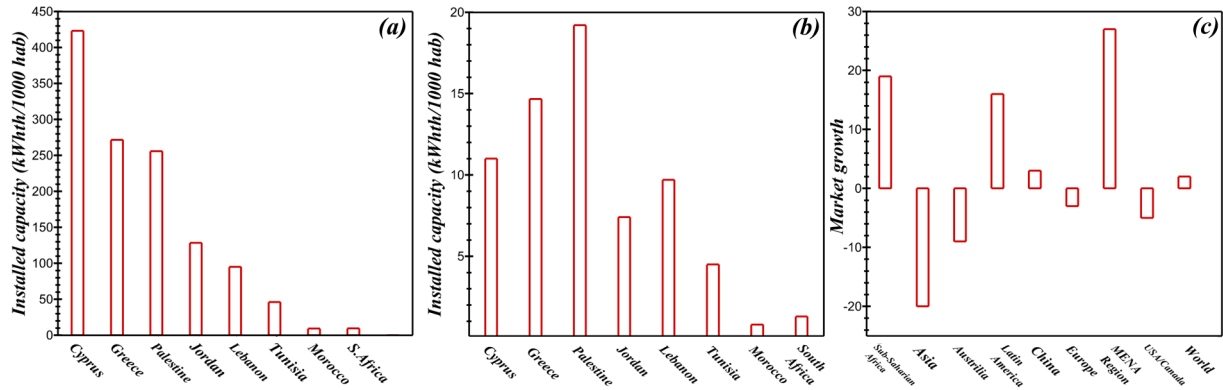


Figure 4: (a), (b)- Distribution of the total installed capacity by collector's type in 2013. (c)- Installed capacity per 1000 kWh in some considered countries of the world. [3]

Market growth of thermal collectors

Towards the end of 2013, a total capacity of 55.0 GWth, corresponding to 78.6 million square meters of solar collectors has been installed worldwide. This means an increase in the new collector installations by 1.8% compared to 2012. As presented in Fig. 5 more than three quarters of all installed solar thermal systems are thermosyphon systems, the rest are forced circulation systems.

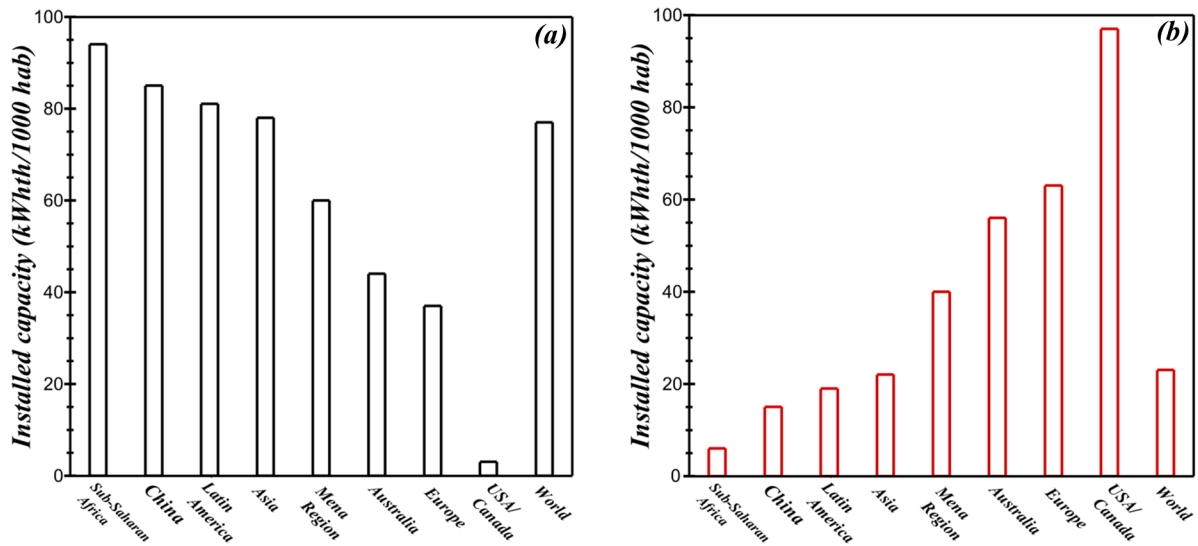


Figure 5: Growth in the market for thermal collectors 2012/2013. (a)- Thermosyphon system, (b)- Forced circulation system.

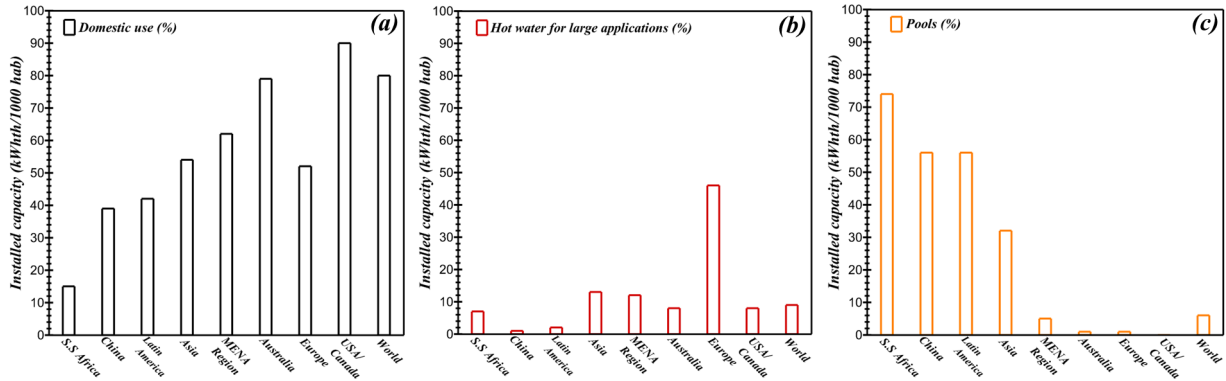


Figure 6: New installed capacity per 1000 kWh in some countries of the world.

There was positive market growth in the period 2012/2013 in China, Latin America, the MENA region and sub-Saharan Africa, while in Europe, Asia (excluding China), the United States, Canada and Australia the number of solar thermal system installations dropped between -3% and -20%. In order to situate the efforts made by Morocco to promote the penetration of solar thermal collectors into the market, the same sample of countries presented in Fig. 6 was considered and the market evolution has been assessed by considering different applications, such as domestic hot water production, combined systems, hot water production for large applications, pools and other applications.

4.3.2. Classification of the world's SWH market

Generally, more than three quarters of all installed solar thermal systems are thermosyphon systems, the rest are forced circulation systems (Fig. 5). The regions where this trend is not observed are the USA/Canada, Europe, and Australia with 97%, 63% and 56% respectively where forced circulation systems are the most used technologies. Indeed, thermosyphon systems are more common in hot climates, such as in Africa, South America, southern Europe and the MENA region [68]. In these regions, thermosyphon systems are more often equipped with FPC, while in China, the typical thermosyphon system used for the production of domestic hot water is equipped with ETC [4].

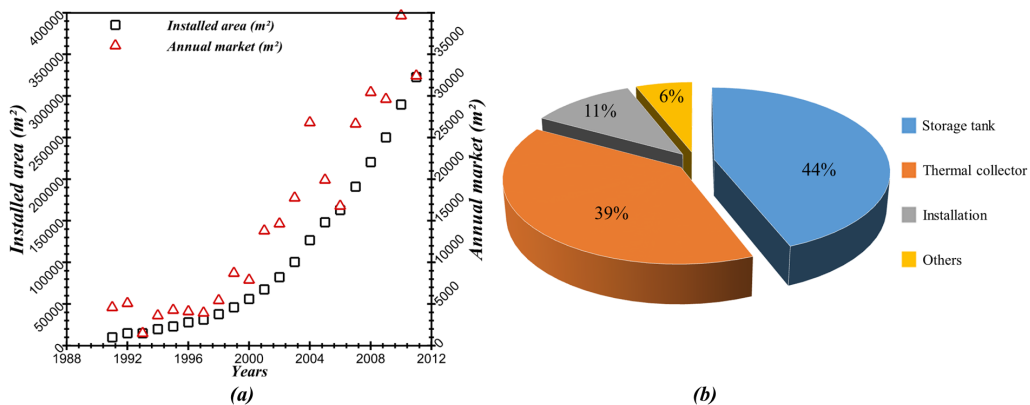


Figure 7: Market classification by SWH's type [4], [5].

Low and medium temperature solar thermal collectors are used in several applications such as space heating, swimming pools, domestic hot water production, air conditioning, and other specific industrial applications [69]. Depending on the range of the temperature required for each application, one specific or different type of collectors can be recommended. By the end of 2013, there were approximately 111 million solar thermal systems worldwide. Of these, 6% were used to heat swimming pools, 80% were used for *DHW* production in individual houses, and 9% were attached to large *DHW* systems for houses, hotels, hospitals, schools (tertiary sector) [70]. approximately 3% of the world’s installed thermal capacity is provided for both *DHW* and space heating (combined solar systems). Other applications accounted for about 1% of installed solar systems (Fig. 7). They include the application of district heating networks, industrial processes or refrigeration machines using a thermal energy source such as absorption and adsorption technologies [5].

Concerning the African countries, the United States and Australia, the majority of installed solar systems are used for heating swimming pools. This trend is reversed especially for Asian countries and Europe. For the *MENA* region, the use of sanitary hot water comes first of all in the fields of applications [71].

4.4. Market situation of SWHs in Morocco

4.4.1. History of SWH’s market development

The low temperature solar thermal market in Morocco was launched with the impetus of the implementation of the *Promasol* program [72]. Indeed, the Moroccan Ministry of Energy and Mines (*MEM*) launched this program in 2002 to promote the market of SWHs in Morocco thanks to the improvement of quality and certification, awareness campaigns, and training of installers of qualified SWHs. The management of the program was entrusted to the Center for the Development of Renewable Energies (CDER) under the supervision of the MEM. On the environmental front, *Promasol* has succeeded in decreasing about 1.3 million tons of carbon dioxide (CO₂) since its creation in 2002.

Concerning its economic impacts, *Promasol* has increased the installed area of solar water heaters from about 36000 m² to more than 220000 m² in 2008 [73] (Fig. 7-(a)). In addition, during the same period, this program contributed to the increase in the number of companies active in the *SWHs* sector. In terms of its social outcomes, the program has contributed to the creation of hundreds of jobs directly through the training and certification of installers, and indirectly through the creation and/or expansion of specialized firms. According to recent data from the Ministry of Energy, Mines, Water and Environment [45], the vision for the development of the low-temperature thermal solar sector in Morocco is given in the Tab. 24. In fact, is possible to identify the challenge undertaken by Morocco in the days to come. An annual increase in the installed capacity of *SWHs* of around 4.4% year is therefore expected.

Year	Cumulative area achievable (m ²)	Energy produced (GWh/an)	Energy saved (kTep/an)	CO ₂ avoided (kT)	Power saved (MW)	Job creation
2020	1700000	1190	103	682	400	920
2030	3000000	2100	181	1204	700	1600

Table 1: Prospects for the development of the low-temperature thermal solar sector in Morocco [45].

4.4.2. Socio-economic situation and energy context

According to the trends of the population projections carried out by the High Commission for Planning (*HCP*) [74], an average variant indicates that the population of Morocco will increase

from 30 million inhabitants in 2005 to 38 million in 2030, which is equivalent to an average additional growth of 300000 inhabitants per year. This demographic development would be mainly urban, mainly due to the rural exodus and the urbanization of rural areas. Thus, in 2030 Moroccan cities would house 64% of the country's inhabitants instead of 55% in 2004 [74]. In recent years, the Moroccan economy has been characterized by its macroeconomic stability coupled with low inflation. In 2015, Morocco enjoyed dynamic economic growth with 4,9%, up from 2014. GDP per inhabitant reached 3690 USD/inhabitant in 2013, with a growth of 4,1% compared to 2008 [75]. Worldwide, energy demand is expected to increase by about 85% between 2010 and 2040 due to rising living standards, economic growth and continuous electrification of society [76] due to the unprecedented development context of the national economy and population growth, the Department of Energy projections foresee, in a baseline scenario, almost triple primary energy demand and quadruple it of electricity by 2030 [77].

From one hand, Morocco, which is not an oil-producing country, is facing severe energy constraints due in part to its almost total dependence (about 96% in 2012) on energy imports and high energy consumption of fossil fuels (around 87%) on the other. The import of this amount of energy has a heavy impact on the country's energy bill, which has recorded an average annual growth rate of 18.8% since 2002, reaching 107 billion dirhams in 2012 [78]. On the other hand, energy in the country is subsidized through a compensation fund with a load of 35.9 MMDH in 2013, which fell 26% compared to 2012 when the load was 4.4 MMDH following the entry into force of the price indexation system in 2013 [79]. Aware of this context, Morocco, as part of its national energy strategy, has therefore begun a process of diversifying the national energy mix in favor of renewable energies, while ensuring that it has competitive energy in terms of costs and availability and preservation of the environment. Currently, Morocco is taking up the challenge of raising the share of renewable energies to 52% by 2030. Morocco has a high potential in terms of availability and abundance of renewable resources. Solar energy is placed at the top of these resources with an average sunshine level of 5.3 kW h/m² under annual sunshine durations ranging from 2700 h in the north to about 3500 h in the south [80].

4.4.3. Current state of the market data

In Morocco, *DHW* requirements are mainly provided by gas boilers that differ in size and power [50]. In some specific applications, oil-fired boilers are also considered [66]. For safety reasons, some households prefer electric water heaters. Indeed, the current electric water heaters consumes 6% of Moroccan electricity production, mostly during peak hours [81]. The solar subsidiary is under development in Morocco. Its rate of coverage of demand does not exceed 11% [81]. The most commonly used system in Morocco is the thermosyphon in the residential sector. It accounts for about 95% of the total installed systems. The trend is reversed in the case of the commercial and industrial sector, where forced circulation systems dominate the market [82]. With regard to the installed collector technology, the planar collectors dominate the market with a share of 95%. *ETC* are the second category of thermal collectors used for the production of hot water in Morocco with a price significantly higher than that of *FPCs*. The majority of solar products used in Morocco are imported. Imports of thermal solar equipment constitute about 90% of sales. Local manufacturing remains marginal resulting from relatively high prices [83].

4.4.4. Assessment of SWH's installation cost

Admittedly, the cost of solar equipment is gradually decreasing mainly thanks to the control of the manufacturing process besides to using cheap materials. On the other hand, the price range of a solar thermal system varies depending on its capacity and the technology of collectors used to design the components of individual solar water heaters, namely the storage tank volume, the booster power, pumps of the primary and secondary solar loops and the *power of the internal/external heat exchanger*. According to AMEE [84] and "Amisole" [85], the average cost of a 2 m² solar collector panel with an insulated hot water storage tank in a range of 160 to 200 liters is approximately assessed to be 1060 USD. Generally, solar collectors and storage tanks account for more than 80% of the total cost of the system. During October 2016, we carried out interviews and visits of national actors operating in the field of SWHs in Morocco, such as "Elec-energie" in Fez, "Bet benbassou" and "Chaffoteaux" in Casablanca and "Energypole" in Rabat. We have achieved a general view on the marketed brands, in addition to their characteristics and their selling price. The collected data are summarized in Tab. 25.

SER-GÜN [86]	150	815.25	Flat copper collector 120x194 (150 liters and 200 liters) or two collectors 94x194 (300 liters)	Tanks guaranteed 5 years, Solar collectors guaranteed 8 years
	200	1081.57		
	300	1358.75		
BATITHERM [87]	150	1032.65	Connection accessories pack	Guaranteed on system 8 years
	200	1434.84		
	300	1847.9		
SOLARHEAT [88]	300	2119.65	Two flat collectors (198x101x8.6), magnesium anode, hot-rolled steel, storage tank (2.5 mm thick) treated at 860 C (According to DIN4753))	Tanks guaranteed 5 years, Solar collectors guaranteed 10 years
TUBULAUX [89]	150	652.2	Evacuated Tubes Collectors (ETC)	Guaranteed on system 10 years
	200	923.95		
	300	1630.5		
CHAFFOTEAUX [90]	150	1228.31	Closed circulation system with natural circulation, tests according to EN 12976, flat collectors	10 years guaranteed on panels
	200	1423.97		
	300	2000.08		
IMPERIAL [91]	150	923.95	Two flat collectors	Guaranteed on system 8 years
AUSTRALINOX [92]	200	1250.05	Copper plane sensor. aluminum absorber (2.15 m ²)	Guaranteed on system 5 years
	300	1576.15		

Table 2: Brands of SWH systems marketed in Morocco.

4.4.5. Main industrial actors of SWH in Morocco

Most of the actors operating in the solar field in Morocco are integrated companies specialized in installations, distribution and maintenance activities. It is estimated that there are 50200 retailers and installers on the market according to [83]. There are also two brands that manufacture SWHs in Morocco, such as "Event solar Morocco" and "Giordano Maroc". A list of actors active in some large Moroccan cities is presented in Tab. 4.

It is noted that a group of those actors is interested in the manufacture of storage tanks. From a distribution point of view, the management of solar thermal equipment that are intrinsic to SWHs is not ensured by active and specialized companies but by installers, and small businesses acting as resellers. As for the installation process, SWHs are often installed by the sellers to ensure optimum installation conditions. Moreover, as it has been reported in our interviews and discussions with the actors previously presented in Tab. 4 that in some cases the sellers may outsource the installation activity of individual/collective SWHs. Tab. 3 is presenting the National Energy Outlook Horizon (NEOH) perceived in Morocco towards 2030 [46].

Demand evolution (Average rate of change in %)		Without energy efficiency	With energy efficiency
Electricity		6, 5	5, 7
Petroleum products		3	2, 5
Primary energy		5	4, 2
Demand in 2030	Without energy efficiency	With energy efficiency	Energy saving
Electricity (TWh)	95	81	14
Petroleum products (Mtep)	16, 6	14, 5	2, 5
Primary energy (Mtep)	43	38	6

Table 3: National Energy Outlook Horizon perceived in Morocco towards 2030 [46].

No.	Companies	Type of activity	No.	Companies	Type of activity
1	AG Energie	Marketing	19	Sococharbo	Marketing
2	Batitherm	Marketing	20	Solargie	Marketing
3	Chaffoteaux	Marketing	21	Sunlight Power Maroc	Marketing
4	Clean Energie	Marketing	22	Kefal n/a Supplier	Marketing
5	Energetica	Marketing	23	Temasol	Marketing
6	Energies continues	Marketing	24	Tropical Power	Marketing
7	Energie Innovation	Marketing	25	Event Solaire Maroc	Marketing
8	EnergyPoles	Marketing	26	Atlas Energy Solaire	Marketing
9	First Metal	Marketing	27	Spring power	Marketing
10	Giordano	Manufacturing and marketing	28	Solicap	Marketing
11	H2 Energy	Marketing	29	Solergitech	Marketing
12	sofoton Maro	Marketing	30	Multi Energies Renouvelables	Marketing
13	Itri Environment	Marketing	31	Maroc Energies Renouvelables	Marketing
14	Myfac	Marketing	32	Compagnie Marocaine des Energies	Marketing
15	Noorweb	Marketing	33	Bati Energie	Marketing
16	NRJ International	Marketing	34	Eco3c	Marketing
17	Phototherm	Marketing	35	Suratem	Marketing
18	Sisteclen	Marketing	36	Thephsol	Marketing

Table 4: Active actors in the solar thermal field in Morocco.

4.5. SOL'R SHEMSY project

4.5.1. Main purposes and general overview

Morocco has an important solar renewable energy potential [93]. A national strategy regarding the integration of *SWHs* is perused through the project launched by *IRESEN* in 2016 under the project name *SOL'R SHEMSY* [7], which aims to manufacture and market the first solar water heater made in Morocco for the social concerns [42]. This project has several purposes, the most relevant would be to facilitate the transfer, adjustment and the integration of *SWH* for the social with a competitive price [6]. In addition, this national Moroccan project aims to:

1. The installation of 1.7 million m² of *SWHs* by 2020 (compared with 350000 m² assessed in 2012 through an investment of 500 MAD)
2. The generation of a considerable saving for the state resulting from the saved butane compensation

3. The development of a local sector that creates jobs by encouraging local production of *SWHs*
4. The development of a *SWH* park, white an efficiency and a quality that comply with the most stringent international standards
5. Optimizing the environmental impact through the reduction of greenhouse gas emissions

Fig. 8 presents the aims of *SOL'R SHEMSY* project, which can be summarized in the following points. First, technological purposes that consist in the development of an experimental platform of *SWHs* to evaluate their energy performance and to suggest technological modifications to ensure their adaptations according to the Moroccan context in terms of the amount of the incident solar energy and the consumer's patterns. Secondly, socio-economic aims to improve the regional and national economy of Morocco, through the development of process lines to manufacture *SWHs*. In addition, to encourage the youth to create start-ups specialized in the labelling and accreditation of *SWHs* products imported to Morocco, while offering the possibility to create job opportunities. The environmental protection aspect is also a priority of *SOL'R SHEMSY*, notably through the use of solar energy and to decrease greenhouse gas emissions during the production of *DHW*. The research and development component is also a major asset for *SOL'R SHEMSY*, in particular through the creation of a reliable and recognized testing laboratory and the dissemination of the operating procedures for *SWHs* installation.

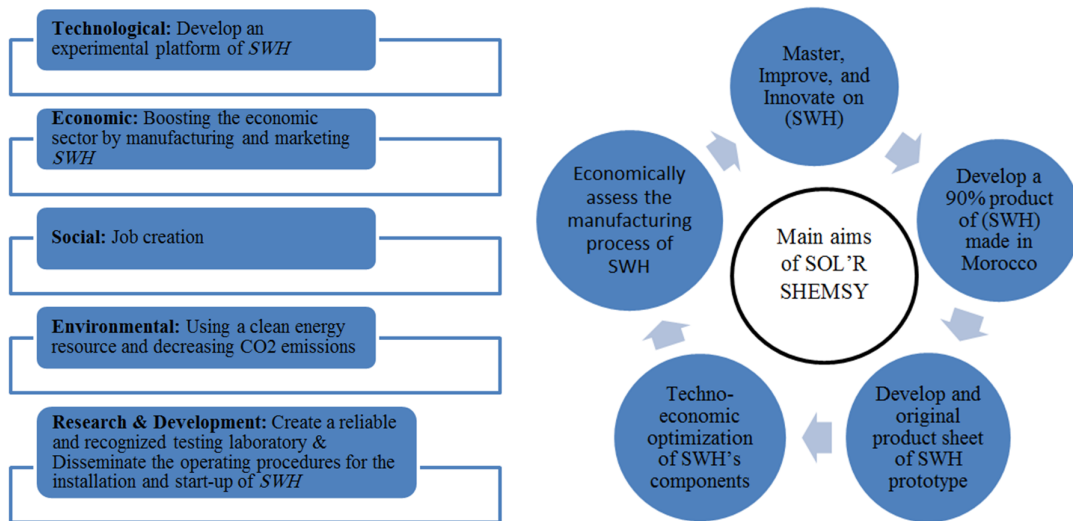


Figure 8: Main aims of *SOL'R SHEMSY* project [6].

4.5.2. *SHEMSY's experimental platform*

To equip the experimental platform of *SOL'R SHEMSY* project, three controllers have been designed and installed in order to record different physical quantities related to the operation of the forced circulation *SWHs* (Fig. 9). These physical quantities are considered as outputs from the *SWH* available in our laboratory and from the *SWHs* installed in several Moroccan cities (Fig. 10). For instance, the temperature at the outlet of the collector field, the inlet temperature of the cold water in the storage tank, the flow rate of the solar primary loop and its available provided thermal energy. The operating cycles of the pump integrated in the solar loop and finally the volume of the consumed hot water in addition to the daily needs.

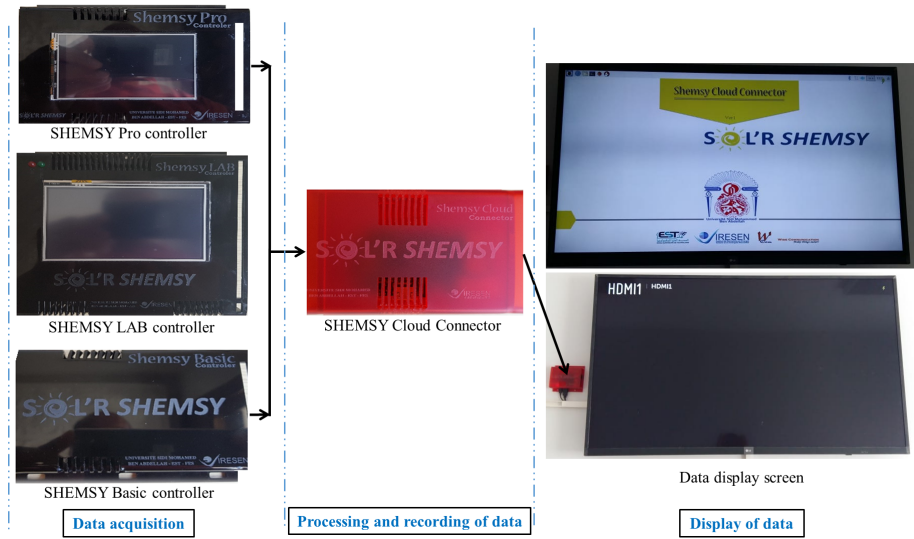


Figure 9: Data acquisition, their processing and recording in "SHEMSY Cloud connector".

Three controller versions have been developed in our laboratory, including "SHEMSY Basic controller", "SHEMSY LAB controller" and "SHEMSY Pro controller". These three collectors are connected to the "SHEMSY Cloud Connector" device that collects and processes the data before their post-processing. It should be noted that 30 controllers will be distributed on several Moroccan families, to determine their domestic hot water needs, in order to create a database regarding the definition of realistic profiles of hot water consumption and to conclude on the technological adaptation of SWHs with respect to the weather conditions of Morocco.

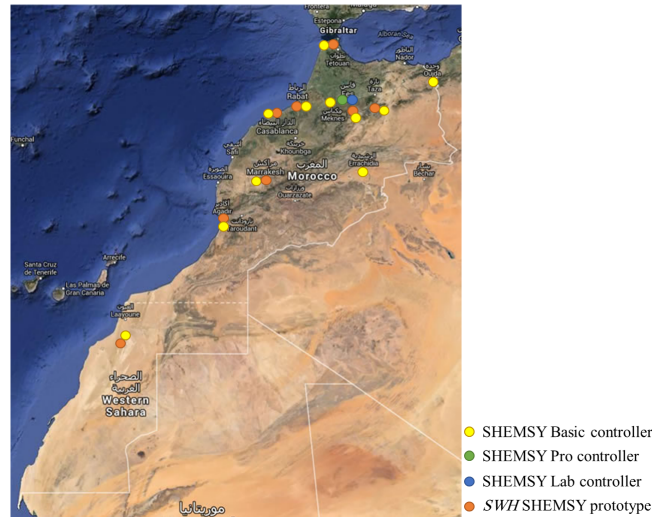


Figure 10: Location of the controllers to be installed in several Moroccan cities.

Fig. 10 presents different cities in Morocco, in which the controllers were distributed to conduct the adaptation and technology transfer study on SWH. "SHEMSY Lab", "SHEMSY Pro controllers", and "SHEMSY Cloud connector" are located in the city of Fez, while "SHEMSY

"Basic controller" and *SWHs* prototypes are integrated in several cities in Morocco. The distribution of the controllers and the prototype that has been selected will help to build a measurements database of the physical quantities, mentioned above, which is necessary to assess the thermal efficiency of *SWHs* that depends mainly on the climatic conditions and the hot water requirement in every city and households. The processing of the measurements derived from the *SWHs* that are located in different cities in Morocco will facilitate their technology transfer, because it would be possible to determine the suitable solar collector technologies, their number and tilt angle for the cities that belong to the same climatic zoning. In addition, to accurately design the volume of the storage tank, which would enhance the solar fraction of the *SWH*, besides to the average power of the booster equipment that should be used to compensate for the insufficient solar energy during the cold periods of the year.

A standard configuration of the forced circulation *SWH* that equips the Moroccan households is presented in Fig. 11(a). It consists of a stratified vertical storage tank with a volume capacity of 300 liters, a control unit which controls the operation of the primary solar circuit pump, a magnesium anode to decrease the deposit of the limestone on the inner walls of the tank and a hydraulic booster system to meet the needs of the consumer when the converted solar energy is insufficient to produce hot water. The experimental platform that we developed is mainly characterized by its modular aspect (Fig. 11(b)), i.e. it allows the integration of additional components. Indeed, it has been equipped with an energy meter that calculates the amount of solar energy converted into thermal energy through the collector. A water flow calculator to build a database of the Moroccan users' load profiles [66].

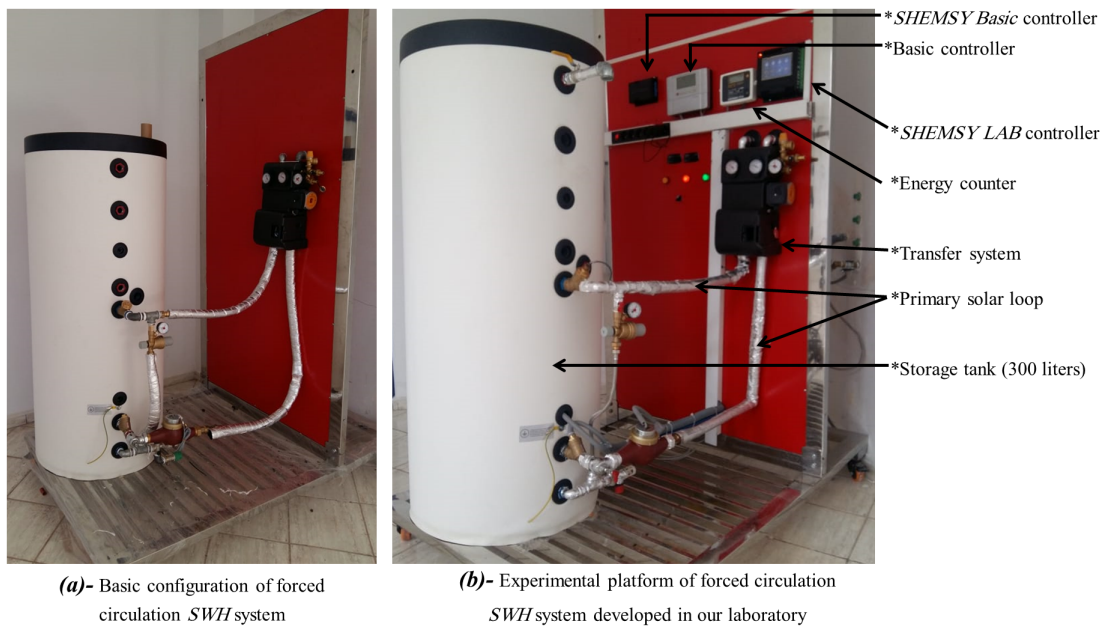


Figure 11: *SHEMSY's* experimental platform. (a)-Basic configuration of forced circulation *SWH* system. (b)- Experimental platform of forced circulation *SWH* system developed in our laboratory.

Currently, the load profile is an input data, which remains a statistical component difficult to define in order to assess the thermal efficiency of *SWHs*. Besides to "*SHEMSY basic controller*", that will be distributed on several Moroccan households in different cities and the "*SHEMSY*

Lab controller". The usefulness of these electronic devices is to control the cycle operation of the primary circuit pump and to record the volume of the consumed hot water. All the recorded data are transferred to the "*SHEMSY Cloud controller*", which handles the data processing and their display.

The high pressure *SHEMSY SWH* presented in Fig. 12 is similar to the ordinary *SWH* that operates on the thermosyphon principle, where the produced hot water has no pressure. The high pressure *SHEMSY SWH* we have designed does not have the limitations and disadvantages of commercial low pressure *SWHs*, because the transfer of solar energy into the water is accomplished according to a completely different principle. In this case, the hot water at the outlet of the *SWH* has the same pressure as the cold water inlet (= the pressure of the sanitary water network of the city). In addition, the heated water does not circulate in the glass absorption tubes for the high pressure *SHEMSY SWH* variant. In fact, the solar energy in the absorption tubes is transferred into the high-pressure hot water storage tank using a series of copper "heat pipe" according to the same principle used in refrigerators [7].

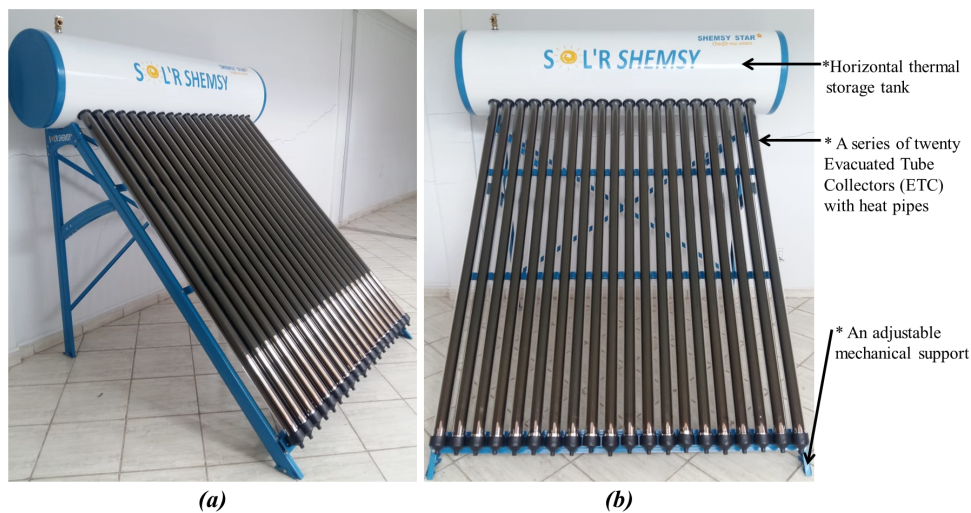


Figure 12: High pressure *SHEMSY SWH* integrating *ETC* with heat pipes [7].

In addition, the high pressure *SHEMSY SWH* offers several benefits compared to the ordinary low pressure *SWH*. For example, *SHEMSY* tubes do not burst during the summer season. Moreover, the installation of the high pressure *SHEMSY SWH* is simple, because the cold water of the city network is connected with its inlet, while the outlet is connected to the inlet of the water heater (gas, electric booster). Therefore, the existing water heater will consume much less energy, since the sanitary water at the inlet is already hot [55].

Fig. 13-(a) presents the components that make the forced circulation *SHEMSY SWH* a scalable prototype. A correctly adjusted Flir thermal camera was used to take thermal images of these components, such as the energy meter (Fig. 13-(b)), the cold input of *DHW* and the hot inlet of the primary solar circuit (Fig. 13-(e)). In addition, a thermal imaging of the primary circuit pump and a thermal image of the high pressure *SHEMSY SWH* are respectively presented in Figs. 13-(c) and Fig. 13-(f). The high pressurized *SWH* integrates twenty *ETCs* where heat pipes with conductive fins are submerged.

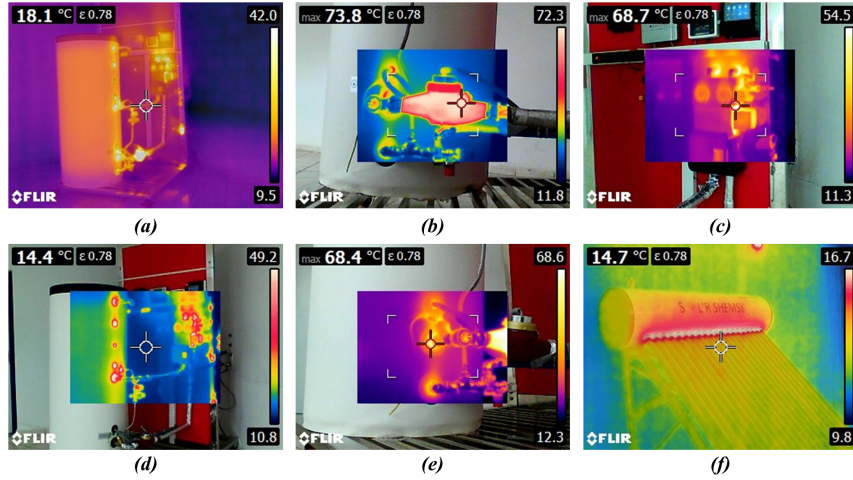


Figure 13: Temperature map of several devices integrated in the experimental *SOL'R SHEMSY* platform.

Two solar collector technologies, oriented to the South [51], were used to constitute the experimental SHEMSY platform, namely *ETC* and *FPC* collectors. The advantage of the present modular experimental platform is that it offers the possibility of a series and parallel coupling of these two technologies, through the use of three servo valves (Fig. 14(b)). The surface of the collector field has been properly selected to meet the heating requirements of 300 liters of *DHW*. The pipes of the solar loop were insulated to decrease the thermal losses, while carrying out the experimental studies. Their main purpose is to evaluate the thermal performance of the *SWH* with *ETC* or *FPC* collectors characterized with an identical apparent surface.

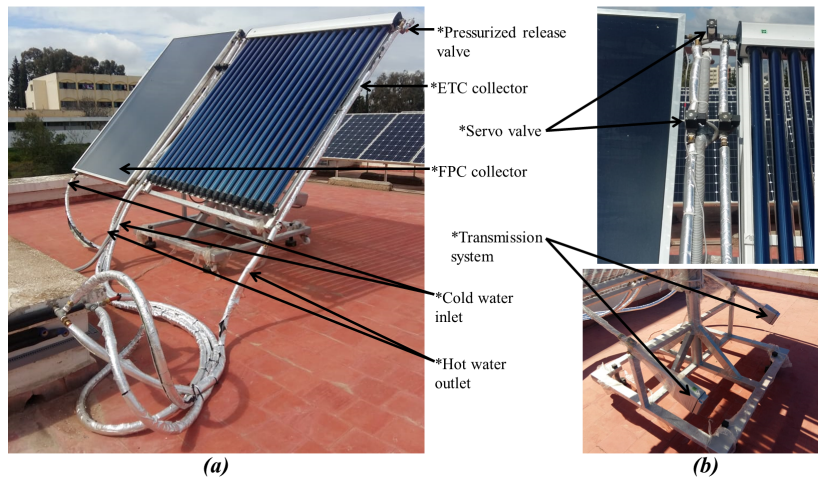


Figure 14: Solar collector field of the experimental SHEMSY platform, constituted from *ETC* and *FPC* technologies.

A transmission system (Fig. 14(b)) was used to adjust the tilt angle of the collectors regarding the incident solar radiations. The temperature measurements at the inlet/outlet of each collector, besides to the inlet/outlet temperature of the collector field are also available. As a result, evaluating the annual performance of *SHEMSY SWH* with forced circulation would be possible. Therefore, we can conclude on the most suitable collector technology, which is located in the region

of Fez, hence, to generalize it on the 3rd climatic zone of Morocco, since the climatic conditions are similar. Fig. 15-(e) presents a temperature map example of the collector map that has been taken using a properly adjusted Flir thermal camera. For example, Figs. 15-(a) and (b) show the maximum local temperature measured at the inlet and outlet of the *ETC*, while Figs. 15-(c) and (d) present the maximum local temperature measured at the inlet and outlet of the *FPC*. The dynamic measurements of these temperatures are necessary to assess the solar fraction of the forced circulation *SHEMSY SWH* [66].

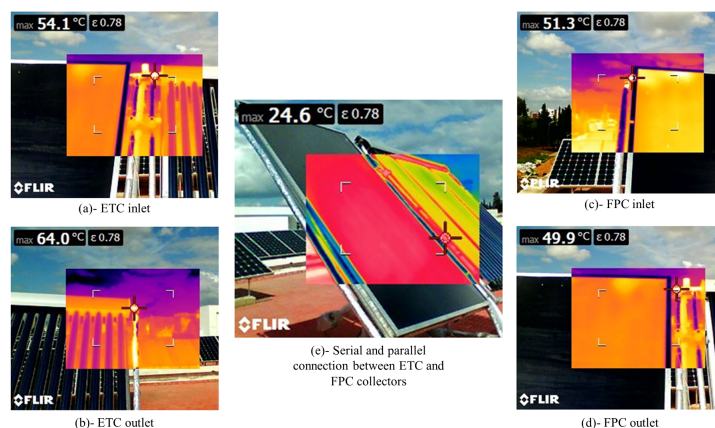


Figure 15: Temperature map of the inlet/outlet of the solar thermal *ETC* and *FPC* connected to the forced circulation *SWH*.

4.6. Solar energy profile in Morocco

4.6.1. Geography of Morocco

Geographical coordinates

Morocco is a country located in North West Africa ($32^{\circ}00'N$ $5^{\circ}00'W$). Its long coastline overlooking the Atlantic Ocean ends beyond the Strait of Gibraltar on the Mediterranean Sea [94]. In the south of Morocco lies the Western Sahara. In the east and south-east, Morocco is bordering Algeria. At some distance from the Atlantic coast are the Canary Islands and Madeira. North of the Strait of Gibraltar is Spain (Fig. 105). Morocco has four main mountain ranges, and it is the only country in the Maghreb to have a huge chain of mountains Atlas. In the south of the country, the Erg Chebbi and Erg Chegaga near the Algerian border, is the largest expanse of stones and sand inside Morocco. Some sand dunes can reach 200 m in height.

General overview of the Moroccan climate

The Moroccan climate is both Mediterranean and Atlantic, with a dry and hot season coupled with a cold and wet season, the end of the warm period being marked by October rains. The presence of the sea attenuates the differences in temperature, tempers the seasons and increases the humidity of the air (400 to 1000 mm of rains on the coast). In the interior, the climate varies according to the altitude. Summers are hot and dry, especially when blowing the hot sirocco or the chergui, summer wind coming from the Sahara. At this season, average temperatures are $22^{\circ}C$ to $24^{\circ}C$. Winters are cold and rainy with frost and snow. In the mountainous regions, the precipitation is very important (more than 2000 mm of rainfall in the Rif or 1800 mm in the Middle Atlas). Pre-Saharan and Saharan Morocco has a dry desert climate.

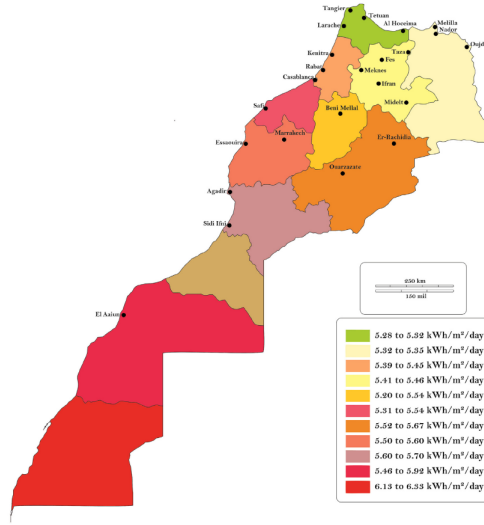


Figure 16: Various solar radiation intensities in Morocco [8].

Local geographical coordinates

The geographical coordinates of 50 Moroccan stations are presented on the Tab. 5. Moreover, the latitude and longitude of each station are considered as input parameters of the equations detailed in the subsection 4.6.2 “Extraterrestrial solar radiation equations”, which allow estimating the incident solar radiations (G_{on}) and the daily radiation’s amount (H_0).

No.	Stations	Lat. (N)	Long. (E)	No.	Stations	Lat. (N)	Long. (E)
1	Rabat	34°00'47"	6°49'57"	26	Guelmim	28°59'13"	10°03'26"
2	Casablanca	33°35'17"	7°36'40"	27	Taurirt	34°24'26"	2°53'50"
3	Marrakesh	31°38'02"	7°59'59"	28	Ifran	31°42'07"	6°20'57"
4	Tangier	35°46'02"	5°47'59"	29	Errachidia	31°55'53"	4°25'35"
5	Fez	34°01'59"	5°00'01"	30	Nador	35°10'05"	2°56'00"
6	Agadir	30°25'12"	9°35'53"	31	Assilah	35°27'54"	6°02'02"
7	Sale	34°03'11"	6°47'54"	32	Berrechid	33°15'55"	7°35'15"
8	Tétouan	35°34'42"	5°22'06"	33	Benslimane	33°36'59,99"	7°06'60,00"
9	Meknes	33°53'36"	5°32'50"	34	Chefchaouen	35°9'40,39"	5°15'47,59"
10	Oujda	34°40'53"	1°54'30"	35	EL Hajeb	33°41'16"	5°22'15"
11	Kenitra	34°15'39"	6°34'48"	36	Ksar el kebir	35°00'01"	5°54'13"
12	Beni mellal	32°20'14"	6°20'59"	37	Tarfaya	27°56'21"	12°55'33"
13	Temara	33°55'40,21"	6°54'18,66"	38	Inezgane	30°21'8,321"	9°33'5,387"
14	El Jadida	33°15'17"	8°30'21"	39	Berkane	34°55'12"	2°19'11"
15	Khouribga	32°52'51"	6°54'22"	40	Bouznika	33°47'21"	7°09'34"
16	Safi	32°17'57"	9°14'13"	41	Skhirat	33°51'7,84"	7°2'20,72"
17	Mohammedia	33°41'09"	7°22'58"	42	Khenifra	32°56'05"	5°39'42"
18	Settat	33°00'03"	7°36'59"	43	Fkih ben salah	32°30'03"	6°41'26"
19	Khemisset	33°49'26"	6°03'58"	44	Sidi slimane	34°15'53"	5°55'33"
20	Taza	34°12'36"	4°00'35"	45	Tan-tan	28°26'16"	11°06'11"
21	Boulemane	33°11'13,369"	4°14'0,01"	46	M'diq	35°40'50,1"	5°19'23,956"
22	Ouarzazate	30°55'08"	6°53'36"	47	Midelt	32°41'06"	4°44'42"
23	Figuiq	32°06'32"	1°13'42"	48	Saïdia	35°5'59,58"	2°17'15,592"
24	Essaouira	31°30'44"	9°46'11"	49	Dakhla	23°41'05"	15°57'28"
25	Larache	35°11'35"	6°09'20"	50	Guercif	34°13'32"	3°21'12"

Table 5: Local geographical coordinates of the considered 50 stations.

The fact of having inventoried these 50 cities has as main aim the assessment of the incident solar irradiations all over Morocco. The estimation of the previously presented solar indicators (G_{on}) and (H_0) would be useful to encourage decision-makers besides to political and industrial actors to facilitate the transfer and generalization of *SWH* technologies for different cities in Morocco.

4.6.2. Extraterrestrial solar radiation equations

The solar radiation on a horizontal plane outside the Earth's atmosphere is calculated using Eq. [1](#) [\[95\]](#).

$$G_{on} = G_{sc}[1 + 0.033\cos(\frac{360 \times n}{365})] \times \cos(\theta_z) \quad (1)$$

where G_{sc} is solar constant ($G_{sc} = 1367 \text{ W/m}^2$). Moreover, n is corresponding to the day of the year (e.g., for the first day of January, $n = 1$), and θ_z is the zenith angle (the angle between a vertical line and the sun's beam) calculated using Eq. [2](#)

$$\cos(\theta_z) = \cos(\delta)\cos(\phi)\cos(\omega) + \sin(\delta)\sin(\phi) \quad (2)$$

where ϕ is the location's latitude of the considered stations (Tab. [5](#)), and δ is the tilt angle defined by Eq. [3](#) [\[96\]](#). Besides, ω is the hour angle (equivalent to 15 degrees per hour from solar noon).

$$\delta = 23.45\sin(360\frac{(284 + n)}{365}) \quad (3)$$

To determine the amount of daily radiation, Eq. [4](#) can be used to assess the amount of daily radiations [\[95\]](#). where (H_0) is expressed in ($\text{J/m}^2/\text{day}$).

$$H_0 = \frac{24}{\pi}G_{sc}[1 + 0.033\cos(\frac{360 \times n}{365})] \times [\cos(\phi)\cos(\delta)\sin(\omega_s) + \frac{2\pi\omega_s}{360}\sin(\phi)\sin(\delta)] \quad (4)$$

$$\omega_s = \cos^{-1}(-\tan(\phi)\tan(\delta)) \quad (5)$$

4.6.3. Incident solar radiations (G_{on})

The evolution of the incident solar radiations (G_{on}) on the 50 stations which are considered as case study in Morocco is presented in Fig. [17](#). Figs. [18](#)(a) up to [18](#)(e) are describing the evolution of (G_{on}) for groups of stations, where each group is composed of 10 cities. The evolution trend of (G_{on}) is a Gaussian presenting maximum values during the summer season. Minimum values of (G_{on}) were recorded during the winter season. It is noted that the daily values of (G_{on}) from several nearby cities are very close. For instance the example of Rabat, Casablanca, Tangier and Tetouan Fig. [18](#) (a). Taza, Khemisset, Settat and Mohammedia Fig. [18](#) (b). Ifran, Nador, Larache and Essaouira [18](#)(c). Assilah, Berrechid, Benslimane and Chefchaouen Fig. [18](#)(d). M'diq, Sidi slimane, Saidia and Skhirat Fig. [18](#) (e). For this reason, we recommend that it would be advantageous to generalize the integration of *SWH* in Morocco according a specified zoning, where the considered cities are presenting similarities in terms of (G_{on}).

The average monthly incident solar radiation (G_{on}) presented in Tab. [7](#) has been evaluated for 50 cities in Morocco. It is important to assess (G_{on}) because it helps to detect the periods of the year described by low solar irradiations per station which are insufficient to maximize the solar fraction of the *SWH* system [\[50\]](#).

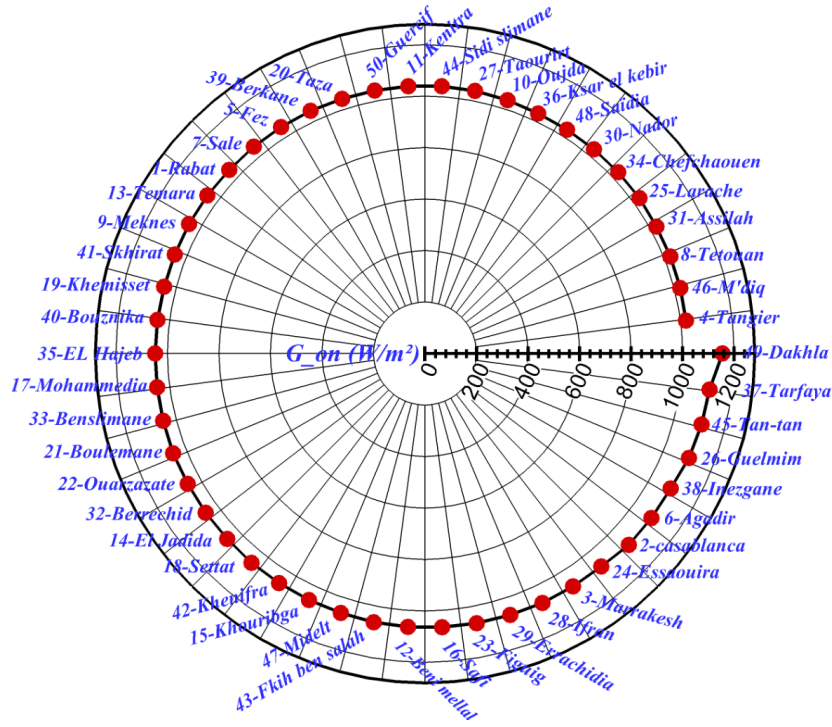


Figure 17: Annual average solar radiation (G_{on}).

Stations	Average (W/m ²)	Min (W/m ²)	Max (W/m ²)	Stations	Average (W/m ²)	Min (W/m ²)	Max (W/m ²)
1-Rabat	1043.61	729.17	1265.58	26-Guelmim	1102.61	826.74	1280.72
2-casablanca	1086.1	774.57	1301.81	27-Taourirt	1038.9	719.86	1264.03
3-Marrakesh	1072.46	776.67	1273.96	28-Ifran	1071.89	774.06	1273.78
4-Tangier	1021.18	693.36	1258.01	29-Errachidia	1068.7	767.58	1267.58
5-Fez	1043.36	728.77	1265.5	30-Nador	1029.7	702.55	1264.45
6-Agadir	1087.08	800.4	1277.38	31-Assilah	1025.4	698.42	1259.4
7-Sale	1043.39	727.25	1265.42	32-Berechid	1053.15	743.14	1268.45
8-Tetouan	1023.93	696.09	1258.88	33-Benslimane	1050.28	738.44	1267.58
9-Meknes	1045.39	730.48	1266.06	34-Chefchaouen	1029.29	704.46	1260.81
10-Oujda	1035.47	714.48	1262.84	35-EL Hajeb	1047.9	734.44	1266.9
11-Kenitra	1040.79	723.04	1264.59	36-Ksar el kebir	1031.36	707.76	1261.52
12-Beni mellal	1064.4	761.69	1271.71	37-Tarfaya	1114.21	844.39	1286.38
13-Temara	1044.96	729.79	1265.92	38-Inezgane	1087.91	798.43	1281.32
14-El Jadida	1053.28	743.35	1268.49	39-Berkane	1042.7	756	1261.82
15-Khouribga	1057.84	750.85	1269.84	40-Bouznika	1046.68	732.59	1266.46
16-Safi	1065.27	760.31	1275.58	41-Skhirat	1045.9	731.32	1266.22
17-Mohammedia	1047.97	734.67	1266.86	42-Khenifra	1057.15	749.57	1269.69
18-Settat	1056.39	748.45	1269.41	43-Fkih ben salah	1062.39	758.23	1271.2
19-Khemisset	1046.25	731.89	1266.33	44-Sidi slimane	1040.7	722.76	1264.62
20-Taza	1041.39	723.87	1264.84	45-Tan-tan	1108.93	835.01	1285.52
21-Boulemane	1051.92	740.99	1268.13	46-M'diq	1023	691.94	1262.1
22-Ouarzazate	1052.05	740.99	1268.13	47-Midelt	1060.22	754.76	1270.53
23-Figuig	1067.12	766.22	1272.46	48-Saïdia	1030.31	706.23	1261.1
24-Essaouira	1074.16	778	1274.33	49-Dakhla	1155.42	924.31	1290.84
25-Larache	1028.92	704.01	1260.62	50-Guercif	1041.19	723.55	1264.78

Table 6: Average, minimal and maximal values of (G_{on}) recorded for 50 Moroccan stations.

Stations	January	February	March	April	May	June	July	August	September	October	November	December
1-Rabat	773.94	908.25	1068.92	1194.11	1252.56	1265.58	1255.01	1210.67	1108.73	953.81	802.51	729.17
2-casablanca	819.67	954.25	1113.8	1235.96	1290.82	1301.81	1292.04	1250.8	1152.21	999.16	848.09	774.57
3-Marrakesh	820.08	949.05	1100.84	1215.36	1265.03	1273.96	1265.23	1228.19	1136.49	991.51	847.15	776.67
4-Tangier	739.08	877.18	1044.21	1177.12	1241.99	1258.01	1246.09	1196.42	1087.04	924.96	768.71	693.36
5-Fez	773.55	907.91	1068.65	1193.92	1252.45	1265.5	1254.91	1210.51	1108.49	953.49	802.13	728.77
6-Agadir	843.08	969.24	1123.57	1225.4	1270.55	1277.38	1269.6	1236.32	1149.91	1010.1	869.38	800.4
7-Sale	773.16	907.56	1076.31	1193.73	1252.95	1265.42	1254.53	1209.37	1108.25	950.44	801.75	727.25
8-Tetouan	742.86	880.56	1055.17	1179	1243.88	1258.88	1246.77	1196.92	1089.42	925.28	772.38	696.09
9-Meknes	776.3	910.34	1078.48	1195.22	1253.85	1266.06	1255.29	1210.62	1110.17	953.03	804.79	730.48
10-Oujda	760.74	896.51	1067.7	1187.76	1249.32	1262.84	1251.44	1204.35	1100.58	940.16	789.72	714.48
11-Kenitra	769.06	903.91	1073.48	1191.77	1251.77	1264.59	1253.52	1207.72	1105.73	947.05	797.78	723.04
12-Beni mellal	806.59	937.16	1099.18	1209.3	1262.1	1271.71	1262.19	1222.35	1128.49	977.93	834.11	761.69
13-Temara	775.62	909.75	1078.02	1194.9	1253.66	1265.92	1255.12	1210.36	1109.76	952.47	804.14	729.79
14-El Jadida	788.8	921.43	1087.07	1201.11	1257.35	1268.49	1258.23	1215.54	1117.79	963.33	816.89	743.35
15-Khouribga	796.07	927.87	1092.04	1204.48	1254.32	1269.84	1259.88	1218.35	1122.18	969.31	823.93	750.85
16-Safi	805.09	935.89	1098.88	1210.52	1264.98	1275.58	1266.08	1225.24	1129.82	977.78	833.11	760.31
17-Mohammedia	780.37	913.96	1081.29	1197.15	1255	1266.86	1256.26	1212.24	1112.66	956.39	808.73	734.67
18-Settat	793.74	925.81	1090.45	1203.4	1258.69	1269.41	1259.36	1217.46	1120.78	967.4	821.68	748.45
19-Khemisset	777.66	911.56	1079.42	1195.87	1254.24	1266.33	1253.61	1211.17	1111.01	954.16	806.11	731.89
20-Taza	769.89	904.71	1074.16	1192.29	1252.11	1264.84	1253.82	1208.18	1106.35	947.81	798.6	723.87
21-Boulemane	786.52	919.47	1085.62	1200.16	1256.82	1268.13	1257.79	1214.77	1116.52	961.54	814.71	740.99
22-Ouarzazate	788.08	919.47	1085.62	1200.16	1256.82	1268.13	1257.79	1214.77	1116.52	961.54	814.71	740.99
23-Figuig	810.98	941.04	1102.15	1211.28	1263.23	1272.46	1263.12	1223.99	1131.11	981.52	838.36	766.22
24-Essaouira	822.4	951.09	1109.83	1216.39	1266.09	1274.33	1265.47	1228.2	1137.86	990.83	849.4	778
25-Larache	750.56	887.43	1060.58	1182.8	1246.25	1260.62	1248.81	1200.15	1094.24	931.7	779.85	704.01
26-Guelmim	869.58	992.43	1140.97	1236.58	1276.72	1280.72	1273.91	1244.56	1165.09	1029	894.96	826.74
27-Taourirt	765.99	901.24	1071.46	1190.42	1250.98	1264.03	1252.85	1206.6	1103.95	944.58	794.82	719.86
28-Ifran	818.6	947.81	1107.39	1214.82	1265.24	1273.78	1264.78	1226.92	1135.74	987.82	845.75	774.06
29-Errachidia	812.14	942.11	1103.65	1213.71	1266.8	1265.42	1267.58	1227.88	1134.03	983.55	839.94	767.58
30-Nador	748.99	886.07	1060.17	1183.92	1249.07	1264.45	1252.65	1202.92	1095.43	931.4	778.74	702.55
31-Assilah	745.13	882.58	1056.77	1180.12	1244.58	1259.4	1247.38	1197.88	1090.84	927.17	774.58	698.42
32-Berrechid	788.59	921.25	1086.93	1201.01	1257.29	1268.45	1258.18	1215.46	1117.66	963.16	816.69	743.14
33-Benslimane	784.03	917.2	1083.8	1198.87	1256.03	1267.58	1257.12	1213.68	1114.89	959.41	812.28	738.44
34-Chefchaouen	751.02	887.9	1061.02	1183.15	1246.5	1260.81	1249.03	1200.46	1094.65	932.15	780.31	704.46
35-EL Hajeb	780.16	913.83	1081.25	1197.17	1255.04	1266.9	1256.3	1212.27	1112.65	956.29	808.54	734.44
36-Ksar el kebir	754.22	890.76	1063.26	1184.72	1247.48	1261.52	1249.87	1201.79	1096.65	934.82	783.41	707.76
37-Tarfaya	886.44	1007.08	1152.42	1245.12	1283.09	1286.38	1280.42	1253.26	1176.65	1043.53	911.7	844.39
38-Inezgane	842.02	968.37	1123.6	1226.85	1273.98	1281.32	1273.4	1238.64	1151.56	1007.86	868.83	798.43
39-Berkane	756	892.29	1064.39	1185.46	1247.91	1261.82	1250.23	1250.23	1097.64	936.22	785.12	785.12
40-Bouznika	778.34	912.16	1079.89	1196.19	1254.43	1266.46	1255.78	1211.44	1111.42	954.72	806.77	732.59
41-Skhirat	777.11	911.07	1079.04	1195.61	1254.08	1266.22	1255.48	1210.95	1110.67	953.7	805.58	731.32
42-Khenifra	794.85	926.84	1091.32	1204.03	1259.09	1269.69	1259.69	1218	1121.56	968.38	822.77	749.57
43-Fkih ben salah	803.25	934.27	1097.03	1207.89	1261.32	1271.2	1261.55	1221.2	1126.61	975.27	830.9	758.23
44-Sidi slimane	768.81	903.75	1073.41	1191.78	1251.8	1264.62	1253.55	1207.74	1105.69	946.91	797.55	722.76
45-Tan-tan	877.38	999.22	1146.63	1241.52	1281.39	1285.52	1279.15	1250.42	1171.63	1036.31	902.97	835.01
46-M'diq	738.66	876.84	1052.89	1178.8	1245.86	1262.1	1249.89	1198.57	1088.93	922.78	768.72	691.94
47-Midelt	799.86	931.22	1094.63	1206.23	1260.34	1270.53	1260.72	1219.81	1124.47	972.43	827.61	754.76
48-Saïdia	752.72	889.36	1062.09	1183.86	1246.91	1261.1	1249.38	1201.04	1095.59	933.49	781.94	706.23
49-Dakhla	963.54	1073.12	1199.11	1271	1290.84	1285.95	1283.46	1270.89	1214.82	1102.73	985.32	924.31
50-Guercif	769.58	904.43	1073.95	1192.15	1252.02	1264.78	1253.74	1208.05	1106.16	947.55	798.3	723.55

Table 7: Monthly solar irradiation (G_{on}) incident on 50 stations of Morocco in (W/m^2).

Hence, its inability to meet the needs of the consumer in terms of domestic hot water production and requirements [66]. The maximum values of (G_{on}) were recorded for April, May, June, July and August for almost the 50 considered stations (Fig. 18). The minimum value of (G_{on}) is 691.94 W/m^2 . In fact, it has been recorded in the city of M'diq during December. While the maximum value of (G_{on}) is 1301.81 W/m^2 recorded in Casablanca during June.

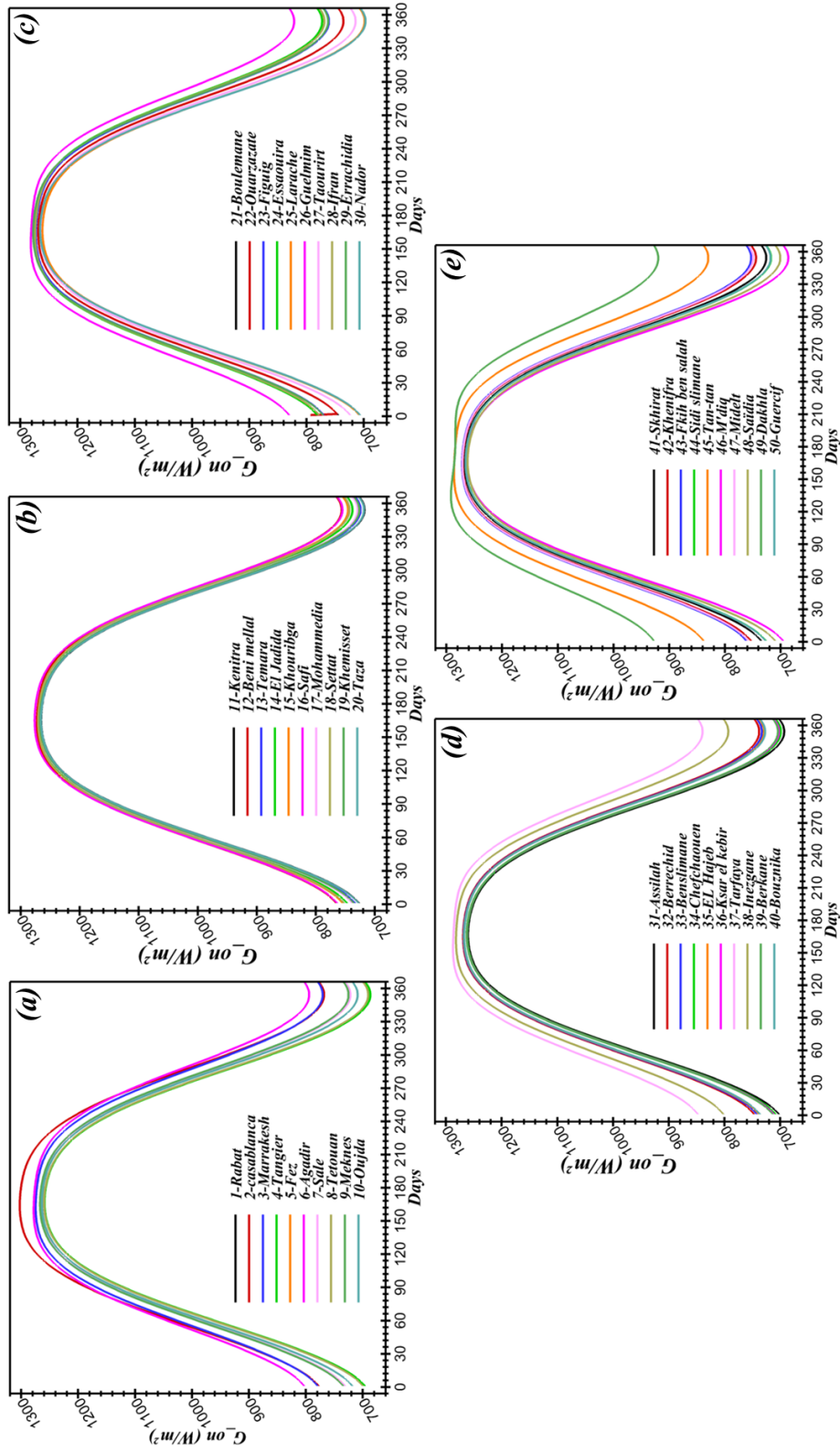


Figure 18: Daily incident solar radiations (G_{on}) for 50 stations in Morocco.

4.6.4. Daily radiation's amount (H_0)

The annual average radiation amount (H_0) is presented in Fig 19. These results were presented on a rosette diagram so that (H_0) incident on the different considered stations could be classified according to a growing trend. Indeed, it has been reported that Tangier and M'diq are two coastal towns receiving a minimum of (H_0), while Tarfaya and Dakhla are two sub-Saharan cities that receive a maximum of (H_0). The average annual radiation's amount (H_0) assessed for 50 stations in Morocco are presented in Tab. 8.

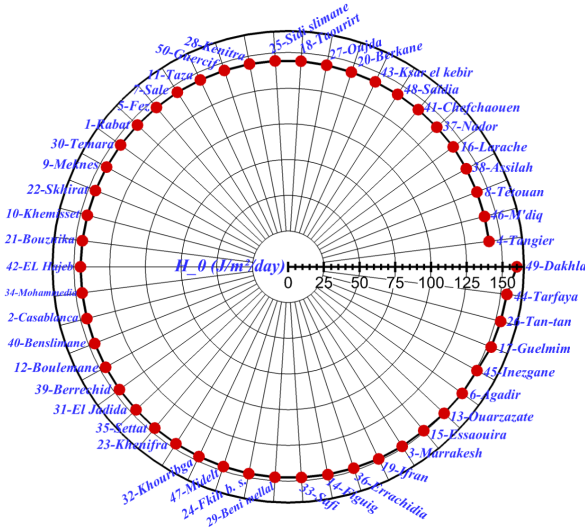


Figure 19: Annual average radiation's amount (H_0).

H_0 (J/m ² /day)									
No.	Stations	min	max	average	No.	Stations	min	max	average
1	Rabat	134.08	152.4	144.81	26	Tan-tan	142.24	161.68	153.62
2	Casablanca	134.75	153.16	145.53	27	Oujda	133.02	151.19	143.66
3	Marrakesh	137.73	156.54	148.74	28	Kenitra	133.69	151.96	144.39
4	Tangier	131.25	149.19	141.75	29	Beni mellal	136.67	155.35	147.61
5	Fez	134.05	152.37	144.78	30	Temara	134.22	152.56	144.96
6	Agadir	139.49	158.55	150.65	31	El Jadida	135.27	153.75	146.09
7	Sale	134.02	152.33	144.74	32	Khouribga	135.85	154.41	146.71
8	Tetouan	131.56	149.54	142.09	33	Safi	136.73	155.41	147.67
9	Meknes	134.27	152.62	145.02	34	Mohammedia	134.6	152.99	145.37
10	Khemisset	134.38	152.74	145.13	35	Settat	135.66	154.2	146.52
11	Taza	133.77	152.05	144.48	36	Errachidia	137.28	156.04	148.27
12	Boulemane	135.1	153.56	145.91	37	Nador	132.23	150.3	142.81
13	Ouarzazate	138.77	157.73	149.88	38	Assilah	131.75	149.75	142.29
14	Figuig	137.02	155.74	147.98	39	Berrechid	135.25	153.73	146.07
15	Essaouira	137.9	156.75	148.94	40	Benslimane	134.89	153.32	145.68
16	Larache	132.19	150.25	142.77	41	Chefchaouen	132.25	150.31	142.82
17	Guelmim	141.5	160.83	152.82	42	EL Hajeb	134.6	152.99	145.36
18	Taourirt	133.46	151.69	144.14	43	Ksar el kebir	132.51	150.61	143.11
19	Ifran	137.62	156.43	148.63	44	Tarfaya	142.91	162.43	154.34
20	Berkane	132.64	150.76	143.25	45	Inezgane	139.59	158.66	150.76
21	Bouznika	134.44	152.81	145.19	46	M'diq	131.39	149.34	141.9
22	Skhirat	134.34	152.69	145.09	47	Midelt	136.15	154.75	147.04
23	Khenifra	135.76	154.31	146.63	48	Saïdia	132.37	150.45	142.96
24	Fkih ben salah	136.43	155.07	147.34	49	Dakhla	148.13	168.38	159.99
25	Sidi slimane	133.69	151.95	144.38	50	Guercif	133.75	152.02	144.45

Table 8: Average annual radiation's amount (H_0) assessed for 50 stations in Morocco.

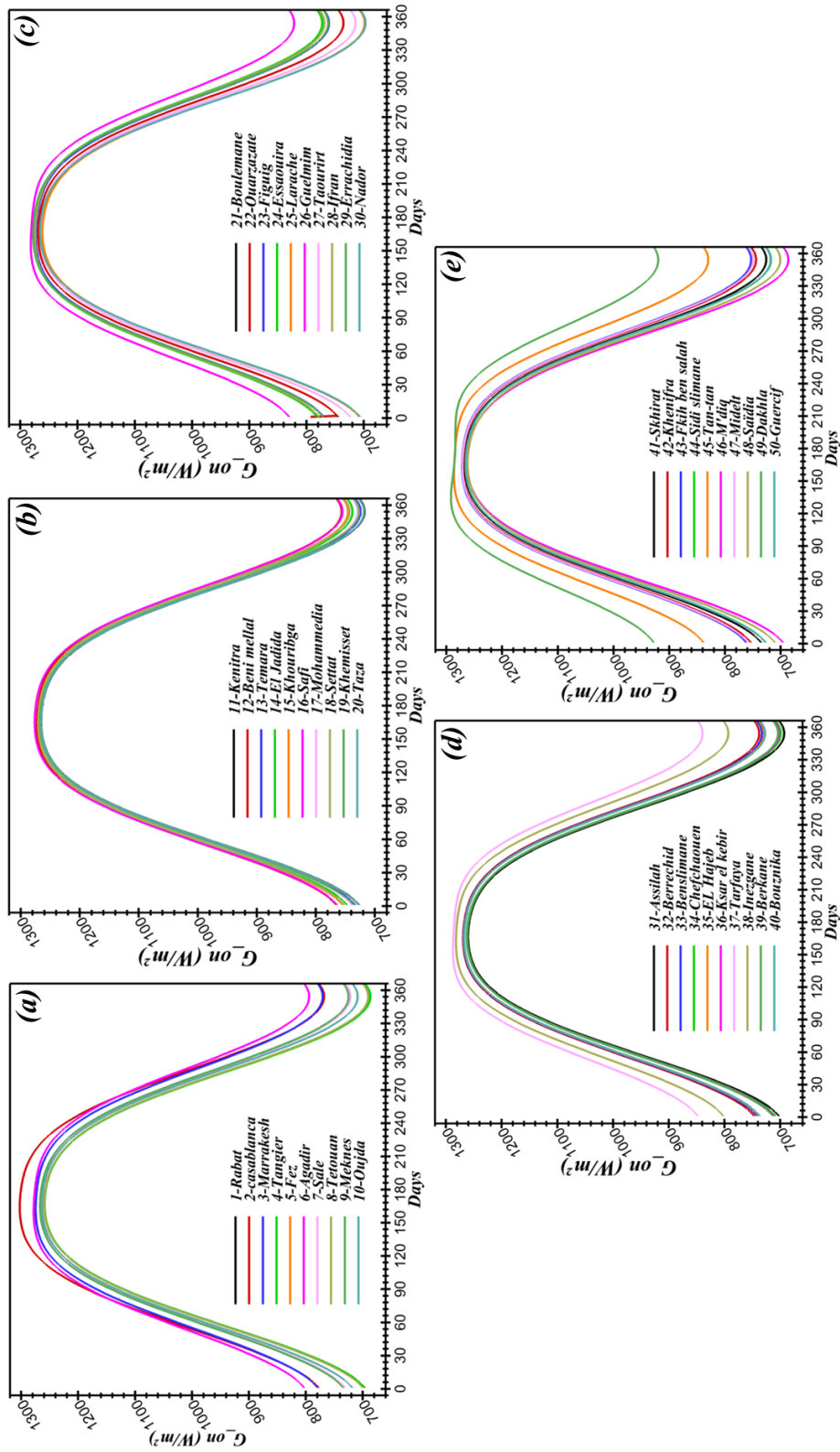


Figure 20: Daily incident solar radiations (H_0) for 50 stations in Morocco.

4.7. Conclusion and policy implications

4.7.1. Conclusions

This chapter suggests a new energy policy that we recommend as strategy intended to be integrated in Morocco. In fact, the motivation that drove us to carry out this work is that *SWH* technologies are not widely known throughout Morocco, even if their energy and thermal efficiency remain better compared to other systems and technologies, which ensure the production of hot water using natural gas or electricity. Hence, this article discusses *SWH* technologies transfer, adjustment and integration as energy policy in Morocco. To begin with, the global market of *SWH* besides to the global overview on their installed capacity in the world has been described. In addition, the world's market growth of thermal collectors has been evaluated, and the general market overview with regard to their total installed capacity in the world has been reported. Moreover, the market situation of *SWH* in Morocco has been described according to socio-economic and energy context, while considering a set of parameters, such as the installation cost and the main local industrial actors, the current state of the market data, the installation cost and the main local industrial actors.

In addition, *SOL'R SHEMSY* project was presented. In fact, it consists of installing *SWH* prototypes in 30 cities of Morocco to assess their performance under different climatic conditions. The measured physical quantities are recorded in a centralized cloud system, which is located in Fez city to carry out the necessary post-treatment, subsequently to conclude on the technological transfer of *SWH* in Morocco.

It is noted that, the amount of minimum, maximum and average values of the daily horizontal radiation have been assessed for 50 stations in Morocco, using Extraterrestrial solar radiation equations, to investigate the feasibility of using solar energy to integrate, adjust and generalize *SWH* technologies in Morocco. The achieved results were helpful, because they provided the available incident solar radiation values that could be used further as a guideline for other studies on installing solar equipment throughout Morocco. Thus, to assist the government to make a decision regarding the installation of more solar power plants such as solar water heaters as energy policy, which aims to promote the energetic efficiency of Morocco.

4.7.2. Policy implications

The following suggested policy recommendations aim to assist the transfer, adjustment and integration of *SWHs* in Morocco. We strongly encourage their implementation, so that the active actors composed of commercial and industrial sectors could become a lever in these technologies. Hence, to achieve multiple socio-economic and environmental benefits.

- Moroccan government should raise awareness of *SWHs* importance comparing them with gas and electric water heaters. Moreover, they have to introduce different source of funding with the support of commercial banks to assist *SWHs* purchase.
- Government have to encourage R&D centers to transform the designed and assessed products in solar energy laboratories into commercial products by providing adequate funds
- Subsidies and loans should be provided to consumers, as it is the case for natural gas in Morocco

- The government should contribute in training human resources interested to work in *SWHs* installations, because the thermal performance of solar collectors depends on several parameters, namely their orientation and tilt angle which must be well adjusted at a particular location by the manpower
- The bulk scale installation of *SWHs* should be encouraged by the government on public and residential buildings
- *SWHs* technologies should be integrated as a national energy policy in the Moroccan environmental strategies to contribute to sustainable development
- Funds and incentives are required to be provided by the government to demonstrate the application of *SHWs*, also to educate the Moroccan consumers, because these hot water production systems are not well known in Morocco
- Foreign investors in *SWHs* should be invited to invest in the Moroccan market and create companies to promote the supply of *SWHs* components
- Students should be encouraged to carry out research projects on renewable energy technologies and more particularly in *SWHs* systems

4.8. *Chapter II: Review on solar thermal stratified storage tanks: insight on stratification studies and efficiency indicators*

4.9. *Introduction*

This chapter is a synthesis of miscellaneous recent experimental and numerical studies carried out on stratified storage tanks for individual and collective solar hot water production applications. In fact, sensitive and latent thermal storage remains very important, because the use of the produced solar thermal energy is not usually instantaneous. Hence, the necessity to properly size and design hot water storage tanks to achieve an increased thermal performance during an applied charging/discharging cycles.

This chapter was written in three parts. The first part provided a sharp insight of the recent studies that have been carried out on the storage tanks connected to solar water heaters (SWHs). Horizontal thermal storage tanks of SWH integrating Evacuated Tube Collectors (ETCs) with heat pipe were also considered in this review. In addition, the experimental approach often used to assess thermal stratified hot water storage tanks was synthesized. Moreover, innovation studies aimed at increasing the thermal efficiency of the storage tanks were presented, either by integrating PCMs or by submerging components such as porous or tilted flat plates inside the tank.

The second part of this chapter presents the equations setting to be established to ensure the physical modeling of thermal stratification within storage tanks. Indeed, two approaches have been detailed: the three-dimensional CFD approach and the two-dimensional formulation based on the introduction of the vorticity stream function equation. Finally yet importantly, the third part of this chapter highlighted a set of thermal performance indicators usually used by the scientific community to evaluate the thermal yield of hot water storage tanks.

Solar water heaters are popular technologies used to harness solar energy, because their investment and maintenance cost are very low [10] (Fig. 21-(a) and (b)). In addition, they are considered as potential contender for enhancing heat transfer and energy gain from solar irradiations [97]. According to Hidalgo et al. [98], several efforts are deployed actually to achieve the balance between domestic hot water consumption of the inhabitants of a building and the solar thermal collector field. Moreover, hot water storage tanks are considered as major sources of energy consumption [29], [99] and miscellaneous researches have shown actually that increasing the thermal stratification level inside the storage tank leads to maximizing its thermal performance, which results in important energy saving [35], [100].

The present review belongs to a Moroccan national project funded by "Institut de Recherche en Energie Solaire et Energies Nouvelles" (*IRESEN*) [6]. Indeed, we assume that important questions raised by the consultants, the research departments and engineers who work on stratified storage tanks and their use in solar domestic hot water production were answered. In fact, this chapter is a synthesis of miscellaneous recent experimental and numerical studies that have been carried out on stratified storage tanks intended to be used in individual [50] and collective solar hot water production applications [66]. The chapter was written in three parts. The first part provided a recent insight regarding the studies that investigated solar storage tanks of different technologies of SWHs such as thermosyphons and forced systems. Also, the auxiliary systems integrated inside the storage tanks to meet the requirements of the produced hot water were presented. Moreover, innovation, experimental and numerical studies performed on stratified storage tanks were also discussed in this first section of the chapter. The second section presents the equation setting to be established to ensure the physical modeling of thermal stratification inside the designed storage

tanks. Indeed, two approaches have been detailed: the three-dimensional CFD approach and the two-dimensional formulation based on the introduction of the vorticity stream function equation. Finally, the third section of this chapter highlighted a set of thermal performance indicators commonly used by the scientific community to assess the thermal efficiency of hot water storage tanks connected to SWHs.

4.10. State of the art

4.10.1. Solar water heaters (SWHs)

A schematic diagram of the thermosyphon SWH is shown in Fig. 21(a). As presented in this figure, the configuration of the storage tank is horizontal and it is integrated above series of ETCs involved in the conversion of solar energy into thermal energy. The water initially stored in the thermosyphon is heated inside ETCs, which are provided with a coating that enhances their solar fraction. The heated water rises by natural convection towards the top section of the horizontal tank, while the cold stored volume fills its bottom zone. Hence, the drawing nozzle of hot water is usually located by thermal designer and engineers at the top of the thermosyphon's tank. Novo et al. [11] released an extensive review of the technologies developed for central solar heating systems using seasonal sensible water storage in large scale basins. In fact, they conducted technical and economic feasibility studies for each system and specifics problems occurred during construction and operation (see Fig. 21(c)).

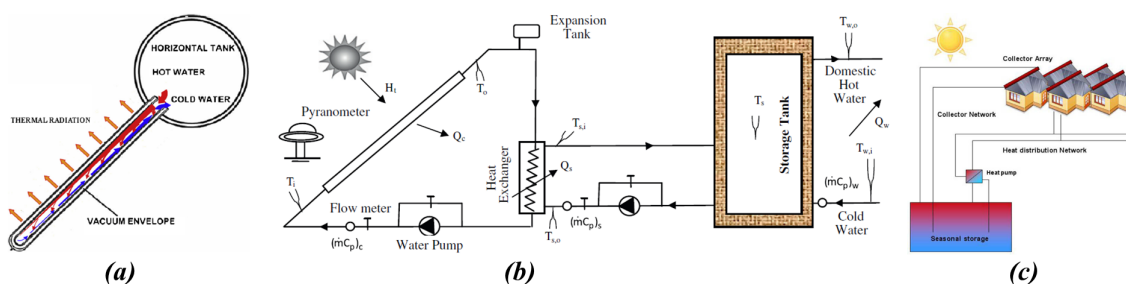


Figure 21: (a)- Scheme of reverse flow in SWHs [9]. (b)- Experimental solar water heating system [10]. (c)- Scheme of CSHPSS [11].

A forced circulation SWH is shown in Fig. 21(b). It consists of two loops, a primary loop also called the solar loop, which is composed of the collector field, the control unit and the recirculation pump. Besides to a secondary loop for storing hot water and which is composed of an external heat exchanger and a vertical storage tank. The control system controls the operation of the pump. Indeed, it triggers when the magnitude of the solar irradiations is higher than a certain threshold and vice versa. The main aim from having this control unit is to enhance the solar fraction of the SWH and to decrease the consumption of the auxiliary system [66]. The stratified tank is filled from the bottom and hot water is loaded from the top. An auxiliary system is submerged in the tank, it can be hydraulic or electric and its operation is triggered when the thermostats integrated in specific positions inside the tank measure temperatures below the set reference temperature defined by the consumer.

Storage tanks with heat pipes are considered as a brand of SWH tanks. Unlike thermosyphons, ETCs are not filled with water but with heat pipes, which are described as essential devices in the solar energy conversion chain. The head of each heat pipe is easily placed into a cylindrical

copper support where heat transfer by conduction occurs. The heat pipe is initially filled with a heat transfer fluid (HTF) that evaporates at low temperatures. The produced vapor releases its latent heat to the cold water initially stored in the horizontal tank to increase its temperature [101]. CFD numerical calculations were already carried out to simulate two-phase closed thermosyphon (TPCT) device, which is integrated in the manifold of ETC collector not connected to the storage part, namely the vertical storage tank. The development of thermal stratification inside this brand of horizontal tanks occurs during a short period, because a temperature in stagnation that is above the saturation temperature of water is reached at each head of the heat pipes and causes the evaporation of the stored water. Indeed, storage tanks with heat pipes are subjected to significant thermo-mechanical loads. Therefore, taken in the name of our Laboratory, detailed thermo-mechanical study has been conducted to optimize the geometry of the horizontal tank and its manufacturing materials, while taking into consideration severe boundary conditions of use [42]. The main implicit aim of this study was to enhance the thermal efficiency of horizontal storage tanks with heat pipes towards enhancing their thermo-mechanical lifespan.

The optimization of a solar ETC using the simulated annealing and three dimensional CFD calculations under the steady state and laminar regime assumptions has been carried out by Ayala et al. [102]. The authors constructed, modeled and assessed 259 different ETC geometries in order to define the parameters that have significant effect on the thermal performance of SWH's collector panel. According to [102], these parameters are the following: the inlet mass flow rate, the tube's diameter and the absorber area of the collector. Hence, they increased the thermal yield of the ETC (26.3%) compared to the initial efficiency of the commercial geometry, by decreasing the absorber area and the length of the tubes. Moreover, Hafez et al. [103] developed a smart adaptive grid model to carry out dynamic simulations of horizontal thermal stratified storage tanks, because according to them, the literature review focuses only on vertical tanks. After validating their suggested model against the experimental data, the authors showed that the number of nodes needed to model the horizontal storage tank affects its thermal yield. In fact, a significant decrease in its efficiency is noticed (32.7%), if the number of the used nodes is not accurate, which is not the case for vertical storage tanks geometries.

The modelling of storage tanks with immersed serpentine heat exchangers has been investigated by Cadafalch et al. [104]. Indeed, the authors developed one-dimensional model based on the multi node approach, corrected by the algorithm of the energy conservative reversion in order to avoid the inverse gradient from occurring. It should be noted that model detailed in [104] helps to predict the thermal efficiency of the vertical tank with internal serpentine. In addition, as discussed by the authors, the one-dimensional developed model can be coupled to other governing equations to handle and describe complex internal fluid phenomena occurring within thermosyphon SWHs. Furthermore, Bataineh et al. [105] carried out unsteady numerical investigations on a sensible heat storage (SHS) unit designed to save energy. This storage unit can be used in various applications such as storing the energy of hot water produced from SWHs systems. Their main idea was to offer an optimal design for the sensible thermal storage tank using natural solid materials. In fact, they used *COMSOL* Multiphysics to assess the effect of three contender materials considered as storage media, to conclude that natural stones are most suitable, because they do not suffer from cracking caused by charging and discharging operating cycles. Moreover, natural stones present higher performances since they can operate under higher temperature ranges.

Monte Carlo method has been used by Rout et al. [106] to conduct a risk analysis of SWHs for east coastal region of India, because their use and diffusion are limited due to their high capital

cost. The main aim behind the analysis carried out by the authors is to check the validity of this perception using the Net Present Value (NPV) tool. In addition, they performed several simulations based on Monte Carlo model, which corresponded to their defined scenarios (current, pessimistic and optimistic) in order to evaluate the risk and viability of solar water heaters. The author's results showed that SWHs are a feasible option that could be transferred and adjusted for east-coastal regions in India.

4.10.2. Storage tank components: heat exchangers and auxiliary systems

In this subsection, two essential devices integrated inside a vertical storage tank are described, namely the heat exchanger and the backup system commonly used to meet the consumer's requirement for insufficient solar energy contribution. The first section presents a brand of heat exchangers connected to the solar loop. While the second part presents the commercialized storage tanks connected to SWHs which are marketed by the leading manufacturers in this solar field.

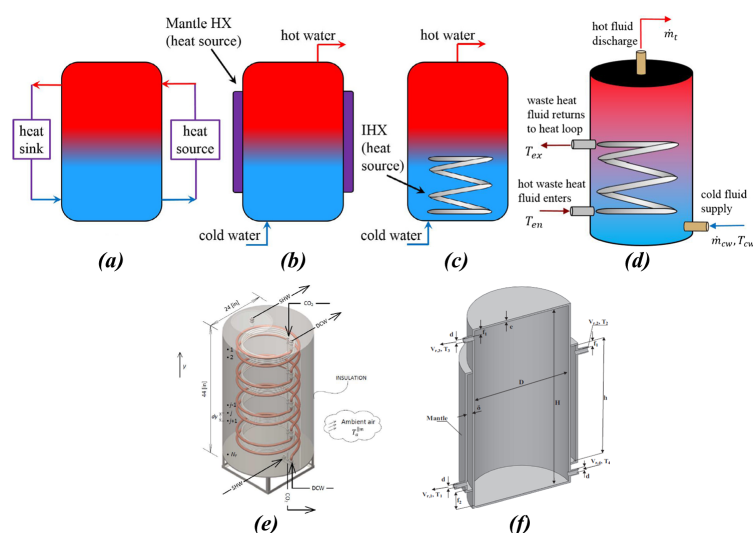


Figure 22: Different configurations of hot water storage tanks. (a)- Storage tank with dual heat sink and heat source mass flow loops [12]. (b)- Storage tank with mantle heat exchanger in contact with the tank's wall [12]. (c)- Storage tank with an internal heat exchanger (IHX) coil [12]. (d)- Schematic of storage tank and IHX [12]. (e)- 3D design of the tank geometry including the heat exchangers [13]. (f)- Schematic cut view of the designed thermal storage tank [14].

Vertical hot water storage tanks equipped with various configurations of thermal heat exchangers are presented in Fig. 22. In fact, a storage tank with dual heat sink and heat source mass flow loops is shown in Fig. 22(a). In addition, a storage tank with mantle heat exchanger in contact with the external wall of the tank is depicted in Fig. 22(b). While Fig. 22(c) shows a storage tank with an internal heat exchanger (IHX) coil previously investigated in [12] (see Fig. 22(d)). Finally, a 3D design of the tank geometry including the heat exchangers is presented in Fig. 22(e) [13]. It should be noted that Arslan et al. [14] assessed the thermal performance of a vertical solar hot water storage tank equipped with a mantle heat exchanger taking into account several discharging operation parameters as presented in Fig. 22(f). The authors were able to preserve pre-established thermal stratification towards controlling Grashof number, which has been calculated through 3D unsteady CFD simulations. Also, they showed that Reynolds number should be kept under certain values to enhance thermal stratification levels.

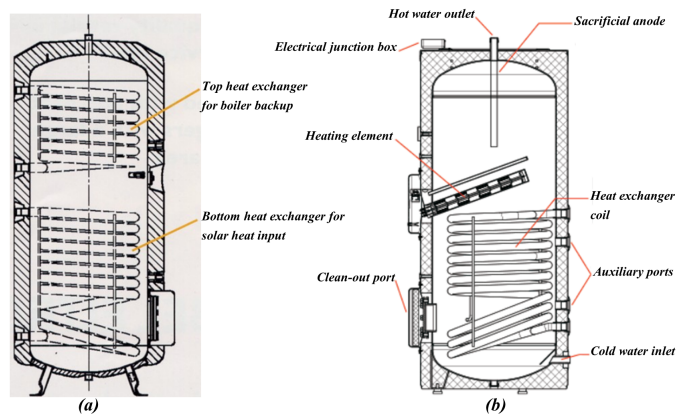


Figure 23: Vertical storage tanks. (a)- with top heat exchanger for boiler backup. (b)- Electrical heating element.

The use of electric back-up is necessary to meet the requirements of the consumer if solar energy supply is insufficient to produce hot water [107]. Fig. 23 shows two vertical storage tanks with different submerged boosters: a top heat exchanger is used as boiler backup for the stratified tank, which is presented in Fig. 23-(a) and an electrical heating device depicted with detailed nomenclature in Fig. 23-(b).

4.10.3. Investigations on stratified storage tanks

4.10.4. Experimental studies

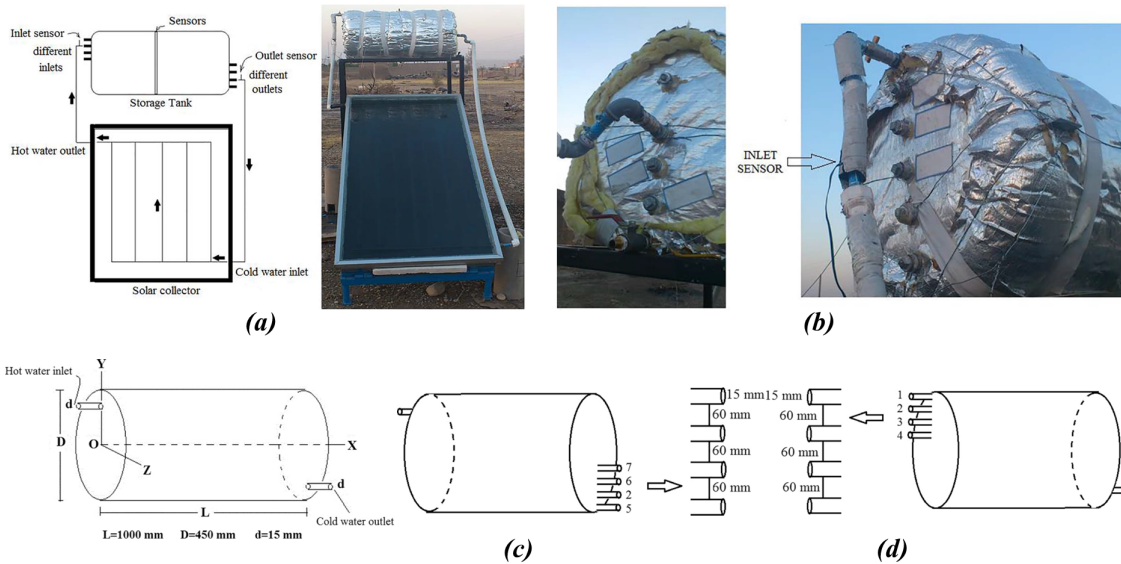


Figure 24: (a)- Thermosyphon SWH in situ and its schematic [15]. (b)- Different cases of hot water inlet to the tank (right) and the cold water outlet (left) [15]. (c)- Different cases of the location of cold fluid at the outlet [15]. (d)- Different cases of the location of the hot water inlet [15].

The charge of a high aspect ratio cavity representing the storage of an integrated collector storage solar water heater (ICSSWH) system has been analysed experimentally by Swiatek et al. [108]. Their major findings were an increased stratification with a shorter submerged plate in the

tank. Also, Heating the storage tank in the middle and inserting a stratification plate help to achieve satisfying stratification.

Another analysis of a conical solar water heater (CSWH) with an attached thermal storage tank, with or without evacuated glass absorber under different operating conditions has been performed by Imtiaz et al. [16] (Fig. 25(a)). With the increase of the inlet flow rate, the maximum efficiency of the CSWH was achieved at a critical flow rate of 6L/min and inversely according to their experimental conclusions. Further, Wang et al. [17] carried out a parametric analysis to evaluate the inlet structure impact on the thermal stratification under different flow rates (1L/min, 2L/min, 3L/min, 4L/min, 5L/min, and 6L/min). The main achieved results related to 6L/min flow rate are the following: first, the Richardson numbers for the three modes were $6,4 \times 10^4$ and 4×10^6 . Second, the fill efficiencies were 0.534, 0.584 and 0.814. Finally the MIX numbers were 0.531, 0.309 and 0.039 (see Fig. 26(a)).

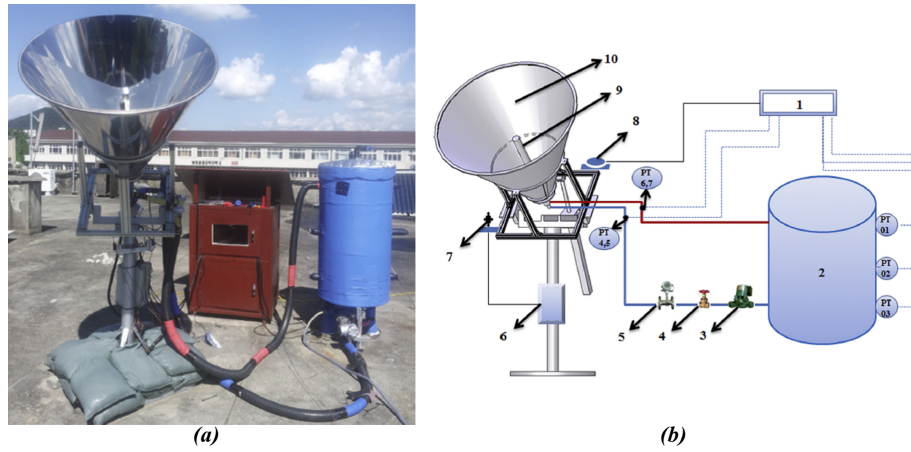


Figure 25: (a)- Experiment setup. (b)- Detail description of conical collector assembly design [16]. 1- data logger, 2- Tank, 3- Pump, 4- Valve, 5- Flow meter, 6- Dual axis tracking system, 7- Sun sensor, 8- Pyranometer, 9- Double tube absorber, 10- Conical concentrator, 11- P/T sensor [16].

The schematic diagram of the experimental apparatus used to measure the temperature inside the tank is presented in Fig. 26(a) [17]. A similar study has been performed by Nash et al. [18]. The schematic of thermocouple locations used in their experimental setting to collect data is shown in Fig. 26(c). Moreover, Murali et al. [19] also worked on the thermal assessment of stratification inside a vertical tank, and Fig. 26(a) presents the location of thermocouples and the design of their implemented diffuser. In addition, fifteen temperature sensors were submerged inside a vertical tank by Dragsted et al. [21] to collect the necessary data in terms of temperature, in order to describe the thermocline evolution while applying charging and discharging cycle. Last but not least, Brown et al. [22] visualized the flow inside a transparent tank by applying a flow rate at the inlet nozzle $\dot{V} = 5.7 \text{ ml/s}$ at an initial temperature $T_i = 49.0^\circ\text{C}$ to evaluate Richardson number found equal to $Ri = 9087.3$.

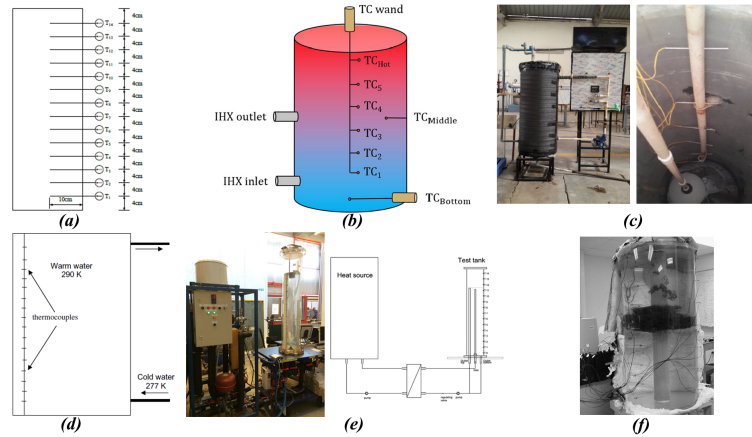


Figure 26: (a)- Schematic diagram of the experimental apparatus [17]. (b)- Schematic of thermocouple locations used in experimental data collection [18]. (c)- Location of Thermocouples and diffuser inside the tank [19]. (d)- Schematic diagram for the experimental setup [20]. (e)- Picture and schematic diagram of test tank made from polymer with an inlet stratifier connected to a heat storage test facility and 15 temperature sensors were located inside de tank [21]. (f)- Flow visualization for an inlet flow nozzle at $T_i = 49.0^\circ\text{C}$ and $\dot{V} = 5.7 \text{ ml/s}$ ($\text{Re} = 500$ and $\text{Ri} = 9087.3$) [22].

Tang et al. [9] investigated through experimental studies the thermal performance of water-in-glass ETC solar water heaters at nights as presented in Fig. 27-(b). They concluded that the reverse flow rate in the SWH is affected by the collector tilt angle and by the collector’s technology (see Fig. 34-(b)).

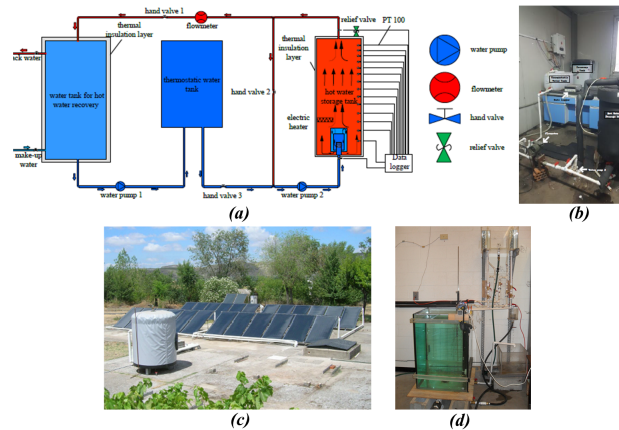


Figure 27: (a)- Schematic view of solar collector connected to the storage tank [9]. (b)- Experimental assessment of thermal storage tank [9]. (c)- Installation in Planta Experimental de Energía Solar, Arganda del Rey (CSIC) [9]. (d)- Experimental setup at the Department of Civil Engineering of the University of Nebraska-Lincoln [23].

4.10.5. Numerical studies

3D unsteady CFD simulations were performed by Wahiba et al. [30] to investigate the effect of several design and operating conditions on the flow behavior, thermal stratification and overall efficiency of a hot water storage tank installed in solar thermal energy systems (Fig. 33-(d)). According to these authors, 3D transient CFD simulations can be used as an effective tool to optimize thermal storage tank parameters at early design stages. Also, new numerical simulation

platform has been developed by Gonzalez et al. [109] to evaluate the commercial viability of thermocline approach, regarding the energetic effectiveness and structural reliability. Thanks to their investigations, they showed that a better storage performance and structural strength could be achieved together with the lowest temperature difference, since their developed code was validated first against the available solar one thermocline case study. Recently, Romanchenko et al. [110] applied techno-economic optimization model to the district heating system located in Goteborg, Sweden, to compare the storage efficiency using hot water tank and the thermal inertia of buildings. The general conclusion based on their findings is that compared to the thermal inertia of buildings, the hot water tank stores more than twice as much heat over the considered year. Hence lower energy losses were recorded. In addition, the cost of their system has decreased by 2% when the hot water tank is added to the district heating system.

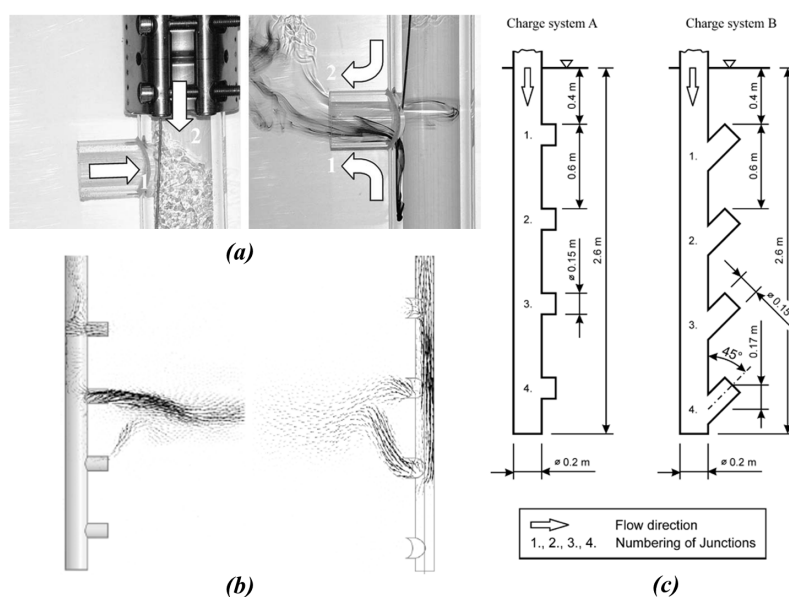


Figure 28: (a)- Development of sucking effects in the fluid mechanical charge systems (Sucking of warmer water) [24]. (b)- Velocity field in the charge system A and the storage tank computed with CFD [24]. (c)- Examined charge designs [24].

Dehghan et al. [111] investigated numerically the dynamic thermal efficiency behavior of a domestic solar heater water storage tank (DSWHS) equipped with a mantle heat exchanger operating in the discharging/charging mode. They found that the pre-established thermal stratification is well conserved during the discharging operating mode for higher values of Grashof number (Gr). Moreover, the tank inflow Reynolds number and the mass flow rates applied at the inlet nozzle diameter should be kept below certain values to provide water with a proper temperature for consumption.

4.10.6. Overwhelming PCMs inside storage tanks

Recently, several studies were conducted to investigate the potential contribution of submerging PCMs within hot water storage tanks for various applications, such as individual/collective hot water production [50] and [66], seasonal storage [11] (Fig. 21(c)) or latent heating of swimming pools to keep their temperature at a comfort ranges during the cold periods of the year, especially

the winter season [12]. It should be noted that, Navarro et al. [25] assessed the performance of a versatile latent heat storage tank using PCMs operating in a temperature range from -10°C to 100°C throughout experimental investigations (Fig. 29(a)). Their studies were carried out in two parts. In fact, the first study is explaining the recommended criteria that should be used to design with accuracy the thermal storage tank. While their second study, presented an experimental assessment that aims to define a set of performance indicators to evaluate the thermal efficiency, such as the enthalpy–temperature curve, the density and specific heat measured for the considered paraffin, besides to the analysis of the vertical stratification evolution inside the tank integrating the PCM. Moreover, the process of integrating PCMs inside several storage tank configurations such as Sodium, Potassium and Lithium salts, besides to the evaluation of the heat transfer fluid (HTF) effect and the calculation of the necessary time required to ensure the charging of the tank have been modeled and investigated by Dadollahi et al. [112]. Indeed, their results showed that the volume of the PCMs is the main factor that affects the charging time of the tank and the velocity field of the HTF.

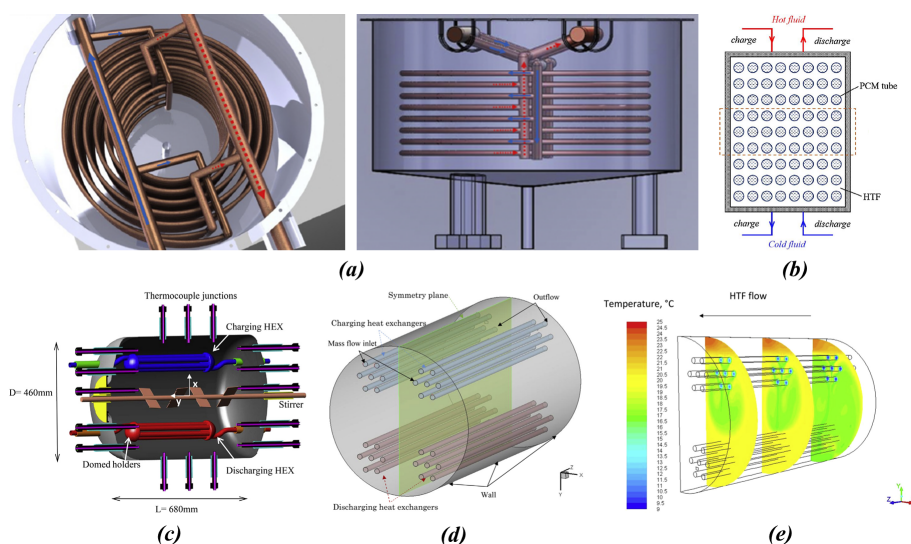


Figure 29: (a)- Upper and front views of the tank. [25]. (b)- Schematic representation of the heat transfer process between the HTF inside the storage tank and the PCM [12]. (c)- 3D cross section view of the PCM storage tank [26]. (d)- 3D representation of the computational field [26]. (e)- Temperature distribution along different cross sections of the tank for a HTF flow rate of 11 g/s after 2 h of charging operating mode [26].

Lu et al. [113] studied the performance of a thermal storage tank integrating PCMs intended to store and release energy to meet the requirements of the hot water loaded by the consumer. Their results showed that different melting point temperatures of the used PCMs could decrease the storing time of heating. Moreover, they concluded that the released heat becomes more important by increasing the PCMs contents which is obvious achievement [114]. According to [115], PCMs could be a good contender to the electric heating devices used in solar water heaters and could contribute in reducing their overall energy bill. Furthermore, three dimensional CFD model has been developed and validated by Allouche et al. [26] to simulate the heat transfer in PCM tubes located inside 100 liters horizontal cylindrical tank (Fig. 29(e)). They defined several performance indicators such as the bulk temperature, the heat transfer rate and the energy recovered from the PCMs. Their results showed that 3D numerical simulations could predict with accuracy the heat

transfer within the storage tank, because for example the relative error between the PCM bulk temperatures assessed numerically and measured experimentally is within the margin of 5%. An experimental performance analysis of a solar water heater using Latent Thermal Energy storage (LTES) in a stratified tank with two different inlet locations has been investigated by Murali et al. [19], to show that stratification is enhanced in both continuous and batch wise discharging because of the use of a diffuser integrated at the bottom inlet nozzle of the tank. Fig. 30(a) presents the schematic illustration of the experimental setup and the HTF path in the heat charging and discharging process investigated by Meng et al. [27]. While Fig. 30(b) shows the evolution of their achieved liquid fraction at $t=2500s$.

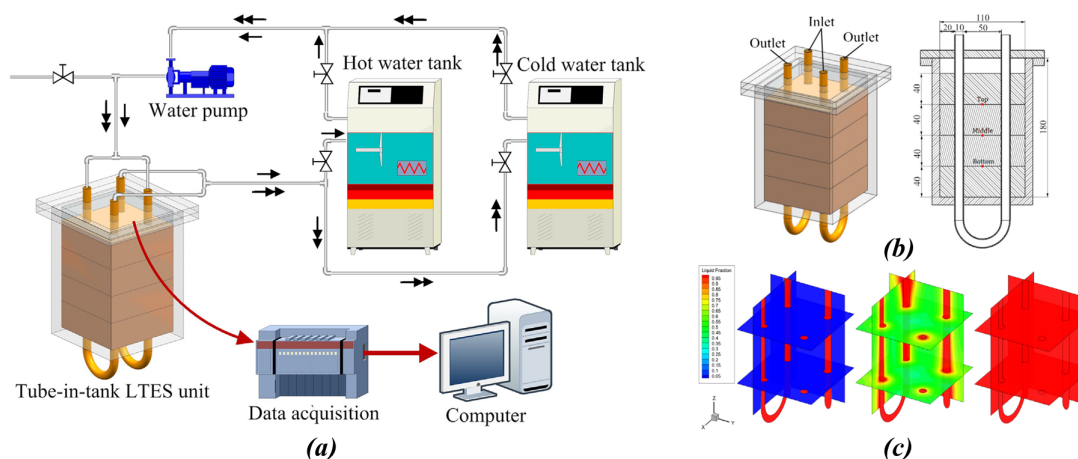


Figure 30: (a)- Schematic illustration of the experimental setup and the HTF path in the heat charging and discharging process [27]. (b)- Schematic illustration of the LTES unit [27]. (c)- Liquid fraction distributions on the cross sections of the LTES unit at different recorded instants during the heat charging process (inlet temperature: $80^{\circ}C$, inlet flow velocity: 0.1 m/s). Liquid fraction distribution at $t= 2500\text{ s}$ [27].

Recently, Tarhan et al. [116] designed a new trapezoidal storage tank of solar water heaters to evaluate its thermal efficiency in two considered cases, namely with and without the integration of PCMs. Indeed, they proposed two designs of their trapezoidal built in storage solar water heater. In the first design, myristic acid was filled into the PCM storage tank, while in the second design, auric acid was filled into the PCM storage tank. The main conclusions drawn from their work are presented as follow: the effect of lauric acid storage unit in stabilizing the temperature of water during the day, besides to the effect of myristic acid in decreasing thermal heat losses that occur at night. Further, Li et al. [12] proposed an optimal design for PCMs intended to be integrated inside thermal storage tank to meet the heating requirements of an open-air swimming pool during the winter season (Fig. 29(b)). In fact, they have developed a simulation platform using both of *TRNSYS* and *Matlab* to design the accurate volume of the PCM storage tank taking into consideration the effect of several decision variables. In addition, their investigations led to an efficient reduction of the PCM storage tank volume without decreasing its storing capacity. Last but not least, Abdelsalam et al. [117] conducted two dimensional CFD simulations using *ANSYS CFX 14.0* code to assess the thermal performances of a hybrid thermal energy storage tank containing coil heat exchanger with submerged PCMs. Their simulation results showed that the heat transfer characteristics were not affected by the gap spacing set between the encapsulated PCMs. Moreover, the fact of increasing the PCM volume fraction beyond 0.15 did not affect the

charging rate of water.

4.10.7. Thermal stratification assessment

The thermal stratification quality in the storage tank is affecting the thermal efficiency of solar water heaters. As reported in [24] if a better thermal stratification is generated and maintained during the dynamic operation cycles of solar storage tanks, the yield of the solar system could be higher (Fig. 28(c)).

Using water to store thermal energy is one of the useful ways in the field of solar energy [17], and it remains the main reason behind the released works on thermal stratification. In fact, Ievers et al. [29] performed CFD three-dimensional numerical simulations using *Fluent* program and exergy analyses, in order to analyze the effects of seven tank geometries and the applied realistic operating conditions on the evolution of the thermal stratification. The major findings drawn from their parametric studies showed that the fact of increasing the aspect ratio of the tank (height/diameter), decreasing the initial values of the flow rates at the inlet/outlet and moving their positions to the outer extremities of the tank help to achieve increased levels of thermal stratification. Further, one-dimensional numerical code, which is based on the finite-difference method and semi-implicit model has been developed by Ghaddar et al. [118] to simulate the liquid stratification behavior within thermal storage tanks. Besides, they modified their suggested model to take into consideration the effect of the turbulence mixing that occurs at the flow inlet of the storage tank due to the diffuser design. It has to be noted that, their complete model has been validated against the experimental results, which allow its use in different applications such as solar energy storage [42], [21] and air-conditioning systems [20].

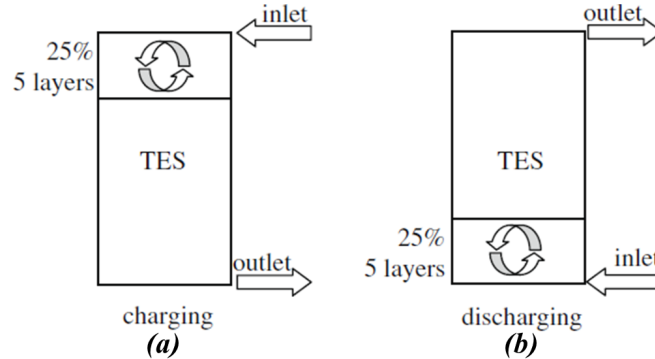


Figure 31: (a)- Charging experiments with full mixing at the top [28]. (b)- Discharging experiments with full mixing at the bottom [28].

Brown et al. [22] suggested the integration of a porous manifold within a vertical 315 liters liquid storage tank to enhance its thermal stratification (Fig. 26(f)). In fact, the aspect ratio of their assessed tank was 4 and efficient energy savings were achieved for a low Richardson number 0.615. It was concluded from their numerical investigations that the porous manifold is decreasing the induced shear mixing between the stored hot water and cold loaded water. Hence, maintaining good stratification. Haller et al. [28] reviewed the methods used to determine the stratification efficiency of several thermal energy storage processes such as the rate of entropy production (Figs. 31 and 32). Steinert et al. [119] developed one-dimensional heat transport equation to describe the transient behavior that occurs during the charge and discharge cycles inside thermal stratified

storage tanks. Indeed, they have achieved accurate results using their code implemented in *Matlab* with much less calculation effort compared to CFD simulations.

Arslan et al. [14] assessed the thermal performance of a vertical solar hot water storage tank equipped with an external mantle heat exchanger installed in a solar domestic hot water (SDHW) system throughout three-dimensional unsteady CFD simulations (Fig. 22(f)). According to their achieved results, thermal stratification is preserved during the discharging cycles for higher values of Grashof number and for Reynolds number below certain limits, especially during hot water loading periods. Moreover, Erdemir et al. [31] placed obstacles in four different distances from the tank bottom to improve its thermal stratification (Fig. 34(b)). According to their established methodology, the analysis of the thermal efficiency was based on several performance indicators such as temperature distribution contours, Richardson number and the temperature of the consumed loaded water.

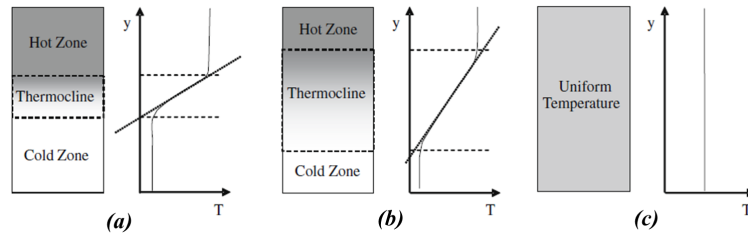


Figure 32: (a)- Different stratification's degrees inside the vertical storage tank with the same amount of the stored energy: Highly stratified, (b)- moderately stratified (c)- unstratified storage (fully mixed) [28].

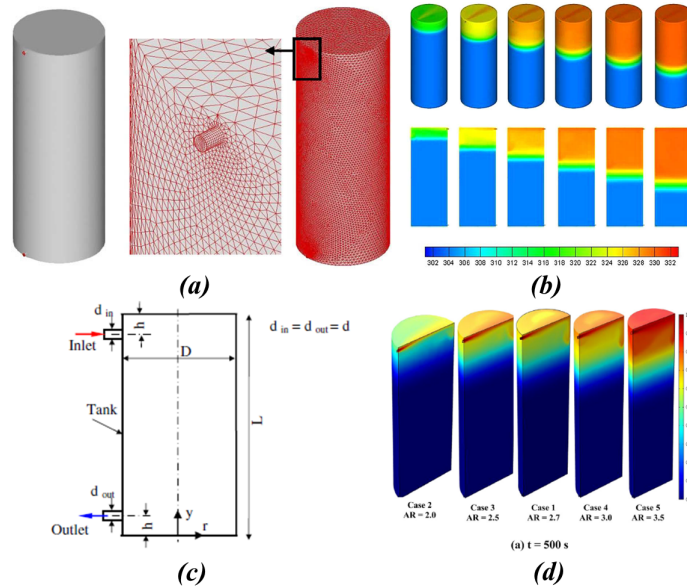


Figure 33: (a)- The physical system and the corresponding numerical model with mesh distribution [29]. (b)- Evolution of the temperature contours of the 3D model from 250 s to 2750 s with 500 s increment (from left to right): top row (three-dimensional), and bottom row (sectioned two-dimensional) [29] [29]. (c)- Schematic view of the center plane of the thermal storage tank design. (d)- Aspect ratio effect at different diameters on the temperature contours ($L = 1194$ mm at $t = 500$ s) [30].

Assari et al. [15] carried out experimental and numerical studies to evaluate the effect of varying the outlet and inlet location nozzles of the fluid in the horizontal cylindrical storage tank to optimize the dynamic process of thermal stratification (Fig. 24(d)). They found that an accurate location of the hot water inlet nozzle results in an improved thermal storage tank stratification, while an appropriate location for the cold water nozzle leads to better collector efficiency. In addition, the same author performed several experimental studies aimed to destruct the thermal stratification of a storage tank. Further, they also evaluated the solar collector performance. It has to be noted that their experimental results were in good agreement with the theoretical results, as it has been reported in the present detailed study [20].

A new method intended to calculate the stratification efficiency of thermal energy storage tanks without taking into consideration storage heat losses has been developed by Haller et al. [121] based on the second law of thermodynamics. They showed that entropy balances could have a great potential to compare the stratification efficiencies for storage components, namely stratification devices. Furthermore, Jordan et al. [122] investigated the effect of cold water inlet on the thermal stratification in small solar domestic storage marketed tanks. In fact, they compared two different marketed inlet designs to increase the solar fraction [123] of the solar water heater, which is related to the decrease of the booster consumption. Last but not least, numerical and experimental studies were carried out on a horizontal cylindrical tank storing water, heated with solar energy to assess the behavior of thermal stratification [124]. They investigated four cases where the cold water injection nozzle has been maintained at the tank's bottom, to conclude finally using Turbulent Mixing Model and Displacement Mixing Model that the inlet divergent conical tube could enhance thermal stratification.

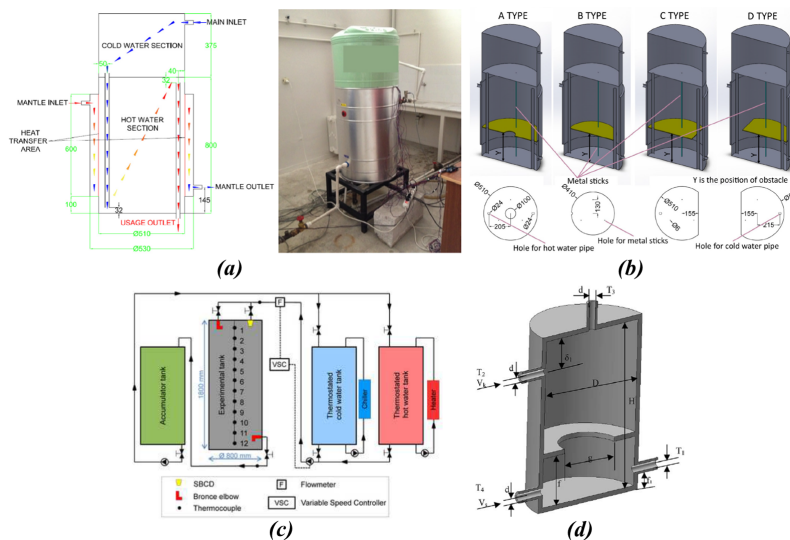


Figure 34: (a)- Schematic view of the vertical mantled hot water tank. (b)- Obstacle location inside the storage tank [31]. (c)- Schematic diagram of the SWH [32]. (d)- Mechanical design for hot water thermal storage tank [33].

In a recent comparison study, Mari et al. [32] compared between the effect of two water inlet devices during a thermal charge process, namely a sintered bronze conical diffuser (SBCD) and a conventional inlet elbow (E) (see Fig. 34(c)). They presented several results, which showed that water stratification is increased during thermal charging with both low and high flows if SBCD

diffuser is used. Moreover, the dimensionless height of the midpoint of the thermocline can be used to quantify the volume of water affected by the mixing produced because of the turbulence. Furthermore, The effect of different obstacles on thermal stratification in a cylindrical hot water tank has been investigated by several numerical analysis carried out by Altuntop et al. [33] (Fig. 34(d)). In fact, the authors show that the fact of placing obstacle in the tank could provide better thermal stratification compared to the no obstacle case. Besides, obstacles having gap in the center have better thermal stratification than those having gap near the tank wall. According to a recent study carried out by Kursun [38], enhancing thermal stratification in hot water tanks helps to increase the efficiency of SWHs. His study aimed to enhance thermal stratification by conducting parametric studies on the insulation part of a vertical storage tank. In fact, the author suggested two insulation designs, namely the truncated cone and the pyramid insulation geometry. Subsequently, they investigated the effect of several parameters on the tank's yield, such as the tank aspect ratio (D/H), the ratio of the bottom insulation diameter to the top insulation diameter (d_i/D_i) and finally the ratio of the bottom insulation thickness to the top insulation thickness (h_b/h_t). The most important result he has achieved is the enhancement of the generated thermal stratification mainly by reducing D/H , d_i/D_i and h_b/h_t ratios.

4.11. Mathematical modeling of thermal stratification

4.11.1. Three dimensional CFD approach

In this review's second section, two numerical approaches commonly used by thermal engineers and researchers were presented. In fact, numerical simulations help to predict with high accuracy the modeling of the fluid flow, energy transfer and thermal stratification development inside the storage tank. Two approaches have been detailed: the three-dimensional CFD approach (Fig. 35(a)) and the two-dimensional formulation based on the introduction of the vorticity stream function equation (Fig. 35(b)). Fig. 35(a) shows a typical configuration of a vertical storage tank equipped with a coil heat exchanger and two hot and cold water nozzles located respectively at the top and bottom levels.

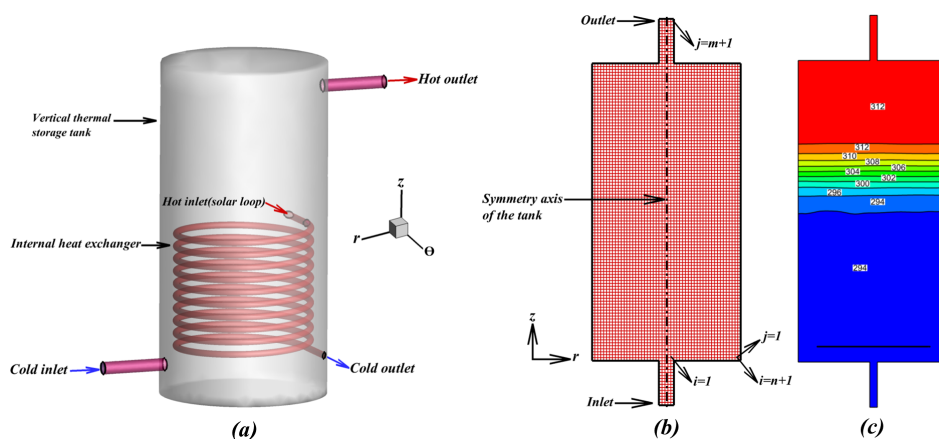


Figure 35: (a)- Vertical thermal storage tank with internal heat exchanger located at the bottom. (b)- The grid applied for the calculations [34].(c)- The effect of injecting cold water at 20°C on the evolution of the static temperature contours at $t=120s$ [35].

This typical 3D configuration of the tank can be simulated numerically using CFD calculations. The stratified tank stores initially hot water and charging/discharging cycles can be simulated after

generating the mesh grid (see Fig. 33(a)) and applying the accurate boundary conditions (see Fig. 33(c)) to highlight the evolution of thermal stratification phenomenon. Consequently, the necessary amendments on the design of the tank or the flow inputs such as the inlet velocity and temperature can be performed to increase the thermal efficiency of the designed tank.

The main advantage of these numerical methods is that it affords additional information that cannot be achieved by performing experimental investigations, which prove to be sometimes very expensive for the assembly [125]. The numerical results that could be promoted are the following: plotting the evolution of the temperature map inside the tank (Figs. 29(e) and 33(b)), to locate and depict hot, cold and recirculation stream function zones Fig. 28(b) to improve. Further, to determine the thickness of the thermocline (Fig. 35(c)). In addition, to assess the evolution of the liquid fraction of PCMs submerged in the tank, if latent heat energy storage is used to enhance the thermal efficiency of the considered vicinity (Fig. 30(c)). Finally, to calculate several performance indicators detailed further in the third section of this chapter (Fig. 39).

4.11.2. Continuity equation

The continuity equation expresses the conservation of the charged water's mass during a consumption cycle applied by the consumer. It is expressed in Eq. 6 according to the coordinate system presented in Fig. 35(a) [126].

$$\frac{\partial \rho}{\partial t} + \rho \left[\frac{1}{r} \frac{\partial(rV_r)}{\partial r} \right] + \frac{1}{r} \frac{\partial V_\theta}{\partial \theta} + \frac{\partial V_z}{\partial z} = 0 \quad (6)$$

4.11.3. Momentum conservation equations

The resolution of the momentum equation gives access to the velocity components of the fluid flow inside the storage tank (V_r, V_θ and V_z) and the evolution of the pressure field. It is expressed on r axis as shown in Eq. 7 [33].

$$\begin{aligned} \rho \frac{\partial V_r}{\partial t} + \frac{\rho}{r} \frac{\partial(r\rho V_r V_r)}{\partial r} + \frac{\rho}{r} \frac{\partial(V_\theta V_r)}{\partial \theta} + \rho \frac{\partial(V_z V_r)}{\partial z} = -\frac{\partial P}{\partial r} + \mu \left[\frac{\partial}{\partial r} \left(\frac{1}{r} \frac{\partial(rV_r)}{\partial r} \right) \right] \\ + \mu \left[\frac{1}{r^2} \frac{\partial^2 V_r}{\partial \theta^2} + \frac{\partial^2 V_r}{\partial z^2} \right] + \mu \left[-\frac{2}{r^2} \frac{\partial V_\theta}{\partial \theta} \right] + \frac{\rho V_\theta^2}{r} + \rho g_r \beta \Delta T \end{aligned} \quad (7)$$

Momentum equation expressed on θ axis is expressed in Eq. 8 [14].

$$\begin{aligned} \rho \frac{\partial V_\theta}{\partial t} + \frac{\rho}{r} \frac{\partial(r\rho V_r V_\theta)}{\partial r} + \frac{\rho}{r} \frac{\partial(V_\theta V_\theta)}{\partial \theta} + \rho \frac{\partial(V_z V_\theta)}{\partial z} = -\frac{1}{r} \frac{\partial P}{\partial \theta} + \mu \left[\frac{\partial}{\partial r} \left(\frac{1}{r} \frac{\partial(rV_\theta)}{\partial r} \right) \right] \\ + \mu \left(\frac{1}{r^2} \frac{\partial^2 V_\theta}{\partial \theta^2} + \frac{\partial^2 V_\theta}{\partial z^2} \right) + \mu \left(\frac{2}{r^2} \frac{\partial V_r}{\partial \theta} \right) - \frac{\rho V_r V_\theta}{r} + \rho g_\theta \beta \Delta T \end{aligned} \quad (8)$$

Momentum equation expressed on z axis is expressed in Eq. 9 [31].

$$\begin{aligned} \rho \frac{\partial V_z}{\partial t} + \frac{\rho}{r} \frac{\partial(r\rho V_r V_z)}{\partial r} + \frac{\rho}{r} \frac{\partial(V_\theta V_z)}{\partial \theta} + \rho \frac{\partial(V_z V_z)}{\partial z} = -\frac{\partial P}{\partial z} + \mu \left[\frac{\partial}{\partial r} \left(\frac{1}{r} \frac{\partial(rV_z)}{\partial r} \right) \right] \\ + \mu \left(\frac{1}{r^2} \frac{\partial^2 V_z}{\partial \theta^2} + \frac{\partial^2 V_z}{\partial z^2} \right) + \rho g_z \beta \Delta T \end{aligned} \quad (9)$$

4.11.4. Heat transport equation

Heat transport equation is expressed in Eq. [10] [127]. In fact, the resolution of this equation allows determining the unsteady evolution of the temperature field inside the storage tank during a charging/discharging cycle.

$$\rho C_p \frac{\partial T}{\partial t} + \rho C_p \vec{u} \cdot \nabla T = \nabla \cdot (\lambda \nabla T) \quad (10)$$

Currently, several CFD softwares are used by engineering services companies, design offices and research and development centers to solve numerically Navier-Stokes equations previously presented in this section. For instance, Ansys Fluent and Comsol Multiphysics [128] softwares, besides to Ansys CFX calculation code [129], which are widely used to achieve this purpose. It should be noted that different numerical resolution approaches are generally used, notably Reynolds Averaged Navier-Stokes (RANS) or Unsteady Reynolds Averaged Navier-Stokes (URANS) approaches by the CFD softwares. In fact, they can simulate and predict the static/dynamic thermal behavior of thermal storage tanks connected to SWHs, in order to help decision-making and the selection of accurate technological solutions that aim to provide optimal designs of the tanks.

Gomez et al. [36] proposed a CFD method to solve numerically the Navier-Stokes equations (Eqs. [6-9]) that allow the calculation of the fluid momentum and the energy transport which occurs inside the hot water storage tank of 150 liters, where the corrugated coil is submerged (Fig. [36]). The authors have applied the Boussinesq approximation Eq. [7] to solve the fluid momentum that occur by natural convection. This approximation has been used to decrease and save the computational time in comparison with other numerical methods that consider the density of the used fluid variable, consequently the need to use very short time step to capture the flow structure besides to the heat transfer rate. It was concluded from the parametric studies performed by Gomez et al. [36] that a good agreement could be found between the CFD results and the experimental measurements, while carrying out the unsteady tests of heating and cooling water stored in the tank.

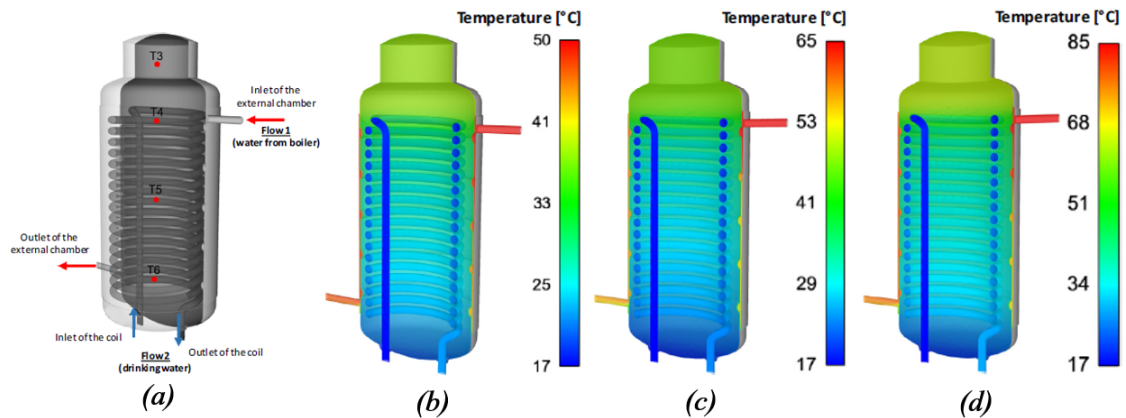


Figure 36: (a)- Vertical storage tank with submerged heat exchanger designed by Gomez et al. [36]. (b)- Temperature contours for CM01, (c)- Temperature contours for CM02 and (d)- Temperature contours for CM03 [36].

Experimental measurement based on Particle Image Velocimetry (PIV) technique and CFD simulations have been carried out by Kumar et al. [130] to investigate the possibility to suppress thermal stratification in a water pool with an immersed heat exchanger. Kumar et al. [130]

suggested the use of three shrouds to suppress thermal stratification in the pool, which is not appreciated by the users. In fact, they were able to show through their CFD investigations that the pool was divided into four compartments enhancing the mixing rate. Hence, the temperature of water near the top area of the pool significantly decreased. Moreover, Kursun et al. [131] assessed the angular position effect (α) comprised between 0-60° of a rectangular hot water tank and its aspect ratio (D/H) with a range of 0.5-1 on the possibility to enhance the thermal stratification capacity of the tank. The main conclusion drawn by the authors is that increasing the tilt angle of the tank from 0° to 60° would increase the thermal stratification of tank, while the decrease of the aspect ratios has a negligible effect on it.

According to Esteve et al. [132], thermal energy storage has become a technology mostly used in the building sector besides to the industries to preserve thermal energy. Hence, the stored energy would be used later. In light of these facts, Esteve et al. [132] suggested the integration of simple inlet devices in storage tanks, because they improve its thermal stratification. These authors carried out three-dimensional CFD simulations, which they have firstly validated against the experimental results, to simulate the evolution of thermal stratification during the charging cycle of the storage tank. The numerical investigations of this research team showed that a simple modification could be performed on the inlet flowrate device to optimize the system efficiency, and the major decision to be taken, which is driven from the numerical simulations, is to use a sintered bronze conical diffuser instead of a conventional bronze elbow inlet, because it enhances thermal stratification.

4.11.5. Two dimensional formulation based on vorticity stream function equation

The three dimensional CFD simulation of laminar/turbulent flows coupled with conduction and convection heat transfer modes that occur inside the stratified storages tanks are expensive in terms of the required computational time and need specific equipment to perform the calculations such as workstations [126] and [133]. In fact, generating an accurate mesh grid and defining a time step that help to capture and reproduce the different physical phenomena related to thermal stratification using 3D numerical simulations increase the physical time of the simulations. Therefore, 3D CFD calculations may be a disadvantage to the scientific community involved in the enhancement of the design of stratified storage tanks. An interesting alternative to 3D numerical simulations is 2D numerical modeling that could simplify the physical phenomena of thermal stratification within storage tanks, but keeping an accurate and acceptable reliability limit. The two dimensional study carried out by Zachar et al. [34] showed that the equation setting presented in this subsection can be used to simulate the development of thermal stratification in stratified tanks, because the results from this two-dimensional modeling based on the vorticity stream function equation showed a good agreement compared to the numerical results achieved from CFX commercial code and the experimental results described in the study of these authors.

4.11.6. Continuity equation

Continuity equation is expressed in the polar coordinates as shown in Eq. [11] [34] according to coordinate system presented in Fig. [35]-(b).

$$\frac{\partial U}{\partial r} + \frac{\partial V}{\partial z} + \frac{U}{r} = 0 \quad (11)$$

4.11.7. Momentum equation

Momentum equation is projected on r axis as mentioned in Eq. [12] [34].

$$\frac{\partial U}{\partial t} + U \frac{\partial U}{\partial r} + V \frac{\partial U}{\partial z} = \frac{1}{\rho} f_r - \frac{1}{\rho} \frac{\partial P}{\partial r} + \nu \left(\frac{\partial^2 U}{\partial r^2} + \frac{1}{r} \frac{\partial U}{\partial r} - \frac{U}{r^2} + \frac{\partial^2 U}{\partial z^2} \right) \quad (12)$$

Momentum equation is projected on z axis as presented in Eq. [13] [34].

$$\frac{\partial V}{\partial t} + U \frac{\partial V}{\partial r} + V \frac{\partial V}{\partial z} = \frac{1}{\rho} f_z - \frac{1}{\rho} \frac{\partial P}{\partial z} + \nu \left(\frac{\partial^2 V}{\partial r^2} + \frac{1}{r} \frac{\partial V}{\partial r} + \frac{\partial^2 V}{\partial z^2} \right) \quad (13)$$

4.11.8. Heat transport equation

Eq. [14] refers to heat transport equation the allows the calculation of the temperature field [7].

$$\frac{\partial T}{\partial t} + U \frac{\partial T}{\partial r} + V \frac{\partial T}{\partial z} = \frac{\lambda}{\rho C_p} \left(\frac{\partial^2 T}{\partial r^2} + \frac{1}{r} \frac{\partial T}{\partial r} + \frac{\partial^2 T}{\partial z^2} \right) \quad (14)$$

4.11.9. Vorticity stream function formulation of the momentum equation

The vorticity equation is derived from Eqs. [11] and [12]. The first equation is differentiated with respect to z and the second one is differentiated with respect to r , also the second equation is subtracted from the first. This notation (Eq. [15]) has been introduced for the vorticity in order to simplify the equation of vorticity transport [34].

$$\omega = \frac{\partial U}{\partial z} - \frac{\partial V}{\partial r} \quad (15)$$

Hence, the vorticity equation takes the following form (Eq. [16] [28]).

$$\frac{\partial \omega}{\partial t} - \frac{U}{r} \omega + U \frac{\partial \omega}{\partial r} + V \frac{\partial \omega}{\partial z} = -\frac{1}{\rho} [rot f]_{\phi} + \nu \left(\frac{\partial^2 \omega}{\partial r^2} + \frac{1}{r} \frac{\partial \omega}{\partial r} - \frac{\omega}{r^2} + \frac{\partial^2 \omega}{\partial z^2} \right) \quad (16)$$

where $f = [f_r, f_z]$. Beyond Eq. [16] an additional equation is needed, because it remains necessary to calculate U and V . Indeed, it is an elliptic equation for the stream-function, ψ derived by $U = -\frac{1}{r} \frac{\partial \psi}{\partial z}$, $V = \frac{1}{r} \frac{\partial \psi}{\partial r}$. Upon putting U and V into Eq. [15] the following equation can be formulated [28]:

$$\frac{\partial^2 \psi}{\partial r^2} - \frac{1}{r} \frac{\partial \psi}{\partial r} + \frac{\partial^2 \psi}{\partial z^2} = -r\omega \quad (17)$$

The boussinesq approximation $\rho(T) = \beta \rho_0 (T - T_0)$ has been applied to express the buoyancy term [134]. Where β is the coefficient of thermal expansion, g is the acceleration of gravity and T_0 is the reference temperature. This equation is used to express the Boussinesq approximation term in the vorticity transport equation [18].

$$\frac{1}{\rho_0} [rot f]_{\phi} = \frac{1}{\rho_0} \frac{\partial \rho(T)}{\partial x} = g\beta \frac{\partial T}{\partial x} \quad (18)$$

The simulation of the fluid flow and heat transfer occurring inside the storage tank requires an accurate use of the physical models. First, it is necessary to define the appropriate materials and boundary conditions. Second, the mesh and the time step must be sufficiently adjusted to reproduce the physical phenomena [135]. Hence, it is recommended to carry out a sensitivity study

on the time step and the number of elements used to generate the mesh grid, in order to determine the required values that should be used. For this reason, the validation of the physical model has to be performed before conducting the targeted parametric studies, based on very specific performance indicators, by comparing the numerical results with those of the experimental studies available in the literature [136].

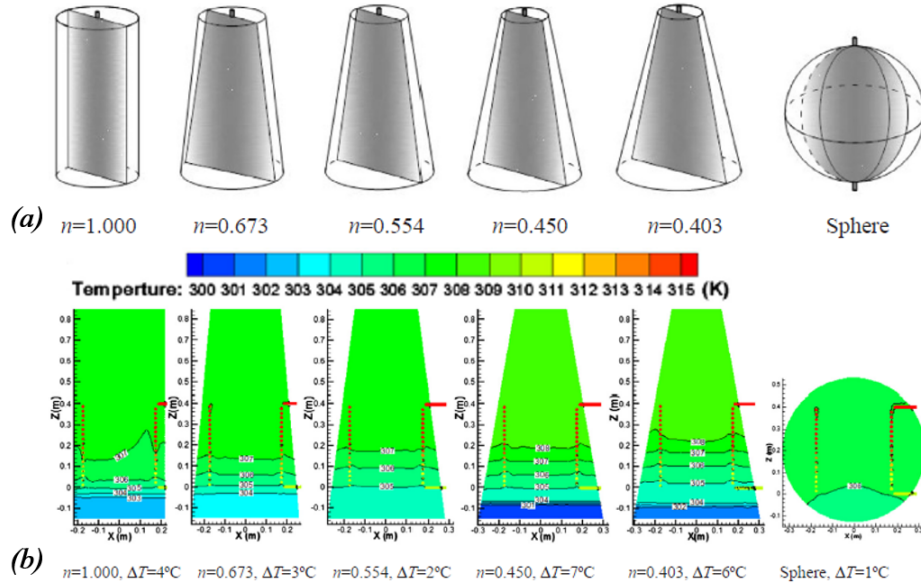


Figure 37: (a)- The considered storage tanks designed and described in [37]. (b)- Temperature fields at $\tau_{ch}=3600$ s [37].

Feifei Cao et al. [37] evaluated the effect of different structures of a thermal storage tank device, namely the cylindrical, the circular and the truncated cone on the evolution of the temperature stratification rate and thermal efficiency during an operating charging cycle. The authors showed that CFD simulations could predict the thermal behavior of the proposed designs. For instance, the spherical tank presented significant symmetrical temperature stratification. Moreover, they showed that a radius ratio ($n=0.554$) for the circular truncated cone tank may lead to better temperature stratification indices and thermal stratification efficiency as shown in Fig. [37].

Special attention has been paid recently to enhance thermal stratification within different geometries of hot water tanks, such as cylindrical and rectangular containers with new shapes of thermal insulation. For instance, the truncated cone and pyramid shapes were numerically assessed by Kursan et al. [38] in order to improve the efficiency of SWHs (Fig. [38]). The authors performed several CFD investigations by changing three key parameters during eight operational hours of the SHW system. The parameters they have evaluated are presented as follows: the aspect ratio of the tank (D/H), the ratio of the bottom insulation diameter to the top insulation diameter (d_i/D_i) and finally the ratio of the bottom insulation thickness to the top insulation thickness (h_b/h_t). To sum up, Kursan et al. [38] showed that the maximum thermal stratification would occur if D/H is maintained at 0.3, d_i/D_i is maintained at 0.75 and finally h_b/h_t is maintained at 0.02.

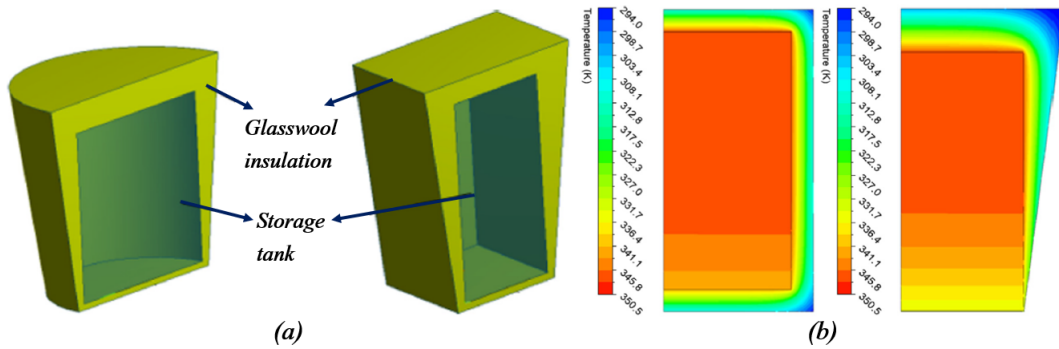


Figure 38: (a)- Geometries of the hot water storage tank designed and evaluated in the released study of Kursun et al. [38]. (b)- Temperature contours of the storage tank for two configurations of the insulation evaluated by Kursen et al. [38]: cylindrical and conical.

Furthermore, El Amin et al. [137] carried out experimental and CFD numerical simulations to assess the thermal behavior of vertical jets within a rectangular water tank according to two cases. The first considered case by these authors is the injection of hot water jet with a uniform inlet temperature in their considered tank. While the second case was the injection of cold water inside the tank with uniform temperature. As reported in their paper, good agreement has been found between the numerical and the experimental results at low temperatures defined as boundary conditions. The authors concluded that CFD simulations are useful because they provide access to several quantities that help making decision regarding the suggested designs of hot storage tanks, such as the pressure field, the temperature and velocity contours besides to different turbulence quantities: turbulence intensity, turbulent kinetic energy and its dissipation rate besides to the vorticity contours...

4.12. Thermal stratification assessment through performance indicators

Miscellaneous methods can be used to assess thermal stratification within water storage tanks. The schematic diagram presented in Fig. 39 summarizes two categories generally used to evaluate thermal stratification. The first category is bifurcated in two classes: dimensional and non-dimensional. The second category is based on the evaluation of the experimental or numerical findings that aim to present the curves necessary to assess the variation of the temperature inside the tank according to well-specified directions (e.g., revolution axis of the vertical tank).

The methods included in this second category are the degree of stratification and its change, besides to the first and second law efficiencies and finally other efficiencies such as the MIX number. These methods are discussed in this section, and the equation setting has been established for each performance indicator to show how it is calculated.

4.12.1. Dimensional and non-dimensional graphical methods

The degree of stratification of a TES could be presented by 2D plots, for instance by representing temperature on one axis and the height of the storage tank on the other axis [34] (Fig. 35 (a)). According to Bouhal et al. [35] the distribution of the temperature at different times of charging/discharging process could be plotted to present numerical results. In fact, the labeling of the axes and the recorded either experimental or numerical data can be dimensional [138] or non-dimensional [139].

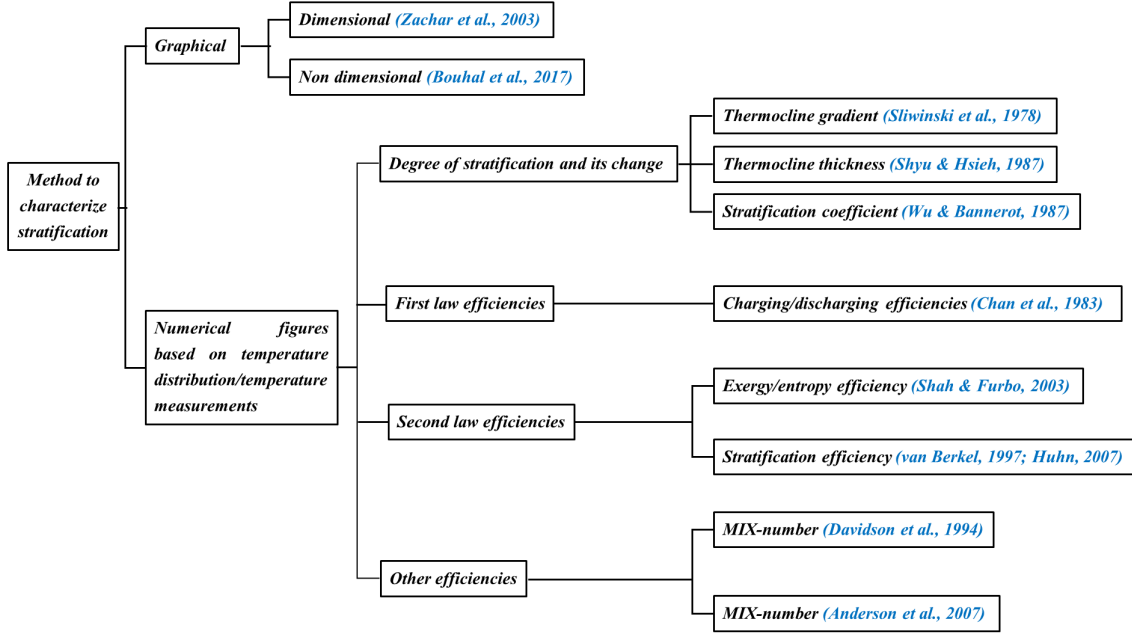


Figure 39: Miscellaneous methods to assess thermal stratification inside water storage tanks.

The non-dimensional value of temperature T^* (see Eq. [20](#) [34](#)) is calculated by dividing the dimensional value of temperature minus the lowest possible value (T_{min}), by the difference between the highest possible temperature value (T_{max}) and the lowest possible value of temperature (T_{min}). In addition, the lowest and highest recorded values depend on the storage tank height (H) and the applied plug flow temperature at the inlet nozzle of the tank (T_{in}) and its initial temperature (T_{ini}) during the charging/discharging process of the performed experiment. Hence, the non-dimensional height (y^*) can be defined as shown in Eq. [19](#). For the charging and discharging process the non-dimensional time t^* expressed in Eq. [21](#) is usually calculated. The minimum time is related to the beginning of the experiment and the maximum time corresponds to the required time necessary to replace the initial volume stored in the tank under the assumption of an ideal plug flow [28](#).

$$y^* = \frac{y}{H} \quad (19)$$

$$T^* = \frac{T - T_{min}}{T_{max} - T_{min}} \quad (20)$$

$$t^* = \frac{t \cdot \dot{m}}{m_{store}} \quad (21)$$

where m_{store} is the stored mass and \dot{m} is the inlet mass flow rate.

4.12.2. Indicators based on temperature distribution and temperature measurements

4.12.3. Stratification number

In this section, the parameters commonly used to assess the efficiency and thermal stratification of sensible and latent heat energy storage tanks are presented. To begin with, the stratification number can be defined as the ratio of the average of the temperature gradients measured at each

time interval to the temperature gradient at the beginning of the charging process assessed at $t = 0$ [35] (Fig. 35(b)). In fact, Saera et al. [140] used the stratification number based on the temperature measurements at equidistant positions in the Thermal Energy Storage (TES) tank to evaluate its efficiency (see Eq. 22 [35]).

$$Str = \frac{(\frac{\partial T}{\partial y})_t}{(\frac{\partial T}{\partial y})_{t=0}} \quad (22)$$

$$(\frac{\partial T}{\partial y})_t = \frac{1}{N-1} \left[\sum_{j=1}^{N-1} \left(\frac{T_j - T_{j+1}}{\Delta Z} \right) \right] \quad (23)$$

$$(\frac{\partial T}{\partial y})_{t=0} = \frac{T_i - T_{ini}}{(N-1)\Delta Z} \quad (24)$$

where (j) represents the nodal points where the temperature is measured. In addition, (N) is the number of nodal points and (ΔZ) is defined as the distance between the nodal points. Moreover, T_i and T_{ini} correspond respectively to the inlet and initial temperature of the HTF. It is noted that the Eqs. 22, 23 and 24 are only applicable, when the temperature is measured at equidistant positions inside the TES tank. However, if the temperature measurements are not made at equidistant positions, the above equations are modified according to the Eqs. 25 and 26, where ΔZ_j is the distance between the j^{th} and $(j+1)^{th}$ nodal points [28].

$$(\frac{\partial T}{\partial y})_t = \frac{1}{N-1} \left[\sum_{j=1}^{N-1} \left(\frac{T_j - T_{j+1}}{\Delta Z_j} \right) \right] \quad (25)$$

$$(\frac{\partial T}{\partial y})_{t=0} = \frac{T_i - T_{ini}}{\sum_{j=1}^{N-1} \Delta Z_j} \quad (26)$$

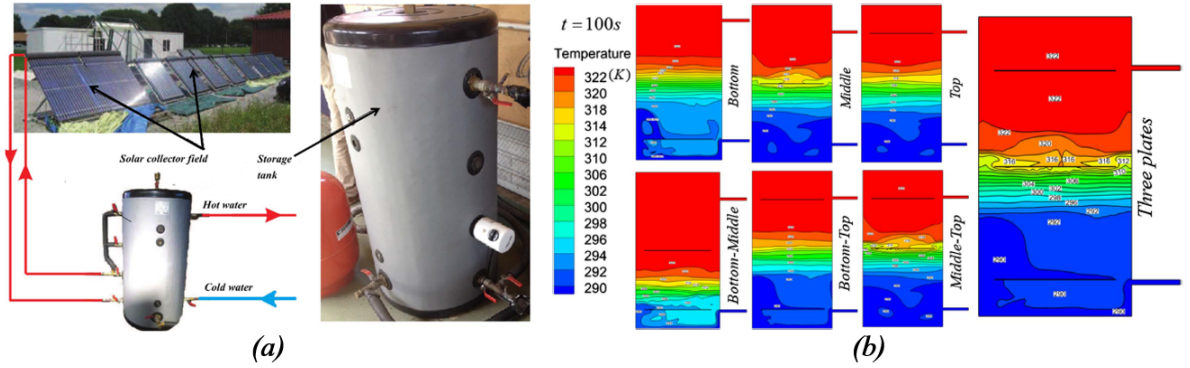


Figure 40: (a)- Vertical storage tank connected to ETC panel [35]. (b)- Temperature map of the storage tank with different configurations of the enhancing stratified plates [35].

More recently, simple inlet devices were suggested by Esteve et al. [132] to evaluate their effect on thermal stratification within a hot water storage tank. Indeed, they used CFD simulations for this thermal assessment purpose, to conclude that the use of low inflow, besides to smooth out inlet velocity could definitely enhance stratification. In addition, Bouhal et al. [35] carried out CFD

numerical modeling and optimization of a vertical solar hot water storage tank presented in Fig. 40 (a) to increase its thermal yield through the integration of stratified plates (Fig. 40 (3)). In fact, they showed throughout the assessment of the stratification number calculated using Eq. 24 that increasing the number of stratified plates submerged within the tank, has not a positive effect on thermal stratification. However, the authors concluded that enhanced thermal performance could be achieved for the flat plate that is located at the middle height of the storage tank.

4.12.4. MIX number

Andersen et al. [141] considered the MIX number as an efficient method to assess thermal stratification in storage tanks, The equation that these authors suggested is a modified formula of the MIX number previously defined by Davidsion et al. [138]. In fact, the MIX number ratio presented in Eq. 27 do not take into consideration the heat lost coefficient at the surroundings of the stratified storage tank, because it is not necessary. It is determined by the first moment of energy, based on the distribution of the temperature levels and energy inside the tank. Most commonly, the MIX number ranges are from 0 to 1, with $MIX = 1$ corresponds to a fully-mixed tank, while $MIX = 0$ is representing a perfectly stratified tank. In order to calculate this stratification performance indicator, the energy momentum of the experimental tank (M_{exp}) Eq. 28 is assessed first and it is related to the energy momentum of two theoretical cases namely, ($M_{stratified}$) Eq. 35 and ($M_{fully-mixed}$) Eq. 37. It is noted that both of those cases are storing the same amount of energy as the experimental tank: a perfectly stratified tank ($M_{stratified}$) and a fully-mixed tank ($M_{fully-mixed}$).

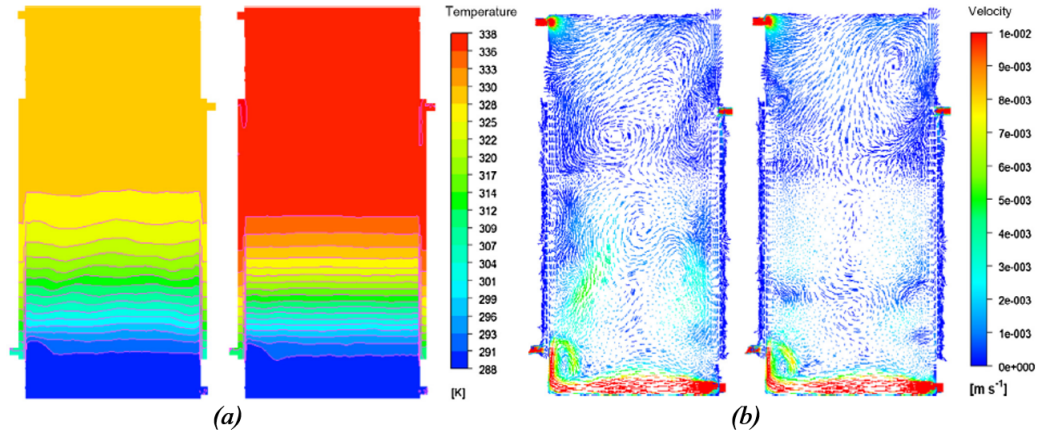


Figure 41: (a)- Temperature contours and (b)- velocity vectors for Grashof number (Gr) below 5×10^{10} at $t^* = 1$ [14].

$$MIX = \frac{M_{stratified} - M_{exp}}{M_{stratified} - M_{fully-mixed}} \quad (27)$$

where

$$M_{exp} = \sum_{i=1}^n y_i E_i \quad (28)$$

$$E_i = \rho V_i C_p T_i \quad (29)$$

If the tank is stratified ($M_{stratified}$), the stored total energy could be considered the same as the amount of the energy obtained from the experiments (see Eq. 30). Also, if T_{hot} and T_{cold} represent experimental data, in this cas V_{cold} and V_{hot} are determined respectively by Eqs. 33 and 34.

$$E_{stratified} = E_{exp} \quad (30)$$

where

$$E_{exp} = \sum_{i=1}^n E_i \quad (31)$$

and

$$E_{stratified} = V_{hot}\rho C_p T_{hot} + V_{cold}\rho C_p T_{cold} \quad (32)$$

The position of the thermocline ($y_{stratified}$) is defined using Eq. 33, if the volumes at cold and hot temperatures are identified.

$$V_{cold} = \pi \frac{D^2}{4} y_{stratified} \quad (33)$$

$$V_{hot} = V_T - V_{cold} \quad (34)$$

The energy momentum of the stratified tank is assessed using Eq. 35, because the height of the thermocline, V_{hot} and V_{cold} are already determined.

$$M_{stratified} = \sum_{i=1}^n E_{stratified,i} y_i \quad (35)$$

The energy achieved from the experiments is also used to evaluate the fully-mixed case Eq. ($M_{fully-mixed}$) as presented in Eq. 36.

$$E_{fully-mixed} = E_{exp} \quad (36)$$

The energy momentum of the fully-mixed tank is assessed using Eq. 37.

$$M_{fully-mixed} = \sum_{i=1}^n E_{fully-mixed,i} y_i \quad (37)$$

where

$$E_{fully-mixed} = V_i \rho C_p T_{fully-mixed} \quad (38)$$

The numerical results derived from the CFD simulations could be useful to define and evaluate the MIX number. For instance, if the assessed storage tank is cooled from a high temperature to a lower temperature by injecting cold flow rate during a discharging process, the temperature contours intrinsic to the configuration of a perfectly stratified tank and a fully mixed tank can be calculated [14] (Fig. 41). Recently, Dragsted et al. [21] assessed thermal stratification for a hot water tank with different inlet stratifiers by performing experimental investigations. They used the Mix number as performance indicator to test the effect of different inlet stratifiers designed

from two manufacturers, namely Solvis GmbH & Co KG and EyeCular Technologies ApS. They concluded that the stratifier from EyeCular Technologies ApS had a better performance in terms of maintaining the thermal stratification in the storage tank. Further, the MIX number is used to predict the destruction of stratified storage tanks connected to solar thermal collectors [120]. For example, experimental investigations were carried out by Assari et al. [120] to define the parameters which affect solar stratified tanks and the thermal yield of the collectors that consist of the primary circuit of SWHs. The authors performed four experiments with different combinations on the conventional thermosyphon SWH system and its hot water storage tank to conclude that decreasing the temperature of the layers located at the bottom of the tank would increase the solar collector efficiency.

4.12.5. Richardson number

Richardson number can be defined as the ratio of buoyancy forces to mixing forces as given by Eq. 39. In fact, it is an effective indicator of stratification performance assessment, because it considers various aspects of the storage tank such as its geometry, the inlet velocity of the charged fluid, and the temperature at the top and bottom layers of the tank [39].

$$Ri = \frac{g\beta H(T_{tp} - T_{bt})}{v_{sf}^2} \quad (39)$$

where

$$v_{sf} = \frac{\dot{V}}{\pi r^2} \quad (40)$$

T_{tp} and T_{bt} correspond to the temperature of water measured at the top and the bottom of the TES tank. Moreover, (H) is the distance between the cold and hot sides of the tank. Also, \dot{V} and v_{sf} represent the volumetric flow rate and superficial velocity of HTF at the TES tank. Finally, r is the radius of the inlet nozzle. Tinaikar et al. [142] carried out detailed numerical and experimental studies to analyze the effect of the internal mixing on the stratification efficiency of a single storage tank unit using Richardson number. In fact, the authors showed through the use of a spatio-temporal method that the merged single vortex pair peels back the thermocline layer, which causes the mixing of the hot and cold fluids. Tab. 9 presents Richardson number effect on thermal stratification from earlier research studies.

Authors	Considered parameter	Results	Conclusions on stratification
Zurigat et al. [143]	stratification number	Ri < 3.6	Inlet geometry has important effect on stratification
Ghajar and Zurigat [144]		Ri > 10	Inlet effect can be neglected
van Berkel et al. [145]		Ri > 10-20	Clear mixing is observed
Brown and Lai [146]		Ri = 0.615	Stratification is appearing

Table 9: Richardson number effect on thermal stratification.

For thermal stratified thermal storage tanks where PCMs are submerged, Oro et al. [147] have defined Richardson ratio expressed in Eq. 41. This ratio is interesting, because it evaluates the integral of the Richardson number along the charging/discharging processes.

$$\varepsilon(R_i) = \frac{(R_i)_{pcm}}{(R_i)_{water}} \quad (41)$$

where

$$(R_i)_{pcm} = \int_{j=0}^{end} (R_i)_{pcm,j} dt \quad (42)$$

$$(R_i)_{water} = \int_{j=0}^{end} (R_i)_{water,j} dt \quad (43)$$

4.12.6. Charging efficiency

Ramana et al. [148] defined the charging efficiency of the TES system as the ratio of the instantaneous heat transfer to the maximum heat transfer, at a given temperature and at well-defined flow rate of the HTF applied at the inlet nozzle of the storage tank (see Eq. 44).

$$\eta_{ch}(t) = \frac{T_i - T_o(t)}{T_i - T_{ini}} \quad (44)$$

where T_i and $T_o(t)$ are the fixed inlet and the instantaneous outlet temperature of the HTF respectively, while T_{ini} is defined as the initial temperature of the fluid stored in the tank. A numerical study of heat transfer and flow characteristics in hot water stores was performed by Hahne et al. [149] using the charging efficiency as performance indicator. For instance, they showed that increasing the height to diameter ratio (H/D) would improve the charging efficiency without exceeding the limit of H/D = 4.

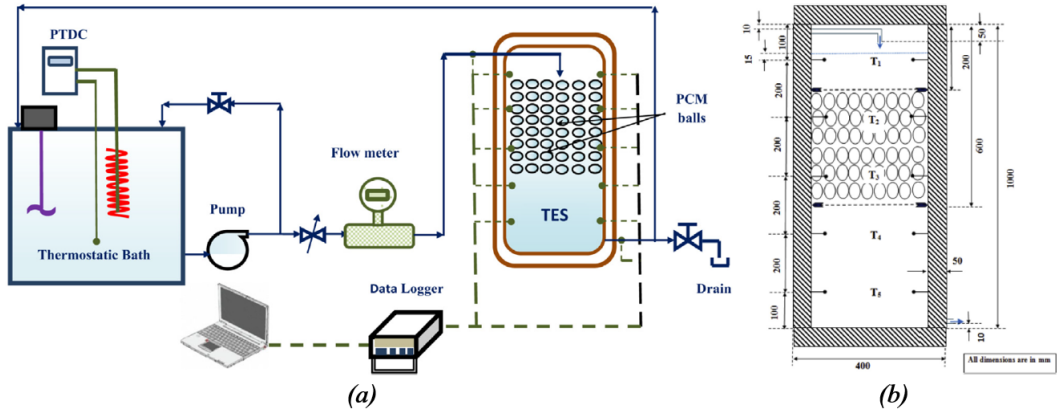


Figure 42: (a)- Schematic layout of the experimental setup designed by Kumar et al. [39]. (b)- Dimensions of the TES tank with the selected location of the sensors [39].

The charging efficiency has been used as a key performance indicator in the experimental study carried out by Kumar et al. [39], to highlight the role of submerging PCMs inside a thermal storage tank on its stratification behavior as shown in Fig. 42. According to their investigations, the authors concluded that increasing the inlet temperature of the HTF fluid would enhance the charging efficiency of the tank, because of the increase of the heat transfer between the PCMs and the working fluid flow.

4.12.7. Storage efficiency

The storage efficiency of the charging process has been defined according to Chan et al. [139] as the actual energy change at time divided by the maximum energy change after ideal plug flow replacement of the entire storage (see Eq. 45).

$$\eta_{storage}(t) = \frac{T_{avg}(t) - T_{ini}}{T_i - T_{ini}} \quad (45)$$

where T_i , T_{ini} and $T_{avg}(t)$ represent respectively the inlet temperature of the HTF, initial and mass average temperature of fluid charged in the storage tank.

4.12.8. Cumulative Charge Fraction (CCF)

According to the experimental investigations conducted by Oro et al. [147] on the stratification analysis in packed bed thermal energy storage systems, the equations presented previously remain suitable for sensible heat energy storage system (EST). In fact, they fail to predict the stratification behavior for both sensible and latent heat energy storage system. Thus, the Cumulative Charge Fraction (CCF) is defined to take into account sensible and latent energy storage (see Eq. 46 [39]). CCF is the ratio of cumulative heat transferred to the storage tank at a considered point in time, to the maximum storage capacity of the TES tank. It is noted that Eq. 46 can be used only in the case of a fixed hot inlet nozzle of the HTF, with a temperature above the melting liquidus point temperature of the PCM and remains not applicable in other cases.

$$CCF = \frac{\int_0^t Q_{ins} dt}{m_f C_{p,f} + m_{pcm} \Delta H_f + m_{pcm} (C_{p,s})_{pcm} (T_s - T_{ini}) + m_{pcm} (C_{p,l})_{pcm} (T_i - T_L)} \quad (46)$$

where

$$\int_0^t Q_{ins} dt = \sum_{k=1}^n Q_{ins}^k \Delta t \quad (47)$$

$$Q_{ins}^k = \dot{m}_f \times c_{p,f} \times (T_i - (\frac{T_0^{k-1} + T_0^k}{2})) \quad (48)$$

where, T_o and T_i are the outlet and inlet temperature of the HTF respectively, and T_{ini} is the initial temperature of the fluid in the storage tank. T_s and T_L are defined as the solidus and liquidus temperature of the PCM respectively. Also, m_f and m_{pcm} are the mass of HTF in the storage tank and mass of the used PCM respectively. Further, $C_{p,f}$ is the specific heat of fluid in the storage tank, $(C_{p,s})_{pcm}$ and $(C_{p,l})_{pcm}$ are the specific heat of PCM in solid and liquid phase respectively and ΔH_f is the latent heat capacity of the PCM. Last but not least, Q_{ins}^k is the instantaneous heat transfer rate at the k_{th} time step, 'n' is the number of time steps and Δt is the size of each time step. \dot{m}_f is the mass flow rate of HTF at the inlet nozzle of the storage tank.

Kuma et al. [39] investigated the effect of submerging PCMs inside a thermal storage tank on its stratification behavior through an experimental study focusing on the charging process. The authors analyzed the stratification behavior of the tank using the CCF indicator, previously presented in Eq. 46, for both the TES systems: with and without integrating the PCMs. In fact, they achieved enhanced stratification in sensible TES system at lower HTF inlet temperature for specific flow rates. On the other hand, they found that adding PCM capsules would improve the stratification capability of the tank, because the temperature difference between the inlet of the HTF and PCM melting temperature increased.

4.12.9. Exergy efficiency

The second law of thermodynamics is useful when the energy will be used to produce work. In this case, the thermodynamic limit of the produced work can be used to define the stored exergy. Indeed, a “dead state” reference has to be defined in order to calculate values based on exergy analysis. This reference state is corresponding to the thermodynamic state of the environment. Better stratification is related to more pronounced temperature gradients inside the TES. In fact, these TES contain usually more exergy than comparative TES systems with similar energy but with less pronounced stratification. As a result, the second law of thermodynamics could be used as effective approach to provide interesting information regarding the stratification efficiency. According to Rosengarten et al. [150], the exergy charging efficiency of a stratified thermal storage tank of a solar water heater can be expressed as presented in Eq. 49. The authors showed that exergy analysis is an accurate approach to describe thermal stratification because it takes into consideration exergy destruction and the exergy delivery temperatures.

$$\eta = 1 - \frac{T_0}{H(T_{inlet} - T_{avg})} \sum_{i=1}^N \ln\left(\frac{T_{inlet}}{T_i}\right) \Delta h \quad (49)$$

where T_0 is the dead state or reference temperature, which can also be the initial temperature of the experimentation or numerical simulation.

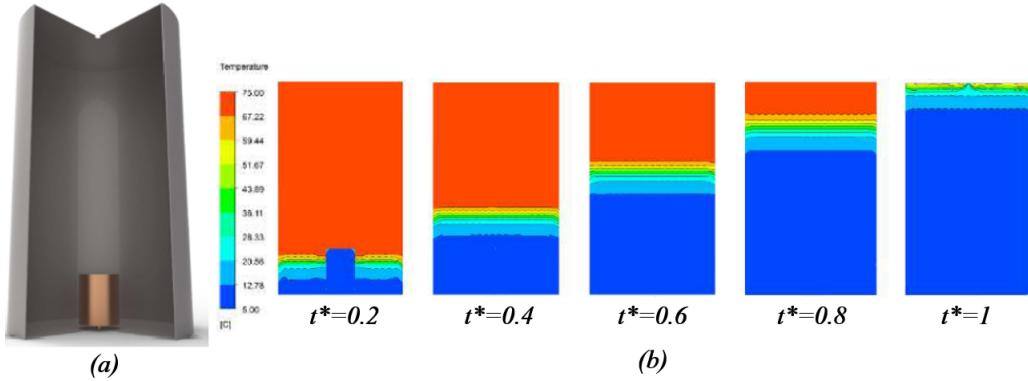


Figure 43: (a)- Thermal storage tank with an integrated equalizer [40]. (b)- Temperature contours evolution for a constant flow rate of 1 liter/min [40].

Most recently, Osorio et al. [151] carried out an exergy analysis of discharging multi tank thermal energy storage systems with constant heat flux. They showed using this performance indicator that superior efficiency of two-tank systems is achieved during the entire timespan. Moreover, the authors proved that the pumping effects and the energy losses are negligible and the efficiency is improved by dividing the storage system. Finally yet importantly, an experimental research, which was followed by three-dimensional (3D) unsteady CFD simulations on a novel equalizer (designed and integrated at the bottom section of the thermal stratification tank) were carried out by Wang et al. [40]. In fact, according to this research, heat storage is considered as an important field in the use of solar energy. These authors used miscellaneous performance indicators to evaluate their parametric studies, such as exergy, the Richardson number, the fill efficiency and the MIX number. They were nonetheless able to conclude that increasing the flow rate injected from the new equalizer shape shown in Fig. 43, would decrease the Richardson number and increase the

exergy at the beginning of the charging process because it has decreased later, by contrast with the MIX number. Most importantly of all, the equalizer suggested by this research team allowed the decrease of the mixing process between cold and hot water, which help to enhance thermal stratification.

4.13. Conclusion

This chapter presents a synthesis of experimental and numerical studies carried out on stratified storage tanks connected to SWHs integrated in green-buildings. In fact, it is vital to design with accuracy hot water storage tanks in order to enhance their thermal yield. The first section of this chapter highlighted recent studies aimed to investigate the efficiency and viability of SHWs and their associated storage tanks. First, a focus has been placed on seasonal storage. Second, recent innovation studies aimed to enhance the thermal efficiency of the storage tanks were presented, either by submerging PCMs or by integrating additional components or new injector's designs in the tank. For instance, a storage tank with a Richardson number greater than 1, implies that it will present better thermal performances because the buoyancy forces overcome the mixing forces.

The second part of this chapter presents the equation setting to be established to ensure the physical modeling of thermal stratification inside storage tanks. Two approaches have been detailed: the three-dimensional CFD approach and the two-dimensional formulation. The advantage of the numerical methods is to provide additional information such as plotting the temperature map inside the tank and to locate the recirculation stream function zones.

To conclude with, the third section of this chapter highlighted a set of thermal performance indicators usually used by the scientific community to evaluate the thermal yield of hot water storage tanks. In fact, two methods were presented: the graphical method and the numerical figures methods based on both temperature and distribution measurements. An example of these performance indicators is the following: dimensional and non-dimensional indicators, thermocline gradient, stratification coefficient, exergy and stratification efficiency and finally the MIX number.

5. Part II: Thermomechanical efficiency enhancement of individual *SWHs* integrating *ETC* with submerged heat pipes using numerical simulations

5.1. *Chapter III: Performance optimization of a two-phase closed thermosyphon through CFD numerical simulations*

5.2. *Introduction*

In this chapter, a comprehensive CFD modeling was built to reproduce the pool boiling in the evaporator section and the liquid film condensation in a closed thermosyphon. The suggested model was validated by experimental results, and a good agreement was observed. Evaporation, condensation and phase change are included by Lee model coupled with the two-phase VOF model. The CFD results of the studied wickless heat pipe in terms of temperature contours, vertical velocity and volume fractions were exploited to understand the phenomenon which occurs inside the thermosyphon that could not be visualized by empirical or experimental work. A parametric study was conducted in order to optimize the performances of the thermosyphon designed for the application of solar thermal energy: the heating of domestic hot water. Several performance indicators were defined to quantify this optimization: Nusselt number, the heat transfer coefficient, mass transfer rate, the heat flux transferred by the condenser section, contours of temperature, vertical velocity of vapor, volume fraction, and the efficiency of the thermosyphon. Our optimization results showed that the efficiency of the closed thermosyphon was improved to reach a new performance of 84.71% thanks to the integration of the tilted fins on the lateral surface of the condenser section.

In many industrial fields, the component development is conducted by the increase in performance and the miniaturization of electronic systems, safety of nuclear reactors and solar heating systems resulting in an increase of the heat dissipation. The thermal management of these components has become a major challenge. As conduction or air convection cooling systems are no more efficient to transfer such high heat fluxes so alternative cooling techniques (two-phase thermal control devices) have to be used such as heat pipe (HP) and two phase thermosyphon (TPTS). The major components of the heat pipe are a sealed container, working fluid, and a wick structure. The wick structure lines the pipe inside wall, which provides the structure to develop the capillary action causing the condensate to return from the condenser to the evaporator.

The use of the thermosyphon is dating back several decades and the first application started at the 40 s. The applications of the thermosyphon are diversified and also used in several fields: solar thermal applications, industrial cooling and modern applications such as thermal engineering systems (space application [152], heat exchanger [153], electronic industries [154] and solar systems [155]). A thermosyphon can be defined as a wickless heat pipe and the condensate returns from the condenser by gravitational force to the evaporator. It's a closed cylindrical tube which contains a heat transfer fluid. It is called passive because it does not need heat (heating power) to transform the energy between the source and the sink. Thermal conductivity is well improved due to the phase change (liquid/vapor) and it remains definitely higher than any know metal [156]. Hence, there has been a considerable research focused on developing better models to predict the heat transfer achievement for a given temperature difference. Aung et al. [157] have numerically investigated the effect of riser diameter and its inclination angle on system parameters in a two-phase closed loop thermosyphon solar water heater. It is observed that the optimum inclination angles and diameters for solar heat flux, circulating mass flow rate and heat transfer coefficient in two-phase thermosyphon system do not coincide. From this work, better understanding and useful information are provided for constructing two-phase thermosyphon solar heaters.

Actually, several million heat pipes are manufactured each month for applications in CPU cooling and laptop computers according to Shabgard et al. [158]. In fact, numerical modeling,

analysis, and experimental simulation of heat pipes have significantly progressed due to a much greater understanding of various physical phenomenon in heat pipes as well as advances in computational and experimental methodologies. Recently, Shah et al. [159] have performed numerical and experimental investigation of core cooling of Li-ion cells using heat pipes that compare their performance with other cooling approaches. The results show that a solid metal rod may be equally effective as a heat pipe and successfully prevent overheating due to malfunction. Another study performed by Danielewicz et al. [160] concerns three-dimensional numerical model of heat losses from district heating network pre-insulated pipes buried in the ground. The studies investigated the challenges in modelling the energy losses of heating networks and have analyzed the factors that influence them. The verification of the simulation was conducted on a test stand in-situ and based on the measurements of the testing station, a database for the final version of the numerical model was developed and a series of simulations were performed. They have presented an innovative method to identify the energy losses of underground heating network pipelines and to quantify the temperature distribution around them, in transient working conditions.

Moreover, Poplaski et al. [161] have worked on a complete thermal network analysis for a cylindrical heat pipe and have identified the dominant thermal resistances. The working model was developed to simulate high and low temperature heat pipe operation for both transient and steady state modes of operation. It was found that the vapor core thermal resistance can become significant as the operating temperature increases; however, the largest thermal resistances are those corresponding to the external heat transfer fluids. A detailed model have been performed by Ranjan et al. [162] including the effects of the wick micro-structure on the overall heat transfer rate. Two numerical models were used and coupled to predict the performance of a heat pipe with a screen wick. The first was a macro-model where the phase-change rates and the pressure/temperature at the solid-liquid interface were obtained through an energy balance at the interface. The second model examined the wick micro-structure and computed the phase change rates from the liquid meniscus formed in the pores.

Furthermore, a novel thermosyphon configuration have been proposed by Nair et al. [163] with rectangular internal fins at the condenser. In order to simulate the operation of a thermosyphon, a modified steady state theoretical model and synergistic approach by combining VOF model and lumped parameter model are used. The study analysis of effect of increasing fins inside the condenser section of the thermosyphon. An innovative counter-current two-phase thermosyphon have been presented by Schreiber et al. [164] features multiple pools cascaded along the evaporator section and liquid are accumulated in the pools until they overflow to spread the working fluid. The numerical control volume model and experimental validation are discussed.

Tong et al. [165] have experimentally analyzed the performance of R744 two-phase thermosyphon loop. The study shows that there is usually some fluid that circulates in the loop without changing phase and the maximum heat transfer ability is achieved at the fill ratio around 100%. The obtained results show that lowest driving temperature difference is achieved at the fill ratio around 62% and the thermosyphon loop with a lower fill ratio is more likely to fluctuate at small heat loads.

Zhang et al. [166] have developed a generalized model for two-phase thermosyphon loops (TPTLs) in which the downcomer can be partially liquid filled or fully liquid filled under different conditions. The model is used to analyze the flow and heat transfer features of a TP TL. The results show that the downcomer is partially liquid filled in the case of small temperature difference and refrigerant charge. Additionally, the heat transfer rate first increases then decreases with the

increase of refrigerant charge, and first increases linearly then increases relatively slowly with the increase of temperature difference.

Rahimi et al. [41] worked on CFD modeling of flow and heat transfer in a thermosyphon. They used the volume of fluid (VOF) technique to model the interaction between these phases. They showed that CFD technique can successfully model the complex heat and mass transfer. Bandar Fadhl et al. [1] used the volume of fluid (VOF) model available in *Ansys Fluent* to conduct their simulations. They observed a good agreement between the CFD temperature profiles and experimental temperature data. The CFD results of their work showed that *Fluent* with the VOF method can successfully model the complex phenomena inside the thermosyphon.

Gedik et al. [167] worked on the experimental investigation of the thermal performance of a two-phase closed thermosyphon at different operating conditions. They studied the influence of several parameters on the efficiency of the TPCT such as the working fluids, operating conditions as inclination angles, heat inputs and flow rates of cooling water at the condenser section. They characterized each fluid tested by optimal operating conditions which lead to the optimal performances of the thermosiphon.

Feng Jiang et al. [168] worked on Heat transfer enhancement in a closed thermosyphon with thermally conductive PA6/water. They conducted in their experiments the effects of filling ratio, heat flux and solid holdup to study the heat transfer performance. They reveals through their results that three-phase closed thermosiphon lead to an enhancement of heat transfer performance in comparison with two-phase closed thermosyphon (TPCT) filed with pure water. The response of a thermosyphon under pulsed heat inputs conditions have been studied by Kafeel et al. [169]. They simulated using a full scale axisymmetric model and using the two fluid methodologies within Eulerian multiphase domain the behavior of the TPCT under pulsed heat conditions. Their numerical modeling is different from that of Fadhl. [1] that have imposed a heat transfer coefficient as a boundary conditions on the side surface of the condenser to model the conjugate heat transfer between the head of the thermosyphon and the jacket of cooling which cover it.

Jouhara et al. [170] simulated a three-dimensional complex multiphase geyser boiling in a two-phase closed thermosyphon (TPCT). They showed that CFD can predict a boiling regime and the pattern occurring. They have validated their CFD findings with two of their experimental facilities. They noted that the simulated time of the phase change did not exceed six seconds. This gives an idea on the heavy computational time but also on the important means of calculations that were deployed.

From the literature research previously presented which describes recent studies that have been conducted on the thermosyphon, the number of numerical works remain limited and the heat transfer process mechanism in this system is far from well-understood. Thus, the aim is to present new efficient shapes of a closed thermosyphon based on several experimental studies on this device in order to contribute to the enhancement of heat transfer and minimization of flow losses. Hence, the main objective of this numerical study is to investigate the phase change in a thermosyphon subjected to specific terms and conditions that are related to the targeted field: the solar thermal application.

5.3. Mathematical model

5.3.1. Physical model and basic equations

Fig. 44 represents a description of a closed thermosyphon used to heat a cool water entering a cylindrical exchanger. A simplified diagram of vacuum tube collector is represented. The double

glazing, the reinforcement which improves the heat transfer were not represented besides the metal support and the thermal insulation of the exchanger. Passive operation is as follows: the incident solar radiation on the thermosyphon vaporizes a fraction of the heat transfer fluid. The ascending vapor comes into contact with cold water filling the exchanger. This transfer of mass and energy can heat water which benefits from the latent heat of vapor trapped in the head of the thermosyphon. The vapor phase becomes again liquid and goes down at the bottom of the thermosyphon by effect of gravity while the output water from the exchanger becomes hot.

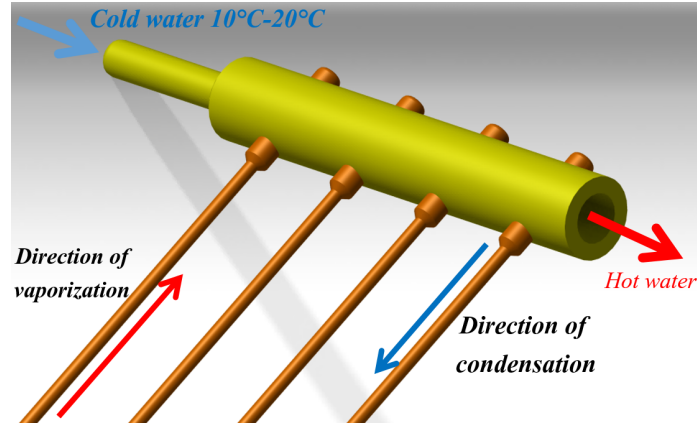


Figure 44: Energy transfer mechanism by a series of wickless heat pipes inserted into a cylindrical exchanger.

In this chapter, a numerical model for a two-dimensional cylindrical wickless heat pipe has been developed to analyze the heat transfer mechanism. This numerical study is divided into two main steps:

1. Validation of the numerical code used to simulate the phase change (liquid/vapor).
2. Parametric study aiming to optimize the performance of the heat pipe to be used as a passive device in the solar thermal collector.

The current numerical investigation is based on Volume Of Fluid (VOF) model which allow the surface tracking of two or more immiscible phases [171]. The volume fraction of each new phase is added to calculations. The sum of the fractions of all the phases in a control volume are equal to one. CFD modeling allows to solve the equations of Navier-Stokes simultaneously. In these equations, the density (ρ), the dynamic viscosity (μ) depend on the volume fraction of each phase and they are calculated by the formulas (Eqs. 50 and 51). The fraction of the phase present in a grid cell is represented by the quantity α_l , α_v that respectively indicates the liquid and vapor fractions.

$$\rho = \alpha_l \rho_l + (1 - \alpha_l) \rho_v \quad (50)$$

$$\mu = \alpha_L \mu_L + (1 - \alpha_L) \mu_V \quad (51)$$

The code numerically treats the mesh grid, which is filled by the two non-miscible phases, as follows:

- If the cell is filled by the liquid phase: $\alpha_l = 1$

- If the cell is filled by the vapor phase: $\alpha_v = 1$
- if a cell is simultaneously filled by the two phases liquid and vapor: $0 < \alpha_l < 1$

5.3.2. Continuity equation for VOF model (volume fraction equation)

The *lee* model [172] is a mechanistic model with a physical basis. In this model, the liquid-vapor mass transfer (evaporation and condensation) is governed by the vapor transport equation (Eq. 52), where \dot{m}_{lv} and \dot{m}_{vl} are the rates of mass transfer due to evaporation and condensation, respectively and they are expressed in $kg s^{-1} m^{-3}$.

$$\frac{\partial \alpha_v \rho_v}{\partial t} + \nabla \cdot (\rho_v \alpha_v \vec{u}_v) = \dot{m}_{lv} - \dot{m}_{vl} \quad (52)$$

- v : vapor phase
- α_v : vapor volume fraction
- ρ_v : vapor density
- \vec{u}_v : vapor phase velocity

Eqs. 53 and 54 are used to define positive mass transfer as being from the liquid to the vapor for evaporation-condensation problems. Based on the following temperature regimes, the mass transfer can be described as follows:

If $T_l > T_{SAT}$

$$\dot{m}_{lv} = r_v \times \alpha_l \rho_l \frac{T - T_{SAT}}{T_{SAT}} \quad (53)$$

If $T < T_{SAT}$

$$\dot{m}_{vl} = r_l \times \alpha_v \rho_v \frac{T - T_{SAT}}{T_{SAT}} \quad (54)$$

The phase change occurs at constant pressure and depends on the temperature of saturation T_{SAT} .

r_v and r_l are mass transfer time parameters [173] that must be fine tuned. The source term for the energy equation can be obtained by multiplying the rate of mass transfer by the latent heat.

The continuity equation presented previously is called volume fraction equation and it solves the secondary phase. The primary phase is calculated by the Eq. 55:

$$\sum_{L=1}^n \alpha_L = 1 \quad (55)$$

5.3.3. Momentum equation for VOF model

Only one equation of motion is solved in the flow field. The calculated velocity is shared on the two phases. Momentum Eq. 88 is expressed by:

$$\frac{\partial \rho \vec{u}}{\partial t} + \nabla \cdot (\rho \vec{u} \vec{u}) = -\nabla P + \nabla \cdot \tau + \rho g + F_{CSF} \quad (56)$$

The forces applied to the fluid are gravity, pressure, viscous forces of friction as well as the surface tension. The effect of the surface tension is included by adding the term F_{CSF} to momentum equation. This term (Eq. 57) represents the continuum surface force and it was proposed by Brackbill et al. [174].

$$F_{CSF} = 2\sigma_{lv} \frac{\alpha_l \rho_l C_v \nabla \alpha_v + \alpha_v \rho_v C_l \nabla \alpha_l}{\rho_l + \rho_v} \quad (57)$$

where C is the surface curvative and σ_{lv} is the surface tension coefficient. The same expression as [1] was used, to express the coefficient of surface tension σ_{lv} and the density of the liquid phase ρ_l which are a functions of temperature (Eqs. 58 and 59).

$$\sigma_{LV} = 0.09805856 - 1.845 \times 10^{-5}T - 2.3 \times 10^{-7}T^2 \quad (58)$$

$$\rho_L = 859.0083 + 1.252209 \times T - 0.0026429T^2 \quad (59)$$

5.3.4. Energy equation for VOF model

The VOF model treats energy e and temperature T as mass averaged variables Eqs. 60 and 61.

$$\frac{\partial \rho e}{\partial t} + \nabla \cdot (\rho e \vec{u}) = \nabla \cdot (k \nabla T) + \nabla \cdot (p \vec{u}) + S_E \quad (60)$$

$$e = \frac{\alpha_l \rho_L e_l + \alpha_v \rho_v e_v}{\alpha_l \rho_l + \alpha_v \rho_v} \quad (61)$$

$$e_l = C_{p,l}(T - T_{SAT}) \quad (62)$$

$$e_v = C_{p,v}(T - T_{SAT}) \quad (63)$$

The thermal conductivity k of the mixture depends on the conductivity of each phase present in the field (Eq. 64). S_E is a source term of energy which calculates the energy transferred during evaporation and condensation.

$$k = \alpha_l k_l + (1 - \alpha_l) k_v \quad (64)$$

5.3.5. Heat transfer model in the metal wall

The physical model used to describe the heat transfer in the metal wall of the thermosyphon is expressed in Eq. 65. The heat transfer occurs by conduction in the metal wall, and a two-dimensional unsteady state has been considered as a simplifying hypothesis.

$$\rho_w C_w \frac{\partial T}{\partial t} = k_w \left(\frac{\partial^2 T}{\partial x^2} + \frac{\partial^2 T}{\partial y^2} \right) \quad (65)$$

Where ρ_w is the density of the material wall, C_w is the metal wall specific heat capacity and k_w represents its thermal conductivity.

5.4. Validation methodology of the numerical VOF model

The validation of the two-phase (VOF) model used during our numerical study is a basic step which precedes the geometric changes on the thermosyphon aiming to enhance its performances. Our study is based on the work of Fadhl et al. [1] to achieve this goal. In fact, as mentioned in the introduction, they have numerically modelled the distribution of the temperature in a two phase closed thermosyphon (TPCT) using VOF model, after its validation with their experimental results under the same operating conditions.

The experimental device presented in Fig. 45 [41] was implemented by Alizadehdakhel et al. [41] to validate their CFD model. The same experimental set-up was used to carry out the experimental tests on a typical wickless heat pipe besides to the validation procedure initiated by Fadhl et al. [1].

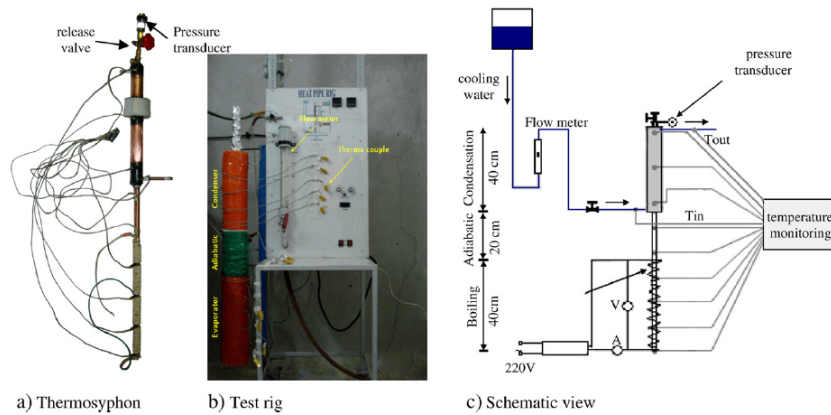


Figure 45: Experimental setup of Alizadehdakhel et al. [41].

5.4.1. Description of the experimental device

A two-phase closed thermosyphon (TPCT) is inserted in a heating electrical resistance. A water coolant circuit was used to condense the vapor resulting from the evaporation of the working fluid. The section of the evaporator is half filled with distilled degassed water. A measurement instrumentation equips the device to measure the heating power in the evaporator, the temperature by using thermocouples as well as a flow meter to measure the flow on the level of the condenser.

A wickless heat pipe consists of three sections: the evaporator section located at the bottom of the thermosyphon, an adiabatic section in the middle to avoid the interactions with the external medium and the condenser section located at the top of the thermosyphon.

The performance indicator used during this study is the temperature. The local measure of the temperature along the circumference of the thermosyphon is taken by six thermocouples: one thermocouple on the adiabatic section and five thermocouples stuck on the circumference of the condenser section. The objective of using five thermocouples that were made from an alloy of (NiCr / NiAl) is to prove the nonexistence of non condensable gases (NCGs) [1].

5.4.2. Description of the experimental procedure of Fadhl et al. [1]

Fadhl et al. [1] applied a constant flux on the circumference of the evaporator to simulate the phase change, and a zero flux on the surface of the adiabatic section to reproduce the condition of the thermal insulation. It is not possible to model the flow of water in the cooling circuit, since

our simulation is two dimensional. Several empirical expressions of the heat transfer coefficient can model the heat transfer that occurs between the jacket which coats the condenser and the condenser section. The expression of the heat transfer coefficient that brings us closer to validation and which has also been used by fadl et al. is presented in Eq. [85](#)

$$h_c = \frac{Q_c}{2\pi r L_c (T_{c,avg} - T_\infty)} \quad (66)$$

Where h_c is the condenser heat transfer coefficient, T_∞ is the average temperature of the condenser cooling water, $T_{c,avg}$ is the condenser average temperature and Q_c is the rate of heat transfer from the condenser, L_c is the condenser length.

Fadhl studied the response of this pulsated thermosyphon by six different values of heating power 100.41, 172.87, 225.25, 275.60, 299.52, 376.14 (W). Two extreme configurations were chosen to validate their results, because to reach the steady state of this numerical simulation is a heavy computational duty. For this reason two configurations were defined *i.e.* the case where the flow applied on the circumference of the evaporator is minimal (172.87 W), then maximum (376.14 W).

Tab. [10](#) introduces the values of the heating powers applied at the evaporator Q_{in} , the rate of heat transfer from the condenser Q_c , the average temperature of the condenser cooling water $T_{c,avg}$ and the heat transfer coefficient used as boundary conditions h_c .

Evaporator	Condenser cooling water	Condenser		
		Q_c (W)	$T_{c,avg}$ (K)	h_c (K/Wm ²)
Q_{in} (W)	T_∞ (K)			
172.87	301.45	162.6	318.07	707.6
376.14	309.4	336.6	330.33	1163.5

Table 10: Experimental conditions used for the numerical study.

5.4.3. Solution strategy and convergence criteria

Unsteady simulations were carried out to model the evaporation-condensation phenomena. A time step of 2×10^{-4} s gives a courant number (CFL) ([94](#)) between 0.5 and 3, knowing that it should not exceed 250 for VOF model ([171](#)). As it is mentioned in the work of Fadhl, the steady state mode is reached at the end of 60s.

$$CFL = \frac{u_x \Delta t}{\Delta x} + \frac{u_y \Delta t}{\Delta y} \quad (67)$$

Where Δx and Δy are the space steps discretization and Δt is the time step discretization.

The SIMPLE algorithm was used for the pressure-velocity coupling, a first order numerical scheme for momentum and energy equations discretizations. Geo-Reconstruct and PRESTO were used for the discretization of the volume fraction and the pressure interpolation scheme respectively. Our numerical calculations were considered convergent when the scaled residual of the mass and velocity is less than 10^{-4} and less than 10^{-9} for energy.

The vapour phase is defined as being the primary phase and the liquid phase is defined as the secondary phase. The *Lee* model is used to describe the transfer of mass and energy when the temperature of the liquid reaches the saturation temperature $T_{SAT} = 373$ K.

5.4.4. Simulation model

A 2D numerical model is used during this work to simulate the transfer of mass and energy in the wickless heat pipe. The thermosiphon is made of copper. Its length is 0.5m, its internal diameter is 20.2 mm and the thickness of copper is 0.9 mm. According to the experiment, it is divided into three sections, the evaporator section 200 mm, the adiabatic section 100 mm and the condenser section 200 mm. Half of the evaporator (100) mm is filled with the heat transfer fluid, in this case it is distilled water. Eight monitors were defined on the side circumference of the thermosiphon, keeping the same location of the thermocouples mentioned in the experiment. Thermocouples $T_{c,1}$ up to $T_{c,5}$ are used to determine the average temperature of the condenser.

Structured quadrilateral grid of 80000 elements was used to improve the simulation performance and accuracy. In fact, this grid number has led to the convergence of the temperature results independently of the mesh at the adiabatic and the condenser sections (Fig. 47), knowing that Fadhl et al [1] used a structured quadrilateral grid of 69092 elements while carrying out the validation step. Two test cases were used for the validation of our model. The positioning of the monitors for the numerical temperature's measurement is presented in Fig. 46.

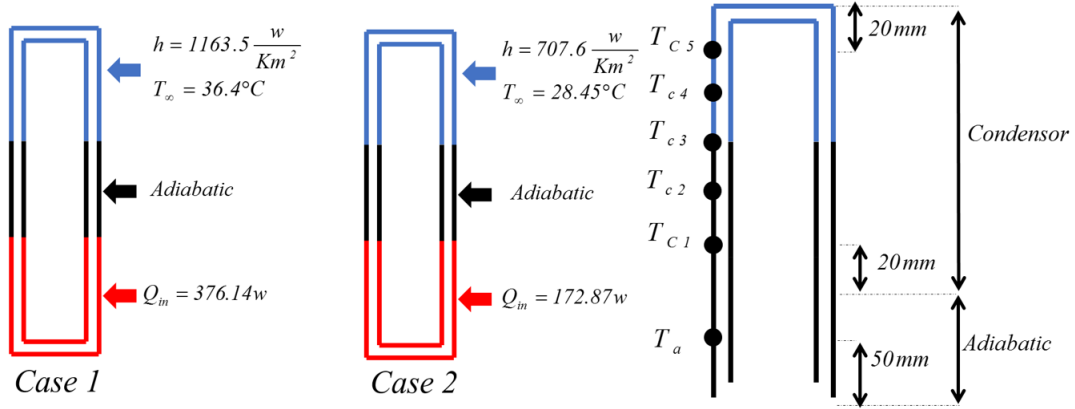


Figure 46: The thermocouples positions on the thermosiphon and the reviewed cases for validation.

The total thermal resistance of the thermosiphon TPCT was calculated by applying the electrical analogue (Eq. 68).

$$R_{exp} = \frac{\Delta T_{e-c}}{Q} = \frac{T_{e,avg} - T_{c,avg}}{Q_{evaporator}} \quad (68)$$

The average temperature of adiabatic and condenser are calculated by the following equations.

$$T_{a,avg} = T_a \quad (69)$$

$$T_{c,avg} = \sum_{i=1}^5 \frac{T_{c,i}}{5} \quad (70)$$

5.4.5. Uncertainty analysis

According to Fadhl et al. [1] the main source of the experimental error came from the temperature readings. The temperature measurement on the thermosiphon's circumference, namely the

adiabatic and condenser sections was carried out using K-type thermocouples with a measurement uncertainty of $\pm (0.05\% \text{ rdg} + 0.3 \text{ }^\circ\text{C})$ and $0.5\% \text{ rdg}$ for the power readings. An equation which is providing the propagation of uncertainties was discussed in the work of Taylor et al. [175]. In fact, it was found in the experimental work of Fadhl et al. [1] that the maximum uncertainty parameter associated with the propagation of uncertainties was around 5.5% , which is an acceptable value in engineering applications [175].

5.4.6. Validation results

Tab. [11] presents the values of the experimental temperatures measured by Fadhl and al. at the adiabatic section and condenser section, as well as its numerical temperatures. Our temperatures are also presented, they were used to calculate the relative error which is compared with the error of Fadhl. A slight difference of 1.48% is listed in the adiabatic section. As regards the condenser section, a difference which does not exceed 0.7% is quantified.

Tab. [12] presents the average experimental temperatures of the adiabatic and the condenser sections measured by Fadhl. They were compared with our numerical temperatures once again. The relative error is calculated to justify the validity of the two phase VOF model with a transfer of mass and energy. A difference of 1.48% is estimated on the adiabatic while an error of 0.32% is estimated on the condenser.

Tab. [13] represents the second test case, where the flux applied on the evaporator is minimal. It presents the experimental temperatures recorded by Fadhl et al. They were compared with our numerical temperatures to estimate the relative errors. It is an approach similar to the previous one, used to validate the case of maximum applied heat flux. Indeed, the margin of difference in the relative error in the adiabatic section is 2.65% . At the condenser, our error has improved and the maximum difference was 2.36% (thermocouple $T_{c,4}$).

Sections	Positions	$T_{experimental}$	$T_{Numeric\ Fadhl}$	$T_{Our\ Simulations}$	Fadhl's errors %	Our errors %
Adiabatic	T_a	342.75	370.11	375.20	7.98	9.46
Condenser	T_{c1}	328.95	327.12	326.25	0.56	0.8
	T_{c2}	325.55	323.66	321.52	0.58	1.23
	T_{c3}	332.45	323.15	321	2.80	3.44
	T_{c4}	331.35	322.70	321.05	2.61	3.10
	T_{c5}	333.35	323.17	324.71	3.05	2.6

Table 11: Validation of case 1 - Comparison of the numerical temperatures and the relative errors assesment.

Sections	Positions	$T_{exp\ avg}$	$T_{Numeric\ avg}$	$T_{Our\ Simulations}$	Fadhl's errors %	Our errors %
Adiabatic	T_a	342.75	370.11	375.20	7.98	9.46
Condenser	T_{c1}	330.33	323.96	322.906	1.92	2.24
	T_{c2}					
	T_{c3}					
	T_{c4}					
	T_{c5}					

Table 12: Validation of case 1 - Comparison of the average temperature error on the level of the adiabatic section and the condenser section.

Sections	Positions	T_{exp}	$T_{Numeric\ Fadhl}$	$T_{Our\ Simulations}$	Fadhl's errors %	Our errors %
Adiabatic	T_a	327.45	362.41	371.13	10.68	13.33
Condensor	T_{c1}	320.55	329.54	323.83	2.8	1.02
	T_{c2}	318.85	326.54	317	2.41	0.58
	T_{c3}	317.95	325.95	315.72	2.52	0.70
	T_{c4}	317.05	325.64	315.92	2.71	0.35
	T_{c5}	315.95	327.13	321.77	3.54	1.84

Table 13: Validation of case 2 - Comparison of the numerical temperatures and the relative errors assesment

Fig. 47 summarizes the validation of the previously presented results in Tabs. 11, 12 and 13. Our numerical results are in good agreement with the literature results. Hence, the two-phase VOF model, as well as the *Lee* model which describes the mass transfer are validated, and they can be used to numerically assess and optimize a new thermosiphon geometric shape.

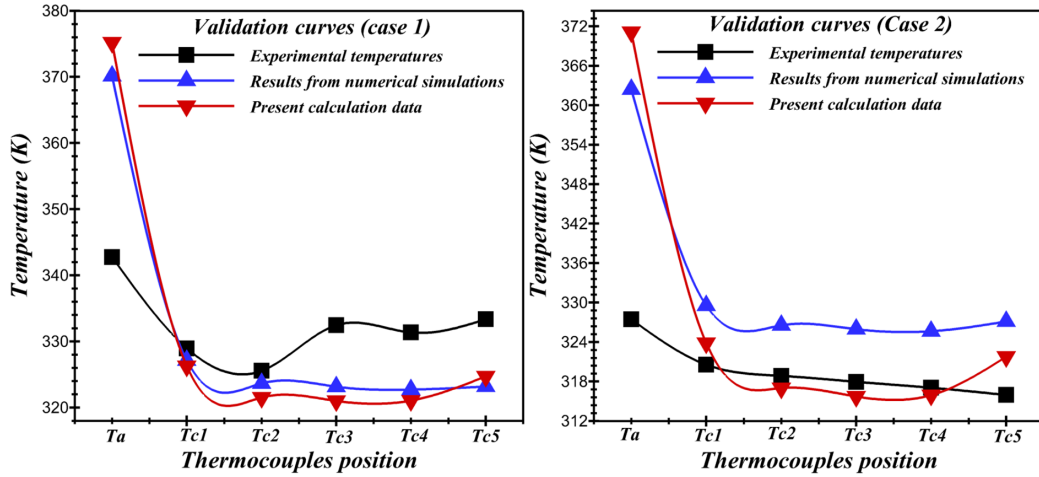


Figure 47: Comparison of temperatures evolution for different positions.

According to Fig. 10, the temperatures results present good agreement as a results the Ansys *Fluent* code used to model the two phase change (liquid-vapor) at the thermosiphon is validated.

The evolution of the vapor fraction on 50 s is presented in Fig. 48. At $t = 0$ s liquid and vapor phases are separated by an interface. After one second, the first bubbles of vapors start to be created at the internal wall of the evaporator section, where the heat flux was applied. The rise of the vapor bubbles is fast which disturbs the balance of the liquid phase. At $t = 5$ s we notice the detachment and an abrupt separation of a few drops of water, because of the rise of the vapor bubbles of more important size towards the adiabatic section. We also notice that the bubbles begin to form from the bottom of the thermosiphon.

The quantity of vapor increases at the evaporator which enrich the condenser with heated vapor. The amount of water decreases in the evaporator, but it is compensated by the liquid film coming from the condenser by gravity through condensation phenomenon. This numerical model is used to conduct the parametric studies in the following section.

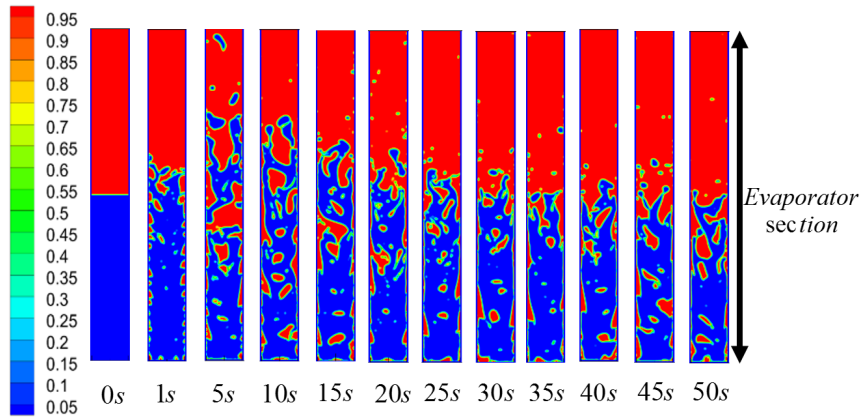


Figure 48: Case 1 - The vapor fraction contours evolution as a function of time.

5.5. Assessed geometries and computational mesh

A parametric study is conducted to improve the heat transfer at the condenser section. Two different geometries were proposed for investigations purposes: a smooth condenser and a condenser with fins configurations. This new design is characterized by the tilt angle which separates the adiabatic zone from the condenser, the used tilt angle is 60° . Fig. 49 represents the geometries which are the subject of the parametric study. Dimensions of each configuration are indicated. The quarter's evaporator section is filled with the heat transfer fluid, water was used in our case.

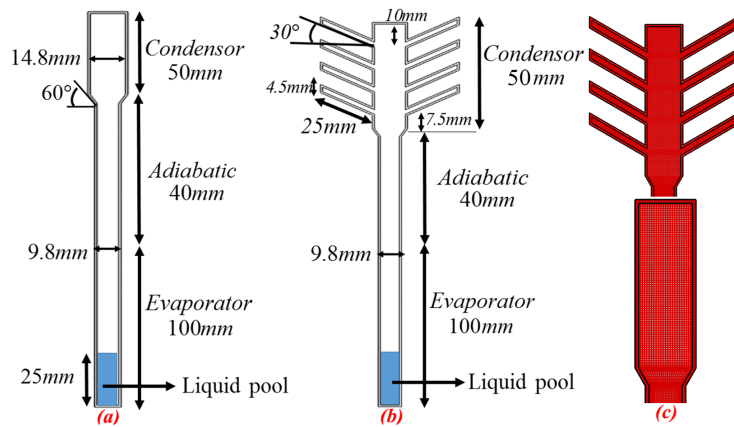


Figure 49: Thermosyphon new design. (a): Smooth condenser. (b): Condenser with fins. (c): Structured mesh grid of the condenser section of the studied configurations (smooth and with fins).

5.6. Boundary conditions and CFD solution procedure

A mesh sensitivity analysis was conducted in order to provide the grid-independency of the simulation results. The number of elements was increased from 58000 and 52000 to 68000 and 62000 for the cylinder with fins and smooth cylinder configurations respectively. In addition, great attention has been provided to the refinement of the internal walls of the evaporator, adiabatic and condenser sections, as well as the two interfaces which connect the middle section (adiabatic) with the two sections concerned by evaporation and condensation. The aim of these meshing strategy

refinements is to properly describe these zones and to ensure liquid drops and vapor bubbles appearance throughout the thermosyphon.

No appreciable variation at the condenser section, for both the studied configurations (smooth and cylinder with fins) in terms of mean temperature value (always lower than 2%) was measured, ensuring the suitability of the present meshes. As a conclusion, a sensitivity analysis on the domain size was first carried out and the mesh independence check has been performed. It was found that 58000 and 52000 for the cylinder with fins and smooth cylinder configurations respectively would describe properly and with accuracy the simulations ahead.

The last two configurations suggested in the previous section are subjected to the following boundary conditions: the evaporator section is heated with a flux $Q_{evap} = 172.87$ W. The adiabatic section is insulated $Q_a = 0$. The condenser section is subjected to a constant temperature condition $T_c = 25^\circ C$. This presupposes that the temperature of the fluid crossing the exchanger is $25^\circ C$.

The modeling is two-dimensional and VOF model previously validated was also used (Mathematical model, section 2). For the smooth condenser configuration, a time step of $10^{-4}s$, $2 \times 10^{-4}s$ leads to convergence. On the other hand, the configuration with fins requires a time step between $5 \times 10^{-5}s$ and $10^{-4}s$ so that the solution converge. This is due to the geometrical complexity which disturbs the flow of the heat transfer fluid.

5.7. Flow visualization of CFD simulation results

The time required to simulate 30s of the physical phenomenon of one configuration lasts 28 days, knowing that the parallel computing was launched on a Z600 workstation (16 CPUs, 32GB RAM).

A set of parameters to quantify the phenomenon of the phase change which occurs inside the thermosyphon were defined: Nusselt number, heat transfer coefficient, mass transfert rate and the heat flux transferred by the condenser section.

Nusselt number (Eq. (71)) is defined at the inner wall of the condenser section to characterize the heat transfer with the vapor which goes up to the head of the thermosyphon. Fig. 50 presents its evolution for the studied configurations: Smooth condenser and Condenser with fins. It was monitored for each time step in order to assist the comprehension of its curve evolution.

$$Nu = \frac{hL_c}{\lambda} \quad (71)$$

$$h = \frac{Q_c}{T_p - T_\infty} \quad (72)$$

Where Nu is the Nusselt number, h is the heat transfer coefficient, L_c is the characteristic length (the length of the condenser section) and λ is the copper thermal conductivity. An increasing Nusselt number means that the heat transfer between the inner wall of the condenser and the vapor is important. The vapor begins to condense after releasing its latent heat. Therefore, the condensed liquid film goes down again by gravity crossing the adiabatic section to be added to the existing fraction in the evaporator section. The internal lateral surface of the condenser is thus cooled and the Nusselt number decreases.

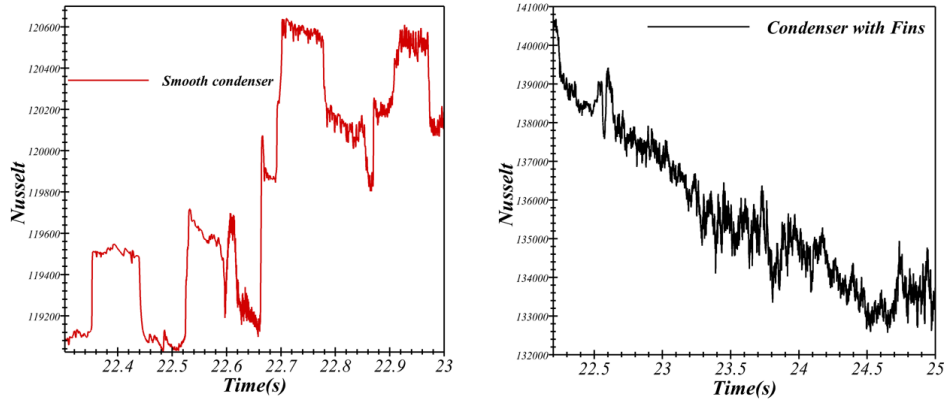


Figure 50: Nusselt number for both configurations. On the left: Smooth condenser. On the right: Condenser with fins.

The geometry of the studied configurations affect Nusselt number evolution. For the Smooth condenser, Nusselt function takes the shape of a sawtooth with an increasing amplitude. Over the interval $[22.3s; 22.66s]$ the mean maximum amplitude is 119750. From $t = 22.66s$, Nusselt number increases to reach 120600. Two teeth having as limit this value will be alternated on the interval $[22.66s; 23s]$.

As presented in Fig. 50, the Nusselt function of the configuration with fins lasts 2.8s. The results were monitored starting from $t = 10s$ to make sure that the initial conditions will not affect the previously defined performance indicators. Nu was monitored in the previous case *i.e.* at the end of each time step. The figure is presenting a set of peak and fluctuations which gives an idea on the frequency of condensation. At $t = 22.2s$, Nusselt number associated to the configuration with fins is higher than that of the smooth configuration ($Nu_{Fins} = 140600 > Nu_{Smooth} = 117176$). Nusselt associated to configuration with fins continues to decrease until reaching 113800.

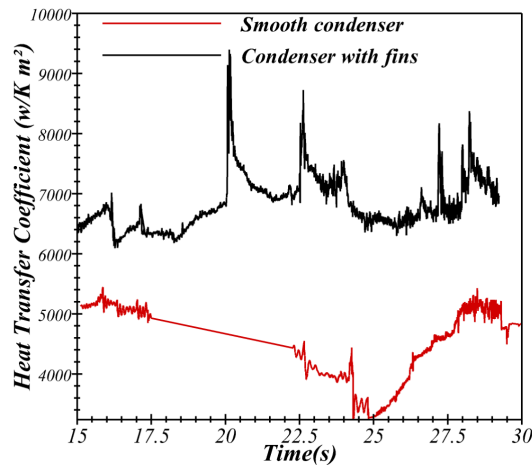


Figure 51: Evolution of the heat transfer coefficient for both configurations as a function of time.

Fig. 51 shows the evolution of the heat transfer coefficient (Eq. (72)) for both configurations as a function of time. It was monitored at the internal section of the condenser. It provides an idea about the exchange that occurs between the vapor phase and the inner surface of the condenser

cooled by the imposed temperature. We notice that $HTC_{Fins} > HTC_{Smooth}$ throughout the interval [15s; 30s].

The HTC presents peaks and fluctuations for the studied configurations. The number of peak of the configuration with fins is higher than that of the smooth configuration. At $t=20s$, the effect of the fins is clear, because HTC increases up to $9200 W/Km^2$ while for the smooth configuration HTC is decreasing and has reached as mean value $4600 W/Km^2$. The heated vapor is trapped at the fins which enhance the released time of its latent heat.

Fig. 52 presents the evolution of the heat flux transferred by the condenser section according to time for the smooth condenser and the condenser with fins.

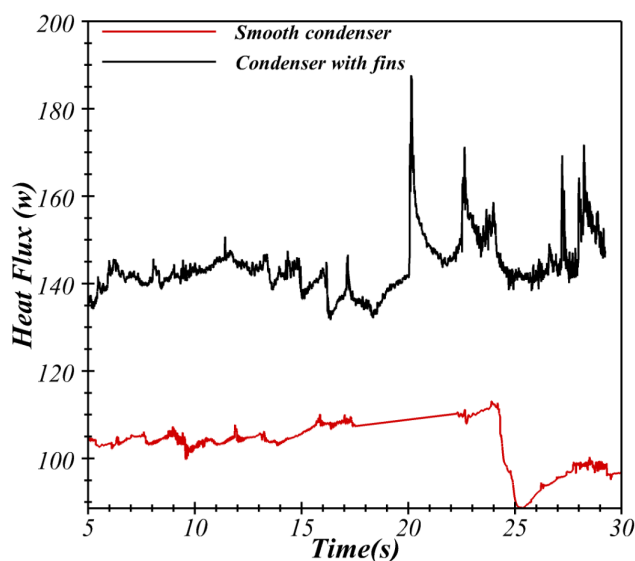


Figure 52: Evolution of the heat flux transferred by the condenser section according to time.

The average flux transferred by the smooth condenser configuration equals to 118.69 W. While the average flux transferred by the fin's configuration equals to 146,45 W. The efficiency of the closed heat pipe is given by the Eq. (73) [176].

$$\eta = \frac{Q_c}{Q_{in}} \quad (73)$$

The efficiency of the smooth configuration is 68,65%. The efficiency of the configuration with fins is 84,71%. To conclude, the thermal performances of the first configuration were optimized by a percentage of 16.05%.

Fig. 53 presents the evolution of the mass transfer rate as a function of time at the condenser section for the studied configurations. MTR can be defined as the amount of evaporated or condensed mass. It was monitored on the evaporator and the condenser sections. The following notations were used:

- A negative sign is assigned to the condensed mass
- A positive sign is assigned to the vaporized mass

The MTR associated to fins configuration is higher than the MTR associated to the smooth configuration at the condenser section ($MTR_{avg\ Fins} > MTR_{avg\ Smooth}$). The use of the fins increases the mass flow of the condensed vapor. Therefore, the heat flux transferred by this configuration is definitely higher than the smooth one.

MTR was also monitored for each step time. In fact, it is a variable quantity which has peaks of small frequencies. The average vaporized value at the condenser section is almost identical at the interval [11s; 13.4s].

At $t = 15.15s$, MTR_{Fins} decreases sharply and then fluctuates around the average value equal to $0.2kg/s/m^3$ which is below the averaged MTR_{Smooth} equal to $0.8 kg/s/m^3$. The actual result could be explained by the fact that the configuration with fins is condensing the amount of vapor that turns into liquid water film. The liquid film is going to be mixed with the pool boiling volume fraction and will decrease its temperature. As a result, MTR_{Fins} would be less than MTR_{Smooth} on the interval [15.15; 18.50s].

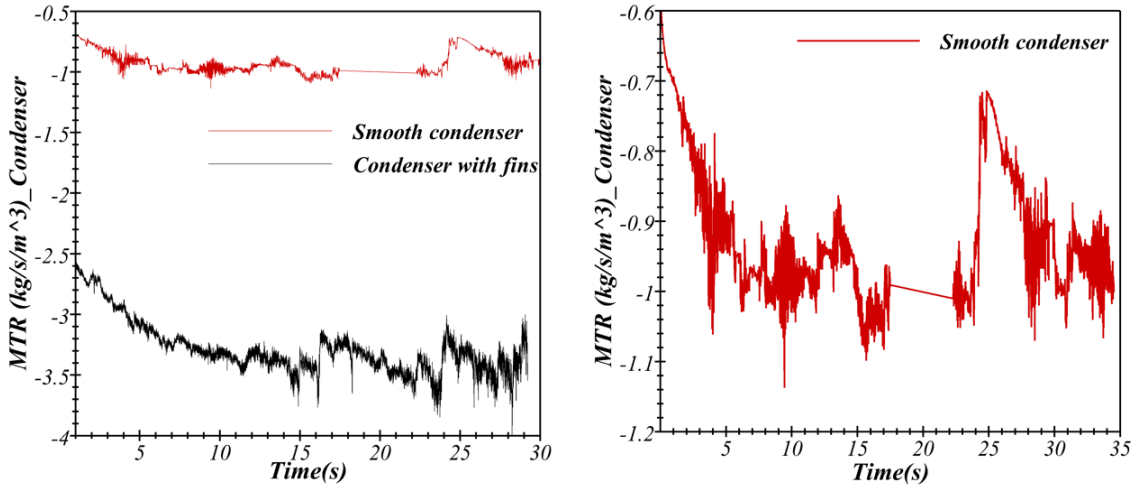


Figure 53: Evolution of mass transfer rate at the condenser section as a function of time. On the left: both configurations are presented. On the right: Scale enlargement of the MTR variation in the smooth condenser.

Fig. 54 presents the static temperature contours evolution over a period of 30 s for the smooth condenser configuration. At $t = 0s$, the vapor temperature field was initialized slightly close to the saturation temperature $T_{SAT} 373.16K$, while the liquid temperature was initialized slightly lower than the saturation temperature $373.14K$. Thereafter, the vapor produced on the evaporator section goes up to reach the condenser section. The vapor releases its latent heat to be transformed into a thin sliding liquid layer which adheres the walls of the condenser, the adiabatic sections and ended up joining the section of the evaporator. From $t = 10s$, the growth of two circular areas at low temperature $290K$ is noticed at the condenser bottom section. They characterize the suspension of the droplet liquid coming from the condensation of the vapor as presented in Fig. 56

The maximum temperature which is reached at the end of 30 seconds is located at the adiabatic section $T = 390K$. The profile of the temperature contours is similar to that of a candle whose shape is affected by the low temperature applied at the condenser section.

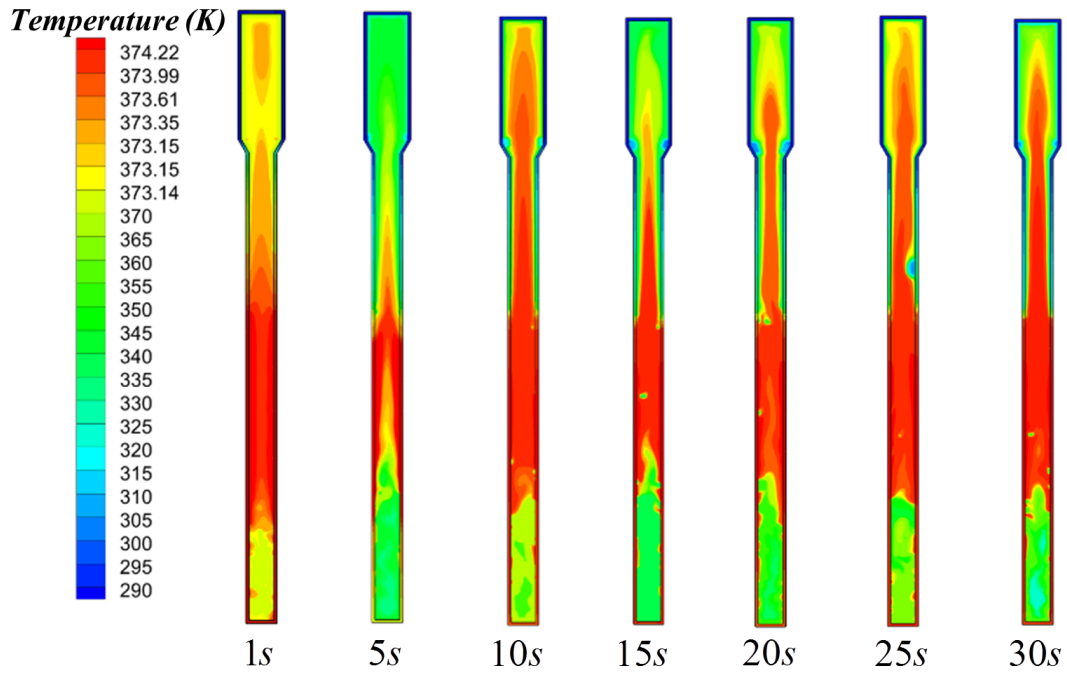


Figure 54: Evolution of the static temperature contours (K) over a period of 30 s - Smooth condenser.

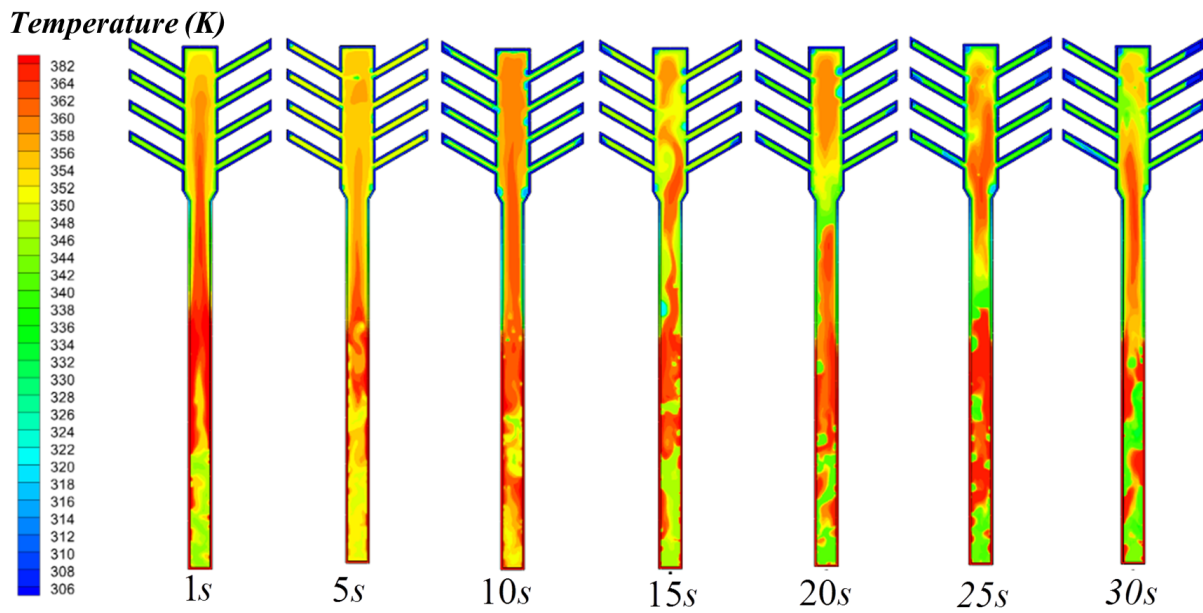


Figure 55: Evolution of the static temperature contours (K) over a period of 30 s - Condenser with fins.

Fig. 55 shows the evolution of the static temperature contours for fins configuration over a period of 30 s. The shape of the static temperature contours are different from those of the smooth configuration, and their values on the condenser section level are lower to them. According to a comparison between Figs. 54 and 55, the heated vapor extent at both adiabatic sections is

different. Indeed, the extent of the vapor is more important on the smooth configuration than that of the configuration with fins. The expanded form of the ascending vapor towards the head of the condenser section is more disturbed by the condensed liquid film going down by gravity towards the heated liquid pool. The effect of liquid and vapor phases interactions in Fig. 55 at $t = 15s$ and $t = 30s$ is noticed. The growth of several blue color zones of the condensed liquid with are different. They are characterized by low temperature $306^{\circ}K$. It is more common to see them on the upper end of the fins ($t = 20s, t = 25s$ and $t = 30s$), also at the angle between the head of the adiabatic section and the bottom of the evaporator section ($t = 5s$ and $t = 10s$).

The vapor bubbles start to appear in the first seconds of the heating process. In fact, they gain in size and disrupt the shape of the liquid pool. The surface tension between the two phases causes a detachment of a few liquid drops ($t = 10s, t = 20s$) which eventually ends up joining by gravity the liquid pool volume heated on the level of the evaporator section. The first condensed drops appear at the bottom of the condenser section starting from $t = 5s$. Indeed, it starts to gain in volume as indicated at $t = 10s$. A sliding drop at the adiabatic section is presented as presented in $t = 25s$. The process of condensation is cyclic and the vapor fraction contours at $t = 30s$ is similar to that of the instant $t = 5s$.

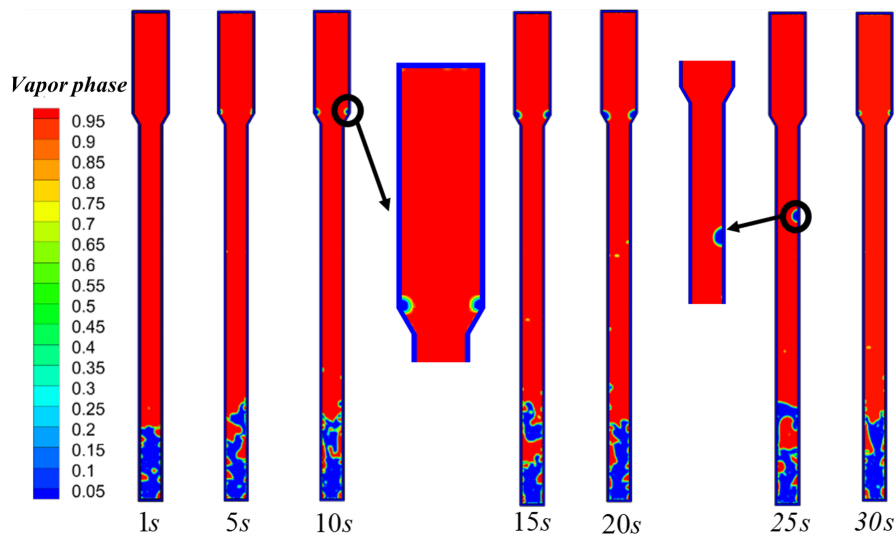


Figure 56: Evolution of vapor fraction contours over a period of 30 s - Smooth condenser.

Fig. 57 is presenting the evolution of the vapor fraction contours over a period of 30s for fins configuration. The condensed mass is more important than that provided by the smooth configuration. It is a difference noticed after comparing the two liquid fractions evaluated at $t = 10s$ on both Figs. 56 and 57. The contours taken at $t = 15s, t = 20s, t = 25s$ and $t = 30s$ provide an idea of the shape of the condensed liquid and its downward momentum that adheres the walls of the thermosyphon. The internal volume of the fins is a volume that promotes vapor condensation. The contours at $t = 30s$ show the condensation of a substantial portion of the vapor which has slid on the inner wall of the fin to join in the first place the area connecting the adiabatic section to the condenser section and thereafter the heated liquid filling the evaporator quarter section ($t = 25s, t = 30s$).

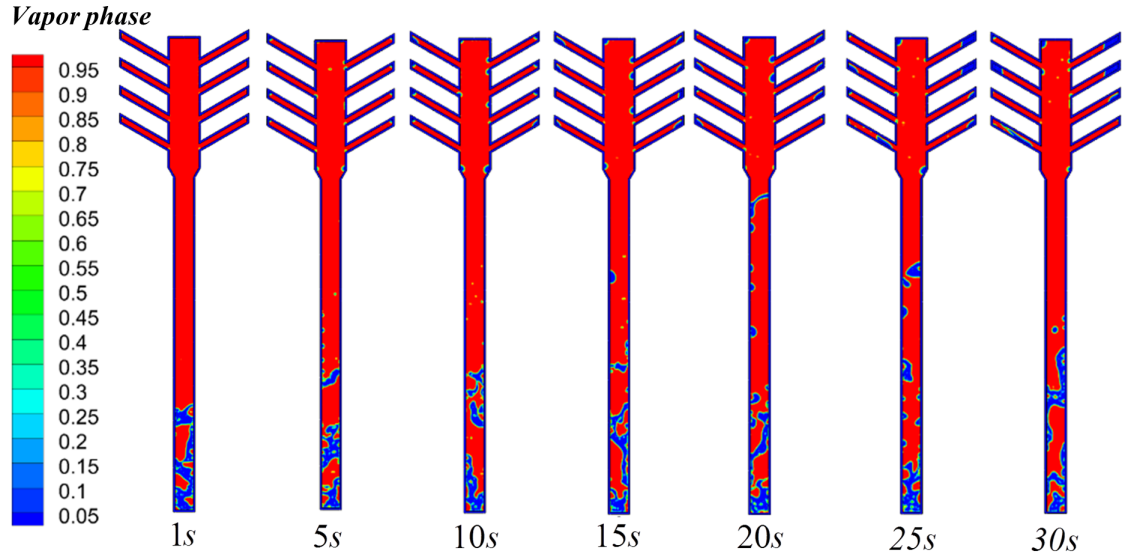


Figure 57: Evolution of vapor fraction contours over a period of 30 s - Condenser with fins.

Fig. 58 presents the evolution of the vertical velocity contours over a period of 30s for the smooth condenser. A fast rise of the vapour phase 0.34 m/s which become more important in particular with a speed of 0.8 m/s as the heating time progress. The vapour phase crosses the adiabatic section with a speed of 0.45 m/s to fit into the condenser section. The temperature of the vapor trapped in the condenser section decreases and it forms a thin liquid film layer which goes down towards the evaporator with a speed of 0.18 m/s. The liquid pool is disturbed by the fast rise of the vapor bubbles adhering the internal wall of the evaporator.

The negative values of the vertical velocity contours (Fig. 58) indicates:

- The return of the condensed liquid to the section of the evaporator by gravity effect.
- The return of the detached and propelled liquid drops because of the fast rise of the vapor bubbles coming from the heated liquid pool.

Fig. 59 presents the evolution of the vertical velocity contours over a period of 25 s for the fins configuration. From the first second, the vapor phase is ascending toward the condenser section with a speed between 0.35m/s and 0.65m/s . From the fifth second a blue area becomes dominant at the condenser section. It is characterized by a ranging speeds between 0.1m/s and 0.35m/s. We explain this by the falling condensed liquid. The two instants $t = 10s$ and $t = 15s$ show that condensation and evaporation is a continuous cyclic process. Indeed, the velocity contours illustrated at $t = 5s$ show that condensation overrides evaporation and vice versa from $t = 10s$, where we see the rise of bubbles of vapor from the section of the evaporator to the condenser section and then they are trapped in the fins.

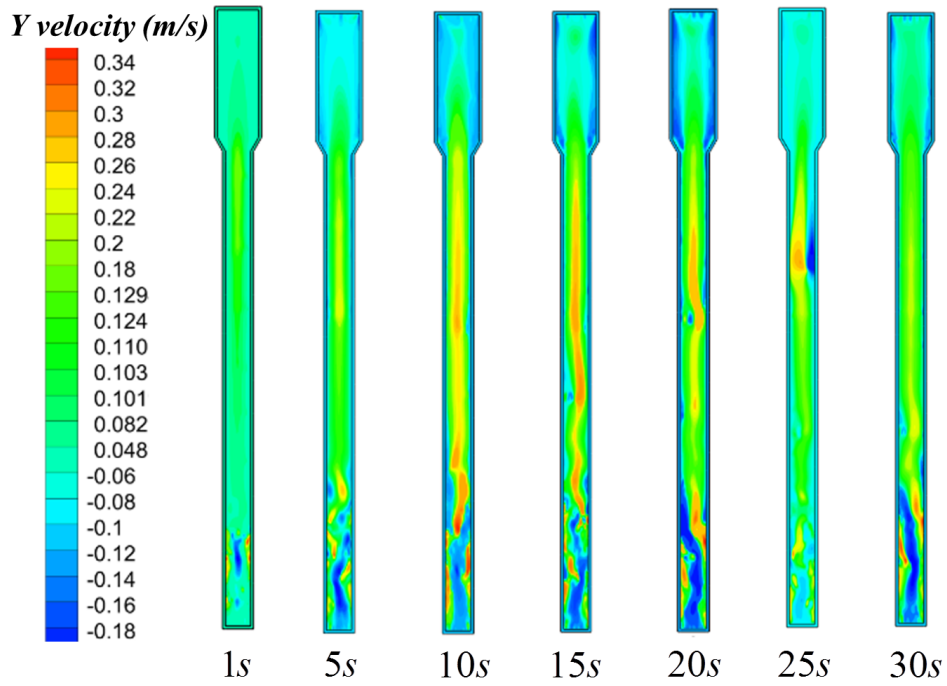


Figure 58: Evolution of the vertical velocity contours (m/s) over a period of 30 s - Smooth condenser.

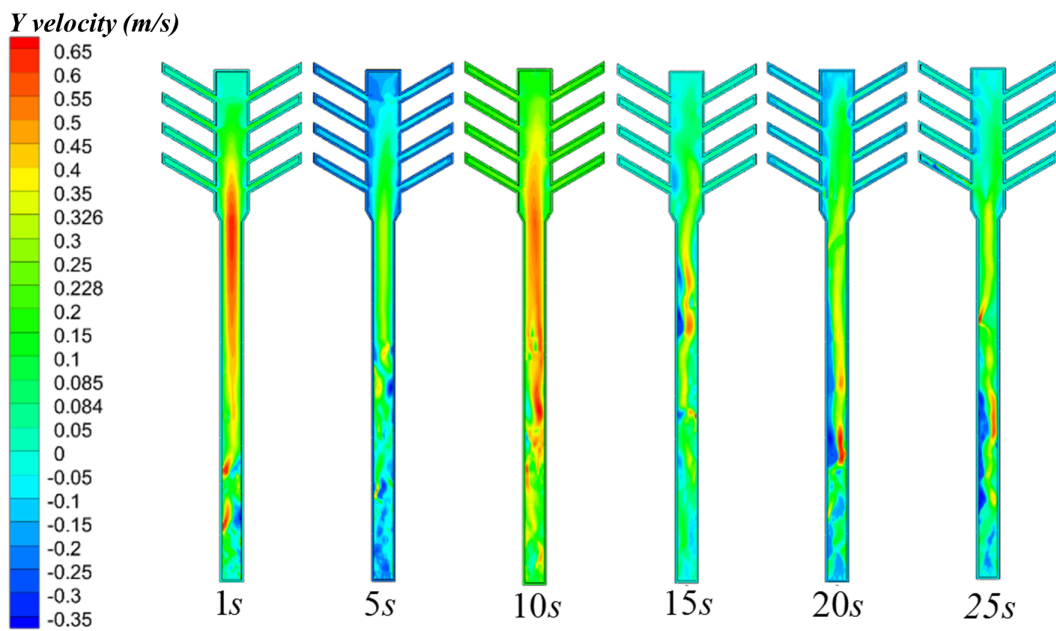


Figure 59: Evolution of the vertical velocity contours (m/s) over a period of 25 s - condenser with fins.

5.8. Conclusion

This chapter investigates the two-phase VOF and *Lee* models validation. Thus, those numerical models were used to assess mass, energy transfer, as well as the overall efficiency of the

thermosyphon. The models validation was reached from the experimental and numerical results available in the literature. The local temperature in two sections and their average temperatures were our validation indicators. In this model, the ascending vapor speed to the condenser and the velocity of the liquid film going down to the evaporator filled with the heated liquid pool were quantified. A numerical framework for analyzing two different configurations of the thermosyphon were conducted which are integrated into the internal exchanger of the vacuum tube solar collector panel. Indeed, two different geometries were numerically investigated mainly by the shape of the head of the condenser (the smooth condenser, and the condenser with fins). Moreover, a set of performance indicators were defined to assess the energy transfer velocity between the evaporator and the condenser sections (temperature contours, phase volume fraction, contours of vertical velocity, Nusselt number, heat transfer coefficient, mass transfer rate, the flux transferred by the condenser section and the efficiency of the thermosyphon). It was found that the efficiency of the closed thermosyphon was improved to 16.05%, to reach a new performance of 84.71% thanks to the tilted fins integrated on the lateral surface of the condenser section.

5.9. *Chapter IV: Thermo-mechanical strength analysis for energy storage improvement of horizontal storage tanks integrating evacuated tube collectors*

5.10. *Introduction*

In the present chapter, a two dimensional axisymmetric Finite Element Method (FEM) is developed to carry out a thermo-mechanical analysis on a horizontal storage tank intended to storage hot water for a domestic application. The purpose of these numerical simulations is to assess the thermo-mechanical behavior of a horizontal tank with evacuated tube collectors, and consequently to suggest a new design which ensures an optimum mechanical strength according to severe applied operating conditions in terms of temperature and pressure. To achieve this goal, a thermo-mechanical 1-way sequential coupling has been used as a solving method. The physical model suggested in this study and the simulations procedure was described under detailed assumptions. In fact, the main hypotheses in the current formulation were the thermo-elastic behavior of the tank's materials and the steady state assumption analysis.

This chapter outlines three studies that were performed to extend the lifespan of the horizontal storage tank, through the definition of a suitable material and an optimal design. The main conclusions of the assessment are that the optimal configuration which avoid the appearance of the stress concentration zones is the configuration (c), where $R_i = 11$ mm and $R_e = 14$ mm, because the stress on the tank's shell was better applied. Moreover, the effect of the material's selection was carried out, and it was found that stainless steel is the optimal material. Last but not least, a set of simulations were conducted to investigate the tank shell thickness on which the thermo-mechanical constraints were applied. The thickness $t = 2$ mm was presenting an optimal mechanical behavior with regard to the studied operating conditions.

Evacuated Tube Solar Collectors (ETC) have become one of the main challenging technologies to heat water for individual social/grouped housing [177, 50]. A series of heat pipes inserted in the evacuated tubes are integrated in the horizontal tank in order to heat the stored water [178]. Several problems occur with the storage tank which use heat pipes as a heating device, especially in the countries where solar irradiance rate is high, as it is the case for North Africa's and Middle East and North Africa (MENA) countries [179]. Consequently, customers lose confidence in this renewable solar energy technology because the mechanical strength of the tank is quickly degraded by the cracks which appear at the welds remaining the main cause of its rupture. Besides, thermal expansion is also a frequent type of strain that is unpredictable. In fact, there are of course other factors according to the nature of the considered loads such as moisture, as well as material corrosion [180]. As a result, customers substitute solar water heaters by electric or gas heating devices two polluting energy sources [179].

The thermomechanical interaction is a branch of the mechanics which treats regarding the coupling methodology the thermal effect on the structural behaviour [181, 182]. The FEM is an effective tool for this purpose, because the approach based on the classical theories only give the necessary information for the preliminary design [183, 184].

Several studies were published regarding the multi-physical problem, particularly thermo-mechanical studies. According to Lie et al. [185] the inbuilt finite element method (FEM) available in the commercial software Ansys can be used to solve the coupling between the heat transfer and the stress model. In fact, they worked on the thermoelastic and the heat transfer analysis of a 3D model of a steel composite stove which was validated against experimental measurements. They

accessed to additional simulation results such as the distribution of the temperature, the strain and the stress fields. Thereafter, they started their own optimization study without conducting experimentation. Moreover, Huang et al. [186] studied the thermomechanical behavior of a Kambara reactor with various anchors which operates at extremely high temperatures throughout a coupled thermo-fluid stress analysis. They used CFX solver and finite element method (FEM) to simulate and analyze its thermal fatigue. They accessed to important results such as: the flow field, temperature profiles, thermal stress, through numerical simulations, which were in good agreement with the available empirical data.

An other FEM using the commercially available Ansys software was investigated by Milan Zmindak et al. [187]. They analysed a concrete structure that is surrounding a nuclear reactor through a finite element thermo-mechanical transient analysis. They performed their simulations by means of the FEM using the commercially available Ansys software. More recently, Wang et al. [188] conducted numerical finite element calculation to study thermal stress and structure optimization of a neck tube with vertical cryogenic insulated cylinders subjected to thermo-mechanical loads using Ansys tools. Furthermore, using 2D simulations, Galantucci et al. [189] studied a hot rolling process with an approach based on a thermo-mechanical analysis using a finite element method (FEM-Ansys 5). Their results showed that the design could be improved through an iterative parametric procedure which provides the temperature in the roll, the plate, the stress and the strain fields using a transient analysis.

An other nonlinear thermoelastic model was set by D. Riedlbauer et al. [190] to simulate the thermomechanical behaviour in the selective laser melting process. In addition to this, Ansys software was used by Belhocine et al. [191] to conduct a 3D fully coupled thermo-mechanical simulation, so as to assess the stress fields, strain and temperature distribution of the ventilated vehicular disc which is subjected to the pads pressure. It is important to know that Abaqus is a well known software which is used to model multi-physics problem. In fact, Abaqus which is also a FEM software was used by John A. Shaw [192] to simulate the localized thermo-mechanical behaviour in a NiTi shape memory alloy.

Experimental studies on a metal hydride hydrogen tank were carried out by Souahlia et al. [193] to assess the performance of the storage time and storage capacity by varying two parameters, namely the supply pressure and the cooling temperature of the hydride bed. According to Yan et al. [194], the safety of precipitation strengthened austenitic stainless steels which is used to store hydrogen in tanks is of great interest. In fact, they assessed the cracking and the safety factor of austenitic stainless steel during charging hydrogen inside the storage tank under constant load.

Another technical assessment with regard to compressed hydrogen storage tank systems intended for automotive applications was performed by Hua et al. [195]. In fact, they assessed the performance, besides to the high-volume manufacturing cost of the compressed hydrogen tanks by applying design pressures of 350 bar and 700 bar, which were considered as sufficient to achieve the Well-to-Tank (WTT) efficiency target.

It is concluded from the review above, that up to now, several literature studies have actually relied on the thermo-mechanical simulations, but few of them have focused on the numerical thermo-mechanical assessment of the horizontal storage tank intended to store hot water for domestic application.

The present work develops a two dimensional axisymmetric FEM numerical simulation of a horizontal storage tank under thermo-mechanical loads. It is interesting to note that Ansys is a platform used to solve the thermo-mechanical formulation and to test the strength of the studied

storage tank, since it can solve multi-physical problems [196, 197, 198]. The sequential 1-way coupling of the thermo-mechanical solver integrating the thermal (Steady-State Thermal) and the mechanical modules (Static Structural) were used. The fatigue, creep and plastic strain are not treated but the assumptions retained are detailed and developed further.

This study aims to determine the factors to improve in the tank design model in order to extend its life span, because it is an important device ensuring solar energy storage. Three studies were performed. The first study is a geometrical optimization. In fact, the shape of the storage tank's dished bottoms was maintained as flat and the curvative radius (R_i) and (R_e) were varied to avoid the appearance of the stress concentration zones. The second study was conducted to predict the material effect and hence to facilitate its choice. Indeed, four different materials were assigned to the tank's shell, namely standard steel, stainless steel, aluminium alloy and the copper alloy. Last but not least, the third study presented a set of simulations to investigate the tank shell thickness on which the thermo-mechanical constraints were applied with regard to the studied operating conditions.

A 3D model of the horizontal tank integrating a series of 10 vacuum tubes solar collectors is represented in Fig. 60. The cylindrical part was modeled during this study were the thermo-mechanical stresses were applied.

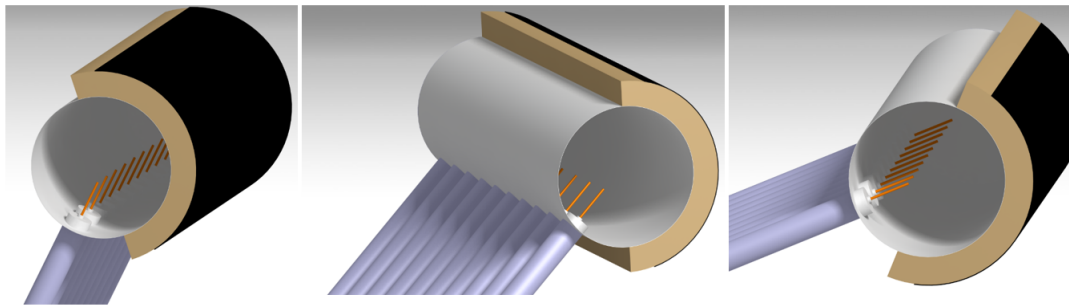


Figure 60: Three-dimensional model of the studied storage tank integrating a series of 10 evacuated tubes with heat pipes.

5.11. Material selection

The quality and the type of the material used to manufacture a domestic hot water storage tanks Domestic Hot water (DHW) cylinder has a high impact on the corrosion resistance and therefore its lifespan. Actually, hot-water tanks are made of enamelled steel (enamel), stainless steel, and less and less of steel coated with copper [199].

The tank material is selected with an appropriate corrosion protection depending on the quality of water to be stored, because it is an important factor which determines its longevity. However, according to the areas, catchment wells, water routing, treatments..., the composition and the corrosive properties of water vary from one place to another, leading to a choice between one of the three types of protection against corrosion: copper, enamel or stainless steel used in hot water storage tanks.

The properties of water must meet a number of requirements, in particular medical requirements, but also pH, which must be within a defined range, and which will affect its aggressiveness. The corrosive properties of water depend on the proportions of the substances that compose it and the way in which they interact with each other. Only a water analysis is going to define with accuracy the best protection against corrosion [200].

Several factors affect water:

- PH value: also known as water acidity. It is the measurement of the amount of hydrogen ions contained in water. Water with low pH is aggressive and would dissolve metals.
- Water Hardness: indicates the amount of calcium and magnesium present in water. The hard waters cause a deposit of limestone on the heating surfaces.
- Aggressive carbon dioxide: it is the amount of free carbon dioxide with corroding properties; The presence of carbon dioxide at low pH and/or hardness values makes the water aggressive.
- Chloride load: a high chloride load can generate aggressive water, especially if it is calcareous.
- Conductivity: measures the composition of water in dissolved salts such as chlorides and sulphates.

Therefore, it is appropriate to select the suitable material for solar hot water storage tanks depending on the quality of the available water.

1. Stainless steel:

It is the most upmarket type of storage tanks. The stainless steel hot water tanks guarantee a remarkable corrosion resistance and guarantee a perfect hygiene even in the most demanding environments. Its surface state is very homogeneous and remains effective even after many years of use, requiring no maintenance, unlike enamelled steel tanks that require a regular replacement of the magnesium anode [201].

The quality of the stainless steel used has a great effect on the corrosion resistance of a hot water tank. It is preferable to choose an austenitic stainless steel (21% chromium and 7% nickel), a family of steels to which chromium is added. In excess of 11% in solution, it causes the appearance of protective layer of chromium oxide that imparts to these steels their inoxidability. There are also ferritic steel grades containing 18% chromium and 2% molybdenum, but almost no nickel. Steel is ferritic, hence it is not sensitive to mechanical corrosion, which means it is resistant to high concentrations of chlorides [202].

Besides the choice of stainless steel, the different stages of the tank manufacture are important. After welding a hot water tank, it is important that the surface which will be in contact with water have a homogeneous composition. For this purpose, a surface scouring is carried out which recreates a uniform film of oxide over the entire internal surface of the hot-water tank. However, even with a stainless steel tank, corrosion may occur. In fact, pitting corrosion is generally not due to a heterogeneity of the material but to the accidental presence of metal dust which, in a damp environment, forms an electric battery. The surface of the steel then forms the cathode and corrodes [203].

2. Enamelled steel:

Enamelled steel hot water tanks are widely available on the market, because they are less expensive than stainless steel tank. Enamel is a smooth material with vitreous properties, applied to the interior of the hot water tank by heating [204]. The vitreous enamel coating provides a "hygienic surface", studies have shown that enamel does not constitute an incubation place for the bacteria [205].

The enamel takes its form and spreads over the steel surface through a heating process at a temperature of about 860°C [204]. However, after treatment, the enamelling surface always

contains microscopic pores which can leave the tank steel surface in contact with water and cause corrosion points. To prevent corrosion, a protective anode is placed inside the enamelled steel hot water tanks. The anode is generally composed of a magnesium-based alloy. Since magnesium is a less noble metal than steel, the anode is "sacrificed" (hence the term sacrificial anode) to prevent corrosion of the steel electrochemically. The pores of the enamel layer are thus filled with calcium and magnesium compounds.

The magnesium anode is consumed at a speed that depends mainly on water quality. Therefore, the anode must be checked regularly for its lifetime and replaced if necessary.

Alternatively, a tank equipped with a titanium anode must be selected, which is permanently connected to a generator which imposes an electric current of a few volts to capture certain minerals naturally present in water (magnesium and calcium) to precipitate them on the walls of the tank and thus to protect it. This system is often referred as "ACI" (Anode to Current Imposed) or "APA" (Electronic Protection Anode) [206]. This protection offers the enormous advantage of lasting in time, but also requires a water rich in magnesium and calcium to be effective.

Finally, there is a dynamic protection which combines the advantages of the magnesium anode and the titanium anode: it is the "hybrid" anode. It is a titanium anode coated with magnesium. Even if the water contains very little magnesium, as soon as the tank is put into service, the current emitted by the anode projects the protective magnesium contained on the anode onto the micro porosities of the enamel covering the tank. This protective barrier is then maintained throughout the life cycle of the tank, thanks to the current applied by the titanium anode. This dynamic protection extends the life of water heaters up to twice as long the water is aggressive.

Hot water storage tanks in enamelled steel are generally considered to be less robust than their stainless steel counterparts [207].

3. Copper:

Lastly, there are a few steel hot-water tanks on the market which are completely covered with a copper layer of 0.4 mm to 0.7 mm thick, welded with argon as a protective gas. The steel tank is resistant to water pressure, while the copper sheet covering it completely prevents corrosion. As a semi-noble and natural metal, copper is resistant to most types of water, including most distribution waters with a minimum pH value. Hot water tanks protected against corrosion by copper, such as stainless steel hot water tanks, do not require maintenance since they do not need protective anode [208].

Copper also has other advantages. In fact, it is an ideal recycling material that can be regenerated many times. Copper is the best choice of material to reduce the risk of legionella, its anti-microbial effect keeps water healthy [209]. Moreover, hot water storage tank made with copper may be used without restriction with potable water, if the pH is greater than or equal to 7.4, or if the pH is between 7.0 and 7.4 and the TOC value (Total Organic Carbon) does not exceed 1.5 mg/l [210].

At low pH, or in the presence of high concentrations of chloride, copper tends to dissolve. Problems of aesthetic orders can then occur causing a discoloration of the porcelain of the sanitary and a greenish coloring of the blond hair in the shower. In case of high chloride concentration, pitting corrosion may occur, but the risk is inversely proportional to the calcium concentration [211].

The following recommendations are presented to assist the selection of the suitable material for the thermal storage tank manufacturing:

- Before choosing a material type for the hot water tank, it is preferable to know accurately the composition of water;
- The stainless steel hot water tank remains to be preferred if the water's quality is unknown and in order not to take risks that will affect the lifespan of the tank;
- It is necessary to privilege products from real tank manufacturers (on their internal line productions) and who master perfectly the enamelling techniques such as *Atlantic* or *Viessmann* [212];
- Finally, whatever the type of the retained tank, in certain cases, it will nevertheless be necessary to install a filter or a specific water treatment to obtain a water quality compatible with its equipment.

5.12. Thermo-mechanical coupling solving method

This section is an equation setting of the physical models solved by Ansys. Heat transfer, stress and compatibility equations and their coupling are written under detailed assumptions knowing that the FEM could be in direct or indirect way. Ansys software solves the thermal elasticity coupling problem with a sequential approach based on the finite element method. It is necessary to consider a coupled analysis which is an interaction between the thermal and the mechanical phenomenon of the storage tank model.

The methods used to solve the thermomechanical coupling are strong coupling [213], weak coupling [214], and 1-way coupling [197]. In this work, the thermo-mechanical 1-way resolution procedure was used. In fact, it is divided into two steps. In the first step, the temperature field is determined after the convergence of the solution towards the steady state. In the second step, the mechanical computation is initialized with the result previously determined (thermal strain) to get displacements at the mesh nodes and stresses at integration points of the finite elements.

We used the same 1-way coupling approach as [185, 215], because the interaction between coupled fields has a low degree of nonlinearities [187]. In the 1-way coupling approach [216], both of the thermal and mechanical phenomenon are correlated sequentially, which means that the thermal model results are considered as boundary conditions for the mechanical model [217].

The computational time of a fully coupled simulation is extensive and remains instable due to nonlinearities of each phenomenon [218]. Therefore, mechanical and thermal procedures in the simulation of hot water storage tank were solved separately. A nonlinear thermal analysis simulation that will be tracked sequentially by a linear static analysis were performed. The previously calculated temperature field is used as the initial thermal load which induced a thermal strain in the mechanical formulation problem.

5.12.1. Thermo-mechanical coupling equations

The mathematical approach formulated in this study is expressed according to the matrix equation which is coupling the vectors of structural load F and thermal load Q . Coupled thermo-elasticity is used to solve the heat conduction equation and thermo-elastic formulation. The 1-way coupling can be expressed by the matrix expression [74].

$$\begin{pmatrix} [M] & 0 \\ 0 & 0 \end{pmatrix} \cdot \begin{pmatrix} \ddot{u} \\ \dot{T} \end{pmatrix} + \begin{pmatrix} [C] & 0 \\ 0 & [C^t] \end{pmatrix} \cdot \begin{pmatrix} \dot{u} \\ \dot{T} \end{pmatrix} + \begin{pmatrix} [K] & 0 \\ 0 & [K^t] \end{pmatrix} \cdot \begin{pmatrix} u \\ T \end{pmatrix} = \begin{pmatrix} F \\ Q \end{pmatrix} \quad (74)$$

where T is the temperature vector, Q is the heat flux vector, u is the displacement vector, $[K]$ is the stiffness matrix, $[K^t]$ is the total conductivity matrix and $[C^t]$ is the specific heat matrix.

5.12.2. Simplifications and assumptions

Simplifying assumptions on the mathematical model were used to analyze the thermomechanical behavior of the tank. To start with, the heat transfer by conduction in the shell, as well as the mechanical analysis were considered stationary. A constant temperature is applied to the inner wall of the tank. The stagnation temperature at the heat pipe head can reach 270°C [156, 219]. This temperature is sufficient to change the phase of the initially stored water into a superheated steam. A very common occurrence in summer seasons in the countries with high sunlight rates [51]. For this reason, a temperature of 270°C [156, 219] was applied as thermal boundary condition. Moreover, the thermal conductivity of the materials was assumed to be constant in the (x,y,z) directions since the used materials are homogeneous. Finally, gravitational forces acting on the modeled system are neglected. Considering these assumptions above, the 1-way coupling model is expressed as follow (Eq. (75)).

$$\begin{pmatrix} [K] & 0 \\ 0 & [K^t] \end{pmatrix} \cdot \begin{pmatrix} u \\ T \end{pmatrix} = \begin{pmatrix} F \\ Q \end{pmatrix} \quad (75)$$

5.12.3. Heat transfer model

According to the stationary regime assumption, the temperature of the tank is determined through the resolution of the heat equation; while the thermal conductivity is independent of temperature. Heat transfer equation is expressed through Eq. (76). In addition to this, boundary conditions are added to the conduction equation to achieve a unique solution. In fact, they were detailed in the following section.

5.12.4. Thermal conduction equation

The governing equations for the steady thermal stress is expressed as follow.

$$\frac{\partial}{\partial x}(\lambda(T) \frac{\partial T}{\partial x}) + \frac{\partial}{\partial y}(\lambda(T) \frac{\partial T}{\partial y}) + \frac{\partial}{\partial z}(\lambda(T) \frac{\partial T}{\partial z}) = 0 \quad (76)$$

where λ is the thermal conductivity of the material $\frac{W}{Km}$.

5.12.5. Stress model

The stress model involves four equation systems written in a steady state assumption: equilibrium equations (Eq. (77)), kinematic equations (Eq. (80)), compatibility equations (Eq. (81)), constitutive equations (Eq. (82)).

Equilibrium equations

The stress tensor inside the computational domain satisfies the equilibrium equations (Eq. (77)).

$$\begin{cases} \frac{\partial \sigma_x}{\partial x} + \frac{\partial \tau_{yx}}{\partial y} + \frac{\partial \tau_{zx}}{\partial z} = 0 \\ \frac{\partial \tau_{xy}}{\partial x} + \frac{\partial \sigma_y}{\partial y} + \frac{\partial \tau_{zy}}{\partial z} = 0 \\ \frac{\partial \tau_{xz}}{\partial x} + \frac{\partial \tau_{yz}}{\partial y} + \frac{\partial \sigma_z}{\partial z} = 0 \end{cases} \quad (77)$$

σ and τ are the components of the stress tensor, where σ is the normal stress, and τ is the shear stress.

The computational domain pressure boundary satisfies Eq. (78).

$$\sigma_{ij}n_j = P_i \quad (78)$$

$$\begin{cases} \sigma_x n_x + \tau_{xy} n_y + \tau_{xz} n_z = P_x \\ \tau_{xy} n_x + \sigma_y n_y + \tau_{yz} n_z = P_y \\ \tau_{xz} n_x + \tau_{yz} n_y + \sigma_z n_z = P_z \end{cases} \quad (79)$$

where σ_{ij} is the stress tensor, $n_j = \{n_x, n_y, n_z\}$ is the normal vector at the surface where the pressure force is applied and $P_i = \{P_x, P_y, P_z\}$ is the surface force vector.

Kinematic equations

The strain vector is related to the displacements as expressed in Eqs. 80

$$\begin{cases} \epsilon_x = \frac{\partial u}{\partial x} & , & \gamma_{xy} = \frac{\partial u}{\partial y} + \frac{\partial v}{\partial x} \\ \epsilon_y = \frac{\partial v}{\partial y} & , & \gamma_{yz} = \frac{\partial v}{\partial z} + \frac{\partial w}{\partial y} \\ \epsilon_z = \frac{\partial w}{\partial z} & , & \gamma_{zx} = \frac{\partial u}{\partial z} + \frac{\partial w}{\partial x} \end{cases} \quad (80)$$

ϵ and γ are the components of the strain tensor, where ϵ is the normal strain, and γ is the distortion strain.

Compatibility equations

Compatibility equations are expressed in equations (Eq. 81).

$$\begin{cases} \frac{\partial^2 \epsilon_x}{\partial y^2} + \frac{\partial^2 \epsilon_y}{\partial x^2} = \frac{\partial^2 \gamma_{xy}}{\partial x \partial y} & , & \frac{\partial}{\partial z} \left(\frac{\partial \gamma_{yz}}{\partial x} + \frac{\partial \gamma_{zx}}{\partial y} - \frac{\partial \gamma_{xy}}{\partial z} \right) = 2 \frac{\partial^2 \epsilon_z}{\partial x \partial y} \\ \frac{\partial^2 \epsilon_y}{\partial z^2} + \frac{\partial^2 \epsilon_z}{\partial y^2} = \frac{\partial^2 \gamma_{yz}}{\partial y \partial z} & , & \frac{\partial}{\partial x} \left(-\frac{\partial \gamma_{yz}}{\partial x} + \frac{\partial \gamma_{zx}}{\partial y} - \frac{\partial \gamma_{xy}}{\partial z} \right) = 2 \frac{\partial^2 \epsilon_x}{\partial y \partial z} \\ \frac{\partial^2 \epsilon_z}{\partial x^2} + \frac{\partial^2 \epsilon_x}{\partial z^2} = \frac{\partial^2 \gamma_{zx}}{\partial x \partial z} & , & \frac{\partial}{\partial y} \left(-\frac{\partial \gamma_{yz}}{\partial x} + \frac{\partial \gamma_{zx}}{\partial y} - \frac{\partial \gamma_{xy}}{\partial z} \right) = 2 \frac{\partial^2 \epsilon_y}{\partial x \partial z} \end{cases} \quad (81)$$

Constitutive equations

The tank material is assumed to be isotropic, thus the total strain is expressed by Eq. (82). The thermal strain is taken into consideration with the term $\alpha(T - T_0)$. Where α is the thermal expansion coefficient and T_0 is the initial tank temperature. Therefore, the thermal strain is expressed by Eq. (83).

$$\begin{cases} \epsilon_x = \frac{1}{E} [\sigma_x - \mu(\sigma_y + \sigma_z)] + \alpha(T - T_0) & , & \gamma_{yz} = \frac{2(1+\mu)}{E} \tau_{yz} \\ \epsilon_y = \frac{1}{E} [\sigma_y - \mu(\sigma_x + \sigma_z)] + \alpha(T - T_0) & , & \gamma_{zx} = \frac{2(1+\mu)}{E} \tau_{zx} \\ \epsilon_z = \frac{1}{E} [\sigma_z - \mu(\sigma_x + \sigma_y)] + \alpha(T - T_0) & , & \gamma_{xy} = \frac{2(1+\mu)}{E} \tau_{xy} \end{cases} \quad (82)$$

$$\epsilon_t = \alpha \Delta T = \alpha(T - T_0) \quad (83)$$

5.13. Thermo-mechanical coupling models

5.13.1. Calculation models building: Geometry, Mesh

5.13.2. Pre-sizing

The thickness of the tank which has been used in the numerical calculations is based on a pre-sizing computation. The shell of the tank is subjected to circumferential $\sigma_{\theta\theta}$, radial σ_{rr} and longitudinal σ_{zz} principal constraints. $\sigma_{\theta\theta}$ is resulting mainly from the internal pressure and from

bed-shell differential thermal expansion [220]. Radial stress σ_{rr} and axial stress are neglected in front of $\sigma_{\theta\theta}$ as simplified pressure vessel theory deduces that the circumferential constraint $\sigma_{\theta\theta}$ which maintains the balance of the cross tank section is greater than the internal radial stress σ_{rr} . $\sigma_{\theta\theta}$ is expressed as follows (Eq. 84).

$$\sigma_{\theta\theta} = p \frac{\phi_{int}}{2e} \quad (84)$$

The used two dimensional axisymmetric thermoelastic model is evaluating all stress tensor components, and only the hoop stress is highlighted.

The tank model was designed using a 3D CAD, as presented in Fig. 61. The tank consists of a cylindrical part ($D/2= 220$ mm, $L= 1000$ mm) and two flats dished bottoms which are welded to the cylindrical ferrule part with curvature radius: R_i and R_e . The tank volume is 150 L and its shell thickness is $t = 2$ mm. The hole series in the cylindrical part are the location of the evacuated tube solar collectors integrated in the tank.

The axisymmetric FE model, the dimensions of the joints between the cylindrical ferrule and the flat dished bottoms, the diameter and the length of the tank are presented in Fig. 61.

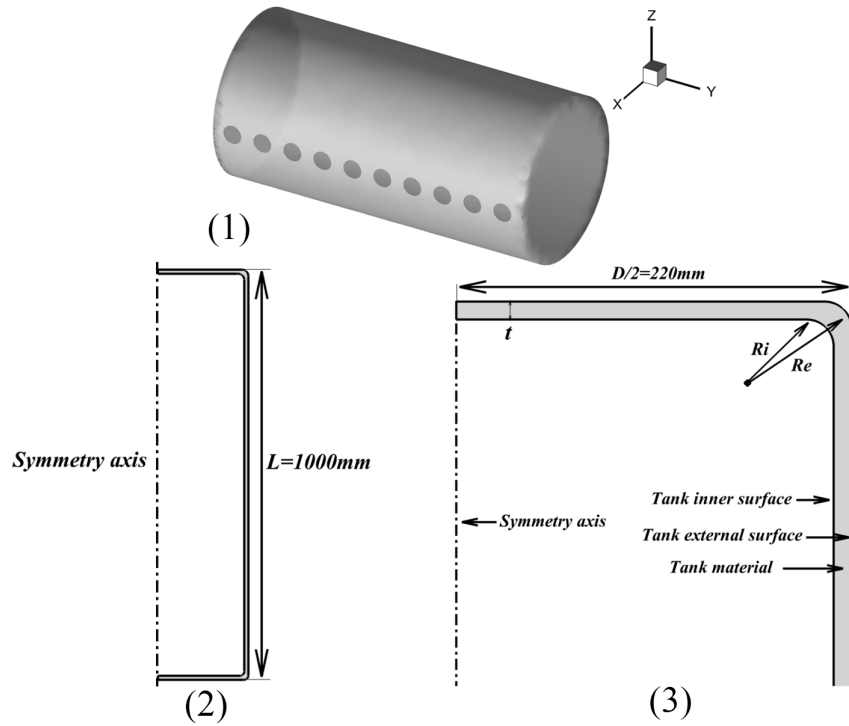


Figure 61: (1)-3D model of the tank. (2),(3)- 2D axisymmetric FE model of the tank.

The thermal and the mechanical meshes were identical for computational optimization purposes. A mapped mesh was used in our case to get more accurate results. A local grid refinement at the joints between the cylindrical ferrule and the flat dished bottoms has been performed.

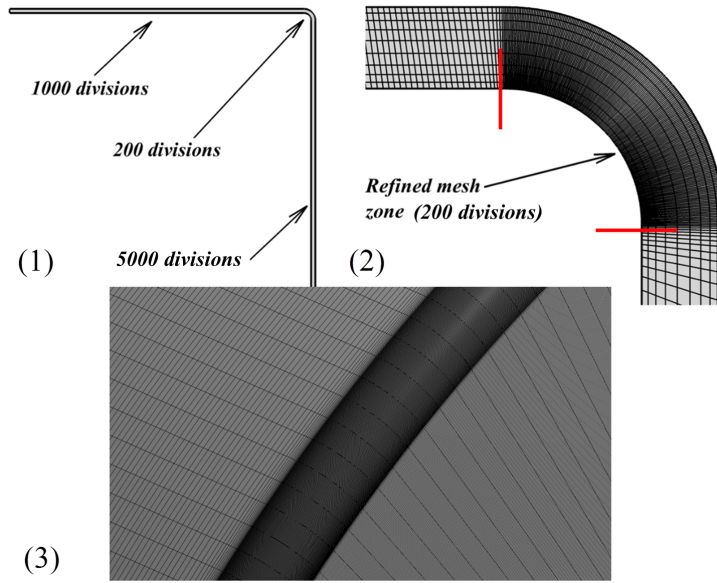


Figure 62: (1)- The tank shell discretization, (2)- the refinement grid structure,(3)- Axisymmetric three-dimensional mesh.

Structured quadrilateral elements were used for the 2D grid generation. The curvilinear part was divided into 200 divisions, while the rectilinear part was divided into 1000 divisions. Thus generating in the case of a 2D modeling 30870 elements as presented in Fig. 62-(1),(2). Further refinement in terms of divisions number was carried out at the connection between the tank's flat dished bottom and its cylindrical part. Axisymmetric 3D mesh was generated from the 2D configuration. A structured cell map was generated at the tank's cylindrical and the flat dished parts. A similar structure was generated for the junction as presented in Fig. 62-(3).

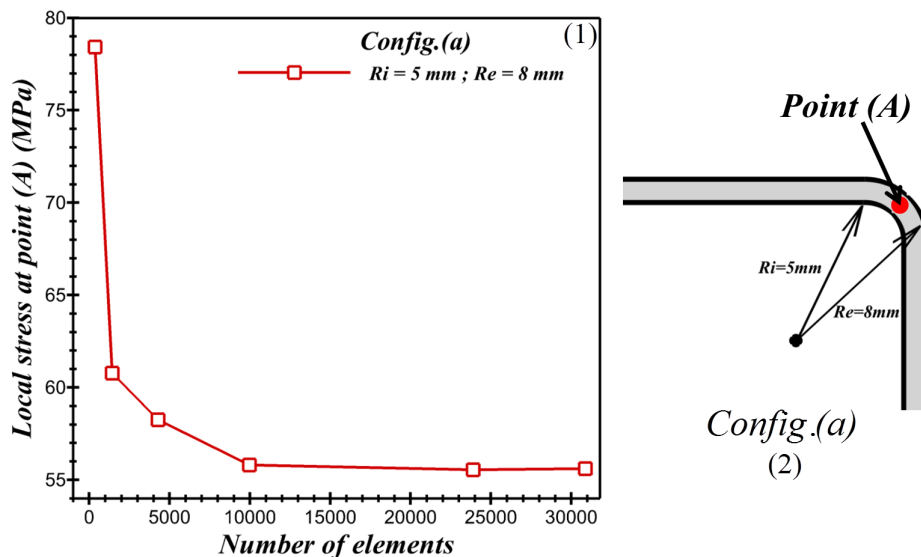


Figure 63: (1)- Mesh convergence test, (2)- Location of point (A) where the local stress was measured.

Mesh convergence test is an important step in this numerical study [221, 222]. The indicator on which this test was carried out is the local stress which was assessed locally at the point (A) Fig 63-(2). The point (A) belongs to the center line of the sheet and represents the midpoint of the junction that binds the cylindrical part and the flat dished bottom. The convergence test was investigated with the configuration (Ri=5 mm and Re=8 mm) (Config.(a), Fig.65). The material that was assigned to the tank's shell was the stainless steel. Six different mesh numbers were used starting with 357 elements and going up to 30870 elements. The applied thermomechanical loads were $T_{stagnation} = 270^{\circ}C$ and $P = 0.7MPa$. The trends of this convergence indicator are presented in Fig. 63. The simulations were launched for an increasing total cell number, while considering the axisymmetric 2D case. The evolution of the local stress is converging to 56 MPa starting from a total cell number equal to 10000 elements. As a result, the simulations including the various parametric studies were conducted using an average of 25000 meshing elements.

5.13.3. Simulations methods and Setting the boundary conditions

5.13.4. Thermal boundary conditions

This section highlights the boundary conditions applied on the CAD model (Fig. 64). Two boundary conditions types were set: a thermal condition where a constant temperature was applied on the internal walls of the tank. Another mechanical condition representing the mechanical effect of the pressure test was also applied on the cylindrical internal tank's walls. In fact, during their manufacturing, the storage tanks are subjected to an operating pressure test to assess their mechanical resistance. They are subjected to a pressure ranging between 0.5 and 0.7 MPa.

The stagnation temperature of the heat pipes could reaches $270^{\circ}C$ [156, 219]. This temperature transforms the water stored in the tank into superheated steam. In order to consider extreme operating conditions, the temperature at the tank's internal walls was assumed equal to $T_{stagnation} = 270^{\circ}C$ [156, 219]. Besides, the outer surface of the tank is covered by an insulating material. Accordingly, zero heat flux on the external wall of the tank was applied (Eq. 85).

$$\lambda \frac{\partial T}{\partial N} = 0 \quad (85)$$

where $\frac{\partial T}{\partial N}$ is the temperature gradient in the normal direction boundary of the tank's shell.

An additional boundary condition which represents mechanical equilibrium is also applied to take into account the 2D axisymmetric resolution approach. Indeed, zero mechanical displacement is applied at both ends of the tank $U_x = 0$ (Fig. 64), while the displacement U_y is maintained free.

As regards the numerical procedure resolution, a physical configuration was established for the heat model separately to the mechanical model, in order to get first the temperature profiles which allow to compute the thermal strain. The thermal results were coupled sequentially with the mechanical model to compute the mechanical displacement. Two stresses must be taken into consideration: thermal stress induced by the temperature shock and the mechanical stress resulting from the operating pressure applied to the internal walls of the tank. The effect of temperature variation on the thermo-physical properties of the material was taken into account because rheological changes of the material properties due to temperature causes the thermal strain, stress and creeping.

The thermomechanical boundary conditions applied to the axisymmetric model of the horizontal tank are presented on Fig. 64. A stagnation temperature of $270^{\circ}C$ [156, 219] and an admissible pressure of 0.7 MPa are applied on its internal surface. The horizontal displacement applied on

the tank's flate dished bottoms was set to zero while it was set to a free value for the vertical displacement direction so as to model correctly the axisymmetric condition.

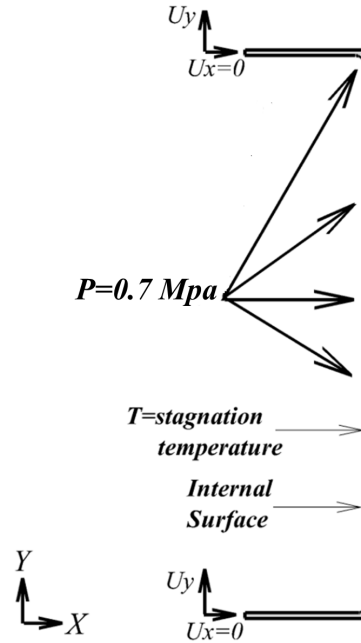


Figure 64: Thermo mechanical boundary conditions applied on the 2D-axisymmetric tank model.

The axisymmetric configuration presented previously presupposes that the studied tank is sealed, not pierced and does not incorporate the evacuated tube solar collectors.

5.14. Results of the simulation

In the present chapter, three studies were carried out to propose an optimal tank model which resists to the real operating conditions detailed in the boundary conditions subsection.

1. *Study 1:* the internal pressure of 0.7 MPa applied to the internal surface of the tank can lead to stress concentration zones where the elastic limit of the material is exceeded. Thus, a parametric study on the curvative radius of the junction which binds the cylindrical part to the flat dished bottoms were carried out. Indeed, five cases were studied (Fig. 65). The sheet thickness estimation to manufacture the tank is based on the pre-sizing formula. 3 mm was picked as the thickness value, since it is the thickness available in our laboratory for experimental purposes. The remaining studies are going to be based on the result outcomes of the study 1.
2. *Study 2:* The optimal configuration which avoid the stress concentration zones appearance was determined through the first study. The second study aims to determine the most suitable material for the tank. Indeed, the mechanical behavior of four materials was studied, the thermomechanical properties are detailed in Tab. 14.
3. *Study 3* is a parametric investigation which aims to determine the optimal shell thickness used for the tank manufacture.

5.14.1. Strength failure desing code

The thermomechanical analysis was described by the following indicators: Von Mises stress [223], Von Mises strain [224], displacements [225]. The Von-Mises stress is calculated as presented in the formula (Eq. (86)). The maximum stress must not exceed the strenght limit to avoid any failure.

$$\sigma_{VM} = \sqrt{\frac{1}{2}[(\sigma_1 - \sigma_2)^2 + (\sigma_2 - \sigma_3)^2 + (\sigma_3 - \sigma_1)^2]} < \frac{\sigma_e}{s} \quad (86)$$

where σ_1 , σ_2 and σ_3 represents the three principal stress respectively, σ_e is the yield stress and s is the safety factor.

5.14.2. Study 1: Geometrical optimization

A great attention should be paid to the structural optimization and to the strength calculation. The first studied case is presented in Fig. 65. The shape of the dished bottoms was maintained as flat and the curvative radii (Ri) and (Re) were varied to avoid the appearance of the stress concentration zones.

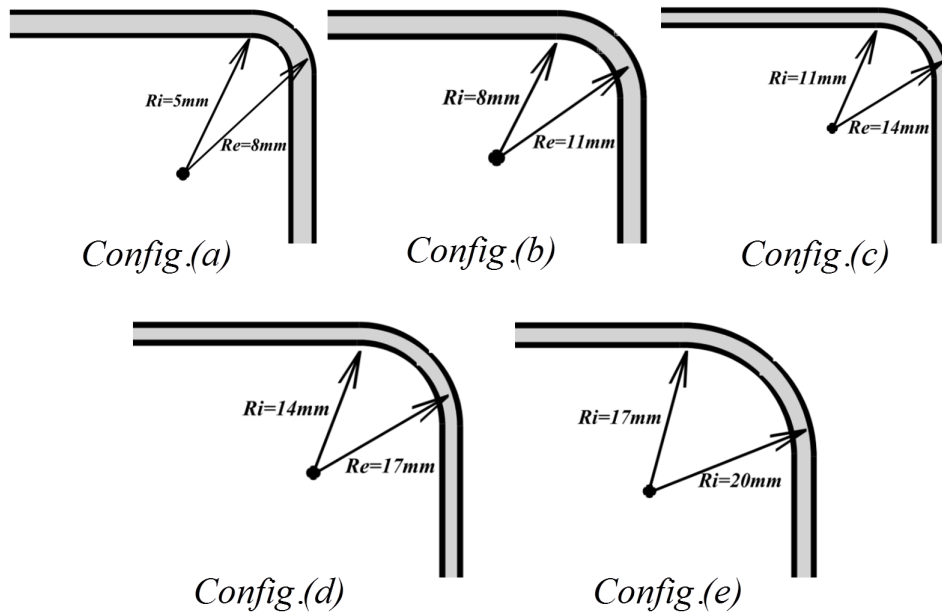


Figure 65: Curvature radius variation of the junction connecting the cylindrical part to the flat dished bottoms to avoid the appearance of the stress concentration zones.

The contours and the numerical values of the stress, the strain and the total displacement along the path (1-2) are presented in the Figs. 66 and 67. Fig 66-(2) shows that the displacement values of the configuration (c) are lower than those of the other configurations (a), (b), (d) and (e). The displacement is equal to 2.5 mm for the configuration (c). The configuration (d) presents a maximum mechanical displacement of 32 mm slightly higher than that of the configuration (e) 31 mm , but largely higher than the displacements of (b) and (a) configurations which are equal simultaneously to 7 mm and 8 mm.

The maximum stress and strain are concentrated at the junction which binds the flat dished bottoms to the ferrule as presented in Fig. 66-(1) for all the configuration under study. The configuration (a) has the maximum stress and strain $\sigma = 55$ MPa, $\epsilon = 0.000275$, while the configuration (e) has the minimum values $\sigma = 52$ MPa, $\epsilon = 0.00026$.

The tendency of the stress-strain curves perfectly reflects the applied thermomechanical loading Fig. 67(1)-(2). Along the radius of the two flat dished bottoms, the stress and the developed strain are minimal and then increase to a maximum peak since the geometry presents an abrupt change in the section orientation of the shell. The values of the stresses and strain decrease but remain greater than $\sigma = 50$ MPa, $\epsilon = 0.00025$. Along the cylindrical part where the pressure of 0.7 MPa is applied.

The contours of stresses and the thermal strain are presented in Fig. 67. The constraints for both (a) and (e) configurations are also presented Fig. 67(1)-(2). The maximum stress is developed at the cylindrical part. For the configuration (e) $\sigma_{max} = 55.541$ MPa , $\sigma_{min} = 6.2543$ MPa. For the configuration (a) $\sigma_{max} = 52.148$ MPa , $\sigma_{min} = 6.6438$ MPa.

Fig. 67-(3) presents the fields of the thermal strain which depends only on the applied stagnation temperature and on the thermal expansion coefficient of the selected material of the horizontal storage tank. These simulations were performed by assigning the standard steel to the shell of the tank.

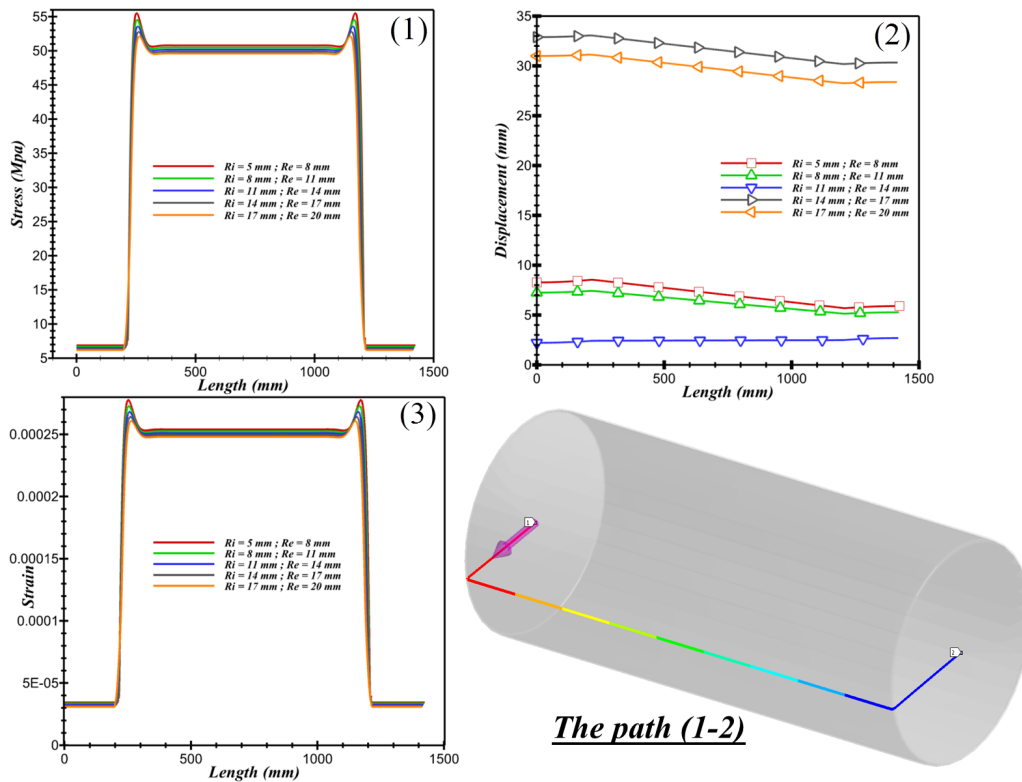


Figure 66: (1)-strain, (2)-Displacement and (3)-stress values along the path (1-2).

The stress and strain fields have a symmetrical shape (Fig. 66(1),(3)) with respect to the vertical plane perpendicular to the rotational axis of the horizontal tank and which cuts it into two parts of the same length (500 mm). Moreover, the maximum stress and strain peaks are due to the

geometrical shape that binds the cylindrical part of the storage tank to the flat dished bottoms, described by the radius of curvature (R_i) and (R_e). Indeed, the stresses and strain are related by the Young's modulus (E) (Eq. 82) [226], which explains the similarity of the achieved tendencies.

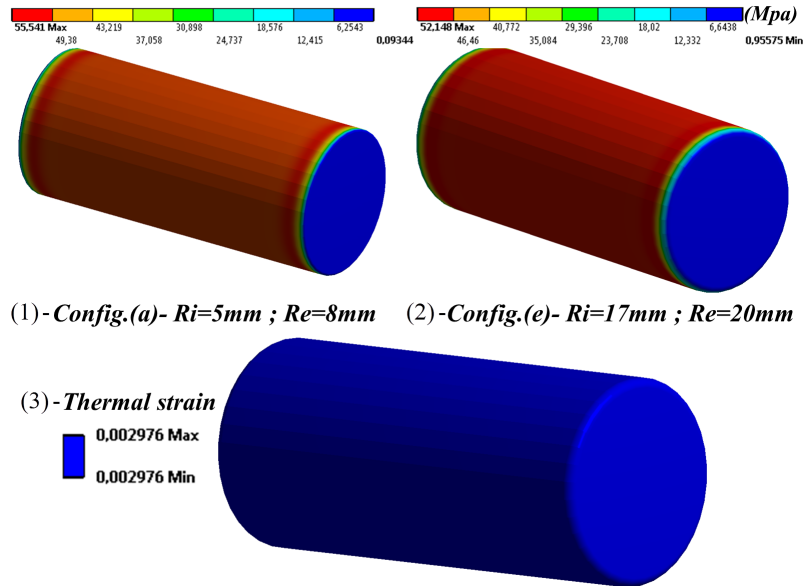


Figure 67: Stress contours (1)-config.(a), (2)-config.(e). (3)-Thermal strain resulting from applying the stagnation temperature on the tank inner walls.

As a result, it is concluded from the first study intended to optimize the geometry on which thermo-mechanical constraints have been applied, that the optimal configuration which avoid the appearance of the stress concentration zones and which better distribute the stress on the tank's shell is the configuration (c), where $R_i = 11\text{ mm}$ and $R_e = 14\text{ mm}$.

5.14.3. Study 2: Material selection effect

The optimal configuration which is the main result of the first study is the configuration-(c). Subsequently, four different materials were assigned to this configuration namely, standard steel, stainless steel, aluminium alloy and the copper alloy in order to study the effect of the material on the mechanical strength of the horizontal tank subjected to thermo-mechanical loads.

The thermo-mechanical properties of the selected materials have a crucial impact on the strength of the storage tank. These properties are the coefficient of thermal expansion, the tensile yield stress [227] and the tensile ultimate strength [228]. Other properties are presented in Tab. 14 such as Young's modulus, shear modulus and compressive yield stress.

The displacements values along the path (1-2) for the selected materials are presented in Fig. 68. The thermo-mechanical displacement at the shell of the stainless steel tank has an optimal value varying between [1.5 mm; 2 mm] along the tank's length equal to 1425 mm. Furthermore, copper alloy and aluminum alloy do not reduce the value of the displacements measured on the path (1-2), because of their tensile ultimate strength which is lower than the values of stainless steel and standard steel. Standard steel could be a contender to manufacture the investigated horizontal tank, because the displacement values do not exceed 3 mm while applying the thermo-mechanical loads.

Properties	Stainless steel	Standard steel	Aluminum alloy	Copper alloy	Units
Density	7750	7850	2770	8300	kg.m^{-3}
Coefficient of Thermal Expansion	1.70E-05	1.2E-05	2.3E-05	1.8E-05	$^{\circ}\text{C}^{-1}$
Reference Temperature	22	22	22	22	$^{\circ}\text{C}$
Young's Modulus	1.93E+5	2E+5	7.1E+4	1.1E+5	MPa
Poisson's Ratio	0.31	0.3	0.33	0.34	
Bulk Modulus	1.693E+5	1.6667E+5	6.9608E+5	1.1458E+5	MPa
Shear Modulus	7.3664E+4	7.6923E+4	2.6692E+4	4.1045E+4	MPa
Tensile Yield Strength	2.07E+02	2.5E+02	2.8E+02	2.80E+02	MPa
Compressive Yield Strength	2.07E+02	2.5E+02	2.8E+02	2.80E+02	MPa
Tensile Ultimate Strength	5.86E+02	4.6E+02	3.1E+02	4.30E+02	MPa
Compressive Ultimate Strength	0	0	0	0	MPa
Isotropic Thermal Conductivity	15.1	60.50	$\lambda = -5\text{E-}04\text{T}^2 + 0.254\text{T} + 144.30$	401	$\text{W.m}^{-1}\text{.}^{\circ}\text{C}^{-1}$

Table 14: Thermomechanical properties of the tank materials.

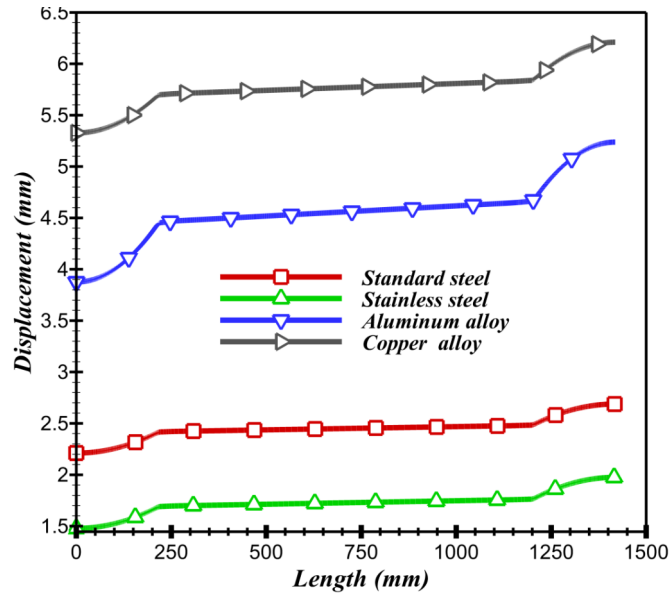


Figure 68: Displacement values measured along the path (1 – 2) for four different materials.

5.14.4. Study 3: Thickness effect

The optimization of the tank's shell thickness was important because it is a parameter that goes into the design of the horizontal storage tank. A similar study, which is based on the same concept and which was intended to optimize the thickness of a composite material, has been released [229]. In fact, a shell thickness optimization of the horizontal tank was carried out according to the third study, in order to reduce its weight, the cost of purchasing the the primary materials for its manufacture and to make easy its shaping by the usual mechanical methods. The applied thermo-mechanical boundary conditions were preserved, as presented in the first and second study. Furthermore, the optimal curvature radius resulting from the previous parametric studies was maintained to avoid the appearance of the stress concentration zones. In addition to this, stainless

steel was used as manufacturing material, because it has ensured high mechanical resistance in terms of strain and stress which were measured along the path (1-2), with respect to the other contender materials .

Five different thicknesses were considered namely, 0.75 mm; 1.25 mm; 1.50 mm; 2 mm and 2.5 mm during this study as presented in Fig. 69. The thermomechanical boundary conditions detailed above were also retained. The mechanical displacement was selected as a performance indicator to make the optimal thickness choice, which is used for manufacturing the thermal storage tank. The displacement evolution along the mean tank fiber (path 1 – 2) is presented in Fig. 69. The curves have a maximum spike which corresponds to the junction between the cylindrical part and the tank’s flat dished bottoms, where the mechanical stresses are concentrated for the five studied thicknesses. The thickness $t = 0.75$ mm induces the maximum displacement values which are between 2 mm and 4.5 mm. On the other hand, it is noted that $t = 2$ mm is the optimized thickness, since the displacement remains minimal with values between between 0.8 mm and 2.2 mm. Therefore, it can be concluded that the thickness $t = 2$ mm ensures an optimum mechanical strength for the horizontal hot water storage tank which integrates evacuated tube with heat pipes.

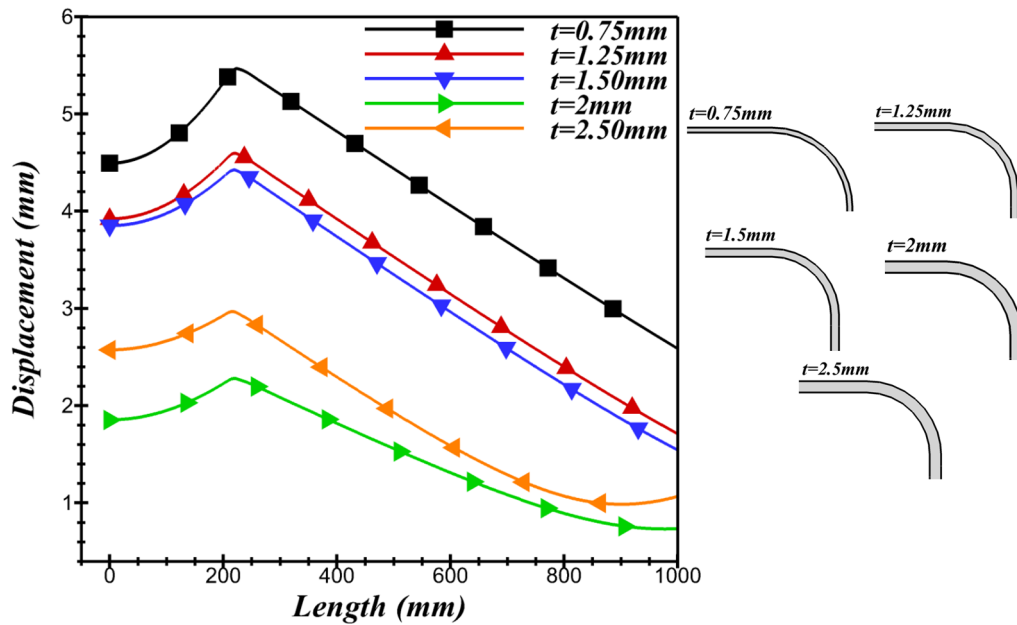


Figure 69: The effect of five different thicknesses on the tank’s shell displacement over the center line (path (1-2)).

5.15. Conclusion

In this chapter, a thermo-mechanical analysis of a horizontal thermal storage tank intended to store hot water for a domestic application has been carried out, using the Finite Element Method (FEM) by combining the steady-state thermal analysis to the static structural analysis. Total Displacements, stresses and strains were simulated through a two dimensional axisymmetric 1-way thermo-mechanical coupling. Thermo-mechanical stress and various parameters which aim to optimize the lifespan of the tank were conducted under extrem temperature and pressure operating conditions, which were based on the strength Von-Mises failure code. The main conclusions to be drawn from this numerical simulation study could be presented as follow:

- The optimal configuration which avoid the appearance of the stress concentration zones and which distribute better the stress on the tank's shell is the configuration-(c), where the curvative radius $R_i = 11$ mm and $R_e = 14$ mm. This result has been achieved through conducting the first study;
- The material choice was investigated through the second study, in order to minimize the mechanical displacements of the tank's shell subjected to thermo-mechanical loads. The stainless steel presented a better mechanical strength compared to standard steel, aluminium alloy and copper alloy. It is noted that this second study has been performed taking into consideration the result of the first study;
- The mechanical displacement has been considered as indicator to select the optimized thickness of the storage tank's shell among five thicknesses. The optimal thickness that should be selected while manufacturing the tank's shell, which is subjected to the thermo-mechanical load have to be equal to $t = 2$ mm.

5.16. *Chapter V: Experimental study and CFD thermal assessment of horizontal hot water storage tank integrating Evacuated Tube Collectors with heat pipes*

5.17. *Introduction*

This chapter presents an experimental study and a set of CFD simulations applied to a horizontal tank storing hot water. Hence, the main purpose of this work is to suggest a new and optimal design of the studied horizontal tank which is considered as the main device in individual solar water heaters integrating Evacuated Tube Collectors (ETC) with heat pipes. An experimental study was carried out to measure the maximum temperature of the heat pipes using a thermal camera. Subsequently, CFD simulations were performed using the previously recorded experimental results. The numerical studies aimed to assess the effect of the heat pipe's number, integrated on the lateral internal shell of the tank, on its energetic performances such as the discharging efficiency.

In fact, four cases were studied according to the number of the used heat pipes (n). Several performance indicators were defined to identify the optimal configuration, such as the heat transfer coefficient assessed at the heat pipe, temperature contours and streamlines, temperature evolution according to specific paths defined inside the storage tank and the discharging efficiency... It was found that the average temperature of the horizontal tank is increased by the rise in the heat pipe's number. On the other hand, the laminar structure of the flow field is disturbed and the outlet temperature of the hot loaded water is also affected. Otherwise, the HTC calculated for the heat pipe close to the outlet of the storage tank for $n=6$ achieved 212.5 W/K.m^2 , while it is 300 W/K.m^2 and 230 W/K.m^2 for $n=8$ and $n=10$, respectively. Moreover, the discharging efficiency of the horizontal storage tank depends mainly on the instantaneous variation of the water's temperature.

5.17.1. *Background*

Hot water consumption is increasing in many countries, especially in Middle East and North Africa (MENA) [66] regions that have, collectively, the world's largest supplies of oil and gas [230]. This explains why individual solar water heaters have become a reliable and efficient solution to ensure the production of hot water [231], while contributing to the reduction of the electric bill [232]. For example in Brazil, on average, over 73% of Brazilian households use these 3–8kW electrical resistance showerheads to provide hot water for domestic consumption which contributes to a load curve that peaks in the early evening, imposing a considerable burden to generation, transmission, and distribution utilities [233]. The literature presents several works in which the energetic performances of thermosyphon solar water heaters have been studied [234]. For instance, the performance of water-in-glass ETC solar water heaters has been assessed using experimental measurements to depict its optical and heat loss characteristics for domestic water heating in Sydney [235]. However, the thermal assessment of solar water heaters using Evacuated Tube Collectors (ETC) with absorbing fins, where heat pipes are integrated is still considered as a new issue. Hence, it has to be analyzed and enhanced further, in order to achieve heating necessities. Therefore, particular attention must be paid to the sensitive storage part in the horizontal storage tank such an important device in solar hot water systems (Fig. 70). We have already worked on the improvement of the thermo mechanical strength of this type of horizontal storage tank [42] by conducting a parametric study which aimed to optimize three essential indicators namely, the thickness of the manufacturing shell, the material and finally the curvature radius which connects the cylindrical part of the tank to its two flat dished bottoms.

We believe that this study is original because first it belongs to a national Moroccan project entitled “*SOL’R SHEMSY*” [6], which aims to design and commercialize the first SWH made in Morocco funded by IRESEN. Second, it helps to understand heat transfer phenomena that occurs inside a domestic horizontal tank integrating on its lateral shell heating sources and which is subjected to dynamic charging/discharging cycles. An exhaustive required consultancy of the literature’s studies showed that the experimental and numerical investigations carried out on the assessment of the energy efficiency of the horizontal storage tank using ETC with heat pipes as heating source are not numerous. Therefore, we were interested to carry out an experimental study to measure the temperature in stagnation of a single heat pipe in the open air by using a thermal camera, and to capitalize on this result considered as thermal boundary condition, which will be useful for conducting unsteady CFD studies to optimize the horizontal storage tank design of the studied SWH.

5.17.2. Literature CFD studies on thermal storage enhancement

Several methods are used to assess thermal storage tanks [147]. Currently, a new inlet device which aim to enhance thermal stratification in a hot water storage tank during the charging mode has been proposed by Mari et al. [32]. They compared the effect of two inlet configurations, namely a sintered bronze conical diffuser (SBCD) and a conventional inlet elbow (E) on the stratification by conducting experimental studies that helped to visualize the evolution of the recorded temperatures, the calculation of the MIX number [147], as well as the description of the thermocline evolution. Another study which aim to enhance thermal stratification in storage tank has been conducted by Brown et al. [22]. They integrated a porous manifold inside the liquid storage tank. In fact, they concluded from the visualization of flow contours that porous manifold could help the reduction of the shear-induced mixing between fluids of different temperature, because it is considered as a factor that affects the thermocline thickness, hence the prevention of good thermal stratification. In addition, a scale model of hot storage-tanks has been designed by Kandari et al. [236] on which experiments were performed to study the effect of the distributor header geometry and the settling mesh on the reduction of the buffer-zone thickness. Their proposed solution in terms of the use of the new header configuration helped to improve thermal stratification and to achieve an efficiency of 85%.

The thermal performance of a solar cooker with ETC integrating heat pipes containing different refrigerants has been assessed by Esen et al. [237], under the climatic conditions of Elazig located in Turkey during summer season (July and August of 2002). Their main findings could be resumed in the following points. First, the maximal temperature of the stored edible oil with 7 liters volume has achieved 175°C. Second, the designed solar cooker could be used to cook several foods, because the cooking period was evaluated between 27-70 min. The same author carried out experimental investigations on three identical small-scale SWH using R-134a, R407C, and R410A refrigerants under various environmental and load conditions [238]. The overall SWH efficiency has been assessed according to two cases, with and without loading water. In fact, they have presented temperature distributions and the achieved thermal efficiencies of the two-phase thermosyphon, which showed good agreements, compared to the literature results.

Moreover, Esen et al. [239] developed a numerical model based on the enthalpy method and compatible with solar assisted cylindrical energy storage tank integrating different phase change materials (PCM) packed in cylinders. They used Gauss-Seidel iteration process to solve the resulting equations. They showed that the key parameters that should be adjusted to increase the thermal performance of the tank are the PCM cylinder radius, the inlet mass flow rate besides to

the inlet temperature of the HTF. Further, the same author worked on the theoretical optimization of the solar-aided latent domestic heating systems [240]. In fact, they used two different models that describe the diurnal transient behavior of the phase change unit. Moreover, they carried out several numerical simulations to investigate the effect of various parameters on the enhancement of the storing time such as the material of the PCMs, the cylinder radius, the inlet mass flow rates and the inlet temperature of the HTF etc. The cylindrical PCMs submerged within the tank which is linked to a solar powered heat pump system was investigated experimentally and theoretically by Esen et al. [241] for space heating purposes. Two-dimensional assumption was considered to solve numerically the heat transfer modeling based on the finite differences methods. Indeed, they have presented key performance indicators related to heating, such as solar radiation amount, space-heating loads besides to the evolution of the stored energy of the tank and its temperature.

Recently, Kenjo et al. [242] developed a model that has been validated against the available experimental results, with the aim to study thermal stratification in a mantle tank integrated in a solar domestic hot water system. Their accurate simulation's results showed that the mixing coefficient could be used to model water flow in the mantle heat exchanger. In the same context of thermal storage efficiency enhancement, Ghaddar et al. [118] developed a numerical one-dimensional model that can be used in solar energy systems such as solar water heaters and air-conditioning systems to describe the behavior and liquid stratification evolution in thermal storage tanks. Their validated model helped to predict the effect of inter-mixing on the reduction of storage tank efficiency.

CFD simulations are also considered as an efficient approach to study, assess and improve the thermal energy storage of horizontal tanks [55] or vertical stratified tanks [35]. Indeed, several recent CFD studies have been released in the literature and which deal particularly with the study and enhancement of the energy indicators that affect the thermal storage of liquids for various applications, in particular solar thermal applications through storing domestic hot water for individual use. For example, Levers et al. [29] conducted seven three-dimensional numerical simulations using *Fluent* CFD program, in order to study the parameters that affect the thermal performance of a hot water system. They showed through their analysis that the tanks aspect ratio, the charging and discharging flow rates of inlet/outlet, besides to their position with respect to the extremities of the tank are the most parameters that affect thermal stratification within the storage tank. Furthermore, the effect of twelve different obstacles integrated inside a cylindrical hot water tank on thermal stratification has been analyzed numerically by Altuntop et al. [33]. Their numerical method has been validated against experimental and numerical results before starting the parametric study which aimed to optimize the residence time of hot water within the tank. They found that the obstacle configuration having the gap located in the center is presenting better thermal stratification than those having the gap near the side wall of the tank.

Moreover, two-dimensional numerical modeling is an efficient and reliable approach that can predict the energy performance of storage tanks and that help to access to additional information difficult to reach experimentally. To illustrate this idea, Bouhal et al. [35] worked on the enhancement of thermal stratification in two configurations of vertical solar hot water storage tanks using different number of flat plates with various tilted positions [31]. Their optimization and numerical modeling was performed based on two dimensional CFD simulations, which helped to define two performance indicators necessary to assess thermal stratification, namely the Richardson number and stratification number. To exemplify more this idea, Bouhal et al. [55] worked on optimizing the energy efficiency of solar horizontal storage tanks integrating evacuated tube collectors based

on parametric studies carried out with two dimensional CFD simulations. They assessed three geometrical shapes of the heat pipes to finally conclude that the rectangular shape represents the optimal configuration, as it helps to reduce the heating time of the stored water and because it improves the thermal exchange between the fluid and the heat pipe.

Investigations	Findings
Bouhal et al. [35] worked on the enhancement of thermal stratification in two configurations of vertical solar hot water storage tanks using different number of flat plates with various tilted positions.	Their optimization and numerical modeling was performed based on two dimensional CFD simulations, which helped to define two performance indicators necessary to assess thermal stratification, namely the Richardson number and stratification number.
Romanchenko et al. [110] compared storage using a hot water tank and the thermal inertia of buildings and they conducted a techno-economic optimization model applied to the district heating system of Goteborg, Sweden	Compared to the thermal inertia of buildings, they found that the hot water tank stores more than twice as much heat over the modeled year, owing to lower energy losses. Further, the total system yearly operating cost decreased by 2% when the hot water tank is added to the district heating system
Dehghan et al. [111] carried out numerical investigation of the unsteady thermal efficiency behavior of a vertical storage tank of a DSWHS with a mantle heat exchanger in the discharge/charge mode	Their pre-established thermal stratification is well preserved during the discharging operation mode for higher values of Grashof number. Moreover, the tank inflow Reynolds number and or its inflow port diameter should be kept below certain values to provide water with a proper temperature for consumption
Imtiaz et al. [16] Analysis of a conical solar water heater (CSWH) with an attached thermal storage tank, with or without a vacuum glass absorber under different operating conditions	The efficiency of their CSWH increased with increasing inlet flow rate, and the maximum efficiency of the system was achieved at a critical flow rate of 6L/min and reciprocally
Murali et al. [19] conducted experimental performance study of a solar water heater using Latent Thermal Energy storage (LTES) in a stratified tank with two different inlet locations	They showed that stratification is enhanced in both continuous and batch wise discharging with a diffuser located at the bottom inlet of the tank
Wand et al. [17] analyzed the inlet structure impact on the thermal stratification under different flow rates (1L/min, 2L/min, 3L/min, 4L/min, 5L/min, and 6L/min)	For 6L/min flow rate, they found that the Richardson numbers for the three modes were $6, 4 \times 10^4$ and 4×10^6 . Also, the fill efficiencies were 0.53493, 0.58493 and 0.81405. Finally, the MIX numbers were 0.53154, 0.30923 and 0.03971
Mari et al. [32] Compared the effect of two water inlet devices during a thermal charge process: a sintered bronze conical diffuser (SBCD) and a conventional inlet elbow (E)	Water stratification has increased during thermal charging with both low and high flows if SBCD diffuser is used. In addition, the dimensionless height of the midpoint of the thermocline can be used to quantify the volume of water affected by the mixing produced by the turbulence
Altuntop et al. [33] analyzed numerically of the effect of different obstacles on thermal stratification in a cylindrical hot water tank	They showed that better thermal stratification is achieved by placing obstacle in the tank compared to the no obstacle case. Besides, obstacle having gap in the center have better thermal stratification than those having gap near the tank wall
Wahiba et al. [30] carried out 3D unsteady CFD simulations to investigate the effect of several design and operating on the flow behavior, thermal stratification and performance of a hot water storage tank installed in solar thermal energy systems	3D transient CFD simulations can be used as an effective tool to optimize thermal storage tank parameters at early design stages
Experimental analysis of the charge of a high aspect ratio cavity representing the storage of an ICSSWH system has been presented by Swiatek et al. [108]	Heating the storage tank in the middle and inserting a stratification plate help to achieve satisfying stratification. Also, stratification was higher with a shorter stratification plate
Development of a new numerical simulation platform to assess the commercial viability of thermocline approach, regarding energetic effectiveness and structural reliability was released by Gonzalez et al. [109]	Their numerical model was first validated against the Solar One thermocline case. Furthermore, a better storage performance and structural strength have been achieved together with the lowest temperature difference

Table 15: Summary of the studies performed on stratified thermal storage tanks

Fertahi et al. [7] enhanced the performance of a two-phase closed heat pipe integrated in horizontal storage tank through CFD simulations. Heat pipes are considered as the main device responsible for converting solar energy into thermal energy transmitted to cold water initially stored in the tank. In fact, they assessed two configurations of the condenser part, which remain the section responsible of the generation of heat and its release. They showed that the performance of the two-phase closed heat pipe could be improved by adding tilted fins on the lateral surface of the condenser section with of percentage of 16%. A summary of the studies performed on stratified thermal storage tanks is presented in Tab. [15].

CFD three-dimensional calculations oriented towards innovation and the proposal of an optimal design of storage tanks were conducted to model and simulate their operation in static or in dynamic mode such as during the charging and discharging cycles. The disadvantage often raised when using this numerical approach is the heavy time allocated to calculations, as well as the necessary equipment to use (powerful workstation) [7] to achieve correct results in an optimal time. For instance, Gasque et al. [243] conducted CFD simulations to study the effect of inner lining

material on thermal stratification inside a hot water storage tank. First, they validated their three-dimensional model against the experimental measurements of temperature, and subsequently, they carried out a parametric study for three different inner lining materials by using different indicators in order to select the most suitable contender which is going to potentially enhance the thermal stratification of the tank. Last but not least, Wahiba et al. [30] presented the results of unsteady three-dimensional CFD simulations intended to design an optimum storage tank for best thermal performances, according to several operating parameters during the charging flow mode. They confirmed that 3D transient CFD simulations could be a reliable tool that aims to optimize the efficiency of thermal storage tanks at early design stages.

5.17.3. Aim of the present study

The aim of the present chapter is to measure experimentally the temperature in stagnation of the heat pipe head using a thermal camera, and to turn the achieved findings to perform CFD calculations intended to assess the thermal efficiency of the solar horizontal storage tank which integrates Evacuated Tube Collector Fig. 70.

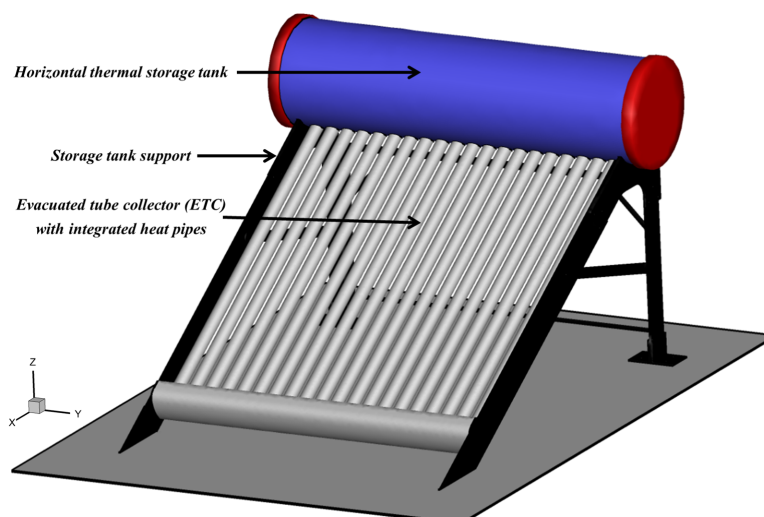


Figure 70: Solar water heater prototype "SOL'R SHEMSY" [6]. The thermal performances of the storage tank are under assessment and improvement stage [42].

Indeed, the experimental achieved temperature will be applied as a thermal boundary condition, during the two-dimensional numerical modeling, on the tubular device where the head of the heat pipes is located Fig. 71(c). The validation of the physical models of *Fluent* calculation code that controls the physical phenomena of heat transfer and flow has been ensured by reproducing the experimental study of Zachar et al. [2], which describes in detail the thermal stratification in a vertical tank that pre-stores hot water subjected to charging and discharging cycles. Four configurations of the horizontal storage tank were considered, namely $n=4$, $n=6$, $n=8$ and $n=10$. Besides, several results were presented to describe and analyze the effect of the heat pipe number on the heat transfer by convection and conduction inside the considered solar storage tank.

5.18. Description of the case study

The three-dimensional numerical design of the horizontal storage tank involved in the simulation studies is presented in Fig. 71. The inner shell of the tank includes a series of ETCs Fig. 71.

(b) equipped with heat pipes which are considered as the main component to heat the cold water initially stored in the horizontal tank. Besides, the internal shell of the tank is covered by a thermal insulation and an external cover Fig. 71-(a).

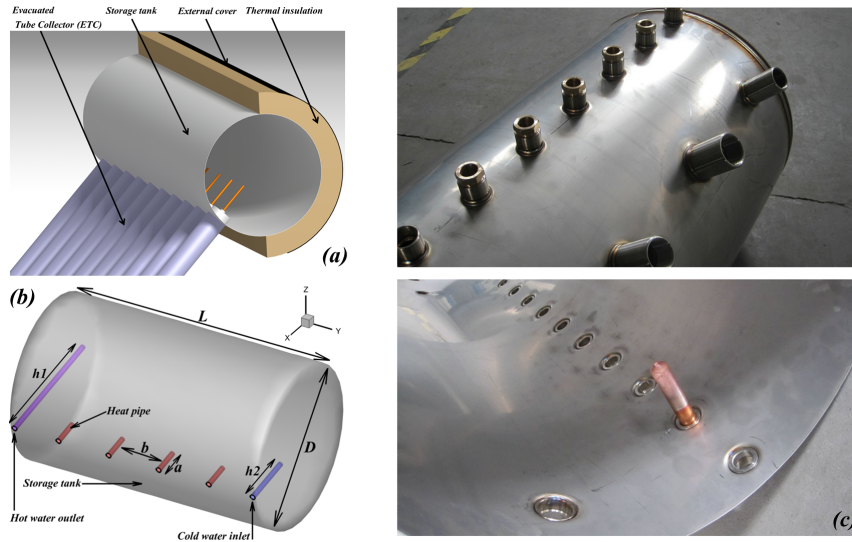


Figure 71: (a)- Inner shell of the horizontal storage tank which includes a series of ETCs where the head of the heat pipes is integrated. (b)-Parameterization of the horizontal storage tank which includes four heat pipes inserted on its internal lateral shell. (c)- Internal shell of the horizontal storage tank integrating heat pipe head made from copper [43].

The studied tank is described by its length $L=1\text{m}$, its diameter $D=0.619\text{ m}$ and its volume $V=300\text{l}$. Fig. 71-(b) is presenting a parameterization of the horizontal storage tank which includes four heat pipes integrated on its internal lateral shell. The length of the heat pipes (a) has been kept fixed, while the spacing (b) is variable and depends on the number of the heat pipes that are located in the horizontal tank (see Tab. 24).

	n=4	n=6	n=8	n=10
b (m)	0.1784	0.1197	0.871	0.663
a (m)	0.100			

Table 16: Values of the length of the heat pipe’s head (a) and the spacing (b) between each heat pipe corresponding to their number (n) inside the horizontal tank.

5.18.1. Parametric study

The aim of this parametric study is to enhance the energy performance of the 300 liters horizontal storage tank. The effect of the heat pipes number and their contribution in heating has been investigated and analyzed. Several performance indicators were defined to identify the optimal configuration, such as the heat transfer coefficient assessed at the heat pipe, temperature contours and streamlines, temperature evolution according to specific paths defined inside the storage tank and the discharging efficiency. In summary, four configurations were considered as presented in Fig. 72, namely $n = 4$, $n = 6$, $n = 8$ and $n = 10$. The length of the heat pipe head and the spacing between each heating source of each proposed configuration are presented in Tab. 24

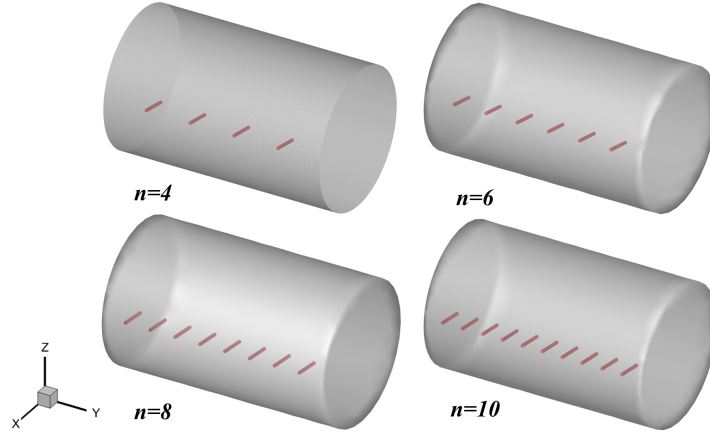


Figure 72: Schematic view of four configurations of the horizontal storage tank integrating different numbers of heat pipes, $n = 4$, $n = 6$, $n = 8$ and $n = 10$.

5.19. Governing equations

The presentation of the equations used to simulate the laminar flow of water inside the horizontal tank and the heat transfer from the heat pipe's head through conduction and convection is detailed in this section.

5.19.1. Continuity and conservation of mass

The equation of mass conservation is expressed in Eq. [87](#) [\[35\]](#), [\[55\]](#).

$$\frac{\partial \rho}{\partial t} + \nabla \cdot \rho \vec{U} = 0 \quad (87)$$

5.19.2. Balance equation for momentum

Eq. [88](#) is representing the momentum equations of water inside the horizontal storage tank [\[35\]](#), [\[55\]](#).

$$\rho \frac{\partial \mathbf{u}}{\partial t} + (\rho \mathbf{u} \cdot \nabla) \mathbf{u} = -\nabla p + \nabla \cdot \tau - \rho \beta (T - T_{ref}) g \quad (88)$$

Where p is the static pressure, τ is the stress tensor (described below), $\rho \beta (T - T_{ref}) g$ is the gravitational body force. Moreover, the stress tensor τ is given by Eq. [89](#).

$$\tau = \mu [(\nabla \mathbf{u} + \nabla \mathbf{u}^T)] \quad (89)$$

5.19.3. Energy equation

The diffusion/convection equation is solved to calculate the temperature field as shown in Eq. [90](#) [\[35\]](#), [\[55\]](#).

$$\rho C_p \frac{\partial T}{\partial t} + \rho C_p \mathbf{u} \cdot \nabla T = \nabla \cdot (\lambda \nabla T) \quad (90)$$

where C_p is the specific heat of the water at constant pressure and λ is the laminar thermal conductivity of the fluid.

5.19.4. Assumptions of the physical models

The unsteady two-dimensional flow and heat transfer equations were governed by the general following assumptions:

1. The working fluid is incompressible
2. The thermophysical properties of the liquid are constant, except for the density that depends on the temperature that is responsible of the thermal buoyancy effect. In fact, Boussinesq approximation has been used [35]
3. The liquid is Newtonian
4. The viscous dissipation is negligible
5. Fluid motion is laminar and two-dimensional

5.20. Storage efficiency and performance indicators

Solar energy is not usually used when it is produced, making the storage system essential [35]. The storage system is designed and sized according to the required autonomy time and the necessary amount of energy, and it must be as efficient as possible to restore the maximum stored energy, which is to minimize heat loss to the outside and improve the thermal efficiency [66].

5.20.1. Thermal efficiency assessment

Thermal efficiency is widely considered criterion used to assess the performance of energy storage systems, because it allows measuring the amount of the available energy and its quality. In general, there are three forms of stratification in a storage tank system [244]. Fully brewed tank where the entire storage system is at uniform temperature, a stratified tank described by a hot temperature zone at the top and a cooler zone at the bottom, separated by a zone of thermal gradients called thermocline, this case has been discussed in the section “CFD code validation”, and will be presented in detail. Finally, a perfectly stratified tank where the thermocline between the hot and cold zones has zero thickness, corresponding to an adiabatic separation of the high and lower temperatures [245]. Thus, the thickness of the thermocline can be an indicator of the degree of stratification: the thicker it is, the less the tank is laminated. It is then possible to realize the interest of a storage system thermally stratified: for the same energy content, the stratified system will have higher temperatures in the upper part and lower in the lower part compared to the tank completely stirred at uniform temperature.

Several parameters affect the thermal efficiency, which can sometimes degrade or reinforce it, depending on the heat transfer method and the operating mode. Indeed, one distinguishes the dynamic mode which corresponds to the charge/discharge of the storage system operating in the static mode, also called cooling, during which the system keeps the energy stored before a new period of charge or discharge. Although static mode is the most common state, dynamic mode plays an important role in real-time analysis [246]. As regards, the phenomena responsible for the destruction of the stratification, the principal ones are the direct injection of the fluid, the flows of natural convection as well as the conduction and the thermal diffusion within the fluid itself (for example through the thermocline) [245], [247]. Regarding the quality and thermal storage efficiency, it is possible to find in the literature a large number of criteria. Hence, there is currently no universally defined method for assessing thermal efficiency, which also makes it difficult to compare different configurations. Tab. 17 shows different methods defined in the literature to characterize the storage efficiency.

Methods to characterize stratification	Graphic methods	With dimensions [14]	
		Without dimensions [131]	
	Data based on temperature measurements	Degree of stratification represented by dimensionless parameters or indices	Thermocline [32]
			Parameters without dimensions [243]
			Coefficient of stratification [35]
		Efficiencies based on the first law of thermodynamics	Recoverable heat fraction [248]
			Efficiency of charge/discharge and storage [249]
		Efficiencies based on the second law of thermodynamics	Energy efficiency and entropic [250]
			Useful energy fraction [251]
		Other methods	Stratification efficiency [252]
Mix [14]			
	Number of storage evaluation [253]		

Table 17: Used methods to assess thermal efficiency storage.

These methods consist of drawing the temperature profile achieved either by numerical modeling or by the acquisition of experimental data. In general, the height (y) of the storage system is defined on one axis and the temperature (T) on another. The advantage of presenting values in dimensionless form is to show results of different experiments or numerical simulations on a single graph with their normalized magnitudes at the maximum height (H) of the studied system as well as at the maximum temperature difference observed $T_{max}-T_{min}$. In the following studies, these two methods will be used as needed, to achieve the used CFD code validation and to assess the efficiency of the proposed horizontal storage tank's configurations.

5.20.2. Discharging efficiency

The discharging efficiency has been defined as performance indicator to assess the thermal efficiency of the considered geometries (see Eq. [91]). The calculation of this thermal efficiency [39] is based on the difference between the cold inlet temperature T_i being charged and the instantaneous outlet temperature loaded from the horizontal tank $T_o(t)$.

$$\eta_{discharging} = \frac{T_i - T_o(t)}{T_i - T_{ini}} \quad (91)$$

5.21. Research methodology

The next section covers the qualitative research methodology used in this chapter. Firstly, an experimental investigation which will be detailed further has been conducted to measure the temperature of one single heat pipe integrated in an ETC positioned outdoor under the climatic conditions of the city of Fez during the first day of November 2017. In fact, the measurement of the temperature in stagnation [42] of the heat pipe is very useful, because it allows quantifying the energy supply of an ETC in terms of temperature/heat flux necessary for the proposal of an optimal design of the storage tank according to energy performance criteria such as the storage efficiency. Subsequently, the temperature in stagnation measured experimentally using a thermal camera will be applied as a thermal boundary condition in the CFD modeling of the charging/discharging flow cycle and the heat transfer modes by convection/conduction occurring within the 300 liters horizontal solar storage tank of the individual solar water heater. Indeed, the storage tank was designed by CAD software, and CFD parametric studies were performed to assess and optimize the number of heat pipes integrated on the lateral shell of the tank. CFD *Fluent* calculation code was used for the numerical resolution of the previously detailed governing equations and to evaluate

the thermal performance indicators necessary for the optimization study such as the average temperature, temperature contours, streamlines, the storage efficiency etc. Before proceeding with the numerical optimization study, the validation of the numerical code is essential. Hence, we have proposed to validate the used numerical code against the experimental study of Zachar et al. [2] carried out on a vertical stratified storage tank.

5.22. Experimental study

5.22.1. Description of the experimental setup

The aim of the experimental study is to measure the maximum temperature, also known as the temperature in stagnation [42] at the head of the heat pipe which is integrated in the Evacuated Tube Collectors with finned absorber using a thermal “FLIR” camera (see Fig. 73(a)). The ETC with the technical characteristics presented in the Tab. 26 is exposed to the solar radiation of Fez city $34^{\circ} 01'59''$ North, $5^{\circ} 00'01''$ West. The experimental measurements were carried out on the first november 2017 and the evolution of the solar irradiation which is incident on the ETC collector, as well as the ambient temperature were measured by using a pyranometer. The measurement results are presented in Fig. 73(b) and (c).

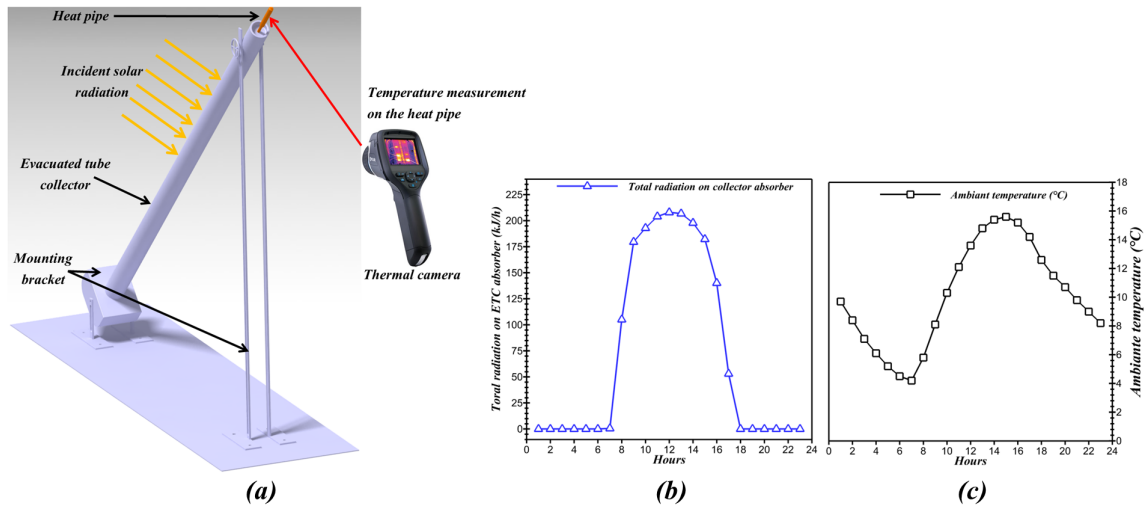


Figure 73: (a)- Experimental setup for measuring the temperature at the head of the heat pipe using a thermal camera. (b)- The total radiation on the ETC absorber measured on the first day of November 2017. (c)- The ambient temperature measured at Fez on the first day of November 2017.

5.22.2. Uncertainty analysis

The ETC collector where the heat pipe is integrated was held in position on a support with a fixed tilt angle, then it was exposed to solar irradiations between 9 am and 15 pm of the first day of November 2017. The head of the heat pipe was exposed to the open air, where the wind speed $u_{avg} = 0.13$ m/s, the air humidity is 25% and it was not a rainy day. The measurement uncertainties of the thermal camera are reported in the Tab. 18

Image data and Optical	
Thermal sensitivity	<0,02 °C to +30 °C
Measures	
Precision	± 1 °C for temperatures between 5 °C and 150 °C ± 2 °C for temperatures up to 1200 °C
Temperature range	-40 to +2000 °C

Table 18: Technical specifications of *FLIR* T1020 thermal imaging camera [47].

Characteristics	Values
Length of the evacuated tube collector	1.800m
External diameter of the evacuated tube collector	58mm
Internal diameter of the evacuated tube collector	47mm
Length of the heat pipes	100mm
Diameter of the heat pipes	27mm
Glass thickness of the evacuated tube collector	1,6mm
Collector materials	Borosilicate glass 3.3 shock-resistant, hail-resistant, 35 mm diameter
Absorption coating	Al-N/Al (copper nitrite)
Absorption >	92% (AM 1.5)
Emittance	7% (100 C°)
Perfect vacuum	P <0.0005
Insulation	Vacuum of 10 ⁻⁴ Pascal
Temperature in stagnation	<220 C°
Heat loss	<0.35W/m ² / C°)
Collector efficiency	90%
The coefficient B =0.84	Characterizes the optical performance of the collector
The coefficient K=1.01	Thermal losses of the collector

Table 19: Technical characteristics of the Evacuated Tube Collector integrating the heat pipe used during the experimental study [6], [43].

5.22.3. Experimental results

5.22.4. Temperature map

The temperatures at the head of the heat pipe were measured for four times of the day, namely 10 am, 11 am, at 12 am and at 14 pm as presented in Fig. [74], the instantaneous maximum temperatures are equal respectively to 55.6 °C, 89.6 °C, 97.8 °C and 121 °C. This experimental study was essential, because it helped to define a variation margin of the heat pipe's temperature. Indeed, it varies between the minimum temperature 48.50°C and the recorded temperature in stagnation equal to 121°C measured in this case at 2 pm during the first day of November 2017. In the next studies, a maximum temperature of 95°C will be applied to the head of the heat pipes during the simulation of the charge/discharge cycles intended to assess the thermal efficiency of the suggested configurations of the horizontal storage tank (n=4, n=6, n=8 and n=10). A temperature below the saturation temperature of water was selected to avoid the evaporation of the stored water. Therefore, the physical model presented in the section "Governing equations" remains valid and could reproduce with accuracy the single-phase flow of water, taking into consideration the heat transfer modes by conduction and convection besides to the buoyancy interactions induced by the effect of water's thermal expansion.

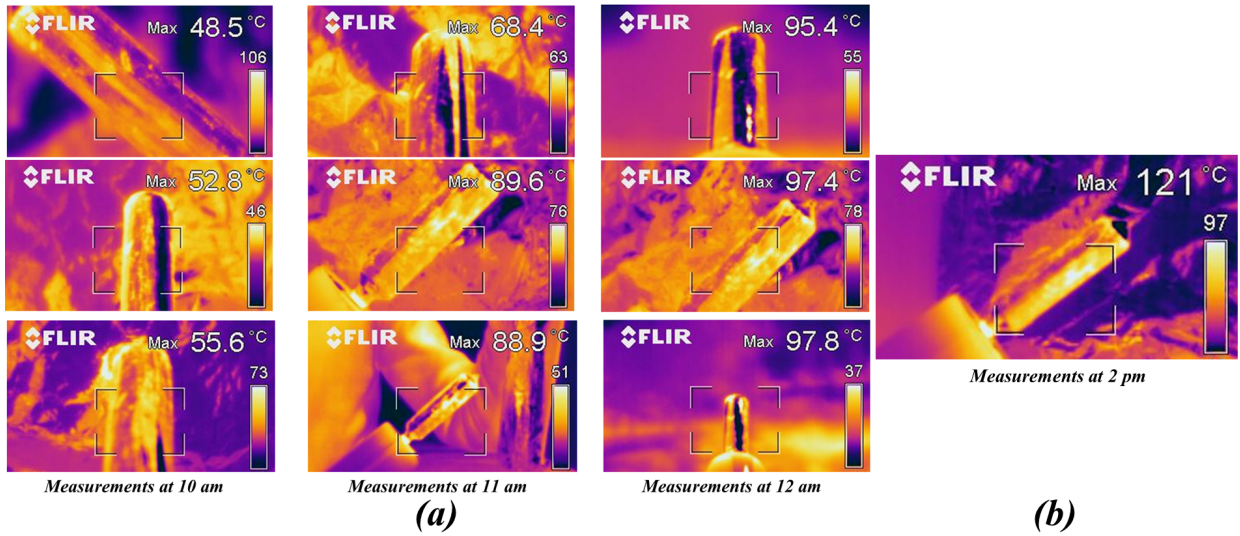


Figure 74: Thermal camera view of the head of the heat pipe. (a)- Measured temperatures at the heat pipe's head below 100°C. (b)- Measured temperature at the heat pipe's head above 100°C.

5.23. CFD code validation

Zachar et al. [2] conducted both experimental and numerical investigations on a transparent storage tank, so as to visualize the development of the thermocline evolution when a dye is injected into water by the injection nozzle located at the bottom of the tank Fig. 75(a). Fig. 75(b) shows a two-dimensional section of the transparent experimental storage tank which presents its dimensions and the position of the flat plate used to enhance thermal stratification. Measuring the evolution of temperature inside the storage tank was achieved by using a tree thermocouple on which a series of 20 thermal sensor were stuck respecting an equidistance. The thermocouple tree is located half way between the wall of the tank and its revolution axis (Fig. 75(b)).

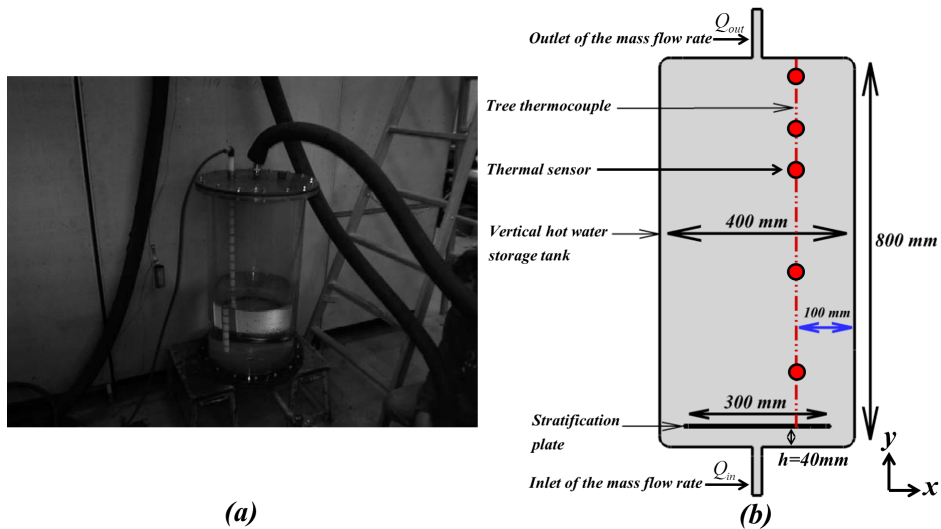


Figure 75: (a)- Picture of the experimental set-up achieved by Zachar et al. [2]. (b)- Representative diagrams of a two-dimensional section of the vertical storage tank that includes a plate for the improvement of thermal stratification.

The experimental measurements which are reported by Zachar et al. [2] were first of all validated through the implantation of their own house program, and thereafter using the CFX commercial code. As far as we are concerned, we used the commercial code OpenFOAM to reproduce the results presented in the study of Zachar et al. [2]. In fact, the validation study is based on the comparison of the experimental recorded temperatures using the thermal sensors against the temperature evolution in the axial direction inside the tank using the numerical results of the CFD simulation code (Fig. 75).

5.23.1. Experimental and numerical study of Zachar et al. [2]

Zachar et al. [2] carried out an experimental study to visualize the thermal stratification and the evolution of the thermocline thickness within a standard storage tank. In our case, the CFD OpenFOAM numerical software was used to reproduce their experimental results. The studied experimental storage tank has a height of 0.800 m and an internal diameter of 0.400 m. The cold water charge and the hot water discharge are performed by two injection nozzles located on the lower and upper disks of the tank, such as the diameter of these apertures is 0.020 m. A very thin flat plate with 0.300 m in diameter has been placed at the lower zone of the tank. It is located at 0.040 m apart from the injection aperture. The aim of having this plate placed at the lower zone of the tank is to decrease the flow velocity coming from the inlet nozzle section. Hence, thermal stratification has been enhanced inside the storage tank.

The operating boundary conditions that has been used for the validation are an applied flow rate at the inlet nozzle $Q_{in} = 0.26\text{kg/s}$. The walls of the tank were maintained adiabatic and a data recording unit has been connected to a computer to ensure the record of the temperatures measured by the thermocouples at the end of each 10 seconds. Transient CFD simulations were performed in order to validate our numerical results against the experimental measurements of Zachar et al. [2]. The SIMPLE algorithm has been used for the pressure-velocity coupling. Besides, the first order Upwind method and the second order scheme were used for the discretization of pressure, momentum, and energy equations respectively. A convergence study of the time step was also conducted with regard to the used cell size equal to 4 mm. In fact, it was found that a time step in the range of 10^{-4} , 10^{-3} is suitable for the simulations and would ensure accurate results. Moreover, the flow regime was supposed to be laminar because of the low flow regime that occurs during the charge/discharge modes which were investigated in the experimental study.

Initially, the vertical tank is supposed to store hot water at a homogeneous temperature of 40°C , while a zero velocity field is assumed before the transient simulation are launched. The numerical solution is supposed to be convergent when the scaled residuals for the continuity, the momentum and the energy equations are less than 10^{-4} , 10^{-5} and 10^{-8} respectively. A parallel processing was launched on a Z600 workstation (16 CPU, 32 Go RAM), and a time step of 5×10^{-4} s was selected to run the simulations. As a result, the computational time lasts 9 hours as an average for a single studied case. The effect of the dimensionless height or the positions y^* (Eq. 92) on the dimensionless temperature T^* (Eq. 93) was considered as an indicator of validation of the experimental study conducted by Zachar et al. [2].

$$y^* = \frac{y}{H} \quad (92)$$

where H is height of the vertical storage tank.

$$T^* = \frac{T - T_{ini}}{T_{ini} - T_{in}} \quad (93)$$

where T_{ini} is the initial temperature of the tank and T_{in} is the charging temperature.

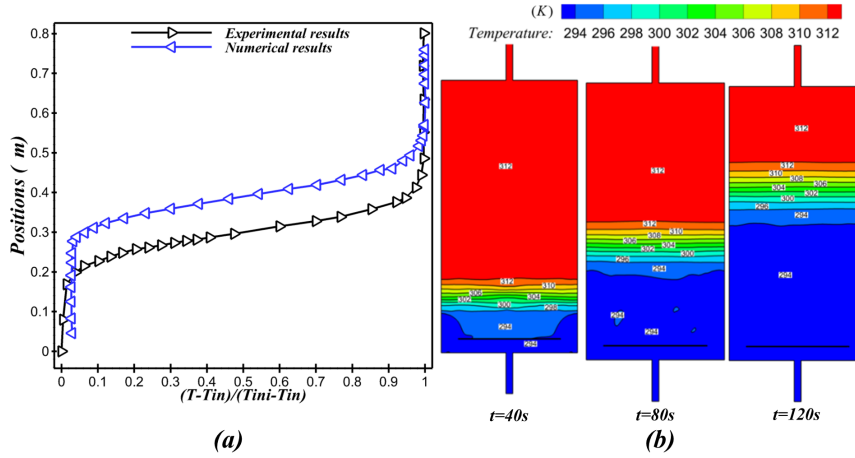


Figure 76: (a)– Effect of the vertical position on the dimensionless temperature (validation curve). (b)- Instantaneous contours of temperature that are corresponding to CFD numerical simulations, and which describe the development of thermal stratification inside the vertical storage tank.

The effect of the vertical positions (y) on the dimensionless temperature T^* is shown in Fig. 76. This figure is presenting the effect of injecting cold water from the nozzle located at the bottom of the storage tank at a temperature of 20°C on the static temperature contours progress, especially at three times $t=40\text{s}$, $t=80\text{s}$ and $t=120\text{s}$. The temperature of the hot water stored initially decreases due to the injection of cold water from the nozzle located at the tank’s bottom.

As presented in Fig. 76-(a), our numerical results approach the experimental measurements, and the gap has been identified by defining the relative error as reported in the Tab. 25. In fact, a good agreement was observed between the experimental measurements of Zachar et al. 2 and our numerical results. Three temperature evolution zones can be distinguished. The first zone, where the temperature difference $T - T_{in}$ is very important, is described by the first quarter of the tank which extends over 0.200 m , which means that the ramp of the curve $y = fct(T^*)$ is significant. However, the difference in temperature over the second quarter which extends over a height of 0.135 m (from 0.2 m to 0.35 m) is less important. Indeed, the dimensionless temperature (Eq. 93) varies between 0.1 and 0.9 , which means that the stratification degree is average. For the last remaining zones $0.35\text{ m} < y < 0.8\text{ m}$, the energy stored within the tank is maximal, because the dimensionless temperature T^* is equal to 1 which means that the thermal stratification is missed in this zone.

Fig. 76-(b) presents the effect of injecting cold water at 20°C over the evolution of the static temperature contours at three times, namely $t=40\text{s}$, $t=80\text{s}$ and $t=120\text{s}$. The temperature map contours show the impact of the charge and discharge modes on the thermocline thickness and hence the stratification constitution.

The discrepancies observed in Fig. 76-(a) can be explained by respecting the assumption of the two-dimensional calculations that have been performed during the simulations. However, the experience is 3D and the effects according to z -axis were not taken into consideration Fig. 76-(b). The relative errors between our simulation results and the experimental dimensionless temperatures measured by Zachar et al. 2 are presented in Tab. 25. A tolerable relative errors are observed, therefore it can be concluded that our simulation results are in a good agreement with the experi-

mental results investigated by Zachar et al. [2].

Experimental results		Our numerical results		Relative error (%)
$\frac{T-T_{in}}{T_{ini}-T_{in}}$	Positions (m)	$\frac{T-T_{in}}{T_{ini}-T_{in}}$	Positions (m)	
0.13	0.24	0.13	0.32	0
0.137	0.24	0.131	0.32	4.37
0.2	0.25	0.2	0.34	0
0.27	0.26	0.27	0.35	0
0.37	0.28	0.37	0.37	0
0.54	0.3	0.54	0.39	0
0.69	0.32	0.68	0.41	1.44
0.84	0.35	0.83	0.445	1.19
0.91	0.37	0.91	0.45	0
0.98	0.41	0.99	0.49	1.02
0.99	0.52	0.99	0.52	0
1	0.55	0.99	0.55	1
1	0.55	1	0.55	0

Table 20: Comparison between the numerical dimensionless temperatures and the relative error's evaluation.

5.24. Mesh independence test and Boundary conditions

5.24.1. Mesh independence test

The mesh independence test was carried out because of its importance in the numerical simulation studies as it has been reported in the thermo-mechanical analysis carried out by Fertahi et al. [42]. In fact, the mesh independence test helps to provide an additional reliability to the achieved results linked to the miscellaneous performed parametric studies. In this considered case study, five structured meshes based on quadrilateral elements were tested to determine the appropriate grid to be used to run the simulations and parametric studies. The meshes that have been proposed to investigate this independence test are presented as follows 15000, 20000, 28000, 36500 and 38000. The evolution of the average temperature measured on the vertical line of the horizontal tank was used as indicator to select the accurate grid that help to achieve the numerical convergence (see Fig. 78-(a)) which depicts the locations of the measurement lines used to evaluate the evolution of the averaged temperature according to different grids.

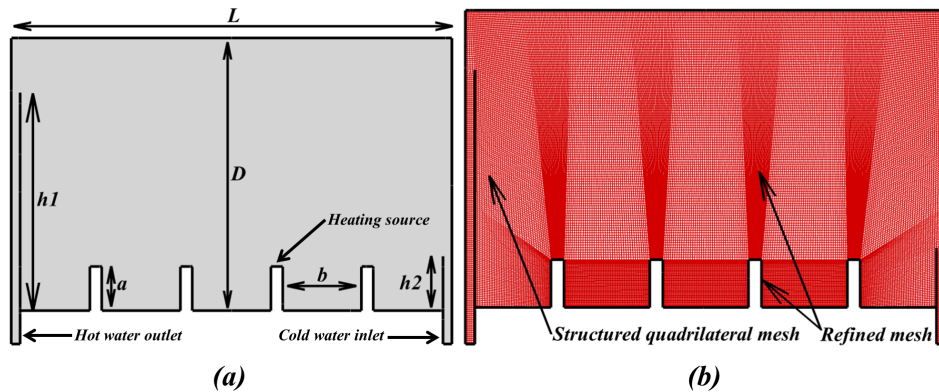


Figure 77: (a)- Symmetrical modeling of the storage tank. (b)- Structured quadrilateral mesh of the fluid field, in addition to the refinement of the meshing elements constituting the different surfaces of the heat pipe's walls.

The evolution of the average temperature along the vertical line, also evaluated at $t=200s$ is shown in Fig. 78 (b). In fact, this temperature evolution has been defined as monitor to ensure the mesh convergence test. The average temperature profile was presented for five grids with different numbers of the meshing elements, from N_1 to N_5 . As shown in the achieved results, the trends of the assessed average temperature present similar pattern. However, it was observed that the temperature profile is reaching a converged pattern with the increase of the meshing elements used to generate the grid and which is slightly beyond 28000 elements. It can be concluded from this mesh sensitivity analysis that the number of elements to be used to generate the accurate fluid field grid is 36500, because a very small changes were recorded concerning the evolution of the average temperature previously assessed on the vertical line that is defined as monitor within the horizontal solar storage tank Fig. 78 (a).

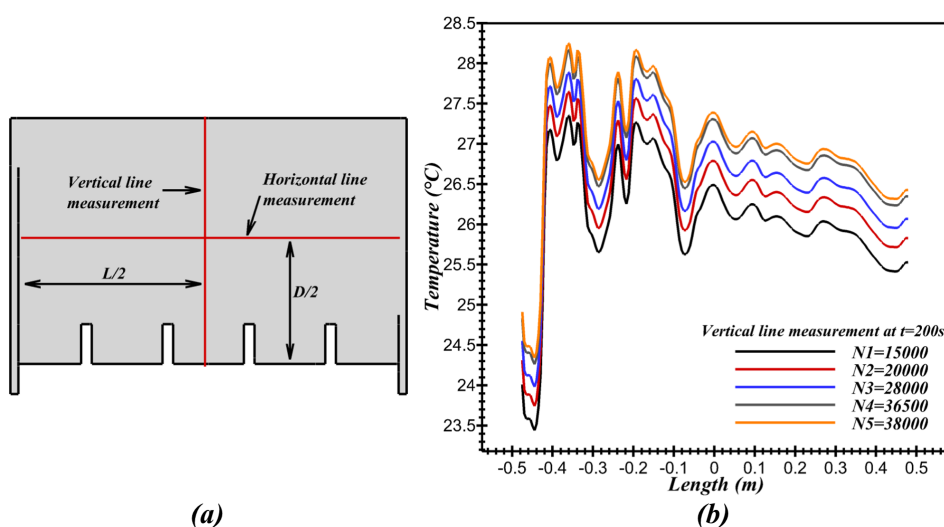


Figure 78: (a)- Line measurement of the average temperature inside the storage tank. (b)- Mesh independence test results.

A local refinement has been applied to the heat pipes that generate heat flux in order to capture the momentum and buoyancy effects of the stored water (see Fig. 77 (b)) [7]. Therefore, the minimum size of the meshing element was 0.0795 mm, and the maximum face size was 3 mm. Besides, the growth factor rate that ensures the homothety of the meshing elements was 1.1. In fact, these settings increased the average quality of the meshed field to 0.91.

5.24.2. Boundary conditions

The locations of the thermal boundary conditions are presented in Fig. 79 (a) and (b). The ETC with finned absorbers incorporating the heat pipes convert the available solar energy into a thermal heat flux at the top of its condenser section as described in the work released by Jafari et al. [254] and Fadhl et al. [101] who have worked on the CFD modelling of a two-phase closed thermosyphon charged with R134a and R404a. As it was planned, the use of the thermal camera during the experimental study helped to predict the evolution margins of the temperature on the head of a single heat pipe. It was found that, the temperature in stagnation ($T_{max} = 121^{\circ}C$) exceeds the saturation temperature of water ($100^{\circ}C$) [170]. Hence, to simulate a single-phase flow including heat transfer preventing the phase change to occur, it has been decided to apply a temperature

slightly lower than 100°C at the heat pipes head. Consequently, a constant temperature $T_{hp} = 95^\circ\text{C}$ has been applied at the heat pipe's head (see Fig. 79(b)) [42]. Moreover, to model a perfect thermal insulation of the horizontal tank, because practically the inner shell of the commercialized tanks is perfectly insulated [15], the surfaces Σ_1 , Σ_2 and Σ_3 were maintained adiabatic.

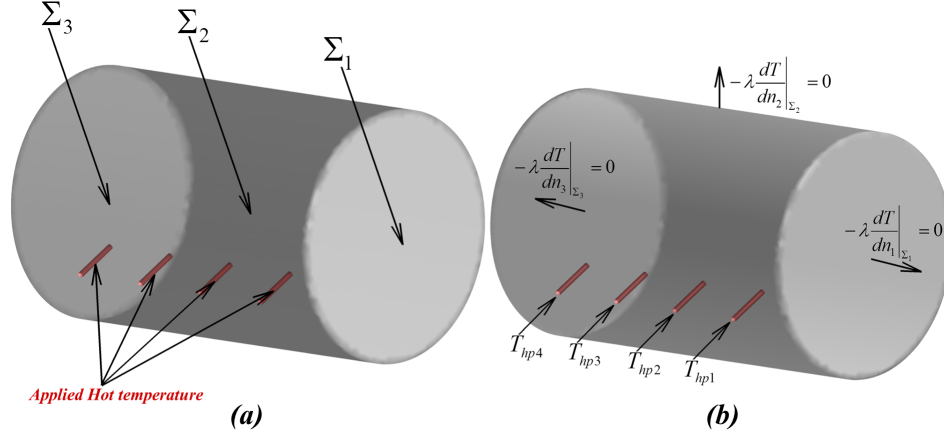


Figure 79: (a)- Locations where the boundary conditions are applied. (b)- Constant heat flux applied at the heat pipes, while the surfaces Σ_1 , Σ_2 and Σ_3 are maintained adiabatic.

5.25. Solution strategy and convergence criteria

Unsteady simulations were carried out to simulate water flow and heat transfer between the stored water and the heat released from the heat pipes located inside the horizontal storage tank. A second order scheme was used in the resolution of the unsteady part of URANS equations. In fact, a time step Δt of 10^{-3} s provided a courant number (CFL) expressed in Eq. 94 between 0.3 and 5 which increased the accuracy of the achieved numerical results [7]. The constant time step has been evaluated using Eq. 95 as mentioned in [255]. Moreover, 85 sub-iterations were performed at each time step. The SIMPLE algorithm has been used for the pressure-velocity coupling. In addition, a second order numerical scheme was used for momentum, energy equations and pressure interpolation scheme discretization respectively. Our numerical calculations were supposed convergent when the scaled residual of the mass, velocity and energy are less than 10^{-5} , 10^{-5} and 10^{-9} respectively. The temperature's field was uniformly initialized at 60°C .

$$CFL = \frac{u_x \Delta t}{\Delta x} + \frac{u_y \Delta t}{\Delta y} \quad (94)$$

where Δx and Δy are the space steps discretization and Δt is the time step discretization.

$$\Delta t = \frac{\tau}{4} = \frac{D}{4\sqrt{g\beta\Delta T D}} \quad (95)$$

5.26. Results and discussion

5.26.1. Effect of heat pipe's number on HTC

The dynamic evolution of the heat transfer coefficient (HTC) is presented in Fig. 80. HTC has been studied for a period of 5 min which corresponds to the time required to ensure the discharge of the horizontal tank. In fact, HTC was calculated numerically using Eq. 96 for each configuration

of the heat pipes integrated into the storage tank i.e. ($n = 4$ Fig. 80(a), $n = 6$ Fig. 80(b), $n = 8$ Fig. 80(c) and $n = 10$ Fig. 80(d)). The heat exchange between the heat pipes where a constant temperature has been applied and the initially stored hot water mass is affected by the cold water charged and the hot water loaded. We can also notice that the HTC's evolution trends are becoming similar by increasing the number of heat pipes from 6 to 10 (see Figs. 80(b), (c) and (d)), and the thermal contribution of the heat pipes becomes constant from the instant $t = 150$ s.

$$h = \frac{q}{A(T_{hp} - T_{\infty})} \quad (96)$$

For instance, the HTC calculated numerically for the heat pipe close to the outlet of the storage tank for the configuration 6 heat pipes (see Fig. 80(b)) is estimated to 212.5 W/K.m^2 . Besides, regarding the configuration 8 heat pipes presented in Fig. 80(c) the HTC has reached 300 W/K.m^2 , finally for the configuration 10 heat pipes shown in Fig. 80(d) the HTC is 230 W/K.m^2 . Moreover, it is noted that the values of HTC at the heat pipe located right next to the outlet of the tank are higher than those of the first heat pipe located near the cold water inlet. This result is explained by to the small temperature difference ($T_{hp} - T_{\infty}$) recorded during the considered discharge cycle.

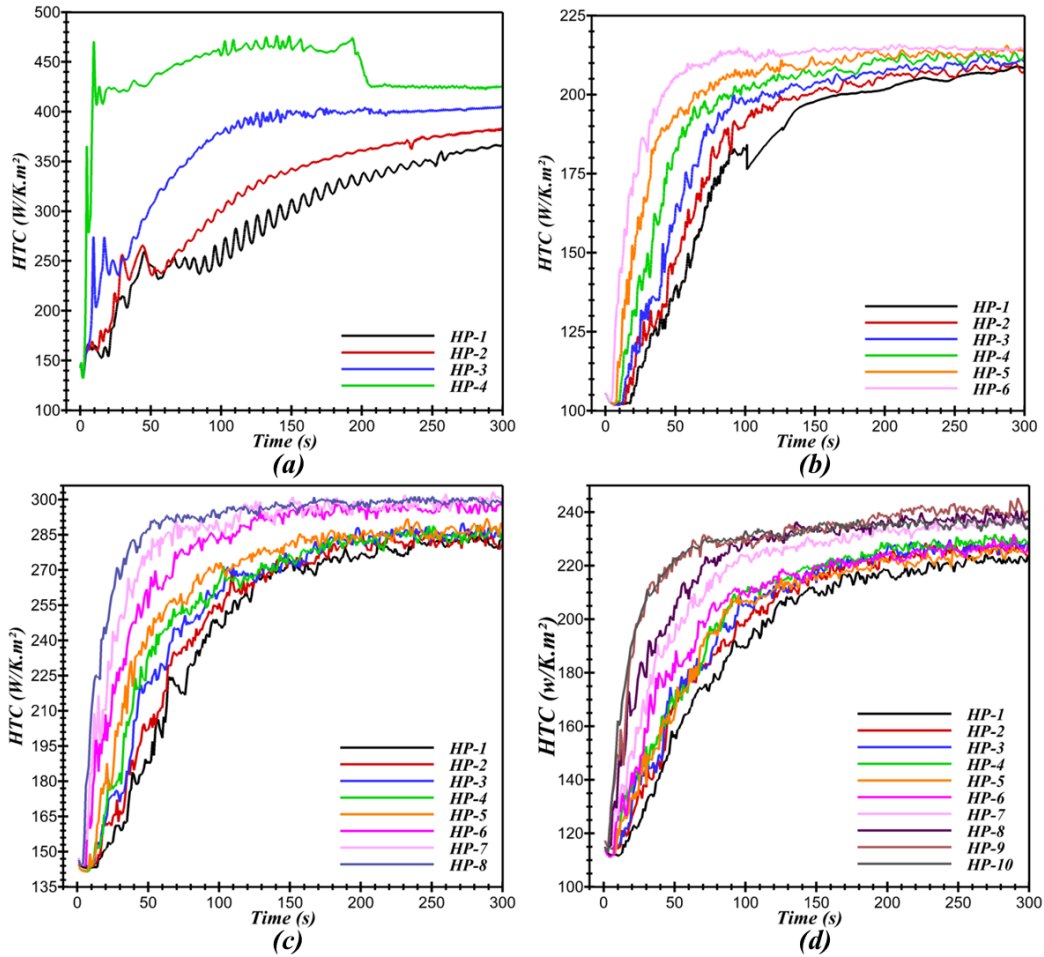


Figure 80: Effect of heat pipe's number on the heat transfer coefficient (HTC) evolution.

Similar studies have been carried out on thermal stratified storage tanks linked to SWH using FPC and ETC technologies. For instance, Tang et al. [9] carried out experimental investigations to analyze the thermal performance of water-in-glass ETC solar water heaters at nights. They found that reverse flow rate in the SWH is affected by the collector tilt angle of the ETC. Also, the reverse flow rate of the SWH was much higher as compared to that in a thermosyphon domestic SWH with FPC. Further, Hasan et al. [256] investigated the effect of the hot water storage tank volume on its efficiency using *Trnsys* program. They concluded with the following results: first, larger storage tanks help to improve the system's efficiency. Second, horizontal and vertical storage tanks provide similar efficiencies and useful solar heat and finally, the SWH performance is better described by the supplied heat to the load instead of the gained solar energy.

5.26.2. Effect of heat pipe's number on the temperature and streamlines contours

The effect of the heat pipe's number on the temperature contours is presented through the results illustrated in Fig. 81. The temperature applied at the heat pipes is 95°C and the velocity inlet of the charged cold water is maintained at $U=0.1\text{m/s}$. Figs. 81-(a), (b), (c) and (d) show the temperature distributions inside the horizontal storage tank (300 liters) with respect to the studied configurations, namely $n = 4$, $n = 6$, $n = 8$ and $n = 10$. After performing the numerical simulations, it appears from the achieved results presented in Fig. 81 that varying the numbers of heat pipes from 4 to 10 disturbs and affects the heat transfer inside the horizontal tank. At early times $t=50\text{s}$, heat transfer by conduction is predominant and the dynamic evolution of the shape's interface created between water and the heat pipes mimics the heated wall's profile. However, as the heating time progresses ($t=150\text{s}$), it is noted that the heat transfer by convection takes over the conduction, and the effect of buoyancy forces becomes important [257]. Through the contours of isotherms, the heat recovered from the heat pipes is transferred by convection to the top center of the horizontal storage tank. Furthermore, temperature gradients become higher near the bottom side of the tank where the heat pipes are located, also the isotherms have a distorted pattern and no symmetrical structure is observed while increasing the heat pipe's number. As a result, the temperature in the top portion of the storage tank remains higher than the bottom portion, because the stored hot water volume is constantly cooled by water coming from its inlet nozzle during the discharge cycle. In addition, the distortion of temperature contours increased with the increase of heat pipe's number due to the buoyancy forces. In fact, the isotherms have a distorted pattern and no symmetrical structure is observed.

Figs. 82 show the streamlines distribution for the studied configurations of the heat pipes integration inside the horizontal storage tank. Figs. 82-(a), (b), (c) and (d) represent the effect of heat pipe's number on flow structures which confirm the same observations highlighted in isotherms contours. In the side edge of the heat pipes, we notice that the effect of heat transfer by conduction is dominant than convection. Comparing the streamlines for different heat pipes number, it may be noticed that when $n = 4$, the streamlines have a concentric elliptical forms. When n is increased ($n = 6$, $n = 8$ and $n = 10$), the flow structures are distorted and a complex structure of the fluid dynamic appears. Consequently, the heat recovered from the heat pipes is transferred by forced convection to the top and near to the outlet nozzle.

As part of the same study, Wahiba et al. [30] carried out 3D unsteady CFD simulations to investigate the effect of several design and operating flow behavior, thermal stratification and performance of a hot water storage tank installed in solar thermal energy systems. They showed through their achieved results that two-dimensional and 3D transient CFD simulations can be used as an effective tool to optimize thermal storage tank parameters at early design stages. Moreover,

Dehghan et al. [11] carried out numerical investigation of the unsteady thermal efficiency behavior of a vertical storage tank of a DSWHS with a mantle heat exchanger in the discharge/charge mode. Their pre-established thermal stratification is well preserved during the discharging operation mode for higher values of Grashof number. Moreover, the tank inflow Reynolds number and or its inflow port diameter should be kept below certain values to provide water with a proper temperature for consumption. In our investigated parametric studies, the Reynolds number has been kept constant and provided laminar flow patten inside the horizontal storage tank. In addition, it is noted that Imtiaz et al. [16] analyzed a conical solar water heater (CSWH) with an attached thermal storage tank, with or without an evacuated glass absorber under different operating conditions. The efficiency of their CSWH increased with increasing inlet flow rate, and the maximum efficiency of the system was achieved at a critical flow rate of 6L/min and reciprocally. In our case, the thermal efficiency of the tank increased with the increase of the heat pipe numbers during the discharging cycle, but the flow pattern was disturbed. In fact, this result was depicted on the temperature contours and streamlines.

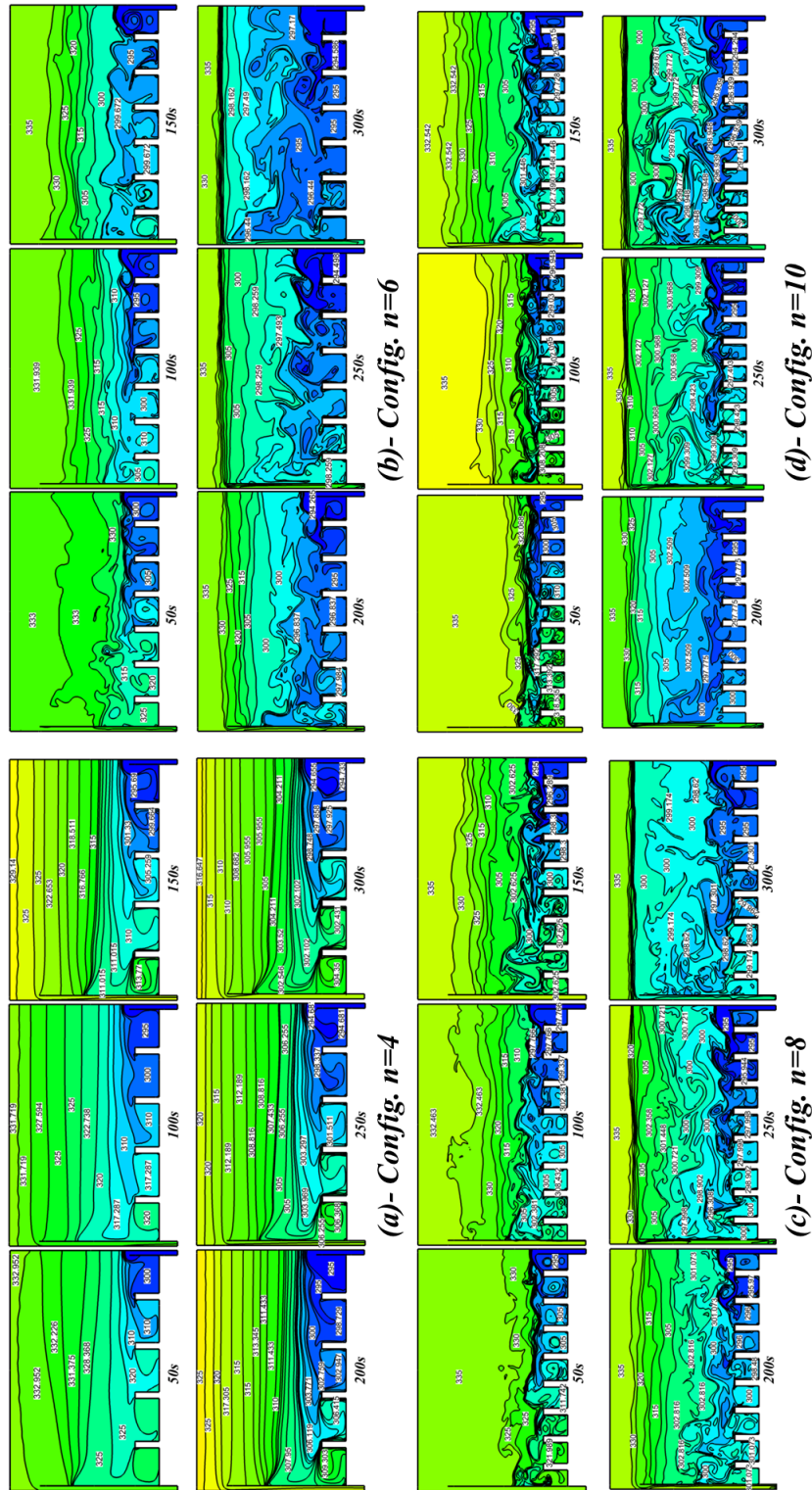


Figure 81: Dynamic evolution of the temperature contours for four configurations, namely $n=4$, $n=6$, $n=8$ and $n=10$.

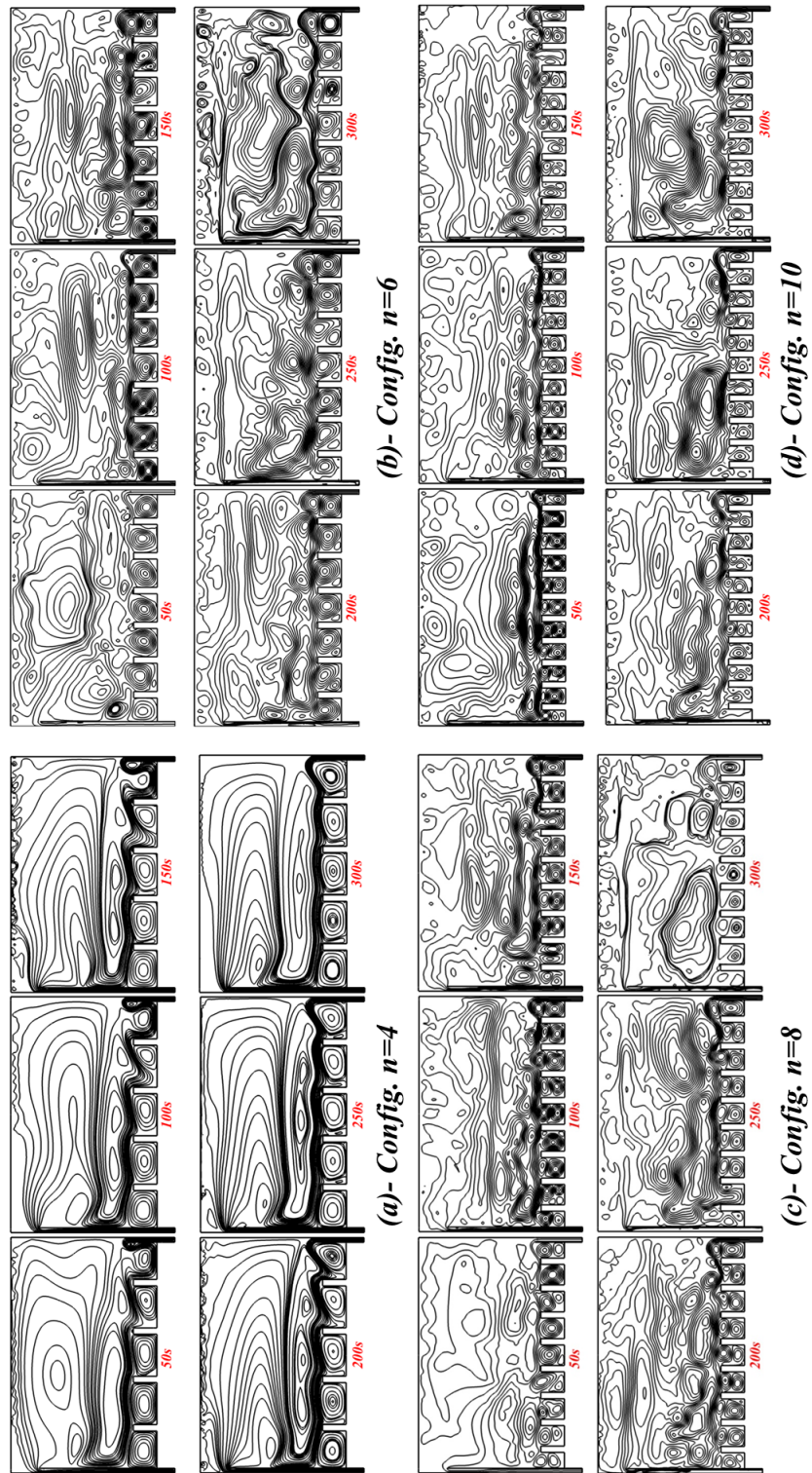


Figure 82: Dynamic evolution of the streamline contours for the fourth considered configurations.

5.26.3. Effect of heat pipe's number on the median temperature

The evolution of temperature along the median horizontal and vertical lines defined at the middle sides of the tank (see Fig. 78-(a)) is presented in Fig. 83 for the investigated four configurations. Five instants were selected to evaluate the unsteady temperature variation during the hot water charging/discharging cycle, including $t = 50\text{s}$, $t = 100\text{s}$, $t = 150\text{s}$, $t = 200\text{s}$, $t = 250\text{s}$ and $t = 300\text{s}$. It is noted that increasing the number of heat pipes affects the temperature evolution trends along both of the horizontal and vertical lines considered as indicator parameters for this current numerical study. For instance, the effect of the configurations $n = 6$ and $n = 8$ (see Fig. 83-(b) and (c)) on the instantaneous trends of the assessed temperatures could be compared with the effect of the basic configuration of the tank which includes four heat pipes ($n=4$). Temperature has decreased with time, because the tank was storing initially hot water, and the amount of the loaded water was simultaneously replaced by cold volume. After 5 min of hot water loading, the temperature monitored along the horizontal line decreased from 57°C to 31°C (for $n=4$ heat pipes). Besides, it has decreased from 57°C to 32°C while considering temperature variation along the vertical line for the storage tank integrating four heat pipes. Fluctuations in temperature, as previously shown in Fig. 83, are explained by the disturbance of the flow's regularity pattern generated by increasing the number of heat pipes, which thus caused multiple cold water recirculation zones as presented respectively by the temperature and streamline contours in Figs. 81, 82.

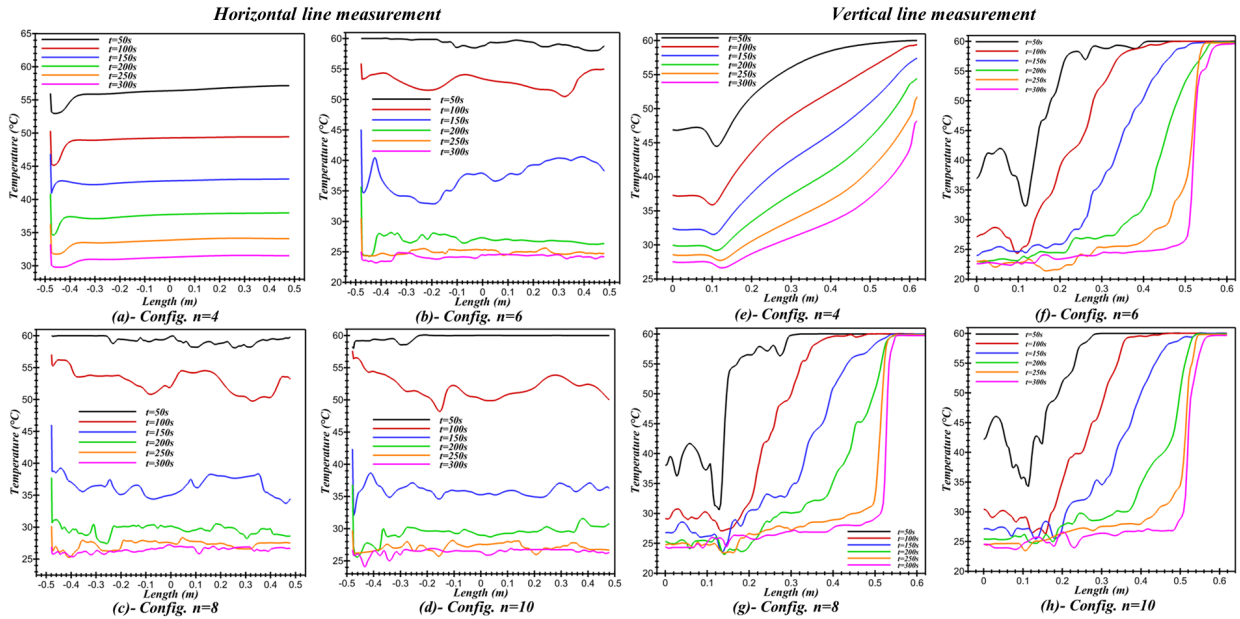


Figure 83: Temperature measurements according to the horizontal and vertical lines for the configurations $n=4$, $n=6$, $n=8$ and $n=10$.

5.26.4. Effect of heat pipe's number on the tank's average temperature and the discharging efficiency

The evolution of the average temperature of the stored hot water subjected to charge/discharge operating cycles is shown in Fig. 84-(a). The numerical simulated time for the discharge operation lasts 5 minutes. We can notice that the average temperature of the horizontal tank is increased by the increase of the heat pipe's number, because additional heat sources are added. Indeed, they contribute to the heating of the charged cold water although the discharge cycle is being applied.

At $t = 200$ s, the achieved average temperature for the basic configuration $n = 4$ is 36°C , while it is 39°C for the configuration $n = 10$. In addition, at $t = 250$ s the average temperature corresponding to $n = 4$ drops to 31°C and it decreases by 4°C for the configuration $n = 10$ to achieve 35°C . As time increases, $t = 300$ s, the average temperature of the horizontal tank drops to 30°C for $n = 4$, and reaches 33°C for the configuration $n = 10$.

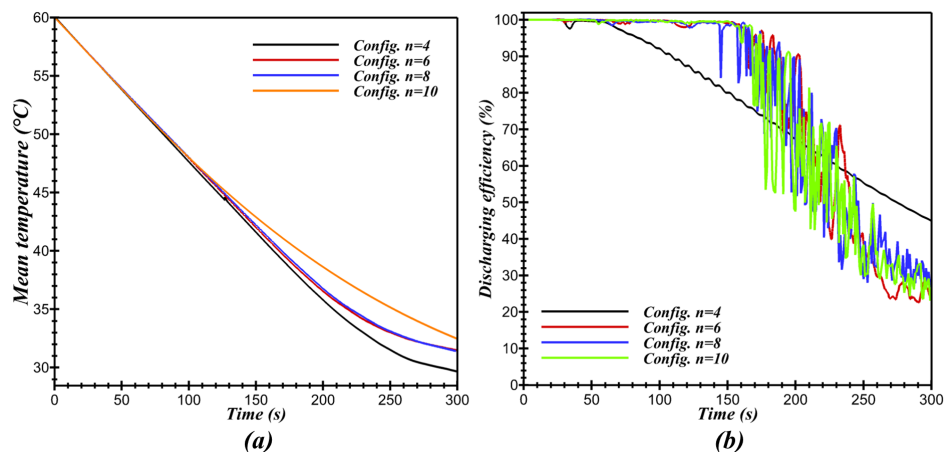


Figure 84: (a)- Evolution of the mean temperature according to the studied configurations. (b)- Discharging efficiency assessed for $n=4$, $n=6$, $n=8$ and $n=10$.

The evolution of the discharging efficiency is presented in Fig. 84(b). As it has been presented in Eq. 91, the discharging efficiency of the horizontal storage tank depends mainly on the instantaneous variation of the temperature of water assessed at the outlet nozzle of the tank $T_o(t)$. It has been shown through the previously achieved results, particularly the temperature contours and the streamlines that the configurations $n = 6$, $n = 8$ and $n = 10$ contribute in the disturbance of the laminar structure of the flow field inside the horizontal tank and causes the appearance of multiple recirculation zones that favor the stagnation of several masses of cold water between the heat pipes. Therefore, the outlet temperature of the hot loaded water is also affected and has a fluctuating trend. Thus, as presented in Fig. 84(b) the instantaneous evolution profile of the discharging efficiency considered as performance indicator for the configurations $n = 6$, $n = 8$ and $n = 10$ is clearly different from that of the basic configuration $n = 4$, characterized by a decreasing variation profile of the outlet drawn hot water which has indeed no fluctuation trend.

5.27. Conclusion

In this chapter, a special attention has been paid to the sensitive energy storage of domestic hot water stored in a horizontal tank where heat pipes are integrated. Indeed, the thermal performance of a 300 liters capacity horizontal tank that initially stores hot water and which is subjected to a charging/discharging cycle was assessed through a set of performance indicators. Consequently, the main purpose of this work is to suggest a new optimal design of the studied horizontal tank considered as the main device in individual solar water heaters (SWH) integrating Evacuated Tube Collectors (ETC) with heat pipes.

First of all, an experimental study was conducted to measure the evolution range of the temperature that the heat pipe integrated in the ETC could achieve using a thermal camera. On the basis of the experimental results, CFD simulations were performed on the horizontal storage tank

to assess the effect of the heat pipe's number, integrated on its lateral internal shell, on its energetic performances (Discharging efficiency). In fact, four cases were studied according to the number of the used heat pipes (n), namely $n = 4$, $n = 6$, $n = 8$ and $n = 10$. The computational code has been validated using the experimental results available on the literature and a good agreement has been achieved. Several performance indicators were defined to identify the optimal configuration, such as the heat transfer coefficient evaluated at the heat pipe regarding each considered configuration, temperature and streamlines contours, temperature evolution according to specific paths defined inside the storage tank, the average temperature and finally the discharging efficiency.

Based on the above results and discussion, it was concluded that the HTC calculated for the heat pipe close to the outlet of the storage tank for $n = 6$ achieved 212.5 W/K.m^2 , while it is 300 W/K.m^2 for $n = 8$ and 230 W/K.m^2 for $n = 10$. Moreover, it was found that the values of HTC at the heat pipe located in the right next to the outlet of the tank are higher than those of the first heat pipe located near the cold water inlet, because the temperature difference ($T_{hp} - T_{\infty}$), recorded during the considered discharge cycle, was small. The average temperature of the horizontal tank is increased by the increase of the heat pipe's number because of rise in heat sources. Indeed, additional heat sources accelerate the heating of the charged cold water although the discharge cycle is applied. Otherwise, the discharging efficiency of the horizontal storage tank depends mainly on the instantaneous variation of the water's temperature assessed at the outlet nozzle of the tank ($T_o(t)$). Increasing the heat pipe's number disturbs the laminar structure of the flow field inside the horizontal tank, thus the outlet temperature of the hot loaded water is also affected and presents fluctuating trend.

6. Part III: Thermal efficiency optimization and enhancement of collective *SWHs* through dynamic simulations

6.1. *Chapter VI: Design and thermal performance optimization of a forced collective solar hot water production system in Morocco for energy saving in residential buildings*

6.2. *Introduction*

This chapter presents a comprehensive study that aims to assess the energetic performances of a solar hot water collective system under a realistic load consumption profile in Morocco. The case study which has been considered in this work is a residential building located in Fez city. Several parameters are involved into the performance assessment of the collective system. Hence, it was essential to identify the parameters on which we will act in order to carry out the parametric study. In fact, the technology of evacuated tube collectors (ETC) with heat pipes were selected as a fixed study parameter, while a set of other indicators were investigated contributing to the collective hot water system design and optimization, such as the solar collector panel total area, the connecting methods between the collector's field which could be serial, parallel or mixed connection, the collective hot water storing volume configurations in addition to the intrinsic optical efficiencies of the world's manufacturers solar collectors. In order to achieve the assessment of the energetic performances of the collective system, four parametric studies were described and carried out to ensure its design and optimization during the dynamic mode operation.

The most relevant findings from this chapter are presented as follows. Incrementing the collector's field area to 120 m² optimizes the thermal efficiency of the collective system, and the hydraulic booster consumption is reduced. Besides, it would be advantageous to use a total area of 80 m² to satisfy the hot water need demand over the four seasons, since the overall collective system thermal efficiency remain above 60%. Moreover, it was possible to ensure a seasonal solar fraction which is greater than 50% by connecting a collective storage tank with a volume of 1500 l and a solar collector panel with an area of 100 m². Last but not least, the effect of the row's number as well as the number of collectors connected per row on the overall collective system's solar fraction was also investigated through this study.

At the present usage level, it is accepted worldwide that the non-renewable energy resources will be available only for a limited period. Accordingly, the need for renewable energy resources has emerged and become very urgent. As an absolutely clean energy, solar energy is one of the most important energy source that has been highlighted so far [258]. Solar water heaters technologies represent a solar thermal application, since they are now well developed and could be easily implemented at a low cost [259].

A number of strategic studies on solar water heaters are available in the literature to investigate various aspects such as their national or international integration in the market, the price of their maintainability, marketing [260]. Recently, in North Africa's and Middle East countries (MENA) [93] several strategic studies on solar water heaters were conducted. For instance, in Algeria, the market potential and the development prospects of the solar water heater field were presented in the work of R. Sellami et al. [69]. Moreover, Mohammed S. Al-Soud et al. [261] studied the integrating possibility of a 50MW concentrating solar power plant for Jordan country. In Lebanon, Isabella Ruble et al. [70] investigated the barriers and the different achievements of domestic solar water heaters. Furthermore, a review on the renewable energy implementation progress in the Gulf Cooperation Council countries was released by Abdul Waheed Bhutto et al. [262]. For residential and hotels applications, Delgado et al. [263] worked on the adaptation and sizing of Solar Water Heaters in Desert Areas. Also, a systematic literature review released by Atika Qazi et al. [264]

is addressing the importance of the artificial neural network in the prediction and design of solar radiation solar systems.

In South Africa, Friedrich Ferrer et al. [265] carried out an average economic performance of solar water heaters for low density dwellings across. The potential and reality of the solar water heater program were studied in Tshwane townships [71], which is a South African City. South Africa was also considered as a studied case in [266], to highlight the low-income housing Residents' challenges with their Government after the integration of Solar Water Heaters (SWH) in buildings.

In Mexico, the Yucatan Peninsula, Victor H. Quej et al. [267] estimated the daily global solar radiation by day of the year in six different located cities. In addition to this, more precisely in urban and rural households also located in Mexico, Rosasflores et al. [268] were interested in the potential energy saving by using solar water heaters. Their study was based on geographical information system.

In China, high priority in the promotion of buildings that are integrating solar water heaters in urbanized areas was presented in [269] through an overview on the potential, recommendations, and experience of this solar technology. Moreover, Frauke Urban et al. [270] proved that solar PV and more precisely solar water heaters are two different energy pathways to decrease the carbon emission in China. An overview about the development of solar water heater industry in China was also presented [271], and an integrated approach to assess the performance of solar water heater in the urban environment was developed by Li et al. [272].

Solar water heaters are considered as a potential application in Turkey [273]. In Australia, S. Rezvani et al. [274] assessed the reliability of solar water heaters through Monte Carlo analysis. Their techno-economic integration possibility into the market was also considered in their study. In Taiwan, Chang et al. [275] presented an outlook for solar water heaters. Also, Lin et al. [276] estimated their payback period for residential buildings.

Actually, energy efficiency has become a priority in buildings. Thus, Vineet Saini et al. [277] carried out an economic analysis of various photovoltaic technologies' types which are integrated with greenhouse solar drying system. Moreover, Energy consumption and water rationalization in shower systems used in dwelling houses for single families was debated by Kordana's study [278]. The energy efficiency design for sustainable housing development was introduced through the studies of Kamand M. Roufehaei et al. [279]. As for another study, Pei Ru Chao [280] focused on the sustainable residential development that are using rainwater-sourced hot water supply through the establishment of water consumption characteristics. Besides, Baljit et al. [281] conducted a review on two major solar integrated applications in building's sector, namely photovoltaic and solar thermal systems such as individual solar water heaters, and Jaisankar et al. [282] released a comprehensive review on solar water heaters. Furthermore, residential and hotel buildings were considered as a case study by David Zambrana-Vasquez et al. [283] to assess the environmental impact of domestic solar hot water systems.

The life cycle environmental impact of a solar water heater was assessed [284]. In fact, Arnaoutakis et al. [285] realized comparative experimental Life Cycle Assessment of two commercial solar thermal devices for domestic applications. Besides, an ontology-based decision was presented in [286] as a supporting tool to optimize the selection of domestic solar hot water system.

Interesting released scientific studies are currently investigating the key parameters in the operating conditions of solar hot water systems. In fact, Bouhal et al. [50] studied the impact of load profile and collector technology on the annual solar fraction savings of solar domestic water

heaters under various Moroccan climatic conditions. In addition to this, Taheri et al. [97] assessed the efficiency of a compact solar water heater. Besides, *Trnsys* simulation tool is currently widely used to model the dynamic operation of solar water heaters [287]. In Quebec, Moreau et al. [288] elaborated a field study of Solar Domestic Water Heaters. They also conducted a set of simulation to enhance the performance of an integrated collector in a storage solar water heater. In India, most of its industries that were taken as a case study are currently using solar energy as an effective process for heating, as detailed in the study investigated by N.S. Suresh [289].

In Morocco, the energy consumption in the building sector is representing the major part of the total energy budget. Since Morocco possesses an important potential of solar energy (an average daily solar radiation which is about $5.3kWh/m^2$ with more than 5000h of sunshine annually [93]) and being part of the country development process and the country sustainability, Morocco tended to exploit in the recent decades this renewable energy by launching several solar projects [290]. Accordingly, the development of solar hot water collective systems in Morocco seems to be a great perspective within the new government strategies for the promotion of renewable energy projects [177]. In fact, the current study belongs to SOL'R SHEMSY, supported by the "Institut de Recherche en Energie Solaire et Energies Nouvelles" (IRESEN-Morocco) which aims to industrialize the first solar water heater system "Made in Morocco" [6], [178] and [35].

In this way, the current work aims to derive a knowledgeable data base for the energetic performance parameters concerning the use and implementation of dynamic solar collective systems in Morocco, because in general, the majority of the research works focuses on hot water individual systems and uses simplified model in the simulations of the collective systems [48] [49] [291]. Accordingly, four parametric studies were presented in this chapter to design the collective solar water heater system and to ensure its optimization during the dynamic mode operation. The combined effects of collector's area and its characteristics, climatic conditions and hot water load profile on the performance of the solar collective system were carried out. In addition to this, simulations were conducted for the currently wide-spread solar collector ETC and four different types of manufacturers were considered to provide useful guidelines about the operation of the hot water collective system under a realistic load profile. In this sense, an energy analysis and performance assessment of this system was achieved, and the system's optimal design was reported.

6.3. Collective system description

The collective system and the residential building involved in this study is presented schematically in Fig. [85]. This configuration approaches a real residential building located in Fez city (Morocco). The building is inhabited by 75 occupants and the daily consumption load was estimated at 80 l per person. Hence, the daily hot water need requirement is estimated at 6000 l/day. The consumption of this volume is controlled by the water load profile which will be described and detailed in the section "Weather data and Load profile".

The collective building under investigation consists of a floor set, such that several apartments are associated with each residential floor. The collective solar system with forced hot water circulation production is set on the terrace of the building. It consists of a solar collector's field using evacuated tubes solar collectors (ETC) connected in series or in parallel, a collective storage tank, a control system, and two hydraulic circuits. The first one is a solar circuit which converts solar energy into thermal energy, while the second one is a hot water distribution circuit that allows meeting the needs requirement of each apartment in the different floors of the building.

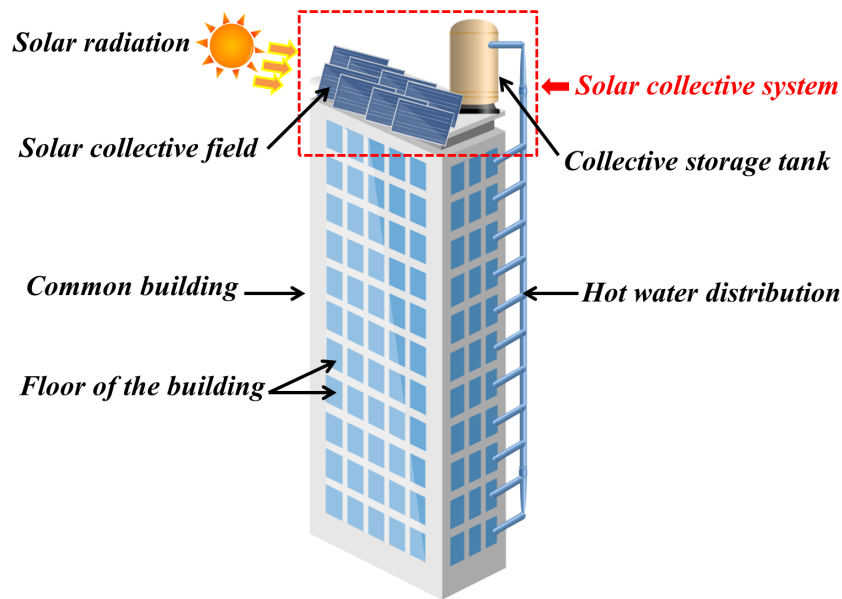


Figure 85: Typical residential building for collective hot water generation [44].

The details of the collective system and its various components are presented in Fig. 86. It integrates a solar tank with an internal heat exchanger, an auxiliary system connected via an internal heat exchanger and a thermostatic temperature control valve. The system consists of a set of solar collectors that supply energy to a DHW tank through an internal heat exchanger located inside the bottom zone. The energy provided to the solar tank is ensured with hydraulic (or an electrical) auxiliary heating system, through a heat exchanger located in the top tank zone.

The system is also equipped with a recirculation circuit in order to afford the desired DHW temperature with a three-way thermostatic valve which mixes the water of the loop of recirculation with warm water of the tank. This element reduces the flow of hot water from the auxiliary flask.

The auxiliary system operates if the storage tank temperature is below the set temperature. This set point temperature value must be higher than the DHW temperature required for consumption. The sizing of the supplement aims to ensure the hot water service in all circumstances and the maximal possible contribution of solar energy.

The control of the primary circuit can be carried out by measuring solar irradiance or by measuring a temperature differential. The pumps operate according to the radiation reaching the collectors, while the temperature differential is between the collectors and the bottom of the tank. The secondary loop can be cross-checked with the primary loop or independently by comparing the temperature of the hot side of the exchanger with that at the bottom of the tank. In all cases, the flow rate of the pumps can be fixed or variable (match-flow system). The system stops the circulation if the temperature of the storage tank or the temperature of the collector is higher than the respective maximum safety temperatures.

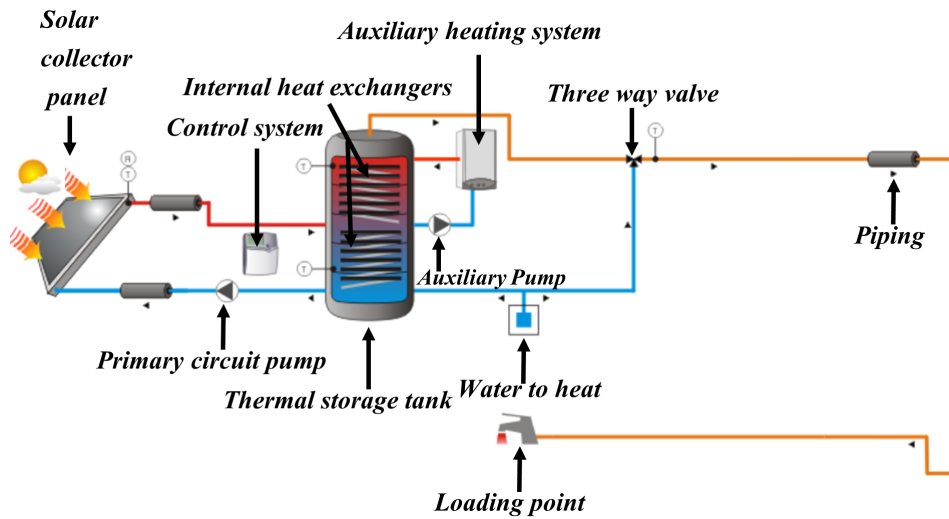


Figure 86: Simplified model of solar hot water collective system [44].

6.4. Weather data and Load profile

6.4.1. Weather data

The average values of the incident solar irradiation on the solar collector field of the collective system, the ambient temperature and the cold water temperature of the climate zone 3 (Fez, $34^{\circ} 03' N 4^{\circ} 58' W$) [93] is presented in Fig. [87]. The evolution of the total horizontal radiation on the solar collector is also presented on the first 15 cold days of January. *Meteonorme* software was used to determine the meteorological data which are intrinsic to the city of Fez in terms of solar radiation flux, ambient temperature and the temperature of the cold water heated over a period which lasts one year.

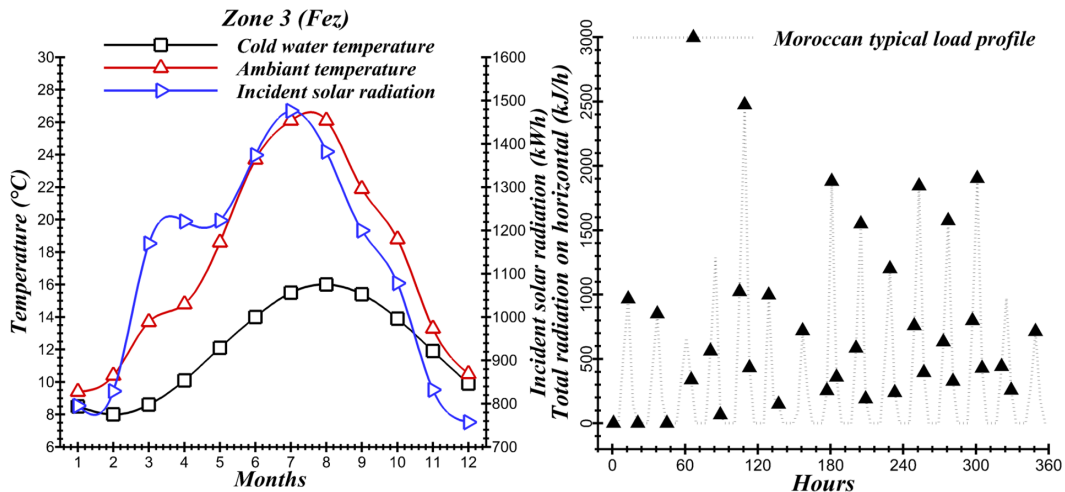


Figure 87: Fez's Weather data which are considered for simulations.

6.4.2. Load profile

A realistic domestic hot water consumption profile for the concerned residence was estimated by recording the need which was loaded by several apartments in the same building (Fig. [88]). This

estimation extends over a period of 24 hours. A monthly averaged estimation over the year was also defined on the same Fig. 88. The maximum hot water consumption was measured between 6h and 8h (840l). Indeed, between 12h and 16h (520 l) and between 18h and 20h, an interval during which the consumption is important (480l). The total of the different loaded volumes over 24 hours is equal to the total requirement previously defined in the balance sheet 6000 l/day.

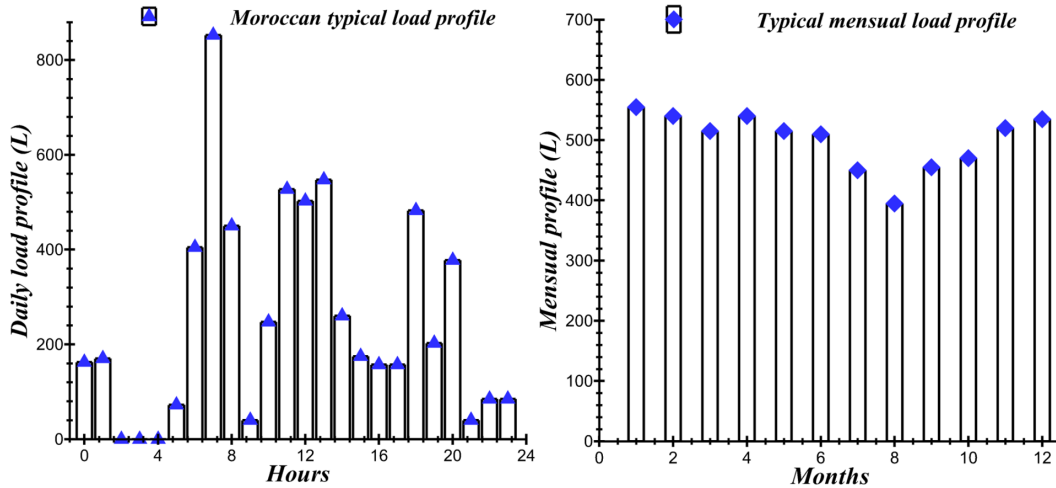


Figure 88: Hot water load profile.

The Domestic Hot Water (DHW) consumption flow rate is presented in Fig. 89. Its evolution over the first 10 days of January was considered. During this cold period of the year, the hot water flow consumed is maximum around noon of each day.

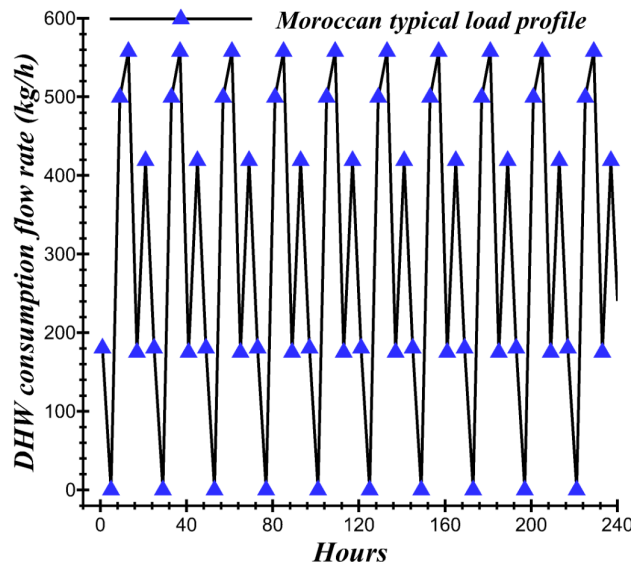


Figure 89: Daily hot water flow rate.

Four parametric studies were carried out in this work aiming to design and optimize the overall efficiency of a forced circulation collective system (Fig. 86). A well-determined domestic hot water

requirement and a load profile which pilots it were considered during this work.

The aim of the first study is to determine the optimum surface area of the solar collector field which maximizes the efficiency of the collective system, namely its solar fraction over the year. For this purpose, several configurations were defined which are acting on the number of collectors constituting the field. The contribution of each collector area in the monthly/annual thermal performance estimation of the collective system was conducted. In addition, the incident solar radiation on the six defined collector's configurations was measured, and its assessment was plotted over a period of the year. Besides, the useful energy gain from collectors for each configuration was estimated. Moreover, determining the relation between the energy consumed by the hydraulic auxiliary booster and the solar fraction of the collective system for different months of the year was investigated. Finally, we sought towards the end of the first study to estimate an overall area of the collector field from which the solar fraction of the collective system becomes optimal, stable and independent of the contribution of the ETC solar collectors inserted in the solar field.

The second study aims to assess the effect of several ETC solar collectors variant's industrialized by different manufacturers (Tab. 26) on the overall efficiency of the collective system. The concerned ETC collector products differ mainly by their three constants commonly used to define its energy performance, in particular η_0 , a_1 and a_2 . To achieve this objective, it was necessary to describe the incident solar radiation on each collector during the 12 months of the year, to estimate the solar energy contribution and the booster consumption. Those investigations will help to assess the trend of the solar fraction for the studied system over one year related to each ETC product. The total area of the collector field was maintained at 60 m² and the volume of the collective storage tank was 2000 l.

The third study aims to demonstrate the arrangement's and connection's effect of various collectors constituting the solar field on the overall efficiency of the collective system. Two configurations were studied, namely the serial and the parallel connection of the collectors. The total area of the collector field was maintained at 60 m² and the volume of the collective storage tank was 2000 l. In order to determine the optimum configuration according to the row number and the collector's number per row, it was necessary to estimate the solar collector's contribution and the auxiliary consumption for each configuration in order to assess their average annual solar fraction and to finally select the optimal.

The fourth study aims to design the collective storage tank in order to ensure the availability of hot water at 45°C. The contribution of the storage tank to the maximization of the seasonal solar fraction of the collective system is the criterion used for its dimensioning. The solar energy contribution was estimated for the four seasons to calculate the solar fraction corresponding to each volume.

6.5. Physical modeling of solar hot water components

6.5.1. Solar collector panel

The collector efficiency is often used to quantify the energy performance of the collector [292].

$$\eta = \frac{Q_u}{A_c I_T} = \frac{\dot{m} C_p (T_{out} - T_{in})}{A_c I_T} \quad (97)$$

Where Q_u is the useful energy to heat the water mass flow \dot{m} entering the collectors field with T_{in} and outgoing with T_{out} temperature. A_c is the total collectors area and I_T is the total solar radiation on the titled surfaces of the collectors.

A quadratic relation was used to define the efficiency of the collectors.

$$\eta = \eta_0 - a_1 \frac{(T_m - T_a)}{I_T} - a_2 \frac{(T_m - T_a)^2}{I_T} \quad (98)$$

where η_0 indicates the zero loss efficiency of the collector, a_1 and a_2 present the first and second order heat loss coefficients which were taken from the *Transol* software (Tab. 26). I_T is the total horizontal radiation, and T_m is the average temperature.

$$T_m = \frac{T_{out} + T_{in}}{2} \quad (99)$$

Where T_{out} and T_{in} are the outlet and the inlet temperatures respectively from the collector, and T_a is the ambient temperature.

6.5.2. Storage tank

The thermal model of a sensible energy storage tank, subjected to thermal stratification, can be modeled by assuming that the tank is divided into N fully-mixed equal volume segments ($N < 15$), as presented in Fig. 90. The stratification degree is determined by the value of N . This model is taking in consideration unequal size nodes, fixed or variable inlets, temperature dead band on booster contribution, variable heat loss coefficients, and losses to gas flue of auxiliary heater are also considered.

6.5.3. Flow streams

As previously mentioned, the storage tank is supposed to contain N fully horizontal layers. Water inlet and outlet are imposed at the top and the bottom segments respectively as shown schematically in Fig. 90.

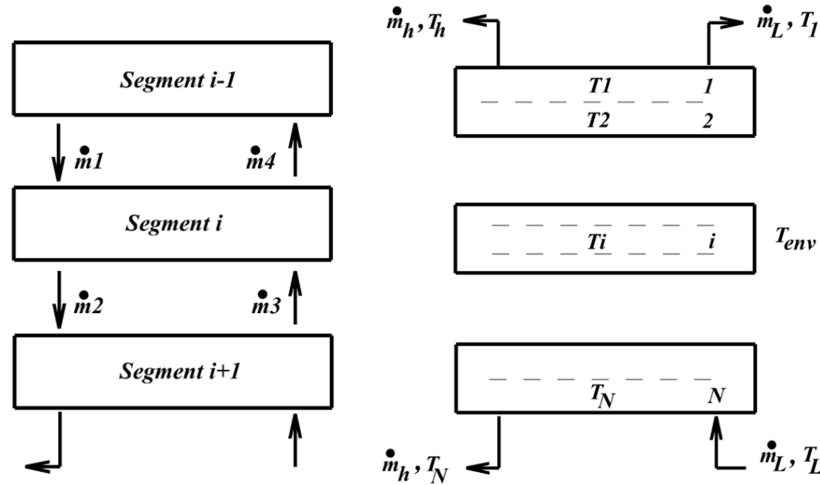


Figure 90: Configuration of a stratified fluid storage tank with a representative flow streams scheme between segments.

The instantaneous energy balance for the storage tank can be written as the following:

$$M_i C_{pf} \frac{dT_i}{dt} = \begin{cases} (\dot{m}_1 - \dot{m}_3) \cdot C_{pf} (T_{i-1} - T_i) & \dot{m}_1 > \dot{m}_2 \\ (\dot{m}_3 - \dot{m}_1) \cdot C_{pf} (T_{i+1} - T_i) & \dot{m}_1 < \dot{m}_2 \end{cases} \quad (100)$$

The temperatures of each of the N tank segments are determined by the integration of their time derivatives expressed in Eqs. [100](#), [101](#). At the end of each time step, temperature inversions are eliminated by mixing appropriate adjacent nodes.

$$M_i C_{pf} \frac{dT_i}{dt} = \begin{cases} \alpha_i \dot{m}_h C_{pf} (T_h - T_i) + \beta_i \dot{m}_L C_{pf} (T_L - T_i) + U A_i (T_{env} - T_i) + \\ \quad + \gamma_i (T_{i-1} - T_i) C_{pf} & g_i > 0 \\ \quad + \gamma_i (T_i - T_{i-1}) C_{pf} & g_i < 0 \\ \quad + \dot{Q}_i & i = 1, N \end{cases} \quad (101)$$

6.5.4. Energy flows

Energy flows and changes in the internal energy are calculated as follows [293](#). The rate of energy loss from the tank to the surroundings \dot{Q}_{env} , including boiling effects if applicable is expressed in Eq. [102](#).

$$\dot{Q}_{env} = \sum_{i=1}^N U A_i (T_i - T_{env}) + \gamma_f \sum_{i=1}^{i=l} (U A)_{f,i} (T_i - T_f) \quad (102)$$

The rate at which sensible energy \dot{Q}_s is removed from the tank to supply the load is expressed in Eq. [103](#).

$$\dot{Q}_s = \dot{m}_L C_{pf} (T_l - T_L) \quad (103)$$

The rate of energy input to tank \dot{Q}_{in} from hot fluid stream is expressed in Eq. [104](#).

$$\dot{Q}_{in} = \dot{m}_h C_{pf} (T_h - T_N) \quad (104)$$

The internal energy change of the tank ΔE is expressed in Eq. [105](#).

$$\Delta E = \frac{V \cdot \rho_f (\sum_{i=1}^N T_i - \sum_{i=1}^N T_i(t = t_0))}{N} \quad (105)$$

6.5.5. Solar fraction

Solar fraction can be defined as the total energy provided by the solar collective system to produce hot water. It is calculated using equation [117](#) [294](#). The solar fraction is the most important indicator to characterize the thermal performance of the collective system compared to the other parameters previously presented, since it takes into account the overall performance of the entire system and not only one single component.

$$f = 1 - \frac{Q_{Auxiliary}}{Q_{load}} \quad (106)$$

Where Q_{load} is the total energy transferred by the collective system to satisfy the heating requirements, and $Q_{Auxiliary}$ is the total auxiliary energy provided to the collective system to support the portion of the total solar energy load which is not sufficient.

6.6. Results and Discussion

6.6.1. First study: Effect of the collector's field area and arrangement

The incident solar radiation on the solar collector field for six studied configurations is presented in Fig. 91. Bar graphs were used to represent the monthly averaged values of the incident energy on the collector field. The trends of the six bar graphs remain similar and follow a normal distribution. Indeed, the incident solar energy is maximum during summer and minimal during the cold periods of the year such as autumn and winter.

This quantity is affected by the number of collector constituting the solar field (see Tab. 24). In fact, it increases according to the number of collectors used to satisfy the energy demand of the requested hot water. For instance, in March, the energy incident on a field comprised of 10 collectors is equal to 3550 kWh. It is increased by a multiplier factor equal to 5.74 since the incident energy becomes 20400 kWh in the case of using of 60 solar ETC collectors. The annual consumption of the hydraulic booster and the solar fraction are presented in Tab. 25.

Number of solar ETC collectors	Total surface (m^2)	Connection of solar collectors	Flow rate of the primary circuit pump (kg/h)
10 Collectors	20	1 row	130
		10 solar collectors connected in series	
20 Collectors	40	2 rows	260
		10 solar collectors connected in series	
30 Collectors	60	3 rows	390
		10 solar collectors connected in series	
40 Collectors	80	4 rows	520
		10 solar collectors connected in series	
50 Collectors	100	5 rows	650
		10 solar collectors connected in series	
60 Collectors	120	6 rows	780
		10 solar collectors connected in series	

Table 21: Collectors field connexion and arrangement.

Number of solar ETC collectors	10	20	30	40	50	60
Average annual consumption of the hydraulic booster (kWh)	4776	2916	2199	1894	1656	1481
Average annual solar fraction (%)	36	62	72	76	79	82

Table 22: Performance of collective system for different arrangement of solar collector.

The evolution of the useful energy gain from collectors of the assessed configurations during the first four cold days of January is presented in Fig. 92. The volume of the storage tank used in this case is 2000 l. For the first day of January, at noon (12h), the useful energy gain for 10 collectors is equal to 17500 kWh. The use of an additional number of collectors maximizes this energy. Indeed, the energy gained by the collector field is multiplied by 4 (80000 kWh) since the number of collectors constituting the field is equal to 60.

The effect of the hydraulic booster energy on the monthly solar fraction of the collective system is presented in Fig. 93. The auxiliary system operates when the solar collector field production is insufficient to heat water to the desired temperature (45°C). Fig. 93 shows that the minimum

solar energy during the cold months of the year is balanced by the contribution of the auxiliary system which is maximized. Therefore, the solar fraction of the collective system decreases and vice versa for the hot periods, i.e. when the thermal energy supplied by the ETC solar collectors is sufficient to meet the user's needs in terms of hot water temperature, the consumption of the hydraulic auxiliary system is reduced which allows to increase the solar fraction of the collective system.

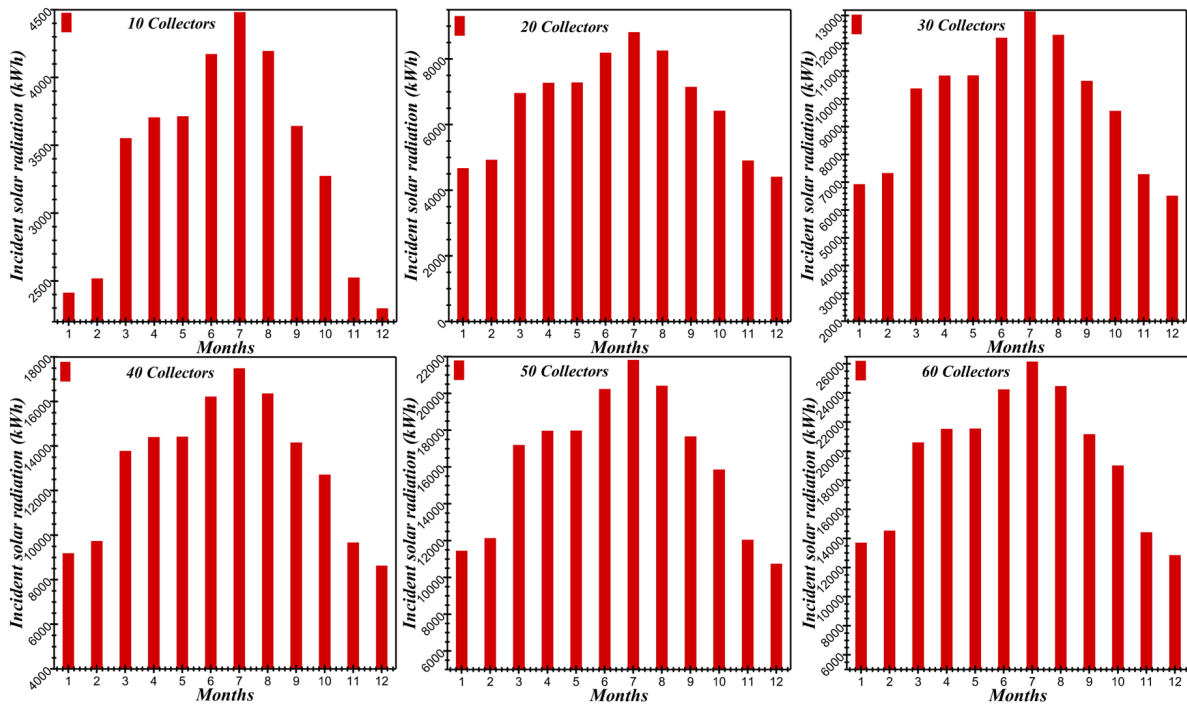


Figure 91: Incident solar radiation for different solar collector's arrangement.

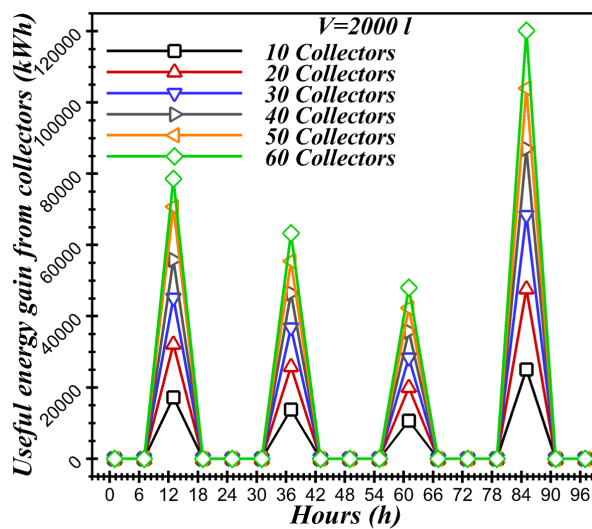


Figure 92: Useful energy gain for different solar collector's arrangement.

In January and while using 10 collectors, the input of the hydraulic auxiliary system is equal to 7017 kWh and the solar fraction is 21%. In September the input of the hydraulic booster is equal to 3345 kWh and the solar fraction is 43%.

By using 20 collectors, the input of the hydraulic auxiliary system in March is equal to 3678 kWh and the solar fraction is worth 56%. In July the input of the hydraulic auxiliary system is equal to 956 kWh and the solar fraction achieve 85%.

For the case of 30 collectors, the input of the booster system in December is equal to 4002 kWh and the solar fraction is 53%. In July the input of the hydraulic auxiliary system is equal to 1620 kWh and the solar fraction is worth 79%.

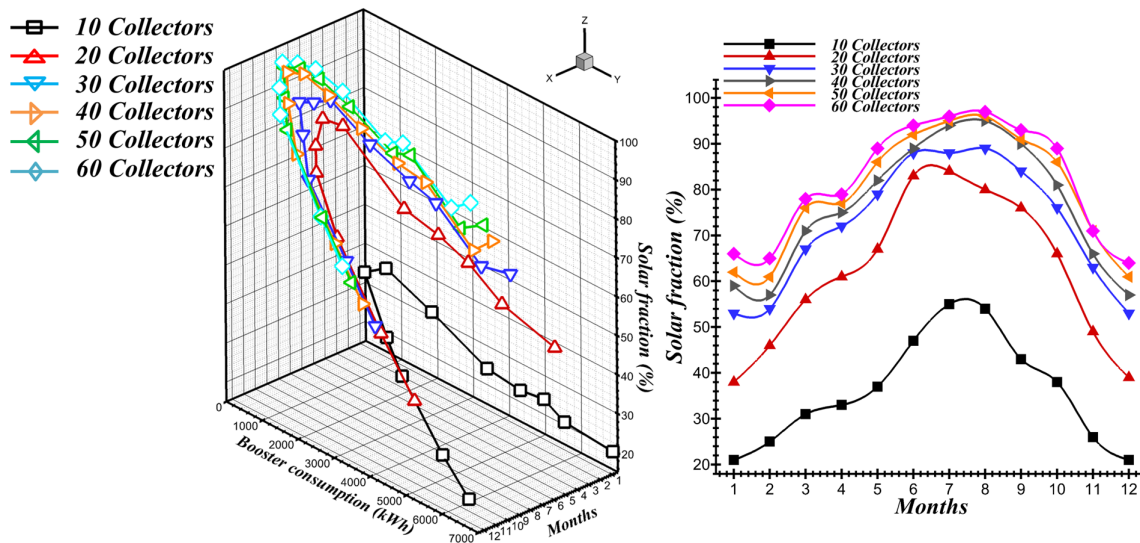


Figure 93: Performance of solar collective system for different solar collector's arrangement.

The evolution of the solar fraction over the year is presented in Fig. 93. Solar fraction tendencies are the same for the six studied configurations; but its monthly values are different from a configuration to another. Incrementing the collector's field overall area to 120 m² (Tab. 24) optimizes the thermal efficiency of the collective system, and the hydraulic auxiliary system consumption is basically reduced .

For January (Winter period), the solar fraction for the collective system corresponding to 10, 20, 30, 40, 50 and 60 collectors reach 21%, 38%, 53%, 59%, 62% and 66% respectively. For November, the collective system's solar fraction corresponding to 10, 20, 30, 40, 50 and 60 collectors achieve 26%, 49%, 63%, 66%, 71% and 71% respectively. For June (Summer period), the collective system solar fraction corresponding to 10, 20, 30, 40, 50 and 60 collectors equals 37%, 83%, 88%, 89%, 92% and 94% respectively.

The average annual solar fraction as a function of solar collector's field area and the seasonal solar fraction evolution of the six configurations according to four seasons are presented in Fig. 94. The annual solar fraction increases with the number of collectors constituting the solar field, but from 80 m², the effect of increasing the total area on the solar fraction margin evolution is minimal (2%). Consequently, it is concluded that the overall performance of the collective system becomes optimal and stable and the addition of solar collectors does not contribute to its improvement.

A solar field which constitutes 10 collectors offers a minimum thermal efficiency compared to

other configurations 20, 30, 40, 50 and 60 collectors. It is preferable to adopt a configuration of 40 collectors, the equivalent of 80 m² to satisfy the need of the hot water demand over the four seasons, because the overall thermal efficiency of the collective system remains above 60%. Typically, the use of an auxiliary energy source is less important considering the available solar thermal energy, being convertible through this number of collectors used.

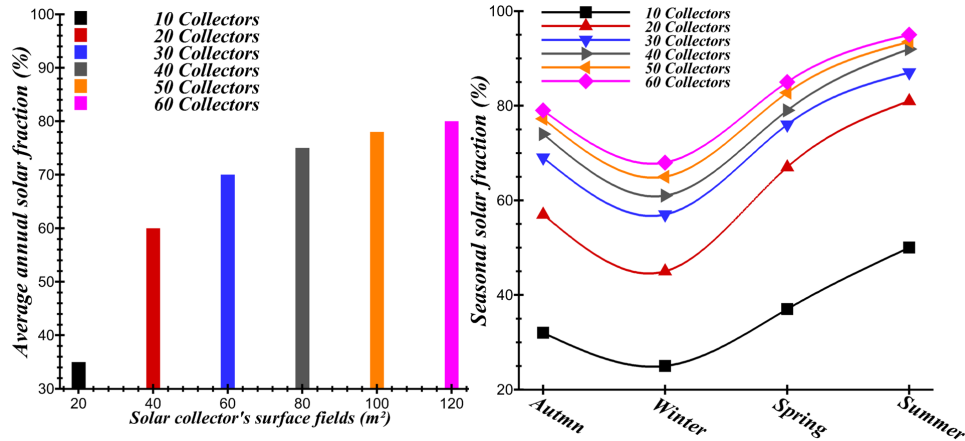


Figure 94: Annual and seasonal solar fraction of the collective system for different solar collector configurations.

6.6.2. Second study: Effect of storage tank's volume

The energy consumption and the solar energy contribution were assessed for five tank's volumes 1000 l, 1500 l, 2000 l, 2500 l and 3000 l during the four seasons (Figs. 96, 97). The auxiliary system consumption decreases by acting simultaneously on two parameters: incrementing the volume of the storage tank and increasing the surface area of the solar collector field. For the volumes from 2000 l to 3000 l, the consumption of the booster system is reduced because the water is mainly heated by the energy exchanged by conduction and convection at the tank's internal heat exchanger. For example, in winter (Fig. 96), using a volume of 1000 l connected to a solar collector field with an area of 40 m² generates a consumption of 5000 kWh. However, using a volume of 2000 l associated with a collector field with an area of 80 m² generates a consumption of 3250 kWh (an estimated saving of 1750 kWh).

For the same volume of 1000 l, the solar energy contribution reach 3400 kWh for the collector field area of 40 m². It increases to 5600 kWh using an overall surface of 80 m² for a volume of 2000 l. The contribution of the hydraulic auxiliary system is maximal for two cold seasons: winter and autumn. The overall efficiency of the collective system decreases during these two periods, but an optimization can be achieved by acting simultaneously on two parameters: The volume of the storage tank and the surface area of the solar collector field. The seasonal average solar fraction remains above 50% throughout the year by combining a collective volume of 1500 l and an available area of 100 m². Another configuration ensures a seasonal solar fraction above 60%. It is an arrangement between a volume of 2000 l and a solar collector field with a surface area of 100 m².

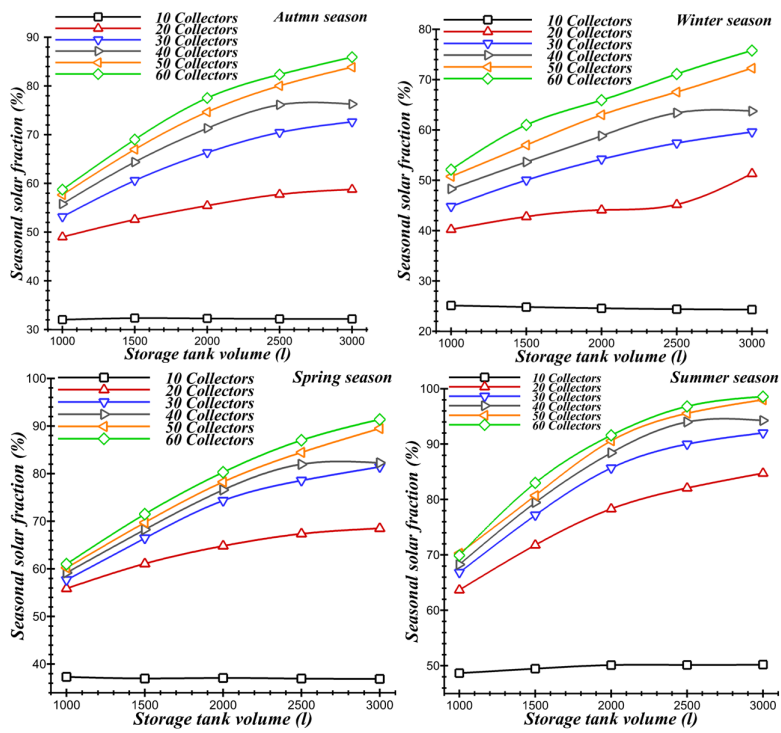


Figure 95: Seasonal solar fraction for different storage tank volumes.

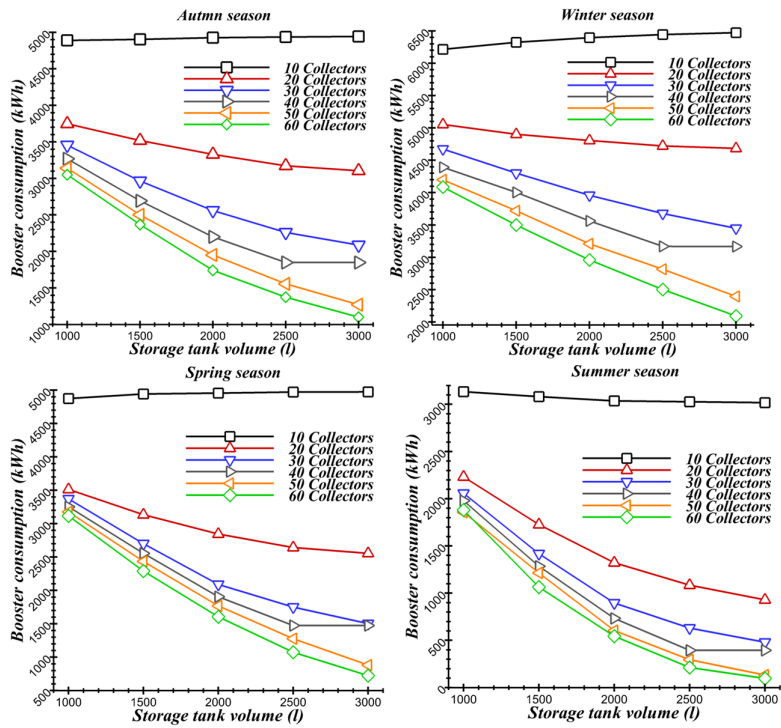


Figure 96: Hydraulic booster consumption for different storage tank volumes.

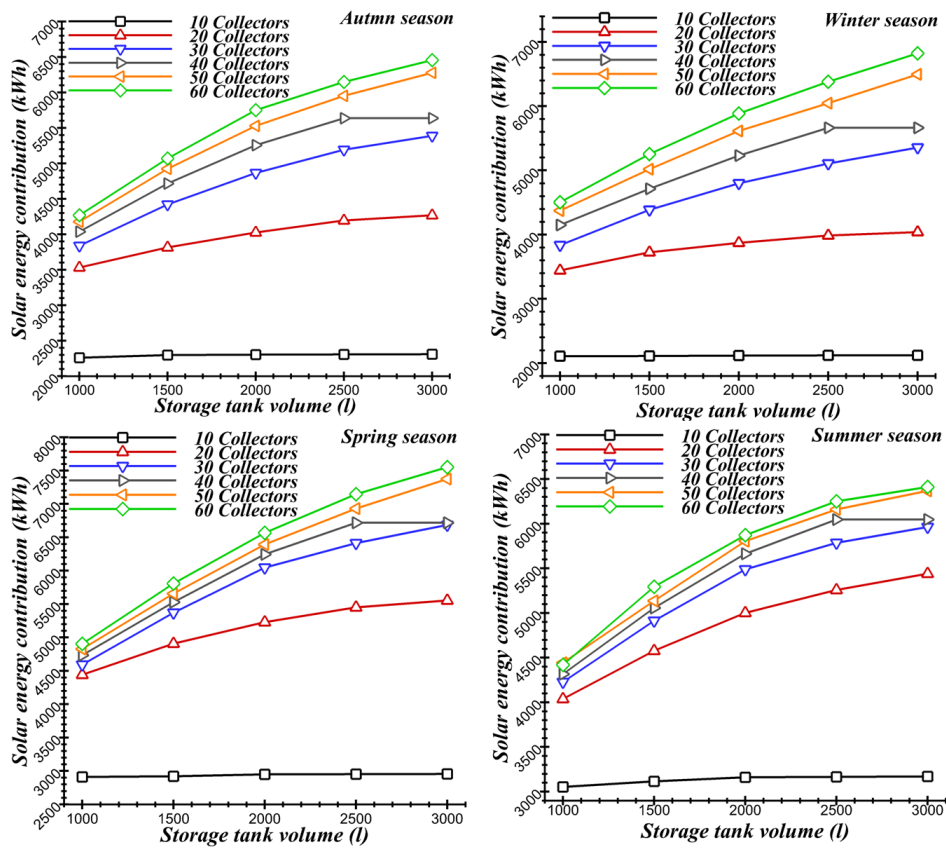


Figure 97: Solar energy contribution for different storage tank volumes.

6.6.3. Third study: Effect of the collector's characteristics from various manufacturers

The estimation of the incident solar radiation on four ETC collector variants over a period of one year is presented in Fig. 98. The manufacturers of the ETC collectors which were assessed are Viessmann Werke GmbH & Co, Thermomax-Inygen, Baxi Calefaccin and Frisquet S.A. The technical characteristics of each ETC product tested and certified by international laboratories are presented in Tab. 26. The annual evolution of the incident solar radiation follows a normal trend. In fact, this parameter is maximal during the Summer season and becomes less important during the autumn and winter seasons.

Manufacturer			η_0	a_1 W/m ² .K ²	a_2 W/m ² .K ²	Height (m)	Q_t 1/h.m ²	C_p kJ/kg.K
Viessmann Werke GmbH & Co	Product	VITOSOL 300-T SP3A 2 m2	0.809	1.370	0.0068	2.030	64.8	8.4830
	Laboratory	ISFH						
Thermomax-Inygen	Product	Thermomax 20	0.750	0.550	0.0153	1.415	72.0	10.78
	Laboratory	CSTB						
Baxi Calefaccin	Product	AR 20	0.750	0.550	0.0153	1.996	72.0	10.78
	Laboratory	ISFH						
Frisquet S.A.	Product	Frisquet TSV2 20	0.750	0.550	0.0153	2.005	72.0	10.78
	Laboratory	CSTB						

Table 23: Intrinsic characteristics of solar collector for various industrial manufacturers [44].

The collective system's solar fraction calculation requires first of all the assessment of the annual solar energy contribution and the annual auxiliary consumption. The ETC collectors are selected from four manufacturers, hence their technical characteristics are totally different. The overall efficiency of the collective system was calculated for a solar collector field with an area of 60 m² connected to a storage tank with a volume of 2000 l (Fig. 99). The solar energy contribution in the solar fraction estimation for Viessmann Werke GmbH & Co manufacturer remains higher than that of the other manufacturers, specifically during the cold periods of the year (months 10, 11, 12, 1 and 2).

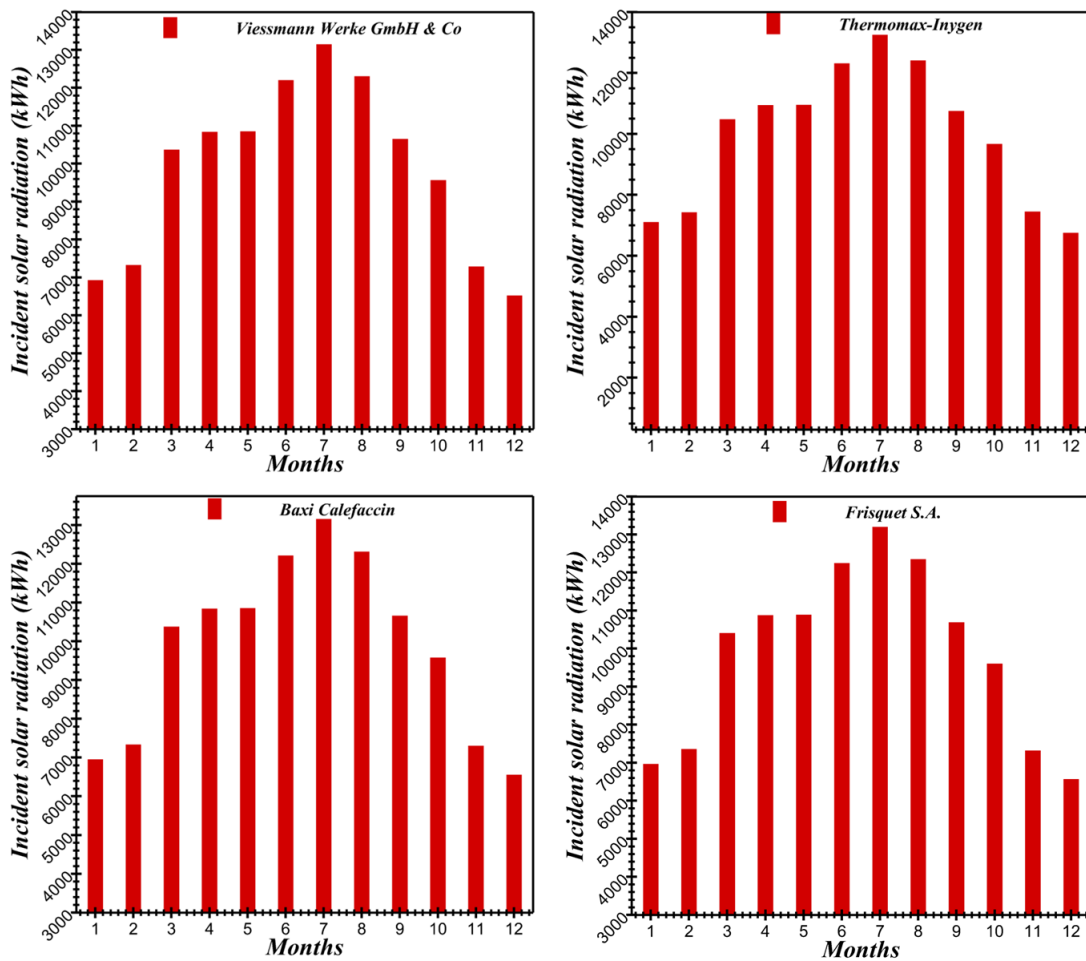


Figure 98: Incident solar radiation for various industrial manufacturers.

This result is reflected in the auxiliary consumption, for example, in January the auxiliary system consumes up to 5100 kWh for Frisquet S.A. manufacturer in order to deliver the required hot water needs. While the same auxiliary system consumes up to 4500 kWh for Viessmann Werke GmbH & Co manufacturer (a monthly saving of 600 kWh). It can be concluded that the product ETC VITOSOL from Viessmann Werke GmbH & Co is the most suitable technology to be used for the studied collective solar application.

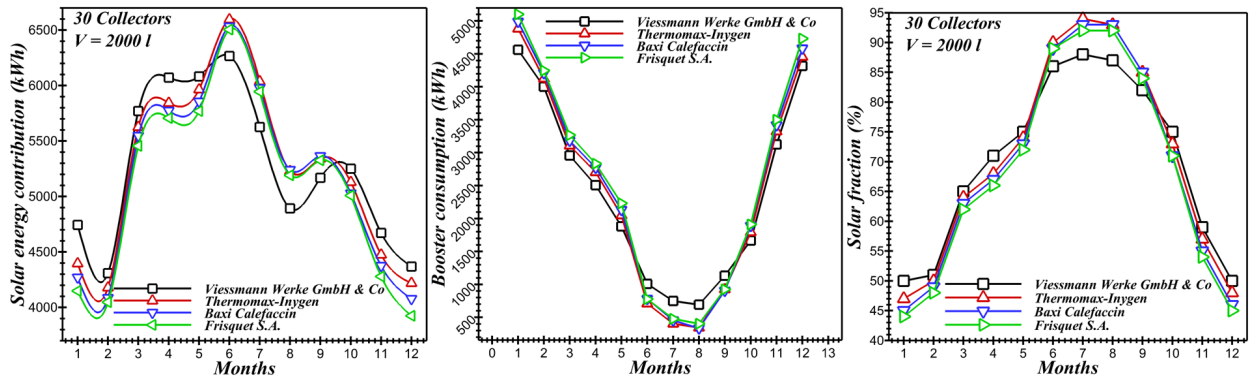


Figure 99: Thermal performance of collective system for various industrial manufacturers.

6.6.4. Fourth study: Effect of collectors arrangement

The collector's arrangement constituting the solar field of the collective system is presented in Fig. 100. Two configurations are distinguished, namely the serial connection and the parallel connection of the collectors. The volume of the storage tank used in this fourth study is equal to 2000 l and the total area is maintained at 60 m². Basically, there are some collective hot water systems in residences which are similar to that presented in Fig. 85 of Fez city. It has been observed that the connection between the solar field collectors is not established considering calculations aiming at maximizing the solar fraction of the system. At present, the connection between the different collectors is only carried out in such a way as to exploit the available surface of the terrace in order to ensure their ergonomic distribution. For this reason, this study was proposed to investigate the effect of the number of rows as well as the number of collectors by row on the overall collective system's solar fraction.

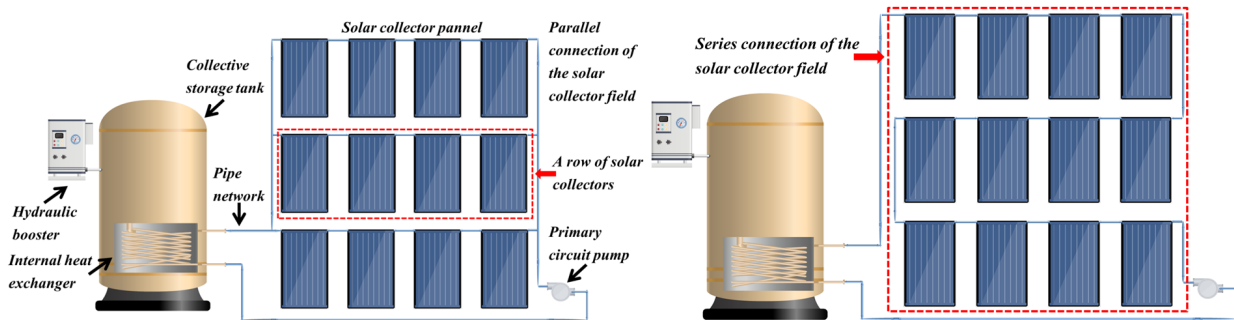


Figure 100: Serial and parallel connection of the collective system's collectors [44].

Depending on the needs and the sunlight of the site, several collectors can be assembled in order to increase the collecting surface. The collector arrangement used to meet the collective hot water production has a considerable effect on its efficiency, in other words on its solar fraction. Several coupling configurations between the collectors which constitute the solar collector field are possible, for instance, serial coupling or parallel coupling. When several collectors are connected in parallel, the circulation flow rate is increased and the temperature of the heat transfer fluid at the outlet of the collector field is not changed. Otherwise, an installation with several collectors connected in series has the effect of increasing the temperature of the heat transfer fluid.

It was necessary to estimate the solar collector's contribution and the auxiliary consumption for each configuration (Fig. 101) in order to determine the optimum of the row's number and the number of collectors per rows. The 6 rows, 5 rows, 10 rows and 3 rows configurations maximize the annual solar fraction of the collective system as it remains above 50%, since the annual booster consumption remains below 4000 kWh and the solar collector's production exceeds 4500 kWh.

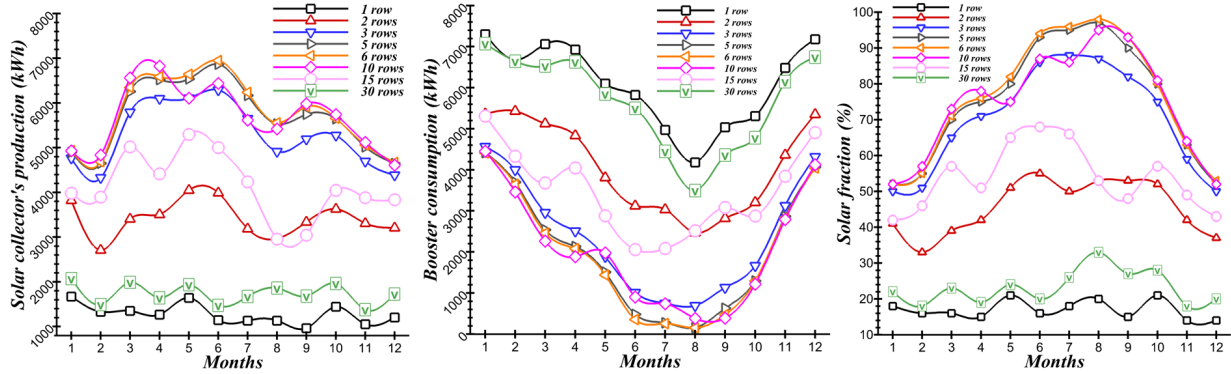


Figure 101: Thermal performance of the collective system for various connections.

The evolution of the average annual solar fraction, the solar collector's production and the auxiliary consumption according to the row's number are presented in Fig. 102. It can be concluded from these three figures that the configurations 6, 5, 10, and 3 maximize the solar fraction to 76%, 74%, 72% and 70% respectively. For this solar collective hot water application, it would be advantageous to connect the collectors constituting the solar field according to the configuration of 6 rows, where each row will connect 5 ETC collectors in series.

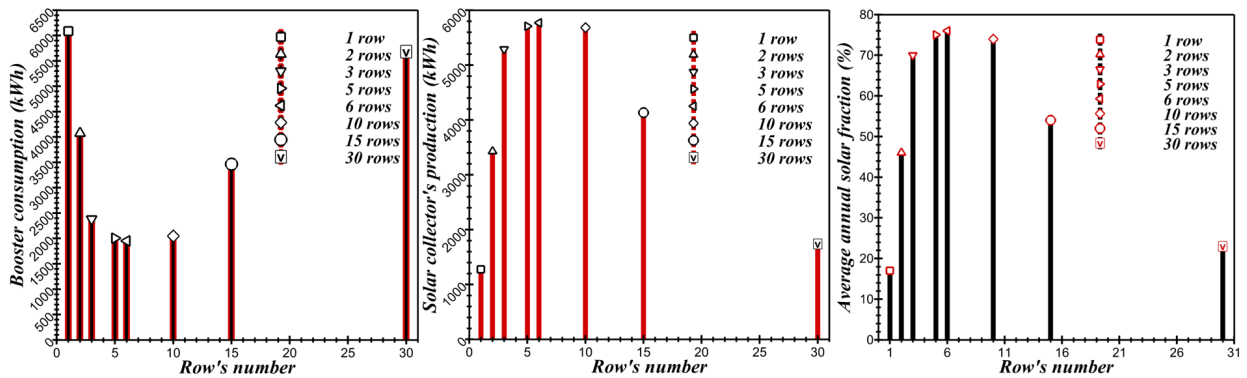


Figure 102: Thermal performance of the collective system for various row's number of solar collectors.

6.7. Conclusion

This chapter aims to assess the performance of a forced solar hot water collective system according to the Moroccan's weather conditions of Fez city. A realistic load profile was considered in this study to describe the hot water consumption profile. Four parametric studies were performed to design the collective solar hot water system and to ensure its optimization. The main findings drawn from the design and the parametric studies are listed as follows.

The First study has shown that increasing the total area of the collectors field to 100 m² maximizes the incident solar radiation, hence the useful energy gained over the year. In addition to this, the progression of the solar fraction margin is reduced to 2% from a certain threshold of the global surface of the solar panel field. Besides, it is found that incrementing the collector's field area to 120 m² optimizes the thermal efficiency of the collective system, and the hydraulic auxiliary system consumption is reduced. Moreover, it has been shown that the overall performance of the collective system becomes optimal and stable which means that adding more ETC collectors to the solar panel does not contribute to its improvement. In fact, for this application, it would be advantageous to use 40 collectors, the equivalent of 80 m² to satisfy the need of hot water demand over the four seasons, since the overall collective system thermal efficiency remain above 60%.

It has been proved through the second study that the auxiliary system consumption decreases by acting simultaneously on two parameters. To increase in the first place the volume of the storage tank and to increase in the second place the surface area of the solar collector field. In fact, an estimated saving of 1750 kWh was reached in winter by switching from (1000 l; 40 m²) configuration to (2000 l; 80 m²). Furthermore, it has been concluded that combining a storage tank with a volume of 1500 l, and a solar collector panel with a surface of 100 m² would ensure a seasonal solar fraction which is greater than 50%.

Regarding the third study, it is shown that the solar energy contribution in the solar fraction estimation for Viessmann Werke GmbH & Co remains higher than the other manufacturers, especially during the cold periods of the year, because the optical efficiency coefficient η_0 is maximum ($\eta_0 = 0.809$), and a_2 is minimal ($a_2=0.0068 \text{ W/K}^2.\text{m}^2$). Moreover, it can be concluded that ETC VITOSOL product from Viessmann Werke GmbH & Co is the most suitable technology to be used for the studied collective solar application.

On another note, the fourth study has shown that the solar collector's connection (Serial or parallel) reflected the effect of the annual fractional savings over the solar hot water collective system's performances. For example, this study evidences the effect of the row's number as well as the number of collectors connected per row on the overall collective system's solar fraction. It has been reported that it would be advantageous to connect the collectors constituting the solar field according to the configuration of 6 rows, where each row is going to connect 5 ETC collectors in series.

6.8. *Chapter VII: Energy performance enhancement of a collective hot water production process equipped with a centralized storage tank*

6.9. *Introduction*

This chapter investigates the thermal performance of a forced circulation collective solar water heater (*SWH*) equipped with a centralized storage tank, throughout dynamic simulations. The main purpose of this study is to identify the parameters affecting the overall efficiency of the collective process, because the literature review focuses on individual *SWH*, rather than collective hot water systems. Hence, being able to suggest general recommendations that would be helpful to guide hot water system designers. A typical residence located in Fez city (Morocco) that shelters 60 occupants was considered as a realistic case study, for which the thermal performances of the collective hot water production system were simulated. Several performance indicators were defined and miscellaneous dynamic simulations were carried out to enhance the process's efficiency. For instance, the incident energy on the solar collector panel, the supplementary consumptions for different storage tank volumes and load profiles, the useful energy gain from the collector's field and the solar fraction of the collective hot water process. The results showed that the Evacuated Tube Technology (*ETC*) is suitable for this collective hot water production application, because the solar fraction of the process remains higher with *ETC*, as opposed to the use of Flat Plate Collectors (*FPC*). Moreover, the centralized storage tank volume affects the annual solar fraction of the collective hot water process. Last but not least, the maximal annual averaged solar fraction was achieved by the *ETC* technology (78%). However, it is equal to 68% for (*FPC*) while maintaining 3000 liters as a centralized storage capacity.

Nowadays, the building sector consumes more than 40% of the primary energy, which is considered as the main contributor to the world energy consumption [295]. Moreover, the requirements for thermal comfort are increasing, which has involved a considerable energy consumption leading to environmental issues, such as emissions, pollution and global warming [296].

SWHs have become a challenging solar thermal application in Morocco. Indeed, the Moroccan government is aware of the socio-economic impact of Domestic Hot Water (*DHW*) production systems. Therefore, an important financial support is provided to research and development universities to promote research activities on *SWHs*, such as "SOL'R SHEMA" project funded by *IRESEN-Morocco* [6], which aims to design and commercialize the first *SWH*, made in Morocco, and which is going to be accessible to a large social scale of users. Currently, collective hot water production in residential buildings is an important issue, which must be taken seriously while applying energy efficiency in the building sector regulations [297]. Indeed, solar water heaters (*SWHs*) are useful solar energy systems that help to achieve this purpose thanks to their technological feasibility and economic attraction compared to other energy devices commonly used to heat water. It should be noted that the main components of any solar energy system are the stratified storage tank, besides to the collectors that absorb the radiation from the sun and transform it to heat. In fact, three types of collectors are widely used in *SWHs* systems namely, Flat Plate Collectors (*FPC*) [298], Evacuated Tube Collectors with heat pipes (*ETC*) [7] and Compound Parabolic Collectors (*CPC*) [299].

As reported in the literature, experimental and simulation studies were performed by the scientific community on individual *SWHs* to assess and enhance their performances. For instance, in Canada, Evarts and his team [300] conducted a survey to evaluate the consumed hot water volume, which is necessary to design *SWHs*. In addition, in Saudi Arabia, Rehman et al. [301] conducted

a techno-economic feasibility study on the integration of *SWHs* for the domestic sector through an optimum selection criteria. Their findings showed that the payback period would be decreased with a higher cost-ratio benefit, if occupant's number is important.

Ayompe et al. [302] validated a *TRNSYS* model for forced circulation *SWHs* under two collector's types, namely *FPC* and *ETC*. In addition, Too et al. [303] evaluated the thermal performance of *SWHs* with narrow mantle heat exchangers using *TRNSYS*. They developed heat transfer correlations in order to model the mantle sides of the storage tank, while Colle et al. [304] analyzed the performances of *SWHs*, which are controlled by weather forecast information. The authors used dynamic simulations to decrease the electric energy peak demand due to the extensive use of electric showerheads (*ESH*) in households. Moreover, Passos et al. [305] studied the feasibility of using domestic *SWHs* as alternative solution to decrease the electricity peak demand in Brazil. In fact, their simulations were performed on an hourly basis.

Martinez et al. [306] elaborated different design approaches and specifications to enhance the thermal performances of *SWH*'s solar network structure. The authors concluded that the number of the collectors in a row and the number of rows in parallel connection would affect the thermal performances of *SWHs*. Similarly, Abdunnabi et al. [307] carried out numerical simulations to predict with accuracy the performances of forced circulation *SWHs*. Meanwhile, in Yunnan province-China, Zhou et al. [308] analyzed the performance of a collective solar domestic water-heating system. They defined several thermal performance indicators to conduct this performance analysis study.

A review regarding the integration of solar water heating system in the building sector has been recently released [309]. Various collectors' types were studied and their efficiencies were compared. The collector's integration possibilities in the building sector were also investigated. Moreover, the review covered important issues concerning the system design, implementation and architectural barriers. Jamar et al. [310] presented a review on different commercial collectors. Their review focused on three principal collectors technologies (*FPC*, *ETC* and *PTC*), comparing the working fluid and the optical characteristics in order to enhance their thermal performances.

On the one hand, Tanha [311] investigated experimentally and simulated the performance of two domestic *SWHs*. Two collector's types were used in their analysis (*FPC* and *ETC*). On the other hand, Benoni et al. [312] conducted an optimization analysis of a thermal storage tank and a *FPC* used by a single-family households, in order to ensure an economic efficiency. Recently, an experimental study has been carried out by Reza et al. [313] to assess the destruction of thermal stratification occurring inside the storage tank of a conventional thermosyphon *SWH*. In fact, thermal stratification destruction is considered as one of the main causes that would affect the performance of the solar collector panel [314]. The main author's result indicated that decreasing the tank's bottom temperature layer would increase the performance of the solar collector panel. Consequently, the overall efficiency of the individual *SWH* system is enhanced. Besides, Alfaro et al. [315] conducted *CFD* simulations to optimize the thermal yield of a commercial solar collector based on the *ETC* technology. The authors performed 3D *CFD* simulations, taking into consideration the laminar case and the steady state assumption to design and construct 259 different collector geometries that were simultaneously modeled and assessed. This research team identified the parameters that affect the thermal performance of the solar collector. They listed them as follows: the internal diameter of the *ETC* tubes, the absorber area and the mass flow rate. Moreover, their optimization's results showed that the minimum absorber area has to be 2.49m², besides the internal diameter of the tubes should be increased by 30%, while their length have to

be decreased by 40%. To conclude with, Alfaro et al. [315] enhanced the thermal yield of *ETCs* using *CFD* simulation with a notable decrease in their cost evaluated at 38.9%.

Furthermore, Garnier et al. [316] carried out numerical and empirical assessments of a novel integrated collector storage solar water heater (*ICSSWH*), which can be used in individual household applications. For instance, their *CFD* simulations showed that high draw-off rate result in increased outlet temperatures from the storage tank, which ensure an improved efficiency. The authors showed that the suggested design of the *ICSSWH* is integrating a submerged heating element that would provide the necessary energy to meet the heating requirement of the user, if solar irradiations are not sufficient. Moreover, according to this research team, the *ICSSWH* can easily be embedded within a structural insulated roofing panel system.

Last but not least, several strategic studies were carried out *SWHs*. Firstly, Yan et al. [317] presented in their study a simplified method, which is based on a life-cycle energy analysis to optimize the design of a solar water heating systems. Secondly, Rezvani et al. [274] used Monte Carlo Analysis to estimate the techno-economic and reliability assessment of *SWHs* lifetime in Australia. Finally, Bessa et al. [318] assessed the importance of integrating *SWHs* as a passive technologies in social housing to decrease pollution and global warming.

The literature presents a significant state of the art on individual *SWHs*, which deals with the improvement of their energy efficiency. This enhancement could be achieved through the optimization of the storage tanks, or through the adjustment of the physical properties of the selective materials used as a coating on the solar collectors, or through the integration of the phase change materials as a latent component to increase the thermal storage of the individual solar systems. However, it should be noted that few studies have been conducted so far on a collective process of hot water production for the tertiary sector, including hotels, hospitals, university residences, restaurants etc. Therefore, up to now, it is difficult to determine the parameters that are likely to affect the solar fraction of the collective process that aims to produce hot water. Thus, this is a prime motivation for our research team to conduct dynamic simulations, in order to determine the set of parameters that can affect its performance.

Heating water for various domestic applications is performed by using electric or gas devices, and this work opens up a new perspective of water heating using solar energy, an abundant resource in Morocco throughout the year [319]. In fact, the aim of this chapter is to take profit from the recent climatic zoning in Morocco to assess the thermal performance of a dynamic solar collective system applied to a residency in Fez. The chapter maps out the collective domestic hot water consumption throughout one state of Morocco and hints at the benefit of using solar collective heating devices as energy saver in domestic building, respectively. Two different solar devices were compared towards their thermal efficiency throughout the whole year, namely *FPC* and *ETC*. Individual personal preferences and habits regarding hot water usage were taken into account as well.

The current analysis is carried out using dynamic simulations, which are based on the computing platform of *TRNSYS*, in order to investigate the combined effect of load profiles, collective thermal storage tank volume, collectors technologies on the overall performances of a forced collective solar water heating system. This numerical study highlights the effect of the parameters cited above on the annual solar fraction saving of the collective hot water production process.

6.10. Description of the studied case

The energy performance of the collective *SWH* system, schematically presented in Fig. 103, has been assessed in a Moroccan residence located in Fez city [34°03'N 4°58'W]. The residence

shelters 60 occupants and the individual consumption was estimated to 80 liters of hot water per person. Hence, the overall daily hot water need is 6000 liters.

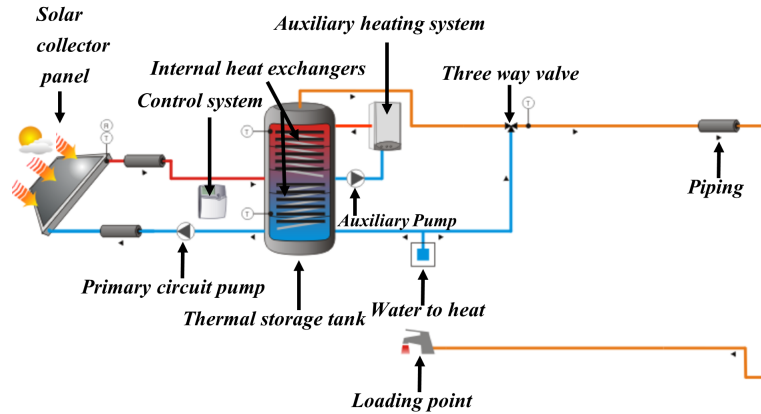


Figure 103: Simplified scheme of the collective hot water process [44].

It should be noted that the distribution of the assessed hot water volume depends on the behavior and the consumption pattern of the inhabitants [320]. In fact, the allocation of the consumed daily hot water among the various months has been taken into account for the considered household as shown in Fig. 107. Additional details will be provided and discussed further in the subsection "Load profile".

6.10.1. Collective system description

The collective system is composed of a solar thermal stratified storage tank, which is connected to an internal heat exchanger [321], besides to an auxiliary system which is an internal heat exchanger connected to a thermostatic temperature control valve.

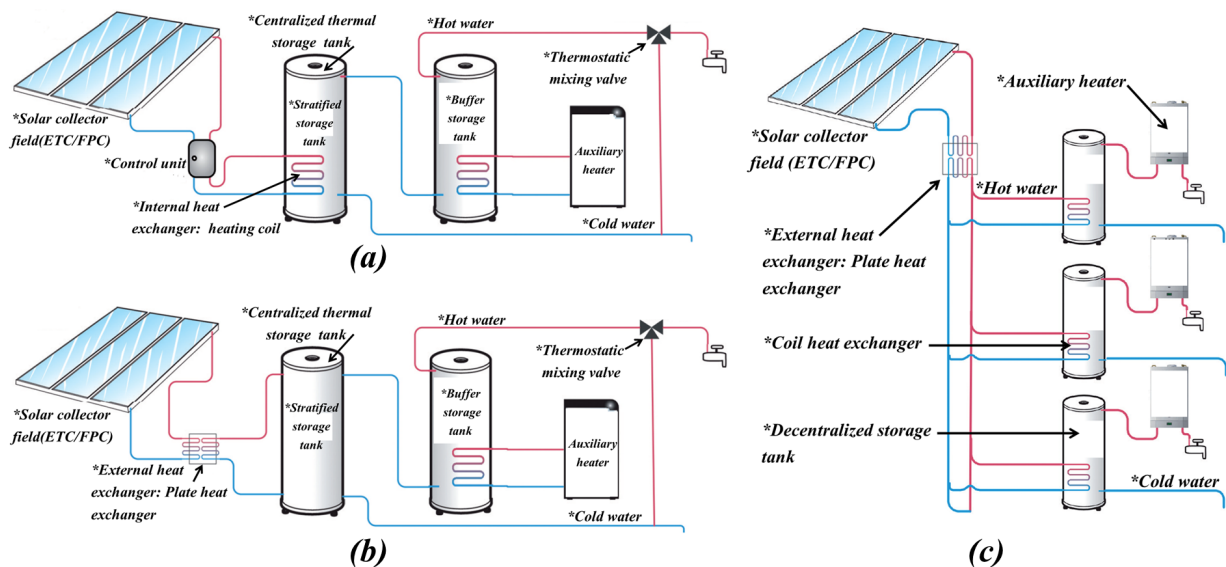


Figure 104: (a)- Centralized storage tank equipped with internal coil heat exchanger. (b)- Centralized storage tank equipped with external plate heat exchanger. (c)- Decentralized storage tank equipped with internal heat exchanger.

The *SWH* collective system consists of a set of solar thermal collectors that supply energy to the domestic hot water (DHW) stored in the tank (Fig. 104). Moreover, the internal heat exchanger is submerged inside the bottom zone of the tank. In fact, the energy provided to the solar tank is ensured with hydraulic or electrical auxiliary heating system, using a heat exchanger located in the top tank zone. In addition, the collective system is equipped with a recirculation circuit, in order to produce the desired *DHW* temperature by the users, using a three-way thermostatic valve which mixes the loop's recirculation water to the warm water previously stored inside the tank. It should be noted that this device decreases the hot water flow from the auxiliary flask.

The auxiliary system operates if the storage tank temperature is below the set temperature defined by the consumer. This set point temperature value must be higher than the *DHW* temperature that is required for the consumption. The accurate design of the auxiliary heating system aims to ensure the hot water service in all the circumstances. Consequently, to get as much benefit from solar energy. Furthermore, the control of the primary circuit is carried out by measuring the amount of the incident solar radiations or by measuring the temperature differential 302. The pumps operate according to the radiation reaching the collectors, while the temperature differential is integrated between the collectors and the bottom side of the tank. The secondary loop can be cross-checked with the primary loop or independently by comparing the temperature of the hot side of the exchanger with the bottom temperature of the tank. In this case, the flow rate of the pumps can be fixed or variable (match-flow system). In fact, the system stops the circulation if the temperature of the storage tank or the temperature of the collector is higher than the respective maximum safety temperatures 305.

The collector technologies used during this study, in order to carry out the forced hot water collective system optimization for low energy consumption and energy storage enhancement, are presented in detail in both Tabs. 24 and 25. For instance, general information such as the manufacturer's signature, the technology's type, the test laboratory as well as technical characteristics, for example optical and thermal efficiencies are presented. Further, Tab. 26 shows the arrangement of the collector field that has been used in this dynamic simulations to meet the heating requirements of hot water. In fact, thirty-one collectors were used to constitute the solar field. They were distributed on 3 rows oriented towards the south. The first and the second rows included 10 collectors respectively, while the third row included 11 collectors. The tilt angle that has been used was 30°. Indeed, according to Agrouaz et al. 511, this tilt angle value helps to enhance the efficiency of the collectors, especially in Fez city. The total apparent area covered by the collector fields is 62.124 m². The arrangement suggested in Tab. 26 was used as a basic and initial configuration to evaluate the annual solar fraction of the collective process intended to produce hot water. Subsequently, a sensitivity study on the effect of the collector coupling and arrangement is proposed in the sub-section 6.12.1.

ETC	Manufacturer	<i>Viessmann Werke GmbH & Co</i>	<i>Jingsu Sunrain Solar Energy</i>	<i>Baxi Calefaccin</i>	<i>Thermomax-Inygen</i>
	Product	<i>VITOSOL 300-T SP3A 2 m2</i>	<i>Sunrain TZ58/1800-25R2</i>	<i>AR 20</i>	<i>Thermomax 20</i>
	Laboratory	ISFH	ISE	ISFH	CSTB
	Averaged price	284 \$ 322			
FPC	Manufacturer	<i>Junkers</i>	<i>Chaffoteau & Maury Rendamax-MT</i>	<i>Energie Solaire S.A.</i>	<i>J. Giordano Industries</i>
	Product	<i>FKT-1s</i>	<i>2.3 V</i>	<i>XX-SEL Vertical</i>	<i>C8 modeles C8/8. S.U</i>
	Laboratory	Fraunhofer	CSTB	CSTB	CSTB
	Averaged price	227 \$ 322			

Table 24: Database of the solar collector panel 44

Additional technical information about the heat transfer fluids (the type and name of the

fluids) used by the certification laboratories to assess the energy performance of various collector's technologies are available in the Transol's manual references [44].

	Manufacturer	a_0	a_1 ($W/K.m^2$)	a_2 ($W/K^2.m^2$)	Height (m)	Q_t ($l/h.m^2$)	C_p ($kJ/kg.K$)	Surface area (m^2)
ETC	<i>Viessmann Werke GmbH & Co</i>	0.809	1.370	0.0068	2.030	64.80	8.4830	2.004
	<i>Jingsu Sunrain Solar Energy</i>	0.734	1.529	0.0166	2.008	70.50	15.60	2.039
	<i>Bari Calefaccin</i>	0.800	1.530	0.0063	1.996	72.00	10.029	2.004
	<i>Thermomax-Inygen</i>	0.750	0.550	0.0153	1.415	72.00	10.78	2.000
FPC	<i>Junkers</i>	0.821	3.699	0.0148	2.080	72.20	10.78	2.230
	<i>Chaffoteau & MauryRendamax-MT</i>	0.820	3.310	0.0181	2.099	72.00	10.78	2
	<i>Energie Solaire S.A.</i>	0.816	3.804	0.0176	2.40	72.00	10.78	2.020
	<i>J. Giordano Industries</i>	0.760	4.003	0.015	2.002	72.00	10.78	2

Table 25: Technical characteristics of the solar collectors panel [44].

Number of rows	Length of rows (m)	Number in series	Distance between rows (m)
3	15.6291	10	3.347

Table 26: Characteristics of the solar collectors field [44].

Figs. 104 represent two categories of the industrial process for the production of solar hot water. The first category is characterized by the centralized hot water storage, as shown in Figs. 104(a) and (b). In fact, the stored hot water volume is important in this case and it can be sized to store 3000 liters. The second category is described in Fig. 104(c) where the storage is individualized, in other words, it is distributed over a set of consumers having a storage tank of reduced volume compared to the centralized storage tank. The centralized production of *DHW* helps to cover the specific needs of the consumer with important volumes during short period. The configuration presented in Fig. 104(a) allows the use of reduced auxiliary systems power according to daily hot water load profile pattern. This result is discussed further in this chapter through the parametric studies that were performed on the storage tank volume of the collective process.

The benefits of a collective hot water process equipped with a centralized storage tank are the low cost of the storage solution and the enhanced performance of the process due to the use of submerged heat exchangers and large storage tank volumes, which leads to lower heat losses compared to the configuration of several tanks. Fig. 104(c) presents a decentralized storage of a collective hot water production process.

6.10.2. Weather data and load profile

Weather data

The Moroccan climate is both Mediterranean and Atlantic, with a dry and hot season coupled with a cold and wet season, the end of the warm period being marked by October rains. The presence of the sea attenuates the differences in temperature, tempers the seasons and increases the humidity of the air (400 to 1000 mm of rains on the coast). In the interior, the climate varies according to the altitude. Summers are hot and dry, especially when blowing the hot sirocco or the chergui, summer wind coming from the Sahara (Fig. 105). At this season, average temperatures are 22°C to 24°C. Winters are cold and rainy with frost and snow. The average temperature then varies from -2°C to 14°C. In the mountainous regions, the precipitation is very important (more than 2000 mm of rainfall in the Rif or 1800 mm in the Middle Atlas). Pre-Saharan and Saharan Morocco has a dry desert climate.

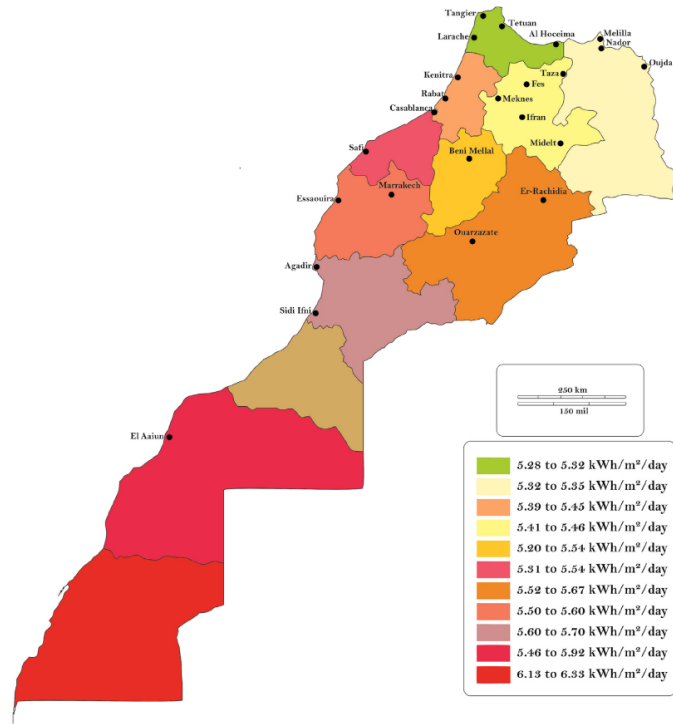


Figure 105: Various solar radiation intensities in Morocco [8].

The meteorological data of Fez city [34°03'N 4°58'W] are defined as the ambient temperature and the incident solar radiation. Moreover, the cold-water temperature refers to the cold water, which fills the tank from the bottom and goes through the hydraulic network of the residence, before it is heated by the solar radiations (Fig. 106-(a)). The incident solar radiation and the total radiation on horizontal correspond to the overall area of the solar collector field of the collective process, which is equal to 62.124 m².

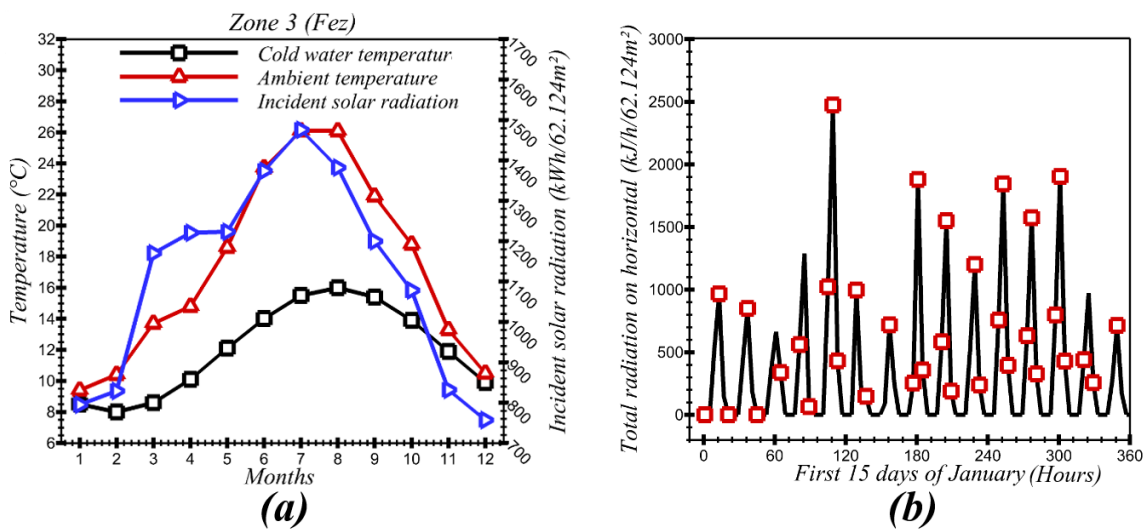


Figure 106: (a)- Fez weather data [44]. (b)- The total radiation on the collector's horizontal [44].

The weather characteristics of the climatic zone 3 (Fez) is continental [93]. Meteonorme software was used to generate the weather data that corresponds to Fez city, because the dynamic simulations require a representative hourly climatic data [323]. It should be noted that the North African climate is common and can be considered as a reference for the Arab Maghreb (AM) countries. The total radiation on the solar collector is independent from the load profile as presented in Fig. 106-(b).

Load profiles

The daily hot water consumption and the heating load profile are considered as the most affecting parameters of the SWH's overall efficiency [107]. In the Moroccan residence, hot water is consumed according to various profiles, which are not well defined up to now, because the consumption of hot water presents a probabilistic pattern that depends on several factors. Hence, the design of the collective SWH remains a complicated issue. Five realistic load profiles were developed based on literature surveys that we have carried out, in order to compensate for this lack of information. The considered profiles per day are listed as follows: *Diario-DTIO*, *Diurno-Day*, *Europeo-European*, *Matinal-Morning* and *Tarde-Afternoon* as shown in Fig. 107. The hot water temperature commonly required by the consumer is equal to 45°C and Fig. 108 is presenting the DHW consumption flow rate, which is corresponding to each load profile throughout the first five days of January (120 hours). In addition, it should be noted that the considered load profiles present the same consumed volume of 6000 liters per day at the set temperature of 45 °C.

For example, the Matinal-Morning profile is characterized by a collective consumption of hot water in the morning and evening.

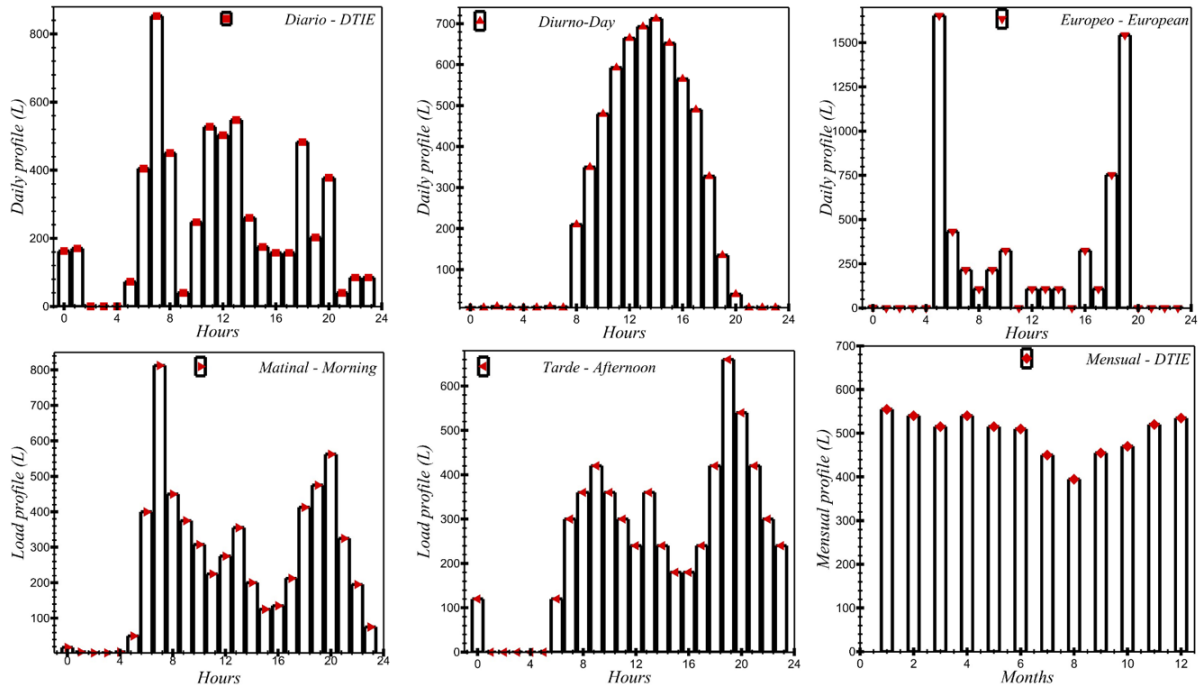


Figure 107: Typical hot water loading profiles used during the dynamic simulations (daily profiles/single monthly profile) [44].

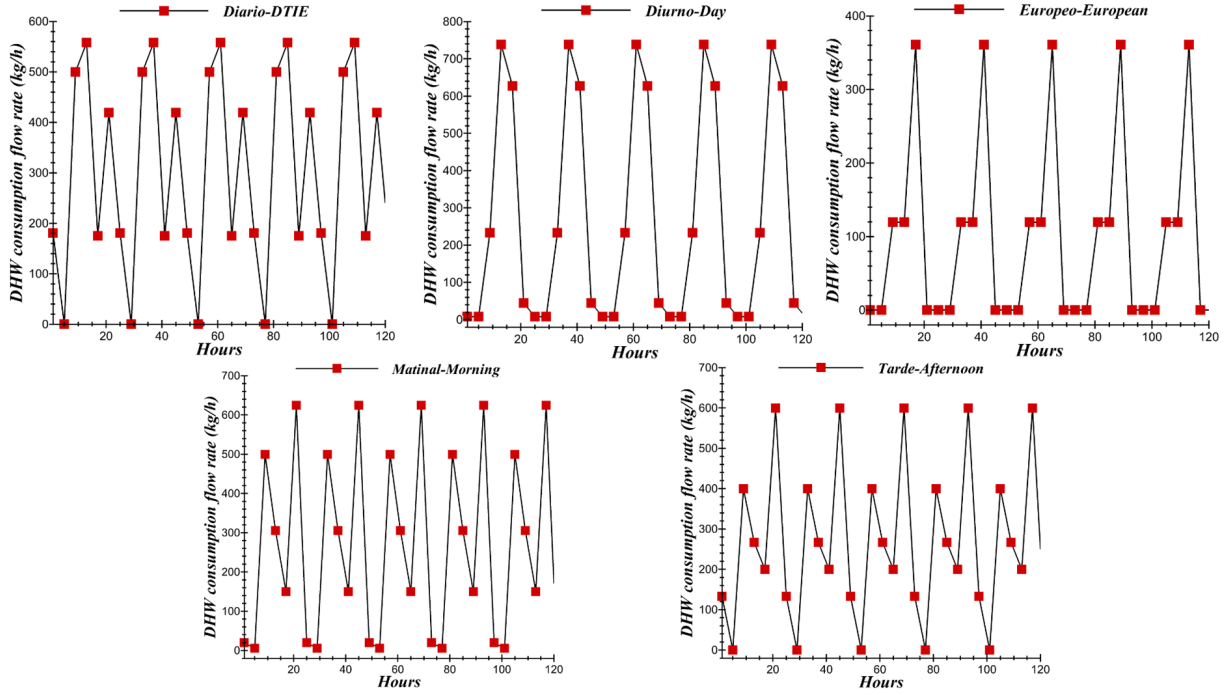


Figure 108: DHW consumption flow rate corresponding to each load profile for the first five days of January [44].

This profile is more suitable for institutions and residences. On the other hand, the profile Tarde-Afternoon presents an accentuated consumption during the afternoon and the evening. In addition, the *Diurno-Day* profile describes a high consumption during the morning between 10 am and 5 pm. The profile Europeo-European corresponds to the countries of the European Union, where the consumer tends to use hot water between 5 am and 7 am and then in the evening between 5 pm and 7 pm. The Diario-DTIE has a general consumption pattern, because it describes a consumption that is spread over the whole day and it does not follow a particular trend.

6.11. Equation setting

6.11.1. Thermal collector

The thermal efficiency of a single collector is expressed in Eq. [107] [292]. Where Q_u is the useful energy to heat the water's mass \dot{m} at the inlet side of the collector's field. In addition, T_{in} is the inlet and T_{out} is the outlet temperature from the solar collector. A_c is the area of the collector, while I_T is the total solar irradiance on the tilted surfaces of the collectors. It is noted that a quadratic relation is used to define the efficiency of one single solar thermal collector as expressed in Eq. [108] [319].

$$\eta = \frac{Q_u}{A_c I_T} = \frac{\dot{m} C_p (T_{out} - T_{in})}{A_c I_T} \quad (107)$$

$$\eta = a_0 - a_1 \frac{(T_m - T_a)}{I_T} - a_2 \frac{(T_m - T_a)^2}{I_T} \quad (108)$$

where a_0 indicates the zero loss efficiency of the collector which represents its optical conversion coefficient. Moreover, a_1 and a_2 represent the first and second order heat loss coefficients by

conduction and convection of the collector, respectively. The numerical values of those parameters are presented in Tabs. [24, 25]. T_m is the average temperature for a single collector given by Eq. [109], where T_{out} and T_{in} are the outlet and the inlet temperatures respectively from one single collector, and T_a is the ambient temperature.

$$T_m = \frac{T_{out} + T_{in}}{2} \quad (109)$$

Our dynamic simulations involve a set of collectors connected either in series or in parallel. Hence, the heated water at the outlet of the first collector module is injected slightly higher at the inlet of the adjacent collector [324]. The collective solar collectors are arranged so that the heat transfer fluid (*HTF*) flows through the collectors in a combined parallel and series pattern. Let us consider twelve collectors, which constitute the collector field of the collective process. In fact, as presented in Fig. [109], the *HTF* flows in a series behavior through each collector in the first row 1, 5 and 9. Moreover, the *HTF* flows in a parallel pattern between the first and the subsequent row.

As shown in Tab. [25], the data supplied by a collector manufacturer are useful to determine the performance of a single collector. However, for a large number of possible array configurations, it is required to develop an accurate method to calculate the array efficiency based on the performance data of a single collector. The first four collectors (1, 2, 3 and 4), presented in Fig. [109], are in parallel and their performance is going to be the equal to the efficiency value assessed by their manufacturer, if the flow throughout each collector is the same as the flow used in the test laboratory. In addition, the second set of the collectors (5, 6, 7 and 8) would also operate according to the manufacturer's data. However, the inlet temperatures of these collectors are equal to the outlet temperatures of the first four collectors. Therefore, their yield would be lower than the collectors 1, 2, 3 and 4. Besides, the collectors 9, 10, 11 and 12 are going to operate at a lower performance than the previous set of collectors, since the inlet temperature is increasing [324].

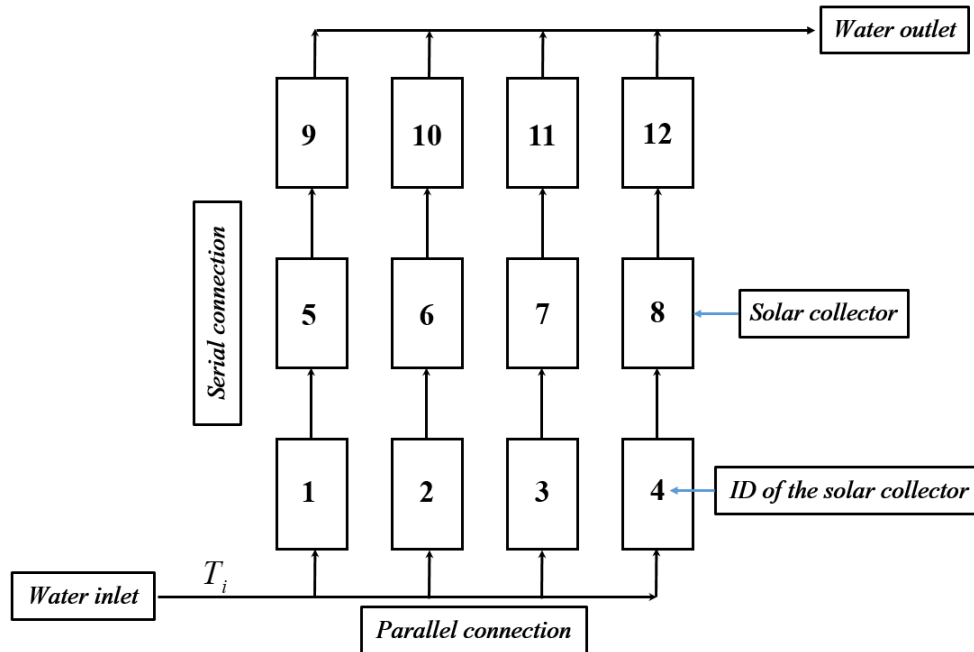


Figure 109: Combined series and parallel flow through a collector array.

An extended method, which is based on the slope/intercept test data of a single collector panel has been developed by Oonk et al. [324] to predict the performance of (N) solar collectors in series (Eq. 110). It should be noted that Eq. 110 can only be used when the fluid Reynold's Number (Re) flowing through the collector is the same as during the laboratory's tests.

$$\eta = (F_R(\tau\alpha)_e)CFN - (F_R U_L)CFN \frac{T_i - T_a}{I_T} \quad (110)$$

$$CFN = \frac{1}{N\psi}(1 - (1 - \psi)^N) \quad (111)$$

$$\psi = \frac{C_2}{GC_p} \quad (112)$$

where η is the performance of N panels in series. $(F_r U_L)$ is slope of the efficiency plot of a single collector. (CFN) is a correction factor corresponding to N collectors connected in series. (T_i) is the inlet temperature and (T_a) is the ambient temperature. In addition, (I_T) is the solar radiation, (GC_p) is the fluid capacitance rate for a single collector, which is defined by the collector's test labs [44]. C_2 is the slope and ψ is defined as the ratio between the slope and the fluid capacitance rate of a single collector.

6.11.2. Storage tank

A single centralized storage tank was used for this collective application. Its volume effect on the annual solar fraction was investigated as presented in Tab. 27. Moreover, the filling and the loading tank's nozzles, besides to the inlet and the outlet positions of the exchanger are presented in Fig. 110 and in Tab. 28.

Volume (l)	H_{tank} (m)	ϕ_{tank} (m)	Internal heat exchanger area (m ²)
1000	2.21	0.76	3.25
2000	1.77	1.2	5.61
3000	2.66	1.2	7.97

Table 27: Dimensions of the centralized tank for each storage capacity [44].

Solar system inlet	Cold water inlet	Solar system outlet	Solar hot water outlet
50% L_{tank}	tank bottom (0% L_{tank})	tank bottom (0% L_{tank})	top tank (100% L_{tank})

Table 28: Location of water injection nozzles (Solar and hot water circuits)

The unsteady energy balance in the tank takes into account the amount of the useful energy gained by the solar collectors Q_u , the hot water energy to load Q_{load} , and the convection losses to the surrounding environment Q_{loss} .

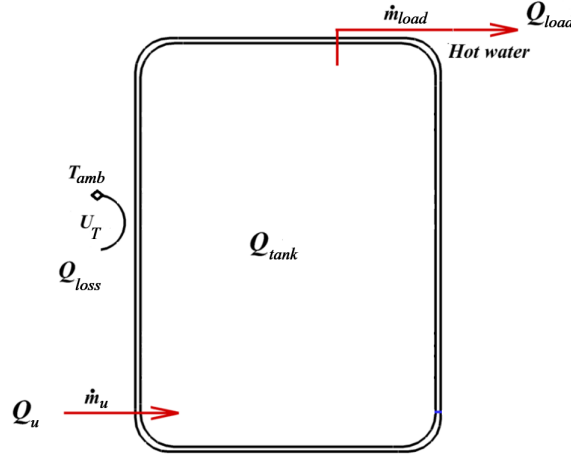


Figure 110: Schematic of the thermal storage tank's energy balance.

The energy balance is expressed using Eq. (113) [325]:

$$Q_{tank} = m_T C_p \frac{dT}{dt} = Q_u - Q_{load} - Q_{loss} \quad (113)$$

The mass stored in the tank m_T is expressed as $m_T = \rho V$. Where ρ is the water's density and V refers to the volume contained inside the centralized tank. Finally, C_p is the specific heat of water. The useful energy Q_u is calculated by Eq. (114). Where $T_{collector}$ is the outlet temperature from the collector, while T represents the temperature of a specific node of the stratified storage tank at the instant t .

$$Q_u = \dot{m}_u C_p (T_{collector} - T) \quad (114)$$

The draw load energy Q_{load} is written in Eq. (115)

$$Q_{load} = \dot{m}_{load} C_p (T_{top} - T_{load}) \quad (115)$$

where T_{top} refers to the top tank's temperature and T_{load} is the temperature of the hot water to load for the consumer. The heat losses from the tank (Q_{loss}) are calculated as mentioned in Eq. (116):

$$Q_{loss} = U_T A (T - T_{amb}) \quad (116)$$

where U_T represents the heat exchange coefficient from water to ambient. In addition, T_{amb} is the ambient temperature, and A is the lateral surface of the tank.

6.11.3. Solar fraction of the collective process

Solar fraction can be defined as the total energy provided by the solar collective system to produce hot water. It is calculated using Eq. (117) [326]. The solar fraction is the most important indicator, which is used to assess the performance of *SWHs* systems, because it takes into account the overall performance of the entire solar system and not only one single device or component [327].

$$f = 1 - \frac{Q_{Auxiliary}}{Q_{load}} \quad (117)$$

Where Q_{load} is the total energy transferred by the collective system to satisfy the heating requirements, and $Q_{Auxiliary}$ is the total auxiliary energy provided to the collective system to support the portion of the total solar energy load, which is not sufficient to ensure heating water.

6.12. Results and discussion

In this chapter, two major parametric studies were carried out to assess the energy performance of the *SWH* collective system equipped with the centralized storage tank.

To begin with, the volume of the storage tank was varied as a first study, and its effect on several performance indicators was analyzed such as: the energy recovered by the solar collectors, the outlet temperature from the collectors, the solar top tank's temperatures, the supplements consumption and the overall solar fraction of the collective process. Furthermore, the effect of the collector field arrangement on the solar fraction for different load profiles was also investigated. We emphasize that the ETC collector, derived from the brand *Viessmann Werke GmbH & Co* has been used to constitute the solar collector panel for the first parametric study.

The second parametric study focuses on the assessment of the collector's technology effect on the solar fraction of the collective *SWH* system. In fact, the system's efficiency was compared by using two different technologies of solar collectors, namely *ETC* and *FPC*.

6.12.1. First parametric study: effect of the storage tank volume

The total volume consumed per day in the collective building is equal to 6000 liters and it is divided according to the load profiles, which are previously detailed in Fig. 107. It should be noted that the maximum volume that is consumed and recorded during a specific period of the day does not exceed 1650 liters. Hence, it is important to study the effect of the centralized tank volume on the evolution of the annual solar fraction of the collective heating water process. Three storage volumes were considered, namely $V = 1000$ liters, $V = 2000$ liters and $V = 3000$ liters. The effect of the storage tank volume for the adopted load profiles on the energy recovered by the evacuated solar collector panel is presented in Fig. 111.

It is noted that the energy recovered by the solar collector is maximal over the year for the highest volume of the stratified storage tank volume ($V = 3000$ liters) 328. Moreover, this recovered energy by the solar panel is affected by the load profiles, as it is shown in Fig. 111.

The energy recovered by the solar collector is enhanced, if hot water's demand is high, for example during the cold period of the year, such as February, March and April. In fact, the primary circuit pump is switched on and the heat transfer fluid is pumped from the internal exchanger located in the lower part of centralized collective storage tank towards the manifolds of the collectors. In addition, the storage tank temperature with a minimal assigned volume increases quickly compared to a higher storage volume, to finally reach the set point temperature. Therefore, the primary circuit pump is switched off, and even if the collector's field is exposed to solar radiations, the heat transfer fluid of the primary circuit loop does not pass through the series of manifolds. Hence, it is not receiving energy from the solar field panel.

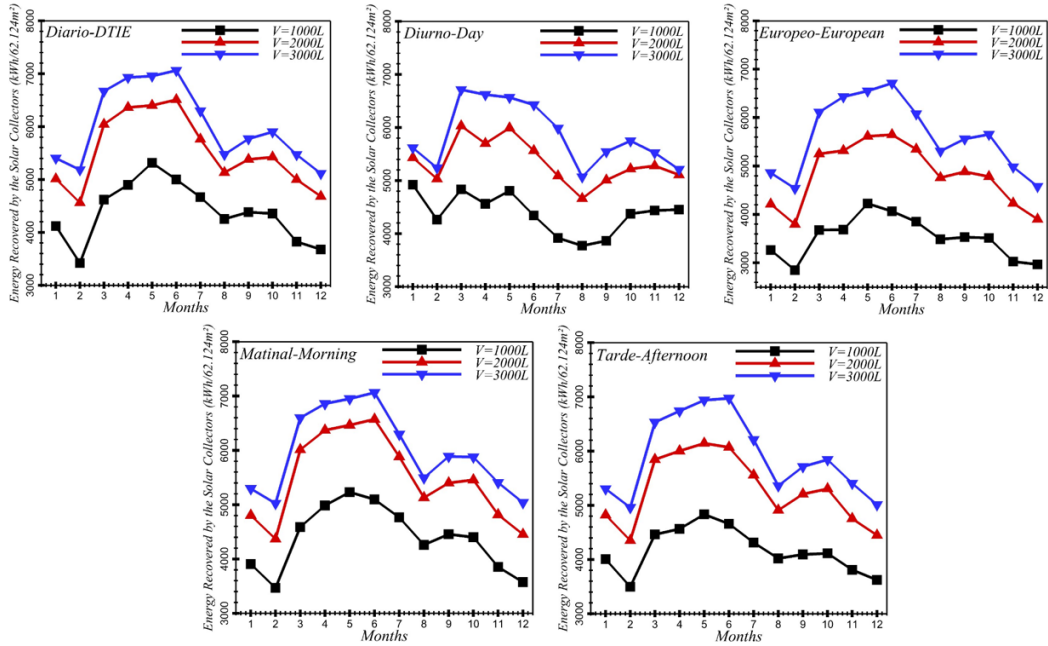


Figure 111: Effect of load profiles and storage tank volumes on the energy recovered by the solar collector.

For instance, the outlet temperature evolution from the solar collector field over the first five cold days of January is presented in Fig. 112. The outlet temperatures from the collector field are below 60°C . As can be observed, the maximal temperature at the solar collector field outlet reaches different values as time progresses. Indeed, the outlet temperature from the collector reaches its maximum peak, when the solar radiations are important. For the *Europeo-European* profile, it is noticed that during the afternoon (15h), the collector outlet temperature is 56°C and it decreases over time, to reach a minimal temperature's value of 10°C in the evening or very early in the morning (6h). As presented in Fig. 112, the maximum temperatures occur only three times, namely at 16h, 62h and 106h for the first five considered and simulated days of January. Indeed, a local maximum has been reached independently from the load profile during the second and fourth days of the first week of January. Therefore, the outlet temperatures of the solar collectors were 12°C and 22°C for the *Europeo-European* profile. Since the solar radiations were insufficient to set off the operation of the primary circuit's pump, which is involved in the heating of the heat transfer fluid, thus, the outlet temperature from the collectors was not as important as the first, third and fifth days of the first week of January.

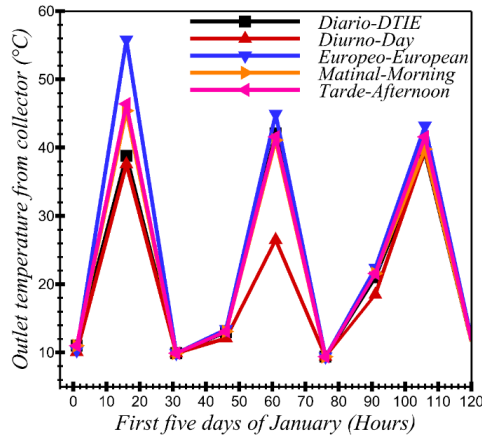


Figure 112: Outlet temperature evolution from collector over the first five days of January.

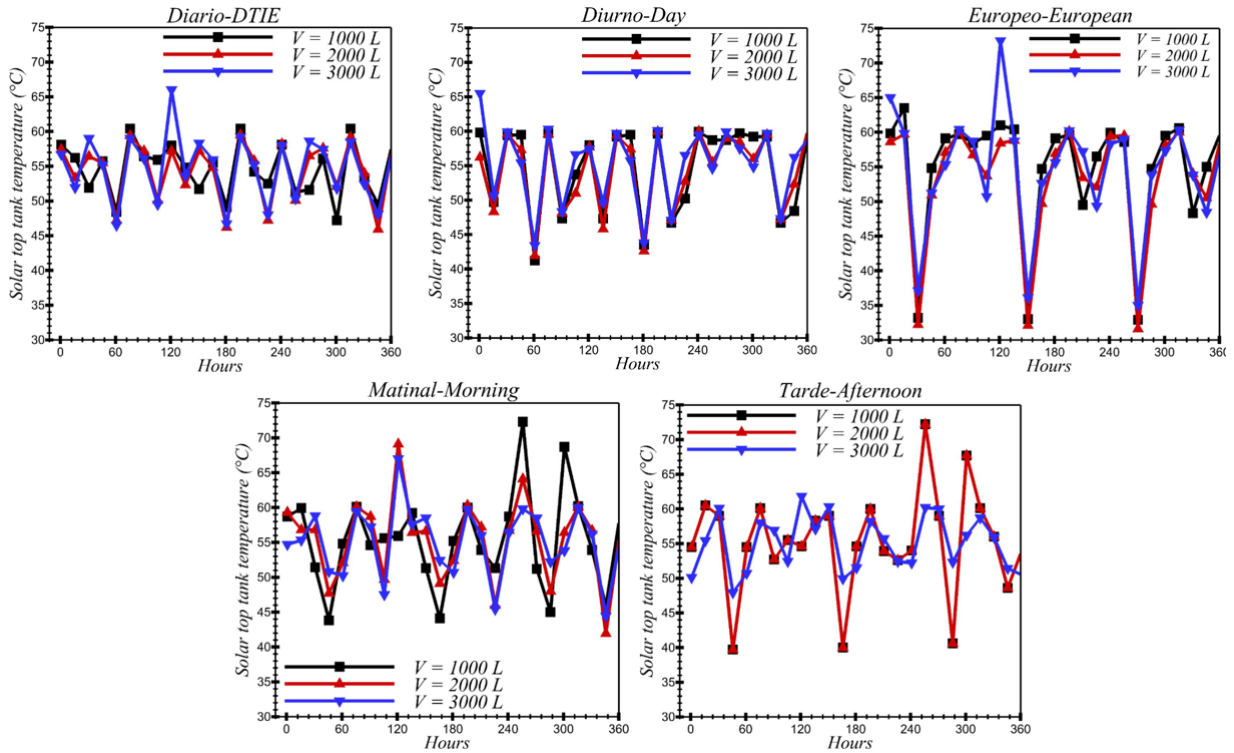


Figure 113: Solar top tank temperature evolution for three different centralized storage tank volumes and for five load profiles on a range of the first 15 cold days of January.

As shown in Fig. [107](#), the Europeo-European load profile is characterized by high DHW consumption between 5h and 7h (1750 liters) and between 17h and 19h (1500 liters). On the other hand, the Tarde-Afternoon load profile is characterized by hot water demands that varies between 200 liters and 400 liters before 17h, reaching 650 liters at 19h and 500 liters at 20h. The difference between these two profiles clearly affects the temperature at the outlet of the storage tank as shown in Fig. [113](#), especially if the effect of the stratified storage tank volume is taken into

account. Therefore, to serve the needs of the consumer whose consumption follows the Europeo-European profile, the use of a large storage tank volume (3000 liters) would be the most appropriate because it would ensure the production of a hot water volume of 1750 liters without affecting the efficiency of the solar collector field, hence, improving the solar fraction of the collective process.

The supplementary consumption was assessed for different storage tank volumes and for the five considered load profiles as presented in Fig. 114. The hydraulic booster as an auxiliary energy source was used to meet the consumers' needs, which are represented by the loading profiles when solar radiations are insufficient, notably during the cold periods of the year. The technical characteristics of the hydraulic booster that has been used during the dynamic simulation are presented in the Tab. 29.

Hydraulic auxiliary system	Manufacturer	Chaffoteaux
	Manufacturer	<i>PHAROS Green 18</i>
	$P_{nominal}$	18 kW
	Set-point temperature	55 °C
	Static differential	5 °C
	Supplement position	90% L_{tank}

Table 29: Technical features of the auxiliary booster 44.

The effect of the tank design is clearly noticeable, because the fact of adding an auxiliary heating source directly affects the overall efficiency of the collective system. Obviously, using a diminished volume of the tank, in this case $V = 1000$ liters, leads to the continuous operation of the auxiliary booster, even if the solar radiations are significant, because the continuous loading of the hot water at 45° C with relatively important flow rates cannot only be ensured by solar energy. Consequently, an optimized volume $V = 3000$ liters of the storage tank would stores an important solar thermal energy, which helps to fill the consumers' needs even in the case of peak demand 329.

The effect of the centralized storage tank volumes on the solar fraction of the collective process for the suggested loading profiles is presented in Fig. 115. The collective system's solar fraction was assessed for five different storage tank volumes varying from $V = 1000$ liters to $V = 3000$ liters, with an incremental volume of 500 liters. For the *Diario-DTIE* profile, the average solar fraction of November, December, January and February is equal to 50%. For April, May, June, September and October the average solar fraction is equal to 80%. The contribution of solar energy compared to the auxiliary booster is clearly enhanced for $V = 3000$ liters volume 330. This result was generalized for the five applied load profiles. Moreover, for the *Europeo-European* profile, the solar fraction was significantly improved from a storage volume of $V = 1000$ liters to $V = 3000$ liters. An enhancement of (20% to 37% for December), (27% to 37% for January), (23% to 44% for February), (25% to 48% for March).

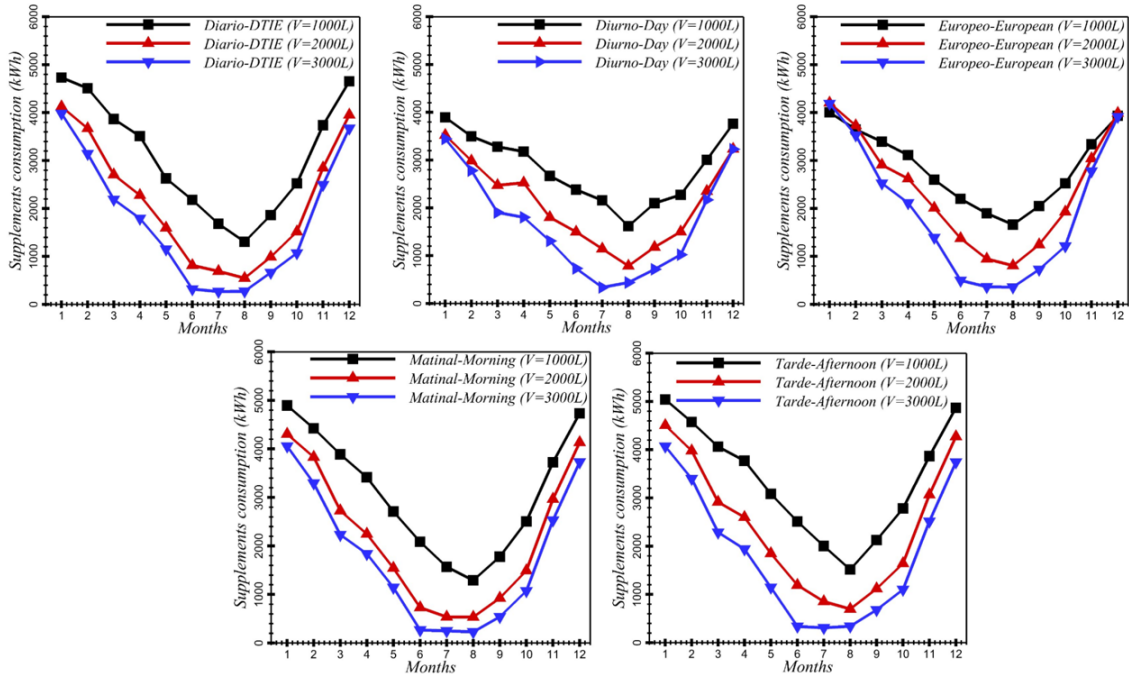


Figure 114: Effect of the load profile on the consumption of the auxiliary booster for different storage tank volumes.

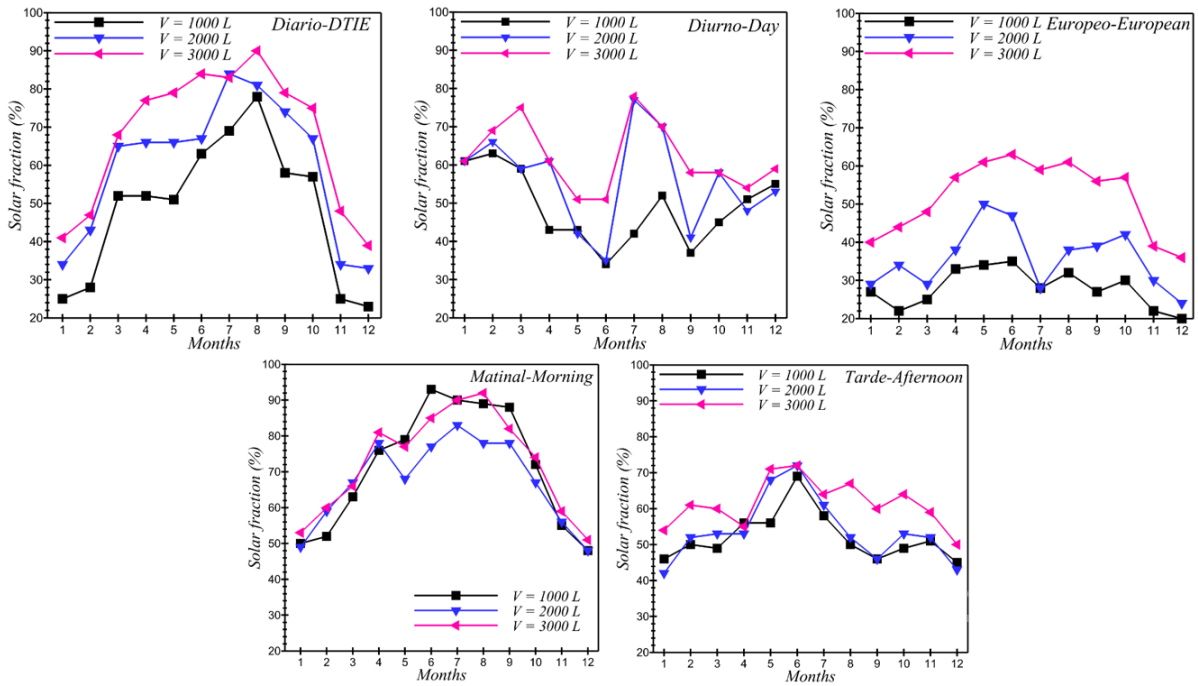


Figure 115: Effect of different storage tank volume on the solar fraction for the considered loading profiles.

Effect of ETC technologies on the annual solar fraction

The effect of the ETC collectors on the solar fraction of the collective system for different volumes of the tank are investigated in this section, according to previous defined load profiles. Four ETCs from different manufacturers (Tab. 25) such as Viessmann Werke GmbH & Co, Jingsu Sunrain Solar Energy, Baxi Calefacchin and Thermomax-Inygen were integrated into the collector field. Each collector product is characterized by the three intrinsic coefficients a_0 , a_1 and a_2 , which affect its operating efficiency.

It has been shown that Jingsu Sunrain Solar Energy's ETC collector maximizes the solar fraction of the collective hot water process. Indeed, it allows reaching a significant solar fraction average over the cold period when the hot water need is high. An average for the months of September, October, November, December, January, February, March, April and May which equals 75.23% for *Diario-DTIE*, 78.22% for *Diurno-Day*, 70.88% for *Europeo-European*, 74.15% For *Matinal-Morning* and 73.77% for *Tarde-Afternoon*.

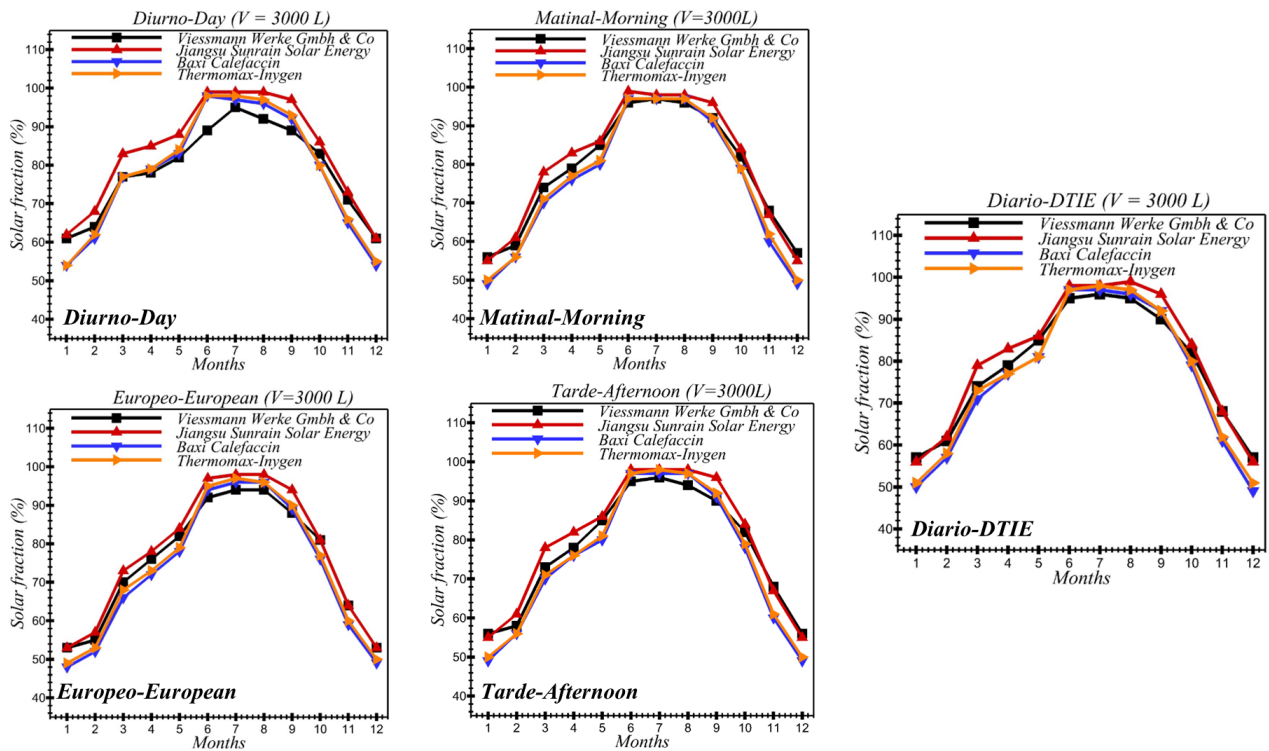


Figure 116: Effect of the ETC collectors designed from different manufacturers on the annual solar fraction of the collective system for a storage tank volume of 3000 liters.

The specific heat capacity (C_p) of the HTF used by the manufacturer "Jingsu Sunrain Solar Energy" is higher than that of the other manufacturers of the ETC collectors that have been considered in the different parametric studies (Tab. 25). As a result, the HTF transfers more energy at the integrated coil heat exchanger integrated at the bottom node the collective thermal storage tank. Consequently, the contribution of the auxiliary heating system is decreased and the solar fraction of the collective process is enhanced. The effect of the ETC technologies on the annual solar fraction over the year using the considered load profiles is presented in Tab. 30. In

this case the volume of the storage tank was $V = 3000$ liters.

Load Profiles		January	February	March	April	May	June	July	August	September	October	November	December
Diario-DTIE	Viessmann Werke Gmbh & Co	57	61	74	79	85	95	96	95	90	82	68	57
	Jiangsu Sunrain Solar Energy	56	62	79	83	86	98	98	99	96	84	68	56
	Baxi Calefacin	50	57	71	77	81	97	97	96	92	79	61	49
	Thermomax-Inygen	51	58	73	77	81	97	98	97	92	80	62	51
Diurno-Day	Viessmann Werke Gmbh & Co	61	64	77	78	82	89	95	92	89	83	71	61
	Jiangsu Sunrain Solar Energy	62	68	83	85	88	99	99	99	97	86	73	61
	Baxi Calefacin	54	61	77	79	83	98	97	96	92	80	65	54
	Thermomax-Inygen	54	62	77	79	84	98	98	97	93	80	66	55
Europeo - European	Viessmann Werke Gmbh & Co	53	55	70	76	82	92	94	94	88	81	64	53
	Jiangsu Sunrain Solar Energy	53	57	73	78	84	97	98	98	94	81	64	53
	Baxi Calefacin	48	52	66	72	78	94	96	96	89	76	59	49
	Thermomax-Inygen	49	53	68	73	79	95	97	96	90	77	60	50
Matinal - Morning	Viessmann Werke Gmbh & Co	56	59	74	79	85	96	97	96	92	82	68	57
	Jiangsu Sunrain Solar Energy	55	61	78	83	86	99	98	98	96	84	67	55
	Baxi Calefacin	49	56	70	76	80	97	97	97	91	79	60	49
	Thermomax-Inygen	50	56	71	77	81	97	97	97	92	79	62	50
Tarde - Afternoon	Viessmann Werke Gmbh & Co	56	58	73	78	85	95	96	94	90	82	68	56
	Jiangsu Sunrain Solar Energy	55	61	78	82	86	98	98	98	96	84	67	55
	Baxi Calefacin	49	56	70	76	80	97	97	97	91	78	60	49
	Thermomax-Inygen	50	56	71	76	81	97	98	97	92	79	61	50

Table 30: *ETC*s collectors technologies effect on the annual solar fraction (%) for the considered load profiles.

Effect of the collector field arrangement on the annual solar fraction

Depending on the consumers' hot water needs and the incident solar radiation of the site, several collectors could be connected, in order to increase the collecting area of the solar field. The current parametric study was carried out for a centralized storage tank volume of 3000 liters and using *ETC*. In fact, the collector arrangement used to meet the collective hot water production has a considerable effect on its efficiency, in other words on its solar fraction (Fig. 117). Several coupling configurations between the collectors, which constitute the solar collector field, are possible. For instance, serial, parallel or mixed coupling.

If several collectors are connected in parallel, the temperature of the *HTF* at the outlet of the collector field is increased. Otherwise, an installation with several collectors connected in series has the effect of decreasing the temperature of the *HTF* at the outlet of the collector field. Parallel and serial configurations were used in this study to enhance the overall efficiency of the collective hot water production process. Thirty one *ETC* collectors, based on the manufacturer *Viessmann Werke GmbH & Co*, were spread over 2, 4, 6, 8 and 10 rows to constitute five configurations. The effect of these arrangements on the solar fraction was assessed for the considered applied load profiles. The improvements recorded regarding the system's solar fraction during the cold season are presented in Tab. 31.

Load profiles		<i>Diario-DTIE</i> (Solar fraction (%))	<i>Diurno-Day</i> (Solar fraction (%))	<i>Matinal-Morning</i> (Solar fraction (%))	<i>Europeo-European</i> (Solar fraction (%))	<i>Tarde-Afternoon</i> (Solar fraction (%))
Decembre	2 rows	37	44	40	40	40
	6 to 8 rows	58	60	54	54	56
January	2 rows	43	48	44	44	42
	6 to 8 rows	57	62	56	54	56
February	2 rows	52	42	38	36	38
	6 to 8 rows	65	68	62	68	62
March	2 rows	68	44	42	40	40
	6 to 8 rows	80	86	78	78	80

Table 31: Effect of *ETC* arrangement on the collective process solar fraction during the cold season.

Currently, the manufacturer "Viessmann Werke" conquers the Moroccan market of solar thermal collectors [319]. It has become a leader in the Moroccan market since it sells its ETC collectors for individual and collective solar applications, such as the production of *DHW*, the heating of swimming pools ... and for other thermal applications, such as heating and cooling production using solar energy. It is for this reason that the *ETC* collectors produced from this manufacturer were used to carry out the parametric study on the arrangement of the collectors and their effect on the solar fraction of the collective process, instead of the *ETC* brand manufactured by "Jingsu Sunrain".

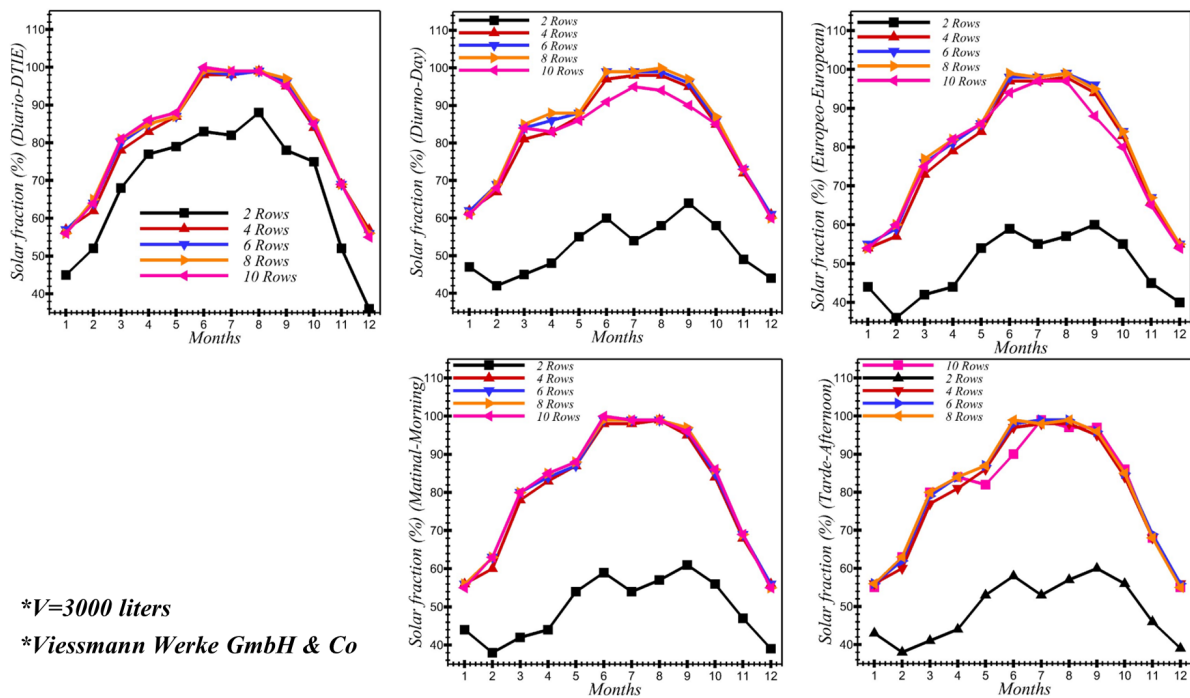


Figure 117: Effect of the collector field arrangement on the solar fraction for different load profiles.

As shown in Fig. 117, the trend of the system's solar fraction for 2 rows is below the other trends which characterize 4, 6, 8 and 10 rows. As a result, the annual solar fraction is improved by increasing the row's number. Six and eight rows enhanced the collective system's solar fraction for almost the five considered load profiles.

Increasing the number of the collectors' rows enhances the solar fraction of the *DHW* production process (Fig. 117). Above a specific number of rows, in our case 6 to 8 rows, the solar fraction does not improve by adding a new series of collectors, because the *HTF* has already received the corresponding maximum energy to its heat capacity. On the contrary, if more rows are integrated in the collector field, greater than 8 rows in this case, pressure drops in the pipes as well as thermal losses by conduction and convection could be generated, and therefore, the fraction of the process is decreased. As a conclusion, for a similar collective application of hot water production, the constitution of a solar collector field where the parallel configuration is predominant would enhance the solar fraction of the collective process. However, additional attention should be addressed to the thermal insulation of the pipes connecting the collectors.

6.12.2. Second parametric study: Collector effect on the annual solar fraction

The second parametric study focuses on the assessment of the collector’s technology effect on the solar fraction of the collective SWH system. In fact, the system’s efficiency was compared by using two different technologies of solar collectors, namely *ETC* and *FPC*.

Effect of the collector technologies on the incident energy on the solar collector plane

This section is intended to study the effect of different solar collector technologies on three performance indicators, namely the solar fraction of the collective hot water process, the useful energy gain from the collectors and the incident energy on the solar collector field. The collector’s characteristics are presented in the Tabs. 24 and 25. Indeed, the incident energy on the solar collector plane was assessed for the *Diario-DTIE* profile and for a centralized thermal storage tank with a volume capacity of $V = 2000$ liters. The effect of several collectors’ brands, which belong to the same technology on the incident energy on the solar collector plane, is presented in Fig. 118. Tab. 32 presents the evolution of the incident energy on the solar collector plane for the cold period of the year. It is noted that the apparent solar collector surface affects the incident energy on the solar collector panel.

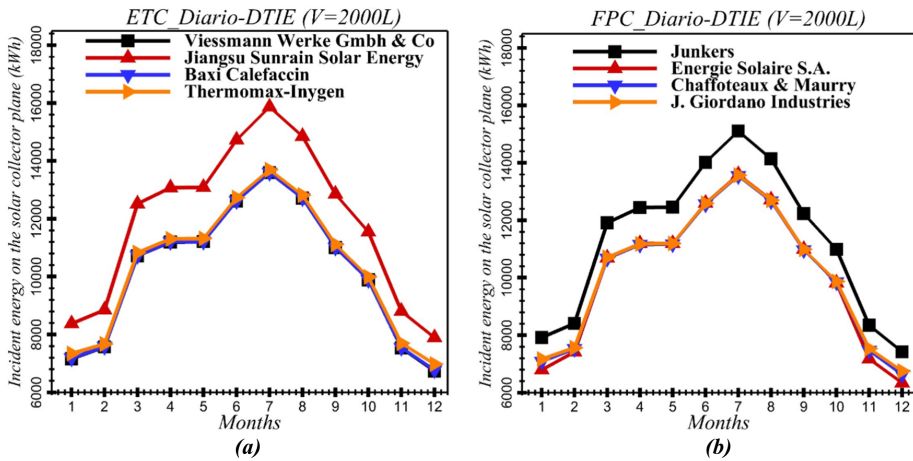


Figure 118: Effect of different collector technologies designed from different manufacturers on the incident energy on the solar collector plane for $V = 2000$ l (*Diario-DTIE* load profile). (a)- *ETC* technologies. (b)- *FPC* technologies.

Incident energy on the solar collector plane (kWh)	November	December	January	February	Mars	April
<i>ETC (Viessmann Werke GmbH & Co)</i>	8735	7790	8300	8790	12490	13000
<i>FPC (Junkers)</i>	8350	7360	7900	8400	11900	12400
Gap in the the incident energy between ETC and FPC	385	430	400	390	590	600

Table 32: Incident energy on the solar collector plane for the cold period of the year.

ETC effect on the useful energy gain from the collector

Two collector technologies were considered in the second parametric study to improve the thermal performance of the collective hot water process. Although the total area of the two variants of *ETC* and *FPC* collectors is equal to 2 m^2 , but the apparent surface that is exposed to the solar

radiations is different, due to the sun's momentum. Indeed, the geometry of the ETCs that is exposed to the solar radiations is tubular [331], while the geometry of the FPCs exposed to the solar rays is flat [332]. It should be noted that the ETCs enhance the conversion of solar energy into thermal energy because of their geometrical shape that does not require a solar radiation tracking system, which is not the case for the FPCs. Therefore, the second parametric study has been carried out to evaluate the gains that *ETCs* technology would bring to the collective production process of domestic hot water compared to FPCs, while testing several certified manufacturers of solar thermal collectors.

The effect of *ETC* on the useful energy gain from the collector is presented in Fig. 119. The useful energy gain from the collectors was assessed for four products of the *ETC* collectors. Moreover, *Diario-DTIE* profile was used as a load profile input for the simulations during the first cold week of January. It has been found that the product of the *Jingsu Sunrain Solar Energy* brand maximizes this indicator to achieve the values presented in Tab. 33. Further, the useful energy gain from the collectors becomes lower in the lack of the solar radiations.

Time (h)	11	36	85	110
Useful energy gain from collector (MJ/h)	112.410	38.714	60.358	154.590

Table 33: Useful energy gain from the collector for Jingsu Sunrain Solar Energy product.

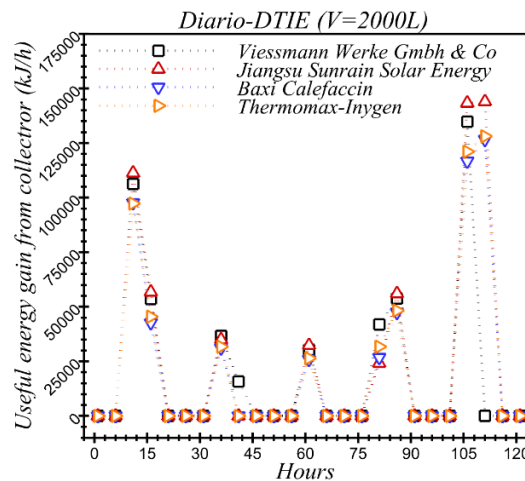


Figure 119: Effect of the *ETC* technology on the useful energy gain from collector for $V=2000$ l (*Diario-DTIE* load profile).

Effect of ETC technology on the annual solar fraction of the collective hot water process

Figs. 120 were presented to compare the energy performance of two different technologies of solar collectors, in order to justify the selection of the collector technology, which would help to meet the requirements of the present solar collective hot water production application. As a first step, a comparison between the energy performance of the *ETC* (*Viessmann Werke GmbH & Co*) and the energy performance of the other *FPCs* collectors was carried out (Fig. 120). In fact, the present study belongs to the project entitled *SOL'R SHEMSY* [6], which aims to manufacture and market on the national Moroccan scale the first *SWH* equipped with *ETC* with heat pipes using as collectors the *Viessmann* product (a choice required by the project's specifications). For this

reason, the *Viessmann Werke GmbH & Co ETC* was selected as a reference product instead of other *ETC* collectors' products.

From one hand, the effect of the *ETC* technology on the annual solar fraction of the collective process is presented in Fig. 120. Further, the solar fraction of the collective system was assessed for three storage capacities, namely $V = 1000$ liters, $V = 2000$ liters and $V = 3000$ liters. Moreover, different products of the *ETC* collectors were compared with the *ETC* collector, notably through the integration of the *Viessmann Werke GmbH & Co* collector product. From the other hand, it has been shown that the solar fraction of the collective process, which uses *Junkers* brand, is enhanced compared to the collective process that uses other *FPC* products. However, the achieved solar fractions remain lower than that of the *ETC Viessmann Werke GmbH & Co*, especially during the cold period of the year i.e. months: October, November, December, January, February, March and April as shown in Tab. 34.

The effect of the collectors' technologies *ETC* and *FPC* on the annual solar fraction of the *SWH* collective system for three volumes of the centralized storage tank is presented in Fig. 120. The collector effect is not predictable for a small tank volume, namely $V = 1000$ liters, however it becomes noticeable as it increases to a volume of $V = 3000$ liters. In addition, the solar fraction of the collective hot water process with a solar collector field constituted with the *ETC* technology is higher than the other configuration of the collective *SWH* system with a solar field based on *FPC* (Tab. 34).

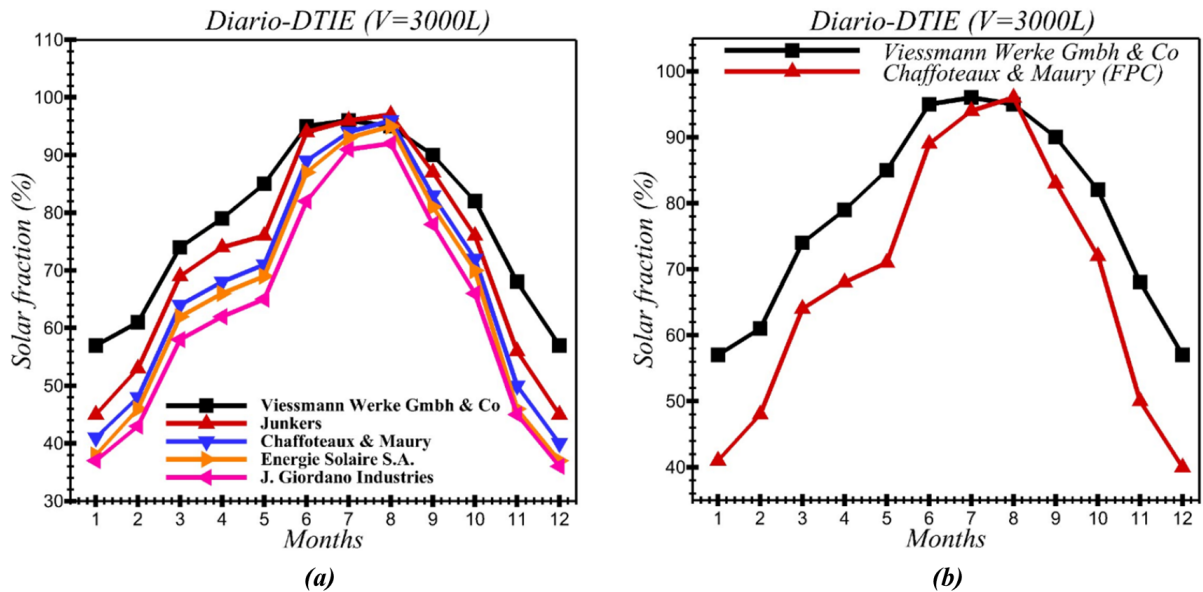


Figure 120: Effect of the *ETC* technology on the solar fraction gains for $V=3000$ l (Diario-DTIE load profile). (a)-Comparison between the annual solar fractions of the *Viessmann* brand (*ETC*) and four different *FPC* brands. (b)-Comparison between the annual solar fractions of the *Viessmann* brand (*ETC*) and *Chaffoteaux & Maury* brand (*FPC*).

The collectors' technologies effect on the annual solar fraction for a centralized storage tank with a volume of $V = 3000$ liters is presented in Tab. 34. The maximal annual averaged solar fraction is achieved by *Viessmann (ETC)* 78%. In contrast, it is equal to 68% for the *Chaffoteau & Maury (FPC)*.

Solar fraction (%)	October	November	December	January	February	March
<i>FPC</i> (Junkers)	78	56	46	46	54	68
<i>FPC</i> (Chaffoteaux & Maury)	72	51	40	41	48	64
<i>ETC</i> (Viessmann Werke GmbH & Co)	85	70	58	58	61	74
The relative gains regarding <i>FPC</i> technology (Junkers)	7	14	12	12	7	6
The relative gains regarding <i>FPC</i> technology (Chaffoteaux & Maury)	13	19	18	17	13	10

Table 34: The solar fraction of the collective process during the cold periode of the year and the relative gains in terms of energy if *ETC* collectors (*Viessmann Werke GmbH & Co*) are used.

The solar fraction of the *DHW* production process largely depends on the availability of solar energy, which is captured and converted by the collector field. It is for this reason that designing properly the collective system to ensure a solar fraction higher than 50%, during the period of the year when the need for hot water is increased, remains a good achievement. As shown in Fig. 120, the solar fraction of the *DHW* process reaches important values between 80% and 95% during the summer period of the year, especially in Mai, June, July, August and September. This result is explained by the fact that during this period of the year, the contribution of solar energy is greater than that of the hydraulic/electrical booster.

It is possible to ensure a stability of the solar fraction of the collective process relative to seasonal periods of the year, which are characterized almost by similar magnitude of solar radiation. On the other hand, ensuring stability of the solar fraction throughout the year remains a very complicated issue, because the amount of solar radiation incident on the collector field is uncontrollable (it is a weather data input), unless technical devices and systems are used to hide the surface of the collector during summer periods.

6.13. Conclusion

In the present study, the thermal performance of a forced circulation collective *SWH* process equipped with a centralized storage tank is assessed, in order to enhance its energy efficiency. A realistic case study has been considered to carry out this analysis. In fact, miscellaneous parametric studies were conducted to meet the collective hot water production need for a social housing (case of multiple apartment blocks) located on the city of Fez, which belongs to the climatic zone 3 in Morocco. Five typical hot water load profiles were used to assess the energy performance of this collective process.

This chapter presents two main parametric studies. The first study focused on the effect of the centralized storage tank volume on the solar fraction of the process. In fact, an undersized volume generates a high consumption rate of the auxiliary system. Hence, the energy efficiency of the process decreases. Moreover, the load profile affects the energy recovered by the solar collector, the outlet temperature from the collector field, the solar top tank temperature and the solar fraction of the collective process. It was found that the parallel connection ensures enhanced solar fraction compared to the series configuration of the collectors.

The second study aimed to shed light on the effect of the collector's technology on the thermal yield of the collective process. Indeed, the collector's technology affects the amount of the incident energy on the solar collector, besides to the useful energy gained. Besides, the solar collectors derived from the same technology with a_0 coefficient slightly equal to 1 and with low values of a_1 and a_2 , ensure enhanced annual solar fractions of the collective process. Finally, the fact of using

a storage tank volume $V = 3000$ liters, connected to ETCs is a suitable choice for this process, because its solar fraction remains higher compared to the use of *FPCs*.

7. General conclusion and perspectives

7.1. General conclusion

This thesis aims to investigate the possibility to achieve a technological transfer of *SWHs* in Morocco, as well as to study the possibility of their adjustment and integration to the national market, taking into consideration the weather conditions and consumption habits of domestic hot water intrinsic to the Moroccan user.

Several studies have been conducted. First of all, we have suggested a new energy policy that we recommend as strategy intended to be integrated in Morocco in the first chapter entitled “*A synthesis on the technology transfer of solar water heaters and inclusion as solar energy policy in Morocco*”. In fact, the motivation that drove us to carry out this work is that *SWH* technologies are not widely known throughout Morocco, even if their energy and thermal efficiency remain better compared to other means which ensure the production of hot water using natural gas or electricity. Hence, we discussed *SWH* technologies transfer, adjustment and integration as energy policy in Morocco. To begin with, the global market of *SWH* besides to the global overview on their installed capacity in the world has been described. In addition, the world’s market growth of thermal collectors has been evaluated, and the general market overview with regard to their total installed capacity in the world has been reported. Moreover, the market situation of *SWH* in Morocco has been described according to socio-economic and energy context, while considering a set of parameters, such as the installation cost and the main local industrial actors, the current state of the market data, the installation cost and the main local industrial actors.

It is noted that, the amount of minimum, maximum and average values of the daily horizontal radiation have been assessed for 50 stations in Morocco, using Extraterrestrial solar radiation equations, to investigate the feasibility of using solar energy to integrate, adjust and generalize *SWH* technologies in Morocco. The achieved results were helpful, because they provided the available incident solar radiation values that could be used further as a guideline for other studies on installing solar equipment throughout Morocco. Thus, to assist the government to make a decision regarding the installation of more solar power plants such as solar water heaters as energy policy, which aims to promote the energetic efficiency of Morocco. Finally, we suggested several policy recommendations which aim to assist the transfer, adjustment and integration of *SWHs* in Morocco. We strongly encourage their implementation, so that the active actors composed of commercial and industrial sectors could become a lever in these technologies. Thus, we could achieve multiple socio-economic and environmental benefits.

Moreover, we presented a synthesis of several recent experimental and numerical studies that have been carried out on stratified storage tanks connected to thermosyphon or forced solar water heaters integrated in individual or collective green-buildings, throughout a review entitled “*Review on solar thermal stratified storage tanks: insight on stratification studies and efficiency indicators*”. It is well known that storing energy using sensitive and latent thermal techniques is important, because the produced solar thermal energy is not instantaneously consumed. Consequently, it is vital to size and design with accuracy hot water storage tanks in order to enhance their thermal yield and stability which are generally affected by various consumption patterns and hot water loading profiles applied by the consumers.

Furthermore, we studied the performance optimization of a two-phase closed thermosyphon through *CFD* numerical simulations. Indeed, the two-phase *VOF* and *Lee* models validations were

investigated. Thus, those numerical models were used to assess mass, energy transfer, as well as the overall efficiency of the thermosyphon. The models validation was reached from the experimental and numerical results available in the literature. The local temperature in two sections and their average temperatures were our validation indicators. In this model, the ascending vapor speed to the condenser and the velocity of the liquid film going down to the evaporator filled with the heated liquid pool were quantified. A numerical framework for analyzing two different configurations of the thermosyphon were conducted which are integrated into the internal exchanger of the vacuum tube solar collector panel. Indeed, two different geometries were numerically investigated mainly by the shape of the head of the condenser (the smooth condenser, and the condenser with fins). Moreover, a set of performance indicators were defined to assess the energy transfer velocity between the evaporator and the condenser sections (temperature contours, phase volume fraction, contours of vertical velocity, Nusselt number, heat transfer coefficient, mass transfer rate, the flux transferred by the condenser section and the efficiency of the thermosyphon). It was found that the efficiency of the closed thermosyphon was improved to 16.05%, to reach a new performance of 84.71% thanks to the tilted fins integrated on the lateral surface of the condenser section.

Further, we carried out a thermo-mechanical analysis of a horizontal thermal storage tank intended to store hot water for a domestic application, using the Finite Element Method (*FEM*) by combining the steady-state thermal analysis to the static structural analysis. Total Displacements, stresses and strains were simulated through a two dimensional axisymmetric 1-way thermo-mechanical coupling. Thermo-mechanical stress and various parameters which aim to optimize the lifespan of the tank were conducted under extreme temperature and pressure operating conditions, which were based on the strength Von-Mises failure code. The main conclusions to be drawn from this numerical simulation study could be presented as follow:

- The optimal configuration which avoid the appearance of the stress concentration zones and which distribute better the stress on the tank's shell is the configuration-(c), where the curvative radius $R_i = 11$ mm and $R_e = 14$ mm. This result has been achieved through conducting the first study;
- The material choice was investigated through the second study, in order to minimize the mechanical displacements of the tank's shell subjected to thermo-mechanical loads. The stainless steel presented a better mechanical strength compared to standard steel, aluminum alloy and copper alloy. It is noted that this second study has been performed taking into consideration the result of the first study;
- The mechanical displacement has been considered as indicator to select the optimized thickness of the storage tank's shell among five thicknesses. The optimal thickness that should be selected while manufacturing the tank's shell, which is subjected to the thermo-mechanical load have to be equal to $t = 2$ mm.

In addition, we paid a special attention to the sensitive energy storage of domestic hot water stored in a horizontal tank where heat pipes are integrated. Indeed, the thermal performance of a 300 liters capacity horizontal tank that initially stores hot water and which is subjected to a charging/discharging cycle was assessed through a set of performance indicators. Consequently,

the main purpose of this work is to suggest a new optimal design of the studied horizontal tank considered as the main device in individual solar *SWH* integrating *ETC* with heat pipes.

First of all, an experimental study was conducted to measure the evolution range of the temperature that the heat pipe integrated in the *ETC* could achieve using a thermal camera. On the basis of the experimental results, *CFD* simulations were performed on the horizontal storage tank to assess the effect of the heat pipe's number, integrated on its lateral internal shell, on its energetic performances (Discharging efficiency). In fact, four cases were studied according to the number of the used heat pipes (n), namely $n = 4$, $n = 6$, $n = 8$ and $n = 10$. Based on the above results and discussion, it was concluded that the *HTC* calculated for the heat pipe close to the outlet of the storage tank for $n = 6$ achieved 212.5 W/K.m^2 , while it is 300 W/K.m^2 for $n = 8$ and 230 W/K.m^2 for $n = 10$. Moreover, it was found that the values of *HTC* at the heat pipe located in the right next to the outlet of the tank are higher than those of the first heat pipe located near the cold water inlet, because the temperature difference ($T_{hp} - T_{\infty}$), recorded during the considered discharge cycle, was small. The average temperature of the horizontal tank is increased by the increase of the heat pipe's number because of rise in heat sources. Indeed, additional heat sources accelerate the heating of the charged cold water although the discharge cycle is applied. Otherwise, the discharging efficiency of the horizontal storage tank depends mainly on the instantaneous variation of the water's temperature assessed at the outlet nozzle of the tank ($T_o(t)$). Increasing the heat pipe's number disturbs the laminar structure of the flow field inside the horizontal tank, thus the outlet temperature of the hot loaded water is also affected and presents fluctuating trend.

We have also designed and worked on the thermal performance optimization of a forced collective solar hot water production system in Morocco for energy saving in residential buildings. In fact, we assessed the performance of a forced solar hot water collective system according to the Moroccan's weather conditions of Fez city. A realistic load profile was considered in this study to describe the hot water consumption profile. Four parametric studies were performed to design the collective solar hot water system and to ensure its optimization. Last but not least, a forced circulation system for hot water production was simulated from an energy performance point of view in order to meet a collective hot water production need for a social housing (case of an apartment block) based on the city of Fez, which is considered to be the climatic zone 3 in Morocco. Five typical hot water load profiles were used to assess the energy performance of this system. These profiles describe various trends in the consumption of hot water (loading time and the quantity loaded). Two main studies were carried out to assess the collective system overall efficiency. Several recommendations were drawn from the design and the parameter study to improve the potential of the solar collective systems in Fez city.

7.2. Perspectives

Among the perspectives considered in this thesis, we suggest carrying out a statistical study to assess the reliability of *SWHs* commercialized in the Moroccan market. We consider that this study is very interesting for *SOL'R SHEMSY* project, because it will provide additional answers to the major problem of adjusting and integrating *SWH* systems in Morocco. The major challenge of this study is to recover and build a database relating to the failure history of *SWHs* components, in order to use the Monte Carlo reliability model.

Secondly, we also suggest carrying out additional research on horizontal and vertical storage tanks to improve the performance indicators related to their thermal stratification and their energy storage efficiency. 3D *CFD* simulations will be performed, and hot/cold water injector geometries

will be tested, as well as several geometries of insulated storage tanks to decrease thermal losses. Moreover, we will attempt to study the feasibility of integrating *PCMs* in storage tanks using *CFD* numerical simulations, to improve the performance of *SWH* at night, because the performance of *ETC* is insufficient to provide the necessary energy to meet the requirements of the produced hot water.

Lust but not least, we plan to perform dynamic simulations using *TRNSYS software* to study the impact of using *SWHs* in various solar thermal applications, such as swimming pool water heating, traditional baths, hotels and restaurants etc. Hence, to conduct economic studies in order to evaluate the gain from solar thermal energy compared to the use of electric energy or natural gas. Besides, we attempt to conduct additional parametric studies on collective systems to optimize their overall yield, as the literature does not provide enough research investigations in the field.

References

- [1] B. Fadhil, L. C. Wrobel, H. Jouhara, Numerical modelling of the temperature distribution in a two-phase closed thermosyphon, *Applied Thermal Engineering* 60 (1-2) (2013) 122 – 131. doi:<http://dx.doi.org/10.1016/j.applthermaleng.2013.06.044>. URL <http://www.sciencedirect.com/science/article/pii/S1359431113004699>
- [2] A. Zachár, I. Farkas, F. Szlivka, Numerical analyses of the impact of plates for thermal stratification inside a storage tank with upper and lower inlet flows, *Solar Energy* 74 (4) (2003) 287 – 302. doi:[http://dx.doi.org/10.1016/S0038-092X\(03\)00188-9](http://dx.doi.org/10.1016/S0038-092X(03)00188-9). URL <http://www.sciencedirect.com/science/article/pii/S0038092X03001889>
- [3] F. Mauthner, W. Weiss, M. Spork Dur, Solar heat worldwide: Markets and contribution to the energy supply, IEA Solar Heating and Cooling Programme: <http://www.slideshare.net/UweTrenkner/worldwide2011-ed2013-lo-res> (2013).
- [4] Z. Yu, D. Gibbs, Encircling cities from rural areas? barriers to the diffusion of solar water heaters in china's urban market, *Energy Policy* 115 (2018) 366 – 373. doi:<https://doi.org/10.1016/j.enpol.2018.01.041>. URL <http://www.sciencedirect.com/science/article/pii/S0301421518300508>
- [5] S. Bahria, M. Amirat, A. Hamidat, M. E. Ganaoui, M. E. A. Slimani, Parametric study of solar heating and cooling systems in different climates of algeria – a comparison between conventional and high-energy-performance buildings, *Energy* 113 (2016) 521 – 535. doi:<https://doi.org/10.1016/j.energy.2016.07.022>. URL <http://www.sciencedirect.com/science/article/pii/S036054421630946X>
- [6] Institut de recherche en energie solaire et energies nouvelles(iresen). URL <http://www.iresen.org>
- [7] S. ed Dîn Fertahi, T. Bouhal, Y. Agrouaz, T. Kousksou, T. E. Rhafiki, Y. Zeraoui, Performance optimization of a two-phase closed thermosyphon through cfd numerical simulations, *Applied Thermal Engineering* 128 (2018) 551 – 563. doi:<https://doi.org/10.1016/j.applthermaleng.2017.09.049>. URL <http://www.sciencedirect.com/science/article/pii/S1359431117339558>
- [8] Y. El Mghouchi, T. Ajzoul, A. El Bouardi, Prediction of daily solar radiation intensity by day of the year in twenty-four cities of morocco, *Renewable and Sustainable Energy Reviews* 53 (2016) 823–831.
- [9] R. Tang, Y. Yang, Nocturnal reverse flow in water-in-glass evacuated tube solar water heaters, *Energy Conversion and Management* 80 (2014) 173 – 177. doi:<https://doi.org/10.1016/j.enconman.2014.01.025>. URL <http://www.sciencedirect.com/science/article/pii/S0196890414000697>
- [10] K. Çomaklı, U. Çakır, M. Kaya, K. Bakirci, The relation of collector and storage tank size in solar heating systems, *Energy Conversion and Management* 63 (2012) 112 – 117, 10th International Conference on Sustainable Energy Technologies (SET 2011). doi:<https://doi.org/10.1016/j.enconman.2012.01.031>. URL <http://www.sciencedirect.com/science/article/pii/S0196890412001112>
- [11] A. V. Novo, J. R. Bayon, D. Castro-Fresno, J. Rodriguez-Hernandez, Review of seasonal heat storage in large basins: Water tanks and gravel–water pits, *Applied Energy* 87 (2) (2010) 390 – 397. doi:<https://doi.org/10.1016/j.apenergy.2009.06.033>. URL <http://www.sciencedirect.com/science/article/pii/S0306261909002694>
- [12] Y. Li, G. Huang, T. Xu, X. Liu, H. Wu, Optimal design of pcm thermal storage tank and its application for winter available open-air swimming pool, *Applied Energy* 209 (2018) 224 – 235. doi:<https://doi.org/10.1016/j.apenergy.2017.10.095>. URL <http://www.sciencedirect.com/science/article/pii/S0306261917315313>
- [13] P.-L. Paradis, D. R. Rouse, L. Lamarche, H. Nesreddine, M.-H. Talbot, One-dimensional model of a stratified thermal storage tank with supercritical coiled heat exchanger, *Applied Thermal Engineering* 134 (2018) 379 – 395. doi:<https://doi.org/10.1016/j.applthermaleng.2018.02.015>. URL <http://www.sciencedirect.com/science/article/pii/S1359431117345544>
- [14] M. Arslan, A. A. Igci, Thermal performance of a vertical solar hot water storage tank with a mantle heat exchanger depending on the discharging operation parameters, *Solar Energy* 116 (2015) 184 – 204. doi:<https://doi.org/10.1016/j.solener.2015.03.045>. URL <http://www.sciencedirect.com/science/article/pii/S0038092X15001723>
- [15] M. R. Assari, H. B. Tabrizi, M. Savadkohy, Numerical and experimental study of inlet-outlet locations effect in horizontal storage tank of solar water heater, *Sustainable Energy Technologies and Assessments* 25 (2018) 181 – 190. doi:<https://doi.org/10.1016/j.seta.2017.12.009>. URL <http://www.sciencedirect.com/science/article/pii/S2213138817304320>
- [16] M. I. Hussain, G. H. Lee, Thermal performance evaluation of a conical solar water heater integrated with a thermal storage system, *Energy Conversion and Management* 87 (2014) 267 – 273. doi:<https://doi.org/10.1016/j.enconman.2014.01.025>

-
- 1016/j.enconman.2014.07.023.
URL <http://www.sciencedirect.com/science/article/pii/S0196890414006542>
- [17] Z. Wang, H. Zhang, B. Dou, H. Huang, G. Zhang, The thermal stratification characteristics affected by a novel equalizer in a dynamic hot water storage tank, *Applied Thermal Engineering* 126 (2017) 1006 – 1016. doi:<https://doi.org/10.1016/j.applthermaleng.2017.06.045>.
URL <http://www.sciencedirect.com/science/article/pii/S1359431116332902>
- [18] A. L. Nash, A. Badithela, N. Jain, Dynamic modeling of a sensible thermal energy storage tank with an immersed coil heat exchanger under three operation modes, *Applied Energy* 195 (2017) 877 – 889. doi:<https://doi.org/10.1016/j.apenergy.2017.03.092>.
URL <http://www.sciencedirect.com/science/article/pii/S0306261917303343>
- [19] G. Murali, K. Mayilsamy, Effect of latent thermal energy storage and inlet locations on enhancement of stratification in a solar water heater under discharging mode, *Applied Thermal Engineering* 106 (2016) 354 – 360. doi:<https://doi.org/10.1016/j.applthermaleng.2016.06.030>.
URL <http://www.sciencedirect.com/science/article/pii/S1359431116309334>
- [20] K. Osman, S. M. N. A. Khaireed, M. K. Ariffin, M. Y. Senawi, Dynamic modeling of stratification for chilled water storage tank, *Energy Conversion and Management* 49 (11) (2008) 3270 – 3273, special Issue 3rd International Conference on Thermal Engineering: Theory and Applications. doi:<https://doi.org/10.1016/j.enconman.2007.09.035>.
URL <http://www.sciencedirect.com/science/article/pii/S0196890408001696>
- [21] J. Dragsted, S. Furbo, M. Dannemand, F. Bava, Thermal stratification built up in hot water tank with different inlet stratifiers, *Solar Energy* 147 (2017) 414 – 425. doi:<https://doi.org/10.1016/j.solener.2017.03.008>.
URL <http://www.sciencedirect.com/science/article/pii/S0038092X1730169X>
- [22] N. Brown, F. Lai, Enhanced thermal stratification in a liquid storage tank with a porous manifold, *Solar Energy* 85 (7) (2011) 1409 – 1417. doi:<https://doi.org/10.1016/j.solener.2011.03.024>.
URL <http://www.sciencedirect.com/science/article/pii/S0038092X11001071>
- [23] E. Palacios, D. Admiraal, J. Marcos, M. Izquierdo, Experimental analysis of solar thermal storage in a water tank with open side inlets, *Applied Energy* 89 (1) (2012) 401 – 412, special issue on Thermal Energy Management in the Process Industries. doi:<https://doi.org/10.1016/j.apenergy.2011.08.001>.
URL <http://www.sciencedirect.com/science/article/pii/S030626191100496X>
- [24] S. Göppert, R. Lohse, T. Urbaneck, U. Schirmer, B. Platzler, P. Steinert, New computation method for stratification pipes of solar storage tanks, *Solar Energy* 83 (9) (2009) 1578 – 1587. doi:<https://doi.org/10.1016/j.solener.2009.05.007>.
URL <http://www.sciencedirect.com/science/article/pii/S0038092X09001170>
- [25] A. López-Navarro, J. Biosca-Taronger, J. Corberán, C. Peñalosa, A. Lázaro, P. Dolado, J. Payá, Performance characterization of a pcm storage tank, *Applied Energy* 119 (2014) 151 – 162. doi:<https://doi.org/10.1016/j.apenergy.2013.12.041>.
URL <http://www.sciencedirect.com/science/article/pii/S0306261913010404>
- [26] Y. Allouche, S. Varga, C. Bouden, A. C. Oliveira, Validation of a cfd model for the simulation of heat transfer in a tubes-in-tank pcm storage unit, *Renewable Energy* 89 (2016) 371 – 379. doi:<https://doi.org/10.1016/j.renene.2015.12.038>.
URL <http://www.sciencedirect.com/science/article/pii/S0960148115305401>
- [27] Z. Meng, P. Zhang, Experimental and numerical investigation of a tube-in-tank latent thermal energy storage unit using composite pcm, *Applied Energy* 190 (2017) 524 – 539. doi:<https://doi.org/10.1016/j.apenergy.2016.12.163>.
URL <http://www.sciencedirect.com/science/article/pii/S0306261916319432>
- [28] M. Y. Haller, C. A. Cruickshank, W. Streicher, S. J. Harrison, E. Andersen, S. Furbo, Methods to determine stratification efficiency of thermal energy storage processes – review and theoretical comparison, *Solar Energy* 83 (10) (2009) 1847 – 1860. doi:<https://doi.org/10.1016/j.solener.2009.06.019>.
URL <http://www.sciencedirect.com/science/article/pii/S0038092X09001546>
- [29] S. Ievers, W. Lin, Numerical simulation of three-dimensional flow dynamics in a hot water storage tank, *Applied Energy* 86 (12) (2009) 2604 – 2614. doi:<https://doi.org/10.1016/j.apenergy.2009.04.010>.
URL <http://www.sciencedirect.com/science/article/pii/S030626190900141X>
- [30] W. Yaïci, M. Ghorab, E. Entchev, S. Hayden, Three-dimensional unsteady cfd simulations of a thermal storage tank performance for optimum design, *Applied Thermal Engineering* 60 (1) (2013) 152 – 163. doi:<https://doi.org/10.1016/j.applthermaleng.2013.07.001>.
URL <http://www.sciencedirect.com/science/article/pii/S1359431113004894>

- [31] D. Erdemir, N. Altuntop, Improved thermal stratification with obstacles placed inside the vertical mantled hot water tanks, Applied Thermal Engineering 100 (2016) 20 – 29. doi:https://doi.org/10.1016/j.applthermaleng.2016.01.069.
URL <http://www.sciencedirect.com/science/article/pii/S1359431116300199>
- [32] E. García-Marí, M. Gasque, R. P. Gutiérrez-Colomer, F. Ibáñez, P. González-Altozano, A new inlet device that enhances thermal stratification during charging in a hot water storage tank, Applied Thermal Engineering 61 (2) (2013) 663 – 669. doi:https://doi.org/10.1016/j.applthermaleng.2013.08.023.
URL <http://www.sciencedirect.com/science/article/pii/S1359431113006042>
- [33] N. Altuntop, M. Arslan, V. Ozceyhan, M. Kanoglu, Effect of obstacles on thermal stratification in hot water storage tanks, Applied Thermal Engineering 25 (14) (2005) 2285 – 2298. doi:https://doi.org/10.1016/j.applthermaleng.2004.12.013.
URL <http://www.sciencedirect.com/science/article/pii/S1359431105000311>
- [34] A. Zachar, I. Farkas, F. Szlivka, Numerical analyses of the impact of plates for thermal stratification inside a storage tank with upper and lower inlet flows, Solar Energy 74 (4) (2003) 287–302.
- [35] T. Bouhal, S. Fertahi, Y. Agrouaz, T. E. Rhafiki, T. Kousksou, A. Jamil, Numerical modeling and optimization of thermal stratification in solar hot water storage tanks for domestic applications: Cfd study, Solar Energy 157 (2017) 441 – 455. doi:https://doi.org/10.1016/j.solener.2017.08.061.
URL <http://www.sciencedirect.com/science/article/pii/S0038092X17307429>
- [36] M. Gómez, J. Collazo, J. Porteiro, J. Míguez, Numerical study of the thermal behaviour of a water heater tank with a corrugated coil, International Journal of Heat and Mass Transfer 122 (2018) 574 – 586. doi:https://doi.org/10.1016/j.ijheatmasstransfer.2018.01.128.
URL <http://www.sciencedirect.com/science/article/pii/S001793101734663X>
- [37] A. Li, F. Cao, W. Zhang, B. Shi, H. Li, Effects of different thermal storage tank structures on temperature stratification and thermal efficiency during charging, Solar Energy 173 (2018) 882 – 892. doi:https://doi.org/10.1016/j.solener.2018.08.025.
URL <http://www.sciencedirect.com/science/article/pii/S0038092X18307941>
- [38] B. Kurşun, Thermal stratification enhancement in cylindrical and rectangular hot water tanks with truncated cone and pyramid shaped insulation geometry, Solar Energy 169 (2018) 512 – 525. doi:https://doi.org/10.1016/j.solener.2018.05.019.
URL <http://www.sciencedirect.com/science/article/pii/S0038092X18304523>
- [39] G. S. Kumar, D. Nagarajan, L. Chidambaram, V. Kumaresan, Y. Ding, R. Velraj, Role of pcm addition on stratification behaviour in a thermal storage tank – an experimental study, Energy 115 (2016) 1168 – 1178. doi:https://doi.org/10.1016/j.energy.2016.09.014.
URL <http://www.sciencedirect.com/science/article/pii/S0360544216312555>
- [40] Z. Wang, H. Zhang, B. Dou, H. Huang, W. Wu, Z. Wang, Experimental and numerical research of thermal stratification with a novel inlet in a dynamic hot water storage tank, Renewable Energy 111 (Supplement C) (2017) 353 – 371. doi:https://doi.org/10.1016/j.renene.2017.04.007.
URL <http://www.sciencedirect.com/science/article/pii/S0960148117303002>
- [41] A. Alizadehdakhl, M. Rahimi, A. A. Alsairafi, {CFD} modeling of flow and heat transfer in a thermosyphon, International Communications in Heat and Mass Transfer 37 (3) (2010) 312 – 318. doi:http://dx.doi.org/10.1016/j.icheatmasstransfer.2009.09.002.
URL <http://www.sciencedirect.com/science/article/pii/S0735193309002188>
- [42] S. ed Din Fertahi, T. Bouhal, A. Arid, T. Kousksou, A. Jamil, N. Moujibi, A. Benbassou, Thermo-mechanical strength analysis for energy storage improvement of horizontal storage tanks integrating evacuated tube collectors, International Journal of Hydrogen Energy 42 (49) (2017) 29370 – 29383. doi:https://doi.org/10.1016/j.ijhydene.2017.10.016.
URL <http://www.sciencedirect.com/science/article/pii/S0360319917339137>
- [43] Energypoles+, créateur d'énergies durables.
URL <http://energypoles.com/solaire-collectif-maroc/shemsy.html>
- [44] Transol.
URL <http://boutique.cstb.fr/fr/transol-3-0.html>
- [45] Ministère de l'énergie, des mines, de l'eau et de l'environnement, stratégie énergétique nationale, horizon 2030.
URL www.orientalinvest.ma
- [46] H. C. au Plan, Croissance économique et développement humain: éléments pour une planification stratégique 2007-2015-rapport (2007).
- [47] Flir systems, thermal imaging, night vision and infrared camera.

- URL <http://www.flir.fr/instruments/content>
- [48] J. Bracamonte, J. Parada, J. Dimas, M. Baritto, [Effect of the collector tilt angle on thermal efficiency and stratification of passive water in glass evacuated tube solar water heater](#), *Applied Energy* 155 (Supplement C) (2015) 648 – 659. doi:<https://doi.org/10.1016/j.apenergy.2015.06.008>.
URL <http://www.sciencedirect.com/science/article/pii/S0306261915007667>
- [49] G. Bourke, P. Bansal, [New test method for gas boosters with domestic solar water heaters](#), *Solar Energy* 86 (1) (2012) 78 – 86. doi:<http://dx.doi.org/10.1016/j.solener.2011.09.004>.
URL <http://www.sciencedirect.com/science/article/pii/S0038092X11003306>
- [50] T. Bouhal, Y. Agrouaz, A. Allouhi, T. Kousksou, A. Jamil, T. E. Rhafiki, Y. Zeraouli, [Impact of load profile and collector technology on the fractional savings of solar domestic water heaters under various climatic conditions](#), *International Journal of Hydrogen Energy* 42 (18) (2017) 13245 – 13258. doi:<https://doi.org/10.1016/j.ijhydene.2017.03.226>.
URL <http://www.sciencedirect.com/science/article/pii/S0360319917312776>
- [51] Y. Agrouaz, T. Bouhal, A. Allouhi, T. Kousksou, A. Jamil, Y. Zeraouli, [Energy and parametric analysis of solar absorption cooling systems in various moroccan climates](#), *Case Studies in Thermal Engineering* 9 (2017) 28 – 39. doi:<http://dx.doi.org/10.1016/j.csite.2016.11.002>.
URL <http://www.sciencedirect.com/science/article/pii/S2214157X16300454>
- [52] T. Bouhal, Y. Agrouaz, T. Kousksou, A. Allouhi, T. E. Rhafiki, A. Jamil, M. Bakkas, [Technical feasibility of a sustainable concentrated solar power in morocco through an energy analysis](#), *Renewable and Sustainable Energy Reviews* 81 (2018) 1087 – 1095. doi:<https://doi.org/10.1016/j.rser.2017.08.056>.
URL <http://www.sciencedirect.com/science/article/pii/S1364032117312017>
- [53] B. Brand, [Transmission topologies for the integration of renewable power into the electricity systems of north africa](#), *Energy Policy* 60 (2013) 155 – 166. doi:<http://dx.doi.org/10.1016/j.enpol.2013.04.071>.
URL <http://www.sciencedirect.com/science/article/pii/S0301421513003248>
- [54] C. Kost, M. Engelken, T. Schlegl, [Value generation of future csp projects in north africa](#), *Energy Policy* 46 (2012) 88 – 99. doi:<http://dx.doi.org/10.1016/j.enpol.2012.03.034>.
URL <http://www.sciencedirect.com/science/article/pii/S030142151200239X>
- [55] T. Bouhal, S. ed Din Fertahi, Y. Agrouaz, T. E. Rhafiki, Y. Zeraouli, A. Jamil, [Towards an energy efficiency optimization of solar horizontal storage tanks and circulation pipes integrating evacuated tube collectors through cfd parametric studies](#), *Sustainable Energy Technologies and Assessments* (2017). doi:<https://doi.org/10.1016/j.seta.2017.10.004>.
URL <http://www.sciencedirect.com/science/article/pii/S2213138817303909>
- [56] R. Chedid, F. Chaaban, [Renewable-energy developments in arab countries: a regional perspective](#), *Applied Energy* 74 (1) (2003) 211 – 220, *energex 2002 - New and Renewable Sources of Energy - Topic I*. doi:[https://doi.org/10.1016/S0306-2619\(02\)00148-4](https://doi.org/10.1016/S0306-2619(02)00148-4).
URL <http://www.sciencedirect.com/science/article/pii/S0306261902001484>
- [57] K. Damerou, K. Williges, A. G. Patt, P. Gauché, [Costs of reducing water use of concentrating solar power to sustainable levels: Scenarios for north africa](#), *Energy Policy* 39 (7) (2011) 4391 – 4398, special Section: Renewable energy policy and development. doi:<http://dx.doi.org/10.1016/j.enpol.2011.04.059>.
URL <http://www.sciencedirect.com/science/article/pii/S0301421511003429>
- [58] S. Griffiths, [A review and assessment of energy policy in the middle east and north africa region](#), *Energy Policy* 102 (Supplement C) (2017) 249 – 269. doi:<https://doi.org/10.1016/j.enpol.2016.12.023>.
URL <http://www.sciencedirect.com/science/article/pii/S0301421516306851>
- [59] A. Eberhard, K. Gratwick, E. Morella, P. Antmann, [Independent power projects in sub-saharan africa: Investment trends and policy lessons](#), *Energy Policy* 108 (2017) 390 – 424. doi:<http://dx.doi.org/10.1016/j.enpol.2017.05.023>.
URL <http://www.sciencedirect.com/science/article/pii/S0301421517303087>
- [60] F. Trieb, H. Müller-Steinhagen, J. Kern, [Financing concentrating solar power in the middle east and north africa—subsidy or investment?](#), *Energy Policy* 39 (1) (2011) 307 – 317. doi:<http://dx.doi.org/10.1016/j.enpol.2010.09.045>.
URL <http://www.sciencedirect.com/science/article/pii/S0301421510007317>
- [61] A. Nouri, M. A. Babram, E. Elwarraki, M. Enzili, [Moroccan wind farm potential feasibility. case study](#), *Energy Conversion and Management* 122 (2016) 39 – 51. doi:<https://doi.org/10.1016/j.enconman.2016.05.058>.
URL <http://www.sciencedirect.com/science/article/pii/S0196890416304368>
- [62] N. Belakhdar, M. Kharbach, M. Afilal, [The renewable energy plan in morocco, a divisia index approach](#), *Energy Strategy Reviews* 4 (2014) 11 – 15. doi:<https://doi.org/10.1016/j.esr.2014.06.001>.

- URL <http://www.sciencedirect.com/science/article/pii/S2211467X14000212>
- [63] A. Alhamwi, D. Kleinhans, S. Weitemeyer, T. Vogt, Moroccan national energy strategy reviewed from a meteorological perspective, *Energy Strategy Reviews* 6 (2015) 39 – 47. doi:<https://doi.org/10.1016/j.esr.2015.02.002>.
URL <http://www.sciencedirect.com/science/article/pii/S2211467X15000036>
- [64] A. Bennouna, C. E. Hebil, Energy needs for morocco 2030, as obtained from gdp-energy and gdp-energy intensity correlations, *Energy Policy* 88 (2016) 45 – 55. doi:<https://doi.org/10.1016/j.enpol.2015.10.003>.
URL <http://www.sciencedirect.com/science/article/pii/S0301421515301312>
- [65] A. Omri, Co2 emissions, energy consumption and economic growth nexus in mena countries: Evidence from simultaneous equations models, *Energy Economics* 40 (2013) 657 – 664. doi:<https://doi.org/10.1016/j.eneco.2013.09.003>.
URL <http://www.sciencedirect.com/science/article/pii/S0140988313001989>
- [66] S. ed Dîn Fertahi, T. Bouhal, F. Gargab, A. Jamil, T. Kousksou, A. Benbassou, Design and thermal performance optimization of a forced collective solar hot water production system in morocco for energy saving in residential buildings, *Solar Energy* 160 (2018) 260 – 274. doi:<https://doi.org/10.1016/j.solener.2017.12.015>.
URL <http://www.sciencedirect.com/science/article/pii/S0038092X17310873>
- [67] H. Dagdougui, A. Ouammi, M. Robba, R. Sacile, Thermal analysis and performance optimization of a solar water heater flat plate collector: Application to tétouan (morocco), *Renewable and Sustainable Energy Reviews* 15 (1) (2011) 630 – 638. doi:<https://doi.org/10.1016/j.rser.2010.09.010>.
URL <http://www.sciencedirect.com/science/article/pii/S1364032110002972>
- [68] K. Chang, W. Lin, T. Lee, K. Chung, Local market of solar water heaters in taiwan: Review and perspectives, *Renewable and Sustainable Energy Reviews* 13 (9) (2009) 2605 – 2612. doi:<https://doi.org/10.1016/j.rser.2009.01.031>.
URL <http://www.sciencedirect.com/science/article/pii/S1364032109000884>
- [69] R. Sellami, N. K. Merzouk, M. Amirat, R. Chekrouni, N. Ouhib, A. Hadji, Market potential and development prospects of the solar water heater field in algeria, *Renewable and Sustainable Energy Reviews* 65 (2016) 617 – 625. doi:<https://doi.org/10.1016/j.rser.2016.07.043>.
URL <http://www.sciencedirect.com/science/article/pii/S1364032116303744>
- [70] I. Ruble, P. E. Khoury, Lebanon's market for domestic solar water heaters: Achievements and barriers, *Energy for Sustainable Development* 17 (1) (2013) 54 – 61. doi:<https://doi.org/10.1016/j.esd.2012.11.004>.
URL <http://www.sciencedirect.com/science/article/pii/S0973082612000920>
- [71] C. Curry, J. A. Cherni, M. Mapako, The potential and reality of the solar water heater programme in south african townships: Lessons from the city of tshwane, *Energy Policy* 106 (2017) 75 – 84. doi:<https://doi.org/10.1016/j.enpol.2017.03.028>.
URL <http://www.sciencedirect.com/science/article/pii/S0301421517301726>
- [72] I. Allali, Promasol: Democratizing access to solar water-heaters, *Growing Inclusive Markets, Morocco* (2011).
- [73] Allali, b. (2011): Promasol : democratizingaccess to solar water-heaters : Gim initiative case study
URL <http://www.growinginclusivemarkets.org>
- [74] Haut-commissariat au plan (hcp), prospectives maroc 2030. quelle démographie?, 2015.
URL <http://www.hcp.ma/>
- [75] Ministère de l'économie et des finances, tableau de bord sectoriel, mai 2015.
URL www.finances.gov.ma
- [76] Exxon mobil, perspectives Énergétiques à l'horizon 2040, 2015.
URL <http://cdn.exxonmobil.com>
- [77] Ministère de l'énergie, des mines, de l'eau et de l'environnement, la nouvelle stratégie énergétique nationale, bilan d'étape, janvier 2013.
URL <http://www.mem.gov.ma>
- [78] Ministère de l'économie et des finances, direction des études et des prévisions financières quel positionnement régional pour le maroc en matière de compétitivité énergétique ?, 2015.
URL www.finances.gov.ma
- [79] Ministère de l'économie et des finances, projet de loi de finances pour l'année budgétaire 2015, rapport sur la compensation, 2015.
URL www.finances.gov.ma
- [80] A. Ouammi, D. Zejli, H. Dagdougui, R. Benchrif, Artificial neural network analysis of moroccan solar potential, *Renewable and Sustainable Energy Reviews* 16 (7) (2012) 4876–4889.

- [81] Haut-commissariat au plan (hcp), prospectives maroc 2030. prospective énergétique du maroc: Enjeux et défis, 2011.
URL <http://www.hcp.ma/>
- [82] A. laraki, Énergies solaire et nergies solaire au royaume du maroc, amisole.
URL <http://marokko.ahk.de/uploads/media/AMISOLE.pdf>
- [83] Ome report for gswh-unep-undp, solar thermal in the mediterranean region: Market assessment report, september 2012.
URL <http://www.solarthermalworld.org>
- [84] Ameer - agence marocaine pour l'efficacité énergétique.
URL www.amee.ma
- [85] A. Tsikalakis, T. Tomtsi, N. Hatziaargyriou, A. Poullikkas, C. Malamatenios, E. Giakoumelos, O. C. Jaouad, A. Chenak, A. Fayek, T. Matar, et al., Review of best practices of solar electricity resources applications in selected middle east and north africa (mena) countries, Renewable and sustainable energy reviews 15 (6) (2011) 2838–2849.
- [86] Sergun solar water heating systems co.
URL <http://www.buyfromturkey.net/BuyFromTurkey/www/CompanyDetails/CompanyProfile.aspx?CompanyID=45>
- [87] Batitherm rabat casablanca maroc - Énergie renouvelable, chauffe-eau solaires.
URL <http://batitherm.ma/>
- [88] " le solaire une energie propre et gratuite, profitez - en ! ".
URL <http://www.greentherm.ma/solarheat.html>
- [89] solar water heaters in morocco.
URL <http://www.adamcom.ma/telecommunication36>
- [90] Chaffoteaux votre partenaire, depuis toujours.
URL <http://www.chaffoteaux.ma/>
- [91] Imperial groupe.
URL <http://www.expertgroupe.com/details-energie-renouvelable-marrakech-maroc.php?id=393>
- [92] Chauffage solaire energie solaire groupes électrogènes (vente, location).
URL <http://www.pagesmaroc.com/groupe,electrogenes,vente,location-MARRAKECH-1011-Australinox.html>
- [93] T. Kousksou, A. Allouhi, M. Belattar, A. Jamil, T. E. Rhafiki, A. Arid, Y. Zeraoui, Renewable energy potential and national policy directions for sustainable development in morocco, Renewable and Sustainable Energy Reviews 47 (2015) 46 – 57. doi:<http://dx.doi.org/10.1016/j.rser.2015.02.056>.
URL <http://www.sciencedirect.com/science/article/pii/S1364032115001458>
- [94] A. Bajoub, A. Sánchez-Ortiz, E. A. Ajal, N. Ouazzani, A. Fernández-Gutiérrez, G. Beltrán, A. Carrasco-Pancorbo, First comprehensive characterization of volatile profile of north moroccan olive oils: A geographic discriminant approach, Food Research International 76 (2015) 410 – 417. doi:<https://doi.org/10.1016/j.foodres.2015.05.043>.
URL <http://www.sciencedirect.com/science/article/pii/S0963996915300302>
- [95] O. Nematollahi, K. C. Kim, A feasibility study of solar energy in south korea, Renewable and Sustainable Energy Reviews 77 (2017) 566 – 579. doi:<https://doi.org/10.1016/j.rser.2017.03.132>.
URL <http://www.sciencedirect.com/science/article/pii/S1364032117304665>
- [96] H. Nfaoui, A. Sayigh, Study of direct solar radiation in ouarazate (morocco), Sustainability in Energy and Buildings: Research Advances ISSN 2054-3743 (2) (2012) 36.
- [97] Y. Taheri, B. M. Ziapour, K. Alimardani, Study of an efficient compact solar water heater, Energy Conversion and Management 70 (2013) 187 – 193. doi:<https://doi.org/10.1016/j.enconman.2013.02.014>.
URL <http://www.sciencedirect.com/science/article/pii/S0196890413001052>
- [98] M. Rodríguez-Hidalgo, P. Rodríguez-Aumente, A. Lecuona, M. Legrand, R. Ventas, Domestic hot water consumption vs. solar thermal energy storage: The optimum size of the storage tank, Applied Energy 97 (2012) 897 – 906, energy Solutions for a Sustainable World - Proceedings of the Third International Conference on Applied Energy, May 16-18, 2011 - Perugia, Italy. doi:<https://doi.org/10.1016/j.apenergy.2011.12.088>.
URL <http://www.sciencedirect.com/science/article/pii/S0306261911008944>
- [99] J. Fan, S. Furbo, Thermal stratification in a hot water tank established by heat loss from the tank, Solar Energy 86 (11) (2012) 3460 – 3469. doi:<https://doi.org/10.1016/j.solener.2012.07.026>.
URL <http://www.sciencedirect.com/science/article/pii/S0038092X12002897>
- [100] T. Bouhal, S. ed Din Fertahi, Y. Agrouaz, T. E. Rhafiki, Y. Zeraoui, A. Jamil, Towards an energy effi-

- ciency optimization of solar horizontal storage tanks and circulation pipes integrating evacuated tube collectors through cfd parametric studies, *Sustainable Energy Technologies and Assessments* 26 (2018) 93 – 104. doi:<https://doi.org/10.1016/j.seta.2017.10.004>.
URL <http://www.sciencedirect.com/science/article/pii/S2213138817303909>
- [101] B. Fadhil, L. C. Wrobel, H. Jouhara, Cfd modelling of a two-phase closed thermosyphon charged with r134a and r404a, *Applied Thermal Engineering* 78 (2015) 482 – 490. doi:<https://doi.org/10.1016/j.applthermaleng.2014.12.062>.
URL <http://www.sciencedirect.com/science/article/pii/S1359431114011910>
- [102] J. A. Alfaro-Ayala, O. A. López-Núñez, F. Gómez-Castro, J. Ramírez-Minguela, A. Uribe-Ramírez, J. Belman-Flores, S. Cano-Andrade, Optimization of a solar collector with evacuated tubes using the simulated annealing and computational fluid dynamics, *Energy Conversion and Management* 166 (2018) 343 – 355. doi:<https://doi.org/10.1016/j.enconman.2018.04.039>.
URL <http://www.sciencedirect.com/science/article/pii/S0196890418303741>
- [103] A. Hafez, M. Kassem, O. Huzayyin, Smart adaptive model for dynamic simulation of horizontal thermally stratified storage tanks, *Energy* 142 (2018) 782 – 792. doi:<https://doi.org/10.1016/j.energy.2017.10.079>.
URL <http://www.sciencedirect.com/science/article/pii/S036054421731784X>
- [104] J. Cadafalch, D. Carbonell, R. Consul, R. Ruiz, Modelling of storage tanks with immersed heat exchangers, *Solar Energy* 112 (2015) 154 – 162. doi:<https://doi.org/10.1016/j.solener.2014.11.032>.
URL <http://www.sciencedirect.com/science/article/pii/S0038092X14005763>
- [105] K. Bataineh, A. Gharaibeh, Optimal design for sensible thermal energy storage tank using natural solid materials for a parabolic trough power plant, *Solar Energy* 171 (2018) 519 – 525. doi:<https://doi.org/10.1016/j.solener.2018.06.108>.
URL <http://www.sciencedirect.com/science/article/pii/S0038092X18306595>
- [106] A. Rout, S. S. Sahoo, S. Thomas, Risk modeling of domestic solar water heater using monte carlo simulation for east-coastal region of india, *Energy* 145 (2018) 548 – 556. doi:<https://doi.org/10.1016/j.energy.2018.01.018>.
URL <http://www.sciencedirect.com/science/article/pii/S0360544218300185>
- [107] T. Bouhal, S. ed Dîn Fertahi, Y. Agrouaz, T. E. Rhafiki, T. Kousksou, Y. Zeraouli, A. Jamil, Technical assessment, economic viability and investment risk analysis of solar heating/cooling systems in residential buildings in morocco, *Solar Energy* 170 (2018) 1043 – 1062. doi:<https://doi.org/10.1016/j.solener.2018.06.032>.
URL <http://www.sciencedirect.com/science/article/pii/S0038092X18305838>
- [108] M. Swiatek, G. Fraisse, M. Pailha, Stratification enhancement for an integrated collector storage solar water heater (icsswh), *Energy and Buildings* 106 (2015) 35 – 43, sl: IEA-ECES Annex 31 Special Issue on Thermal Energy Storage. doi:<https://doi.org/10.1016/j.enbuild.2015.07.005>.
URL <http://www.sciencedirect.com/science/article/pii/S0378778815301213>
- [109] I. González, C. D. Pérez-Segarra, O. Lehmkuhl, S. Torras, A. Oliva, Thermo-mechanical parametric analysis of packed-bed thermocline energy storage tanks, *Applied Energy* 179 (2016) 1106 – 1122. doi:<https://doi.org/10.1016/j.apenergy.2016.06.124>.
URL <http://www.sciencedirect.com/science/article/pii/S0306261916308996>
- [110] D. Romanchenko, J. Kensby, M. Odenberger, F. Johnsson, Thermal energy storage in district heating: Centralised storage vs. storage in thermal inertia of buildings, *Energy Conversion and Management* 162 (2018) 26 – 38. doi:<https://doi.org/10.1016/j.enconman.2018.01.068>.
URL <http://www.sciencedirect.com/science/article/pii/S0196890418300803>
- [111] A. Dehghan, A. Barzegar, Thermal performance behavior of a domestic hot water solar storage tank during consumption operation, *Energy Conversion and Management* 52 (1) (2011) 468 – 476. doi:<https://doi.org/10.1016/j.enconman.2010.06.075>.
URL <http://www.sciencedirect.com/science/article/pii/S019689041000316X>
- [112] M. Dadollahi, M. Mehrpooya, Modeling and investigation of high temperature phase change materials (pcm) in different storage tank configurations, *Journal of Cleaner Production* 161 (2017) 831 – 839. doi:<https://doi.org/10.1016/j.jclepro.2017.05.171>.
URL <http://www.sciencedirect.com/science/article/pii/S095965261731123X>
- [113] S. Lu, T. Zhang, Y. Chen, Study on the performance of heat storage and heat release of water storage tank with pcms, *Energy and Buildings* 158 (2018) 1770 – 1780. doi:<https://doi.org/10.1016/j.enbuild.2017.10.059>.
URL <http://www.sciencedirect.com/science/article/pii/S0378778817320339>
- [114] T. Bouhal, S. ed Dîn Fertahi, T. Kousksou, A. Jamil, Cfd thermal energy storage enhancement of pcm filling

-
- a cylindrical cavity equipped with submerged heating sources, *Journal of Energy Storage* 18 (2018) 360 – 370. doi:<https://doi.org/10.1016/j.est.2018.05.015>
URL <http://www.sciencedirect.com/science/article/pii/S2352152X18302147>
- [115] S. Y. Kee, Y. Munusamy, K. S. Ong, Review of solar water heaters incorporating solid-liquid organic phase change materials as thermal storage, *Applied Thermal Engineering* 131 (2018) 455 – 471. doi:<https://doi.org/10.1016/j.applthermaleng.2017.12.032>
URL <http://www.sciencedirect.com/science/article/pii/S1359431117347804>
- [116] S. Tarhan, A. Sari, M. H. Yardim, Temperature distributions in trapezoidal built in storage solar water heaters with/without phase change materials, *Energy Conversion and Management* 47 (15) (2006) 2143 – 2154. doi:<https://doi.org/10.1016/j.enconman.2005.12.002>
URL <http://www.sciencedirect.com/science/article/pii/S0196890405003353>
- [117] M. Abdelsalam, P. Sarafraz, J. Cotton, M. Lightstone, Heat transfer characteristics of a hybrid thermal energy storage tank with phase change materials (pcms) during indirect charging using isothermal coil heat exchanger, *Solar Energy* 157 (2017) 462 – 476. doi:<https://doi.org/10.1016/j.solener.2017.08.043>
URL <http://www.sciencedirect.com/science/article/pii/S0038092X17307223>
- [118] N. Ghaddar, A. Al-Marafie, A. Al-Kandari, Numerical simulation of stratification behaviour in thermal storage tanks, *Applied Energy* 32 (3) (1989) 225 – 239. doi:[https://doi.org/10.1016/0306-2619\(89\)90031-7](https://doi.org/10.1016/0306-2619(89)90031-7)
URL <http://www.sciencedirect.com/science/article/pii/0306261989900317>
- [119] P. Steinert, S. Göppert, B. Platzer, Transient calculation of charge and discharge cycles in thermally stratified energy storages, *Solar Energy* 97 (2013) 505 – 516. doi:<https://doi.org/10.1016/j.solener.2013.08.039>
URL <http://www.sciencedirect.com/science/article/pii/S0038092X13003496>
- [120] M. R. Assari, H. B. Tabrizi, M. J. Movahedi, Experimental study on destruction of thermal stratification tank in solar collector performance, *Journal of Energy Storage* 15 (2018) 124 – 132. doi:<https://doi.org/10.1016/j.est.2017.11.004>
URL <http://www.sciencedirect.com/science/article/pii/S2352152X17302517>
- [121] M. Y. Haller, E. Yazdanshenas, E. Andersen, C. Bales, W. Streicher, S. Furbo, A method to determine stratification efficiency of thermal energy storage processes independently from storage heat losses, *Solar Energy* 84 (6) (2010) 997 – 1007. doi:<https://doi.org/10.1016/j.solener.2010.03.009>
URL <http://www.sciencedirect.com/science/article/pii/S0038092X10001131>
- [122] U. Jordan, S. Furbo, Thermal stratification in small solar domestic storage tanks caused by draw-offs, *Solar Energy* 78 (2) (2005) 291 – 300, iSES Solar World Congress 2003. doi:<https://doi.org/10.1016/j.solener.2004.09.011>
URL <http://www.sciencedirect.com/science/article/pii/S0038092X04002841>
- [123] R. Gupta, G. Tiwari, A. Kumar, Y. Gupta, Calculation of total solar fraction for different orientation of greenhouse using 3d-shadow analysis in auto-cad, *Energy and Buildings* 47 (2012) 27 – 34. doi:<https://doi.org/10.1016/j.enbuild.2011.11.010>
URL <http://www.sciencedirect.com/science/article/pii/S0378778811005536>
- [124] S. Alizadeh, An experimental and numerical study of thermal stratification in a horizontal cylindrical solar storage tank, *Solar Energy* 66 (6) (1999) 409 – 421. doi:[https://doi.org/10.1016/S0038-092X\(99\)00036-5](https://doi.org/10.1016/S0038-092X(99)00036-5)
URL <http://www.sciencedirect.com/science/article/pii/S0038092X99000365>
- [125] Z. Ouyang, D. Li, Design of segmented high-performance thermoelectric generators with cost in consideration, *Applied Energy* 221 (2018) 112 – 121. doi:<https://doi.org/10.1016/j.apenergy.2018.03.106>
URL <http://www.sciencedirect.com/science/article/pii/S0306261918304446>
- [126] W. Yaïci, M. Ghorab, E. Entchev, 3d cfd study of the effect of inlet air flow maldistribution on plate-fin-tube heat exchanger design and thermal-hydraulic performance, *International Journal of Heat and Mass Transfer* 101 (2016) 527 – 541. doi:<https://doi.org/10.1016/j.ijheatmasstransfer.2016.05.063>
URL <http://www.sciencedirect.com/science/article/pii/S0017931016303544>
- [127] S. Pal, M. Phaniraj, Determination of heat partition between tool and workpiece during fsw of ss304 using 3d cfd modeling, *Journal of Materials Processing Technology* 222 (2015) 280 – 286. doi:<https://doi.org/10.1016/j.jmatprotec.2015.03.015>
URL <http://www.sciencedirect.com/science/article/pii/S0924013615001181>
- [128] G. Lomonaco, W. Borreani, M. Bruzzone, D. Chersola, G. Firpo, M. Osipenko, M. Palmero, F. Panza, M. Ripani, P. Saracco, C. M. Viberti, Initial thermal-hydraulic assessment by openfoam and fluent of a subcritical irradiation facility, *Thermal Science and Engineering Progress* 6 (2018) 447 – 456. doi:<https://doi.org/10.1016/j.tsep.2018.03.003>
URL <http://www.sciencedirect.com/science/article/pii/S2451904917303013>

- [129] T. Höhne, S. Kliem, U. Bieder, [Iaea crp benchmark of rocom pts test case for the use of cfd in reactor design using the cfd-codes ansys cfx and triocfd](#), Nuclear Engineering and Design 333 (2018) 161 – 180. doi:<https://doi.org/10.1016/j.nucengdes.2018.04.017>. URL <http://www.sciencedirect.com/science/article/pii/S0029549318304527>
- [130] S. Kumar, R. Grover, H. Yadav, P. Vijayan, U. Kannan, A. Agrawal, [Experimental and numerical investigation on suppression of thermal stratification in a water-pool: Piv measurements and cfd simulations](#), Applied Thermal Engineering 138 (2018) 686 – 704. doi:<https://doi.org/10.1016/j.applthermaleng.2018.04.070>. URL <http://www.sciencedirect.com/science/article/pii/S1359431117375816>
- [131] B. Kırşun, K. Ökten, [Effect of rectangular hot water tank position and aspect ratio on thermal stratification enhancement](#), Renewable Energy 116 (Part A) (2018) 639 – 646. doi:<https://doi.org/10.1016/j.renene.2017.10.013>. URL <http://www.sciencedirect.com/science/article/pii/S0960148117309746>
- [132] I. J. Moncho-Esteve, M. Gasque, P. González-Altozano, G. Palau-Salvador, [Simple inlet devices and their influence on thermal stratification in a hot water storage tank](#), Energy and Buildings 150 (Supplement C) (2017) 625 – 638. doi:<https://doi.org/10.1016/j.enbuild.2017.06.012>. URL <http://www.sciencedirect.com/science/article/pii/S0378778816320667>
- [133] T. Bouhal, O. Rajad, T. Kousksou, A. Arid, T. El Rhafiki, A. Jamil, A. Benbassou, et al., [Cfd performance enhancement of a low cut-in speed current vertical tidal turbine through the nested hybridization of savonius and darrius](#), Energy Conversion and Management 169 (2018) 266–278.
- [134] S. ed Dîn Fertahi, T. Bouhal, T. Kousksou, A. Jamil, A. Benbassou, [Experimental study and cfd thermal assessment of horizontal hot water storage tank integrating evacuated tube collectors with heat pipes](#), Solar Energy 170 (2018) 234 – 251. doi:<https://doi.org/10.1016/j.solener.2018.05.062>. URL <http://www.sciencedirect.com/science/article/pii/S0038092X1830495X>
- [135] I. Toliás, S. Giannissi, A. Venetsanos, J. Keenan, V. Shentsov, D. Makarov, S. Coldrick, A. Kotchourko, K. Ren, O. Jedicke, D. Melideo, D. Baraldi, S. Slater, A. Duclos, F. Verbecke, V. Molkov, [Best practice guidelines in numerical simulations and cfd benchmarking for hydrogen safety applications](#), International Journal of Hydrogen Energy (2018). doi:<https://doi.org/10.1016/j.ijhydene.2018.06.005>. URL <http://www.sciencedirect.com/science/article/pii/S0360319918317853>
- [136] F. Afshari, H. G. Zavaragh, B. Sahin, R. C. Grifoni, F. Corvaro, B. Marchetti, F. Polonara, [On numerical methods; optimization of cfd solution to evaluate fluid flow around a sample object at low re numbers](#), Mathematics and Computers in Simulation 152 (2018) 51 – 68. doi:<https://doi.org/10.1016/j.matcom.2018.04.004>. URL <http://www.sciencedirect.com/science/article/pii/S0378475418300909>
- [137] M. F. El-Amin, A. Al-Ghamdi, [Experiments and numerical simulation for a thermal vertical jet into a rectangular water tank](#), Results in Physics 10 (2018) 680 – 692. doi:<https://doi.org/10.1016/j.rinp.2018.07.016>. URL <http://www.sciencedirect.com/science/article/pii/S221137971731361X>
- [138] J. Davidson, D. Adams, J. Miller, [A coefficient to characterize mixing in solar water storage tanks](#), Journal of Solar Energy Engineering 116 (2) (1994) 94–99.
- [139] A. Chan, P. Smereka, D. Giusti, [A numerical study of transient mixed convection flows in a thermal storage tank](#), Journal of Solar Energy Engineering 105 (3) (1983) 246–253.
- [140] J. Fernández-Seara, F. J. Uhl'á, J. Sieres, [Experimental analysis of a domestic electric hot water storage tank. part ii: dynamic mode of operation](#), Applied Thermal Engineering 27 (1) (2007) 137 – 144. doi:<https://doi.org/10.1016/j.applthermaleng.2006.05.004>. URL <http://www.sciencedirect.com/science/article/pii/S1359431106001700>
- [141] E. Andersen, S. Furbo, J. Fan, [Multilayer fabric stratification pipes for solar tanks](#), Solar Energy 81 (10) (2007) 1219 – 1226. doi:<https://doi.org/10.1016/j.solener.2007.01.008>. URL <http://www.sciencedirect.com/science/article/pii/S0038092X07000175>
- [142] A. Tinaikar, S. Advaita, U. K. Chetia, K. Manu, S. Basu, [Spatio-temporal disruption of thermocline by successive laminar vortex pairs in a single tank thermal energy storage](#), Applied Thermal Engineering 109 (2016) 924 – 935, special Issue: Solar Energy Research Institute for India and the United States (SERIUS) – Concentrated Solar Power. doi:<https://doi.org/10.1016/j.applthermaleng.2016.04.105>. URL <http://www.sciencedirect.com/science/article/pii/S1359431116305932>
- [143] Y. H. Zurigat, P. R. Liche, A. J. Ghajar, [Influence of inlet geometry on mixing in thermocline thermal energy storage](#), International Journal of Heat and Mass Transfer 34 (1) (1991) 115–125.
- [144] A. J. Ghajar, Y. H. Zurigat, [Numerical study of the effect of inlet geometry on stratification in thermal energy storage](#), Numerical Heat Transfer 19 (1) (1991) 65–83.
- [145] J. van Berkel, C. C. Rindt, A. A. van Steenhoven, [Modelling of two-layer stratified stores](#), Solar Energy 67 (1-3)

- (1999) 65–78.
- [146] N. Brown, F. Lai, Experimental study of stratification in a liquid storage tank with a porous manifold, in: ASME 2004 Heat Transfer/Fluids Engineering Summer Conference, American Society of Mechanical Engineers, 2004, pp. 21–28.
- [147] E. Oró, A. Castell, J. Chiu, V. Martin, L. F. Cabeza, Stratification analysis in packed bed thermal energy storage systems, Applied Energy 109 (2013) 476 – 487. doi:https://doi.org/10.1016/j.apenergy.2012.12.082.
URL <http://www.sciencedirect.com/science/article/pii/S0306261913000214>
- [148] A. Ramana, R. Venkatesh, V. A. A. Raj, R. Velraj, Experimental investigation of the lhs system and comparison of the stratification performance with the shs system using cfd simulation, Solar Energy 103 (2014) 378 – 389. doi:https://doi.org/10.1016/j.solener.2014.02.009.
URL <http://www.sciencedirect.com/science/article/pii/S0038092X14000863>
- [149] E. Hahne, Y. Chen, Numerical study of flow and heat transfer characteristics in hot water stores, Solar Energy 64 (1) (1998) 9 – 18. doi:https://doi.org/10.1016/S0038-092X(98)00051-6.
URL <http://www.sciencedirect.com/science/article/pii/S0038092X98000516>
- [150] G. Rosengarten, G. Morrison, M. Behnia, A second law approach to characterising thermally stratified hot water storage with application to solar water heaters, Journal of solar energy engineering 121 (4) (1999) 194–200.
- [151] J. Osorio, A. Rivera-Alvarez, M. Swain, J. Ordonez, Exergy analysis of discharging multi-tank thermal energy storage systems with constant heat extraction, Applied Energy 154 (2015) 333 – 343. doi:https://doi.org/10.1016/j.apenergy.2015.05.018.
URL <http://www.sciencedirect.com/science/article/pii/S0306261915006285>
- [152] E. Mathioulakis, V. Belessiotis, A new heat-pipe type solar domestic hot water system, Solar Energy 72 (1) (2002) 13 – 20. doi:http://dx.doi.org/10.1016/S0038-092X(01)00088-3.
URL <http://www.sciencedirect.com/science/article/pii/S0038092X01000883>
- [153] Z. Zhao, C. Avedisian, Enhancing forced air convection heat transfer from an array of parallel plate fins using a heat pipe, International journal of heat and mass transfer 40 (13) (1997) 3135–3147.
- [154] H. Jouhara, R. Meskimmon, Experimental investigation of wraparound loop heat pipe heat exchanger used in energy efficient air handling units, Energy 35 (12) (2010) 4592 – 4599, the 3rd International Conference on Sustainable Energy and Environmental Protection, {SEEP} 2009. doi:http://dx.doi.org/10.1016/j.energy.2010.03.056.
URL <http://www.sciencedirect.com/science/article/pii/S0360544210001854>
- [155] K. Kerrigan, H. Jouhara, G. O'Donnell, A. Robinson, Heat pipe-based radiator for low grade geothermal energy conversion in domestic space heating, Simulation Modelling Practice and Theory 19 (4) (2011) 1154 – 1163, sustainable Energy and Environmental Protection “SEEP2009”. doi:http://dx.doi.org/10.1016/j.simpat.2010.05.020.
URL <http://www.sciencedirect.com/science/article/pii/S1569190X10001218>
- [156] A. Faghri, Heat pipe science and technology, Global Digital Press, 1995.
- [157] N. Z. Aung, S. Li, Numerical investigation on effect of riser diameter and inclination on system parameters in a two-phase closed loop thermosyphon solar water heater, Energy Conversion and Management 75 (2013) 25 – 35. doi:http://dx.doi.org/10.1016/j.enconman.2013.06.001.
URL <http://www.sciencedirect.com/science/article/pii/S0196890413002975>
- [158] H. Shabgard, M. J. Allen, N. Sharifi, S. P. Benn, A. Faghri, T. L. Bergman, Heat pipe heat exchangers and heat sinks: Opportunities, challenges, applications, analysis, and state of the art, International Journal of Heat and Mass Transfer 89 (2015) 138 – 158. doi:http://dx.doi.org/10.1016/j.ijheatmasstransfer.2015.05.020.
URL <http://www.sciencedirect.com/science/article/pii/S0017931015005037>
- [159] K. Shah, C. McKee, D. Chalise, A. Jain, Experimental and numerical investigation of core cooling of li-ion cells using heat pipes, Energy 113 (2016) 852 – 860. doi:http://dx.doi.org/10.1016/j.energy.2016.07.076.
URL <http://www.sciencedirect.com/science/article/pii/S0360544216310003>
- [160] J. Danielewicz, B. Śniechowska, M. Sayegh, N. Fidorów, H. Jouhara, Three-dimensional numerical model of heat losses from district heating network pre-insulated pipes buried in the ground, Energy 108 (2016) 172 – 184, sustainable Energy and Environmental Protection 2014. doi:http://dx.doi.org/10.1016/j.energy.2015.07.012.
URL <http://www.sciencedirect.com/science/article/pii/S0360544215009068>
- [161] L. M. Poplaski, A. Faghri, T. L. Bergman, Analysis of internal and external thermal resistances of heat pipes including fins using a three-dimensional numerical simulation, International Journal of Heat and Mass Transfer

- 102 (2016) 455 – 469. doi:<http://dx.doi.org/10.1016/j.ijheatmasstransfer.2016.05.116>.
URL <http://www.sciencedirect.com/science/article/pii/S0017931016302940>
- [162] R. Ranjan, J. Y. Murthy, S. V. Garimella, U. Vadakkan, [A numerical model for transport in flat heat pipes considering wick microstructure effects](#), International Journal of Heat and Mass Transfer 54 (1–3) (2011) 153 – 168. doi:<http://dx.doi.org/10.1016/j.ijheatmasstransfer.2010.09.057>.
URL <http://www.sciencedirect.com/science/article/pii/S0017931010005521>
- [163] R. Nair, C. Balaji, [Synergistic analysis of heat transfer characteristics of an internally finned two phase closed thermosyphon](#), Applied Thermal Engineering 101 (2016) 720 – 729. doi:<http://dx.doi.org/10.1016/j.applthermaleng.2016.01.084>.
URL <http://www.sciencedirect.com/science/article/pii/S1359431116300345>
- [164] M. Schreiber, W. W. Wits, G. J. te Riele, [Numerical and experimental investigation of a counter-current two-phase thermosyphon with cascading pools](#), Applied Thermal Engineering 99 (2016) 133 – 146. doi:<http://dx.doi.org/10.1016/j.applthermaleng.2015.12.095>.
URL <http://www.sciencedirect.com/science/article/pii/S1359431115014982>
- [165] Z. Tong, X.-H. Liu, Z. Li, Y. Jiang, [Experimental study on the effect of fill ratio on an {R744} two-phase thermosyphon loop](#), Applied Thermal Engineering 99 (2016) 302 – 312. doi:<http://dx.doi.org/10.1016/j.applthermaleng.2016.01.065>.
URL <http://www.sciencedirect.com/science/article/pii/S1359431116300151>
- [166] P. Zhang, B. Wang, W. Shi, L. Han, X. Li, [Modeling and performance analysis of a two-phase thermosyphon loop with partially/fully liquid-filled downcomer](#), International Journal of Refrigeration 58 (2015) 172 – 185. doi:<http://dx.doi.org/10.1016/j.ijrefrig.2015.06.014>.
URL <http://www.sciencedirect.com/science/article/pii/S0140700715001826>
- [167] E. Gedik, [Experimental investigation of the thermal performance of a two-phase closed thermosyphon at different operating conditions](#), Energy and Buildings 127 (2016) 1096 – 1107. doi:<http://dx.doi.org/10.1016/j.enbuild.2016.06.066>.
URL <http://www.sciencedirect.com/science/article/pii/S0378778816305552>
- [168] F. Jiang, Y. Tan, G. peng Qi, W. jing Chen, X. yu Han, X. lun Li, [Heat transfer enhancement in a closed thermosyphon with thermally conductive pa6/water](#), Applied Thermal Engineering 101 (2016) 322 – 329. doi:<http://dx.doi.org/10.1016/j.applthermaleng.2016.02.053>.
URL <http://www.sciencedirect.com/science/article/pii/S135943111630196X>
- [169] K. Kafel, A. Turan, [Simulation of the response of a thermosyphon under pulsed heat input conditions](#), International Journal of Thermal Sciences 80 (2014) 33 – 40. doi:<http://dx.doi.org/10.1016/j.ijthermalsci.2014.01.020>.
URL <http://www.sciencedirect.com/science/article/pii/S1290072914000234>
- [170] H. Jouhara, B. Fadhl, L. C. Wrobel, [Three-dimensional cfd simulation of geyser boiling in a two-phase closed thermosyphon](#), International Journal of Hydrogen Energy 41 (37) (2016) 16463 – 16476, special Issue: Hydrogen and Fuel Cell Developments: A special issue on the 8th International Conference on Sustainable Energy and Environmental Protection (SEEP 2015), 11–14 August 2015, Paisley, Scotland, {UK}. doi:<http://dx.doi.org/10.1016/j.ijhydene.2016.02.038>.
URL <http://www.sciencedirect.com/science/article/pii/S0360319915319170>
- [171] C. Hirt, B. Nichols, [Volume of fluid \(vof\) method for the dynamics of free boundaries](#), Journal of Computational Physics 39 (1) (1981) 201 – 225. doi:[http://dx.doi.org/10.1016/0021-9991\(81\)90145-5](http://dx.doi.org/10.1016/0021-9991(81)90145-5).
URL <http://www.sciencedirect.com/science/article/pii/0021999181901455>
- [172] W. Lee, A pressure iteration scheme for two-phase flow modeling (technical paper no. la-ur-79-975), Los Alamos, New Mexico, USA: Los Alamos National Laboratory (1979).
- [173] Z. Liu, Y. Li, Y. Jin, [Pressurization performance and temperature stratification in cryogenic final stage propellant tank](#), Applied Thermal Engineering 106 (2016) 211 – 220. doi:<http://dx.doi.org/10.1016/j.applthermaleng.2016.05.195>.
URL <http://www.sciencedirect.com/science/article/pii/S1359431116308845>
- [174] J. Brackbill, D. B. Kothe, C. Zemach, A continuum method for modeling surface tension, Journal of computational physics 100 (2) (1992) 335–354.
- [175] J. Taylor, Introduction to error analysis, the study of uncertainties in physical measurements, 1997.
- [176] R. W. MacGregor, P. A. Kew, D. A. Reay, Investigation of low global warming potential working fluids for a closed two-phase thermosyphon, Applied Thermal Engineering 51 (1) (2013) 917–925.
- [177] F. ED-DIN, Simulation et optimisation des systemes de production d'eau chaude sanitaire solaire (bourse ireden)'co-tutelle de these avec univ. de pau (2016).

- [178] S. Fertahi, T. Bouhal, Y. Agrouaz, T. Kousksou, T. E. Rhafiki, Y. Zeraouli, [Performance optimization of a two-phase closed thermosyphon through cfd numerical simulations](#), *Applied Thermal Engineering* (2017). doi:<https://doi.org/10.1016/j.applthermaleng.2017.09.049>. URL <http://www.sciencedirect.com/science/article/pii/S1359431117339558>
- [179] T. Kousksou, A. Allouhi, M. Belattar, A. Jamil, T. El Rhafiki, A. Arid, Y. Zeraouli, Renewable energy potential and national policy directions for sustainable development in morocco, *Renewable and Sustainable Energy Reviews* 47 (2015) 46–57.
- [180] O. B. Isgor, A. G. Razaqpur, Modelling steel corrosion in concrete structures, *Materials and Structures* 39 (3) (2006) 291–302.
- [181] F. Auricchio, L. Petrini, A three-dimensional model describing stress-temperature induced solid phase transformations: thermomechanical coupling and hybrid composite applications, *International Journal for Numerical Methods in Engineering* 61 (5) (2004) 716–737.
- [182] J. Aboudi, Y. Freed, Two-way thermomechanically coupled micromechanical analysis of shape memory alloy composites, *Journal of Mechanics of Materials and Structures* 1 (5) (2006) 937–955.
- [183] D. Christ, S. Reese, A finite element model for shape memory alloys considering thermomechanical couplings at large strains, *International Journal of Solids and Structures* 46 (20) (2009) 3694–3709.
- [184] B. Yavari, W. Tworzydło, J. Bass, A thermomechanical model to predict the temperature distribution of steady state rolling tires, *Tire Science and Technology* 21 (3) (1993) 163–178.
- [185] Q. Liu, P. Zhang, S. Cheng, J. Niu, D. Liu, [Heat transfer and thermo-elastic analysis of copper steel composite stove](#), *International Journal of Heat and Mass Transfer* 103 (2016) 341 – 348. doi:<http://dx.doi.org/10.1016/j.ijheatmasstransfer.2016.05.100>. URL <http://www.sciencedirect.com/science/article/pii/S0017931015318032>
- [186] D.-S. Huang, F.-C. Huang, [Coupled thermo-fluid stress analysis of kambara reactor with various anchors in the stirring of molten iron at extremely high temperatures](#), *Applied Thermal Engineering* 73 (1) (2014) 222 – 228. doi:<http://dx.doi.org/10.1016/j.applthermaleng.2014.07.042>. URL <http://www.sciencedirect.com/science/article/pii/S1359431114006188>
- [187] M. Žmindák, P. Novák, V. Dekýš, Z. Pelagić, [Finite element thermo-mechanical transient analysis of concrete structure](#), *Procedia Engineering* 65 (2013) 224 – 229. doi:<http://dx.doi.org/10.1016/j.proeng.2013.09.034>. URL <http://www.sciencedirect.com/science/article/pii/S1877705813015415>
- [188] Y. Li, C. Wang, R. Wang, [The thermal stress analysis and structure optimum of neck tube with vertical cryogenic insulated cylinders based on {ANSYS}](#), *Nuclear Engineering and Design* 252 (2012) 144 – 152. doi:<http://dx.doi.org/10.1016/j.nucengdes.2012.05.042>. URL <http://www.sciencedirect.com/science/article/pii/S0029549312003184>
- [189] L. Galantucci, L. Tricarico, [Thermo-mechanical simulation of a rolling process with an {FEM} approach](#), *Journal of Materials Processing Technology* 92–93 (1999) 494 – 501. doi:[http://dx.doi.org/10.1016/S0924-0136\(99\)00242-3](http://dx.doi.org/10.1016/S0924-0136(99)00242-3). URL <http://www.sciencedirect.com/science/article/pii/S0924013699002423>
- [190] D. Riedlbauer, M. Drexler, D. Drummer, P. Steinmann, J. Mergheim, [Modelling, simulation and experimental validation of heat transfer in selective laser melting of the polymeric material {PA12}](#), *Computational Materials Science* 93 (2014) 239 – 248. doi:<http://dx.doi.org/10.1016/j.commatsci.2014.06.046>. URL <http://www.sciencedirect.com/science/article/pii/S0927025614004571>
- [191] A. Belhocine, M. Bouchetara, Simulation of fully coupled thermo mechanical analysis of disc brake rotor, *Wseas Transactions on Applied and Theoretical Mechanics* 7 (3) (2012).
- [192] J. A. Shaw, [Simulations of localized thermo-mechanical behavior in a niti shape memory alloy](#), *International Journal of Plasticity* 16 (5) (2000) 541 – 562. doi:[http://dx.doi.org/10.1016/S0749-6419\(99\)00075-3](http://dx.doi.org/10.1016/S0749-6419(99)00075-3). URL <http://www.sciencedirect.com/science/article/pii/S0749641999000753>
- [193] A. Souahlia, H. Dhaou, S. Mellouli, F. Askri, A. Jemni, S. B. Nasrallah, [Experimental study of metal hydride-based hydrogen storage tank at constant supply pressure](#), *International Journal of Hydrogen Energy* 39 (14) (2014) 7365 – 7372. doi:<https://doi.org/10.1016/j.ijhydene.2014.02.121>. URL <http://www.sciencedirect.com/science/article/pii/S0360319914005199>
- [194] Y. Yan, Y. Yan, Y. He, J. Li, Y. Su, L. Qiao, [Hydrogen-induced cracking and service safety evaluation for precipitation strengthened austenitic stainless steel as hydrogen storage tank](#), *International Journal of Hydrogen Energy* 39 (31) (2014) 17921 – 17928. doi:<https://doi.org/10.1016/j.ijhydene.2014.08.143>. URL <http://www.sciencedirect.com/science/article/pii/S0360319914024847>
- [195] T. Hua, R. Ahluwalia, J.-K. Peng, M. Kromer, S. Lasher, K. McKenney, K. Law, J. Sinha, [Technical assessment](#)

- of compressed hydrogen storage tank systems for automotive applications, *International Journal of Hydrogen Energy* 36 (4) (2011) 3037 – 3049. doi:<https://doi.org/10.1016/j.ijhydene.2010.11.090>.
URL <http://www.sciencedirect.com/science/article/pii/S0360319910023050>
- [196] C. M. Sabliov, D. A. Salvi, D. Boldor, High frequency electromagnetism, heat transfer and fluid flow coupling in ansys multiphysics, *Journal of Microwave Power and Electromagnetic Energy* 41 (4) (2006) 5–17. arXiv: <http://dx.doi.org/10.1080/08327823.2006.11688567>, doi:10.1080/08327823.2006.11688567.
URL <http://dx.doi.org/10.1080/08327823.2006.11688567>
- [197] H. Liu, P. Li, H. Xiao, W. Mu, The fluid–solid coupling analysis of screw conveyor in drilling fluid centrifuge based on {ANSYS}, *Petroleum* 1 (3) (2015) 251 – 256. doi:<http://dx.doi.org/10.1016/j.petlm.2015.07.009>.
URL <http://www.sciencedirect.com/science/article/pii/S2405656115000395>
- [198] M. A. Soto, R. Venkatasubramanian, Ansys-based detailed thermo-mechanical modeling of complex thermo-electric power designs, in: *Thermoelectrics, 2005. ICT 2005. 24th International Conference on*, IEEE, 2005, pp. 219–221.
- [199] J. Holah, R. Thorpe, Cleanability in relation to bacterial retention on unused and abraded domestic sink materials, *Journal of Applied Microbiology* 69 (4) (1990) 599–608.
- [200] C. F. Estrada, L. A. Godoy, T. Prato, Thermo-mechanical behavior of a thin concrete shell during its early age, *Thin-Walled Structures* 44 (5) (2006) 483 – 495. doi:<http://dx.doi.org/10.1016/j.tws.2006.05.005>.
URL <http://www.sciencedirect.com/science/article/pii/S0263823106000668>
- [201] L. L. Shreir, *Corrosion: corrosion control*, Newnes, 2013.
- [202] P. Armstrong, D. Ager, I. Thompson, M. McCulloch, Improving the energy storage capability of hot water tanks through wall material specification, *Energy* 78 (2014) 128 – 140. doi:<http://dx.doi.org/10.1016/j.energy.2014.09.061>.
URL <http://www.sciencedirect.com/science/article/pii/S0360544214011189>
- [203] B. Eker, E. Yuksel, Solutions to corrosion caused by agricultural chemicals, *Trakia Journal of Sciences* 3 (7) (2005) 1–6.
- [204] J. Lawrence, L. Li, J. Spencer, The effects of high-power diode laser radiation on the wettability, adhesion and bonding characteristics of an alumina/silica-based oxide and vitreous enamel, *Surface and Coatings Technology* 115 (2) (1999) 273–281.
- [205] A. S. Fahmy, A. M. Khalil, Wall thickness variation effect on tank’s shape behaviour under critical harmonic settlement, *Alexandria Engineering Journal* 55 (4) (2016) 3205–3209.
- [206] J. Robinson, P. King, Electrochemical behavior of the magnesium anode, *Journal of the electrochemical society* 108 (1) (1961) 36–41.
- [207] D. Lukkassen, A. Meidell, *Advanced materials and structures and their fabrication processes*, Narrik University College, Hin (2003).
- [208] Y.-L. Shen, Thermo-mechanical stresses in copper interconnects – a modeling analysis, *Microelectronic Engineering* 83 (3) (2006) 446 – 459. doi:<http://dx.doi.org/10.1016/j.mee.2005.11.009>.
URL <http://www.sciencedirect.com/science/article/pii/S0167931705005447>
- [209] J. Rogers, A. Dowsett, P. Dennis, J. Lee, C. Keevil, Influence of temperature and plumbing material selection on biofilm formation and growth of legionella pneumophila in a model potable water system containing complex microbial flora., *Applied and Environmental Microbiology* 60 (5) (1994) 1585–1592.
- [210] P. Nwosu, D. Agbiogwu, Thermal analysis of a novel fibre-reinforced plastic solar hot water storage tank, *Energy* 60 (2013) 109 – 115. doi:<http://dx.doi.org/10.1016/j.energy.2013.07.002>.
URL <http://www.sciencedirect.com/science/article/pii/S0360544213005756>
- [211] M. Kouřil, P. Novák, M. Bojko, Threshold chloride concentration for stainless steels activation in concrete pore solutions, *Cement and Concrete Research* 40 (3) (2010) 431–436.
- [212] I. V. Wikholm, Storage type solar water heater, uS Patent 4,003,367 (Jan. 18 1977).
- [213] J. Yang, S. Preidikman, E. Balaras, A strongly coupled, embedded-boundary method for fluid–structure interactions of elastically mounted rigid bodies, *Journal of Fluids and Structures* 24 (2) (2008) 167 – 182. doi:<http://dx.doi.org/10.1016/j.jfluidstructs.2007.08.002>.
URL <http://www.sciencedirect.com/science/article/pii/S0889974607000679>
- [214] Y. Jiang, S. Yoshimura, R. Imai, H. Katsura, T. Yoshida, C. Kato, Quantitative evaluation of flow-induced structural vibration and noise in turbomachinery by full-scale weakly coupled simulation, *Journal of Fluids and Structures* 23 (4) (2007) 531 – 544. doi:<http://dx.doi.org/10.1016/j.jfluidstructs.2006.10.003>.
URL <http://www.sciencedirect.com/science/article/pii/S0889974606001289>
- [215] Y. G. Soloveichik, M. G. Persova, D. V. Vagin, T. B. Epanchintseva, P. A. Domnikov, K. V. Dundukova,

- V. K. Belov, 3d modeling of thermo-mechanical behavior of composite-made nose caps of hypersonic vehicles, *Applied Thermal Engineering* 99 (2016) 1152–1164.
- [216] O. C. Zienkiewicz, R. L. Taylor, *The finite element method for solid and structural mechanics*, Butterworth-Heinemann, 2005.
- [217] M. Joun, Y. Kang, Finite element analysis of temperatures, metal flow, and boll pressure in hot strip rolling (1993).
- [218] C. Borri, W. Zuhlten, Fully simulated nonlinear analysis of large structures subjected to turbulent artificial wind*, *Journal of Structural Mechanics* 19 (2) (1991) 213–250.
- [219] P. Bordui, J. Jacco, G. Loiacono, R. Stolzenberger, J. Zola, Growth of large single crystals of ktiopo4 (ktp) from high-temperature solution using heat pipe based furnace system, *Journal of crystal growth* 84 (3) (1987) 403–408.
- [220] I. González, C. D. Pérez-Segarra, O. Lehmkuhl, S. Torras, A. Oliva, Thermo-mechanical parametric analysis of packed-bed thermocline energy storage tanks, *Applied Energy* 179 (2016) 1106–1122.
- [221] A. Bianchini, G. Ferrara, L. Ferrari, S. Magnani, An improved model for the performance estimation of an h-darrieus wind turbine in skewed flow, *Wind Engineering* 36 (6) (2012) 667–686.
- [222] F. Balduzzi, A. Bianchini, R. Maleci, G. Ferrara, L. Ferrari, Critical issues in the cfd simulation of darrieus wind turbines, *Renewable Energy* 85 (2016) 419 – 435. doi:http://dx.doi.org/10.1016/j.renene.2015.06.048. URL http://www.sciencedirect.com/science/article/pii/S0960148115300719
- [223] Y. Wang, L. Ku, S. Suo, Y. Dang, Z. Ge, Z. Yan, Q. Zhou, Finite element analysis on von mises stress distributions of si dsp, *Materials Science in Semiconductor Processing* 16 (1) (2013) 165 – 170. doi:https://doi.org/10.1016/j.mssp.2012.05.005. URL http://www.sciencedirect.com/science/article/pii/S1369800112000807
- [224] K. Khanna, V. Gupta, S. Nigam, Creep analysis in functionally graded rotating disc using tresca criterion and comparison with von-mises criterion, *Materials Today: Proceedings* 4 (2, Part A) (2017) 2431 – 2438, 5th International Conference of Materials Processing and Characterization (ICMPC 2016). doi:https://doi.org/10.1016/j.matpr.2017.02.094. URL http://www.sciencedirect.com/science/article/pii/S2214785317302924
- [225] M. Cetkovic, Thermo-mechanical bending of laminated composite and sandwich plates using layerwise displacement model, *Composite Structures* 125 (Supplement C) (2015) 388 – 399. doi:https://doi.org/10.1016/j.compstruct.2015.01.051. URL http://www.sciencedirect.com/science/article/pii/S0263822315000707
- [226] K. Renji, S. J. K. Florence, Estimation of strains / stresses in composite panels using statistical energy analysis, *Journal of Sound and Vibration* 408 (Supplement C) (2017) 400 – 410. doi:https://doi.org/10.1016/j.jsv.2017.07.042. URL http://www.sciencedirect.com/science/article/pii/S0022460X17305783
- [227] K. N. Kalfas, S. A. Mitoulis, Performance of steel-laminated rubber bearings subjected to combinations of axial loads and shear strains, *Procedia Engineering* 199 (Supplement C) (2017) 2979 – 2984, x International Conference on Structural Dynamics, EUROLYN 2017. doi:https://doi.org/10.1016/j.proeng.2017.09.533. URL http://www.sciencedirect.com/science/article/pii/S1877705817340444
- [228] Y. J. Chao, Ultimate strength and failure mechanism of resistance spot weld subjected to tensile, shear, or combined tensile/shear loads, *Transactions-American Society Of Mechanical Engineers Journal Of Engineering Materials And Technology* 125 (2) (2003) 125–132.
- [229] K. Ikeya, M. Shimoda, J.-X. Shi, Multi-objective free-form optimization for shape and thickness of shell structures with composite materials, *Composite Structures* 135 (Supplement C) (2016) 262 – 275. doi:https://doi.org/10.1016/j.compstruct.2015.09.011. URL http://www.sciencedirect.com/science/article/pii/S0263822315008478
- [230] J. Hunt, Recent activities in mena countries, *World Pumps* 2011 (1) (2011) 27 – 31. doi:https://doi.org/10.1016/S0262-1762(11)70033-5. URL http://www.sciencedirect.com/science/article/pii/S0262176211700335
- [231] A. M. Mohamed, A. Al-Habaibeh, H. Abdo, S. Elabar, Towards exporting renewable energy from mena region to europe: An investigation into domestic energy use and householders' energy behaviour in libya, *Applied Energy* 146 (Supplement C) (2015) 247 – 262. doi:https://doi.org/10.1016/j.apenergy.2015.02.008. URL http://www.sciencedirect.com/science/article/pii/S0306261915001750
- [232] H. Al-Madani, The performance of a cylindrical solar water heater, *Renewable Energy* 31 (11) (2006) 1751–1763.

- [233] H. F. Naspolini, H. Militão, R. Rüther, The role and benefits of solar water heating in the energy demands of low-income dwellings in Brazil, *Energy Conversion and Management* 51 (12) (2010) 2835–2845.
- [234] R. Tang, Y. Yang, W. Gao, Comparative studies on thermal performance of water-in-glass evacuated tube solar water heaters with different collector tilt-angles, *Solar Energy* 85 (7) (2011) 1381–1389.
- [235] I. Budihardjo, G. Morrison, Performance of water-in-glass evacuated tube solar water heaters, *Solar Energy* 83 (1) (2009) 49–56.
- [236] A. M. Kandari, Thermal stratification in hot storage-tanks, *Applied Energy* 35 (4) (1990) 299 – 315. doi:[https://doi.org/10.1016/0306-2619\(90\)90029-D](https://doi.org/10.1016/0306-2619(90)90029-D).
URL <http://www.sciencedirect.com/science/article/pii/030626199090029D>
- [237] M. Esen, Thermal performance of a solar cooker integrated vacuum-tube collector with heat pipes containing different refrigerants, *Solar Energy* 76 (6) (2004) 751 – 757. doi:<https://doi.org/10.1016/j.solener.2003.12.009>.
URL <http://www.sciencedirect.com/science/article/pii/S0038092X04000027>
- [238] M. Esen, H. Esen, Experimental investigation of a two-phase closed thermosyphon solar water heater, *Solar Energy* 79 (5) (2005) 459 – 468. doi:<https://doi.org/10.1016/j.solener.2005.01.001>.
URL <http://www.sciencedirect.com/science/article/pii/S0038092X05000290>
- [239] M. Esen, T. Ayhan, Development of a model compatible with solar assisted cylindrical energy storage tank and variation of stored energy with time for different phase change materials, *Energy Conversion and Management* 37 (12) (1996) 1775 – 1785. doi:[https://doi.org/10.1016/0196-8904\(96\)00035-0](https://doi.org/10.1016/0196-8904(96)00035-0).
URL <http://www.sciencedirect.com/science/article/pii/0196890496000350>
- [240] M. Esen, A. Durmuş, A. Durmuş, Geometric design of solar-aided latent heat store depending on various parameters and phase change materials, *Solar Energy* 62 (1) (1998) 19 – 28. doi:[https://doi.org/10.1016/S0038-092X\(97\)00104-7](https://doi.org/10.1016/S0038-092X(97)00104-7).
URL <http://www.sciencedirect.com/science/article/pii/S0038092X97001047>
- [241] M. Esen, Thermal performance of a solar-aided latent heat store used for space heating by heat pump, *Solar Energy* 69 (1) (2000) 15 – 25. doi:[https://doi.org/10.1016/S0038-092X\(00\)00015-3](https://doi.org/10.1016/S0038-092X(00)00015-3).
URL <http://www.sciencedirect.com/science/article/pii/S0038092X00000153>
- [242] L. Kenjo, C. Inard, D. Caccavelli, Experimental and numerical study of thermal stratification in a mantle tank of a solar domestic hot water system, *Applied Thermal Engineering* 27 (11) (2007) 1986 – 1995. doi:<https://doi.org/10.1016/j.applthermaleng.2006.12.008>.
URL <http://www.sciencedirect.com/science/article/pii/S1359431106004248>
- [243] M. Gasque, P. González-Altozano, D. Maurer, I. J. Moncho-Esteve, R. P. Gutiérrez-Colomer, G. Palau-Salvador, E. García-Marí, Study of the influence of inner lining material on thermal stratification in a hot water storage tank, *Applied Thermal Engineering* 75 (Supplement C) (2015) 344 – 356. doi:<https://doi.org/10.1016/j.applthermaleng.2014.10.040>.
URL <http://www.sciencedirect.com/science/article/pii/S1359431114009119>
- [244] M. Swiatek, Etude de la convection naturelle et de la stratification thermique dans une cavité inclinée et chauffée au milieu: application aux capteurs solaires autostockeurs, Ph.D. thesis, Grenoble Alpes (2015).
- [245] M. Y. Haller, C. A. Cruickshank, W. Streicher, S. J. Harrison, E. Andersen, S. Furbo, Methods to determine stratification efficiency of thermal energy storage processes—review and theoretical comparison, *Solar Energy* 83 (10) (2009) 1847–1860.
- [246] Y. Han, R. Wang, Y. Dai, Thermal stratification within the water tank, *Renewable and Sustainable Energy Reviews* 13 (5) (2009) 1014–1026.
- [247] A. Barzegar, A. Dehghan, Transient thermal behavior of a vertical solar storage tank with a mantle heat exchanger during no-flow operation., *Journal of applied fluid Mechanics* 2 (1) (2009).
- [248] Z. Lavan, J. Thompson, Experimental study of thermally stratified hot water storage tanks, *Solar Energy* 19 (5) (1977) 519–524.
- [249] M. Rosen, Appropriate thermodynamic performance measures for closed systems for thermal energy storage, *Journal of solar energy engineering* 114 (2) (1992) 100–105.
- [250] E. Hahne, Y. Chen, Numerical study of flow and heat transfer characteristics in hot water stores, *Solar Energy* 64 (1) (1998) 9–18.
- [251] H. Yoo, E.-T. Pak, Theoretical model of the charging process for stratified thermal storage tanks, *Solar Energy* 51 (6) (1993) 513–519.
- [252] L. J. Shah, E. Andersen, S. Furbo, Theoretical and experimental investigations of inlet stratifiers for solar storage tanks, *Applied thermal engineering* 25 (14) (2005) 2086–2099.
- [253] P. González-Altozano, M. Gasque, F. Ibáñez, R. P. Gutiérrez-Colomer, New methodology for the character-

- isation of thermal performance in a hot water storage tank during charging, Applied Thermal Engineering 84 (Supplement C) (2015) 196 – 205. doi:<https://doi.org/10.1016/j.applthermaleng.2015.03.048>.
URL <http://www.sciencedirect.com/science/article/pii/S1359431115002720>
- [254] D. Jafari, A. Franco, S. Filippeschi, P. D. Marco, Two-phase closed thermosyphons: A review of studies and solar applications, Renewable and Sustainable Energy Reviews 53 (2016) 575 – 593. doi:<http://dx.doi.org/10.1016/j.rser.2015.09.002>.
URL <http://www.sciencedirect.com/science/article/pii/S1364032115009338>
- [255] A. Bejan, Convection heat transfer john wiley & sons new york, Nomenclature cross sectional area. RaiPr specific heat 4 (1984).
- [256] A. Hasan, Thermosyphon solar water heaters: effect of storage tank volume and configuration on efficiency, Energy Conversion and Management 38 (9) (1997) 847 – 854. doi:[https://doi.org/10.1016/S0196-8904\(96\)00099-4](https://doi.org/10.1016/S0196-8904(96)00099-4).
URL <http://www.sciencedirect.com/science/article/pii/S0196890496000994>
- [257] B. Baeten, T. Confrey, S. Peceeu, F. Rogiers, L. Helsen, A validated model for mixing and buoyancy in stratified hot water storage tanks for use in building energy simulations, Applied Energy 172 (2016) 217 – 229. doi:<https://doi.org/10.1016/j.apenergy.2016.03.118>.
URL <http://www.sciencedirect.com/science/article/pii/S0306261916304494>
- [258] C. Koroneos, M. Tsarouhis, Exergy analysis and life cycle assessment of solar heating and cooling systems in the building environment, Journal of Cleaner Production 32 (2012) 52–60.
- [259] F. Ascione, N. Bianco, R. F. De Masi, F. de’Rossi, G. P. Vanoli, Energy retrofit of an educational building in the ancient center of benevento. feasibility study of energy savings and respect of the historical value, Energy and Buildings 95 (2015) 172–183.
- [260] S. Kalogirou, Thermal performance, economic and environmental life cycle analysis of thermosiphon solar water heaters, Solar Energy 83 (1) (2009) 39 – 48. doi:<http://dx.doi.org/10.1016/j.solener.2008.06.005>.
URL <http://www.sciencedirect.com/science/article/pii/S0038092X08001552>
- [261] M. S. Al-Soud, E. S. Hrayshat, A 50mw concentrating solar power plant for jordan, Journal of Cleaner Production 17 (6) (2009) 625 – 635. doi:<http://dx.doi.org/10.1016/j.jclepro.2008.11.002>.
URL <http://www.sciencedirect.com/science/article/pii/S0959652608002795>
- [262] A. W. Bhutto, A. A. Bazmi, G. Zahedi, J. J. Klemesš, A review of progress in renewable energy implementation in the gulf cooperation council countries, Journal of Cleaner Production 71 (2014) 168 – 180, special Volume: PSE Asia for Cleaner Production. doi:<http://dx.doi.org/10.1016/j.jclepro.2013.12.073>.
URL <http://www.sciencedirect.com/science/article/pii/S095965261300927X>
- [263] R. Delgado, H. Campbell, Adaptation and sizing of solar water heaters in desert areas: For residential and hotels, Energy Procedia 57 (2014) 2725 – 2732, 2013 ISES Solar World Congress. doi:<http://dx.doi.org/10.1016/j.egypro.2014.10.304>.
URL <http://www.sciencedirect.com/science/article/pii/S1876610214016713>
- [264] A. Qazi, H. Fayaz, A. Wadi, R. G. Raj, N. Rahim, W. A. Khan, The artificial neural network for solar radiation prediction and designing solar systems: a systematic literature review, Journal of Cleaner Production 104 (2015) 1 – 12. doi:<http://dx.doi.org/10.1016/j.jclepro.2015.04.041>.
URL <http://www.sciencedirect.com/science/article/pii/S0959652615004096>
- [265] P. A. F. Ferrer, Average economic performance of solar water heaters for low density dwellings across south africa, Renewable and Sustainable Energy Reviews 76 (2017) 507 – 515. doi:<https://doi.org/10.1016/j.rser.2017.03.074>.
URL <http://www.sciencedirect.com/science/article/pii/S1364032117304100>
- [266] C. Aigbavboa, Low-income housing residents’ challenges with their government install solar water heaters: A case of south africa, Energy Procedia 75 (2015) 495 – 501, clean, Efficient and Affordable Energy for a Sustainable Future: The 7th International Conference on Applied Energy (ICAE2015). doi:<http://dx.doi.org/10.1016/j.egypro.2015.07.437>.
URL <http://www.sciencedirect.com/science/article/pii/S1876610215012059>
- [267] V. H. Quej, J. Almorox, M. Ibrakhimov, L. Saito, Estimating daily global solar radiation by day of the year in six cities located in the yucatán peninsula, mexico, Journal of Cleaner Production 141 (2017) 75 – 82. doi:<https://doi.org/10.1016/j.jclepro.2016.09.062>.
URL <http://www.sciencedirect.com/science/article/pii/S0959652616314032>
- [268] J. A. Rosas-Flores, D. Rosas-Flores, J. L. F. Zayas, Potential energy saving in urban and rural households of mexico by use of solar water heaters, using geographical information system, Renewable and Sustainable Energy Reviews 53 (2016) 243 – 252. doi:<http://dx.doi.org/10.1016/j.rser.2015.07.202>.

- URL <http://www.sciencedirect.com/science/article/pii/S1364032115009077>
- [269] G. He, Y. Zheng, Y. Wu, Z. Cui, K. Qian, [Promotion of building-integrated solar water heaters in urbanized areas in china: Experience, potential, and recommendations](#), *Renewable and Sustainable Energy Reviews* 42 (2015) 643 – 656. doi:<http://dx.doi.org/10.1016/j.rser.2014.10.044>.
URL <http://www.sciencedirect.com/science/article/pii/S1364032114008697>
- [270] F. Urban, S. Geall, Y. Wang, [Solar pv and solar water heaters in china: Different pathways to low carbon energy](#), *Renewable and Sustainable Energy Reviews* 64 (2016) 531 – 542. doi:<http://dx.doi.org/10.1016/j.rser.2016.06.023>.
URL <http://www.sciencedirect.com/science/article/pii/S1364032116302416>
- [271] H. Runqing, S. Peijun, W. Zhongying, [An overview of the development of solar water heater industry in china](#), *Energy Policy* 51 (2012) 46 – 51, *renewable Energy in China*. doi:<http://dx.doi.org/10.1016/j.enpol.2012.03.081>.
URL <http://www.sciencedirect.com/science/article/pii/S0301421512003333>
- [272] D. Li, S. Liao, [An integrated approach to evaluate the performance of solar water heater in the urban environment](#), *Energy and Buildings* 69 (2014) 562 – 571. doi:<http://dx.doi.org/10.1016/j.enbuild.2013.11.044>.
URL <http://www.sciencedirect.com/science/article/pii/S0378778813007512>
- [273] H. Benli, [Potential application of solar water heaters for hot water production in turkey](#), *Renewable and Sustainable Energy Reviews* 54 (2016) 99 – 109. doi:<http://dx.doi.org/10.1016/j.rser.2015.09.061>.
URL <http://www.sciencedirect.com/science/article/pii/S136403211501031X>
- [274] S. Rezvani, P. Bahri, T. Urmee, G. Baverstock, A. Moore, [Techno-economic and reliability assessment of solar water heaters in australia based on monte carlo analysis](#), *Renewable Energy* 105 (2017) 774 – 785. doi:<https://doi.org/10.1016/j.renene.2017.01.005>.
URL <http://www.sciencedirect.com/science/article/pii/S0960148117300058>
- [275] K.-C. Chang, T.-S. Lee, W.-M. Lin, K.-M. Chung, [Outlook for solar water heaters in taiwan](#), *Energy Policy* 36 (1) (2008) 66 – 72. doi:<http://dx.doi.org/10.1016/j.enpol.2007.07.030>.
URL <http://www.sciencedirect.com/science/article/pii/S0301421507003370>
- [276] W. Lin, K. Chang, K. Chung, [Payback period for residential solar water heaters in taiwan](#), *Renewable and Sustainable Energy Reviews* 41 (2015) 901 – 906. doi:<http://dx.doi.org/10.1016/j.rser.2014.09.005>.
URL <http://www.sciencedirect.com/science/article/pii/S1364032114007783>
- [277] V. Saini, S. Tiwari, G. Tiwari, [Environ economic analysis of various types of photovoltaic technologies integrated with greenhouse solar drying system](#), *Journal of Cleaner Production* 156 (2017) 30 – 40. doi:<https://doi.org/10.1016/j.jclepro.2017.04.044>.
URL <http://www.sciencedirect.com/science/article/pii/S0959652617307527>
- [278] S. Kordana, D. Słyś, J. Dziopak, [Rationalization of water and energy consumption in shower systems of single-family dwelling houses](#), *Journal of Cleaner Production* 82 (2014) 58 – 69. doi:<https://doi.org/10.1016/j.jclepro.2014.06.078>.
URL <http://www.sciencedirect.com/science/article/pii/S0959652614006660>
- [279] K. M. Roufehaei, A. H. A. Bakar, A. A. Tabassi, [Energy-efficient design for sustainable housing development](#), *Journal of Cleaner Production* 65 (2014) 380 – 388. doi:<http://dx.doi.org/10.1016/j.jclepro.2013.09.015>.
URL <http://www.sciencedirect.com/science/article/pii/S0959652613006185>
- [280] P. R. Chao, S. Umaphathi, W. Saman, [Water consumption characteristics at a sustainable residential development with rainwater-sourced hot water supply](#), *Journal of Cleaner Production* 109 (2015) 190 – 202, special Issue: *Toward a Regenerative Sustainability Paradigm for the Built Environment: from vision to reality*. doi:<https://doi.org/10.1016/j.jclepro.2015.04.091>.
URL <http://www.sciencedirect.com/science/article/pii/S0959652615004667>
- [281] S. Baljit, H.-Y. Chan, K. Sopian, [Review of building integrated applications of photovoltaic and solar thermal systems](#), *Journal of Cleaner Production* 137 (2016) 677 – 689. doi:<http://dx.doi.org/10.1016/j.jclepro.2016.07.150>.
URL <http://www.sciencedirect.com/science/article/pii/S0959652616310460>
- [282] S. Jaisankar, J. Ananth, S. Thulasi, S. Jayasuthakar, K. Sheeba, [A comprehensive review on solar water heaters](#), *Renewable and Sustainable Energy Reviews* 15 (6) (2011) 3045 – 3050. doi:<http://dx.doi.org/10.1016/j.rser.2011.03.009>.
URL <http://www.sciencedirect.com/science/article/pii/S1364032111001092>
- [283] D. Zambrana-Vasquez, A. Aranda-Usón, I. Zabalza-Bribián, A. Jañez, E. Llera-Sastresa, P. Hernandez, E. Arizabalaga, [Environmental assessment of domestic solar hot water systems: a case study in residential and](#)

- hotel buildings, *Journal of Cleaner Production* 88 (2015) 29 – 42, sustainable Development of Energy, Water and Environment Systems. doi:<https://doi.org/10.1016/j.jclepro.2014.06.035>
URL <http://www.sciencedirect.com/science/article/pii/S0959652614006234>
- [284] C. J. Koroneos, E. A. Nanaki, Life cycle environmental impact assessment of a solar water heater, *Journal of Cleaner Production* 37 (2012) 154 – 161. doi:<https://doi.org/10.1016/j.jclepro.2012.07.001>
URL <http://www.sciencedirect.com/science/article/pii/S0959652612003289>
- [285] N. Arnaoutakis, M. Souliotis, S. Papaefthimiou, Comparative experimental life cycle assessment of two commercial solar thermal devices for domestic applications, *Renewable Energy* 111 (2017) 187 – 200. doi:<https://doi.org/10.1016/j.renene.2017.04.008>
URL <http://www.sciencedirect.com/science/article/pii/S0960148117303075>
- [286] E. Kontopoulos, G. Martinopoulos, D. Lazarou, N. Bassiliades, An ontology-based decision support tool for optimizing domestic solar hot water system selection, *Journal of Cleaner Production* 112 (2016) 4636 – 4646. doi:<http://dx.doi.org/10.1016/j.jclepro.2015.08.088>
URL <http://www.sciencedirect.com/science/article/pii/S0959652615011798>
- [287] R. Shrivastava, V. Kumar, S. Untawale, Modeling and simulation of solar water heater: A {TRNSYS} perspective, *Renewable and Sustainable Energy Reviews* 67 (2017) 126 – 143. doi:<https://doi.org/10.1016/j.rser.2016.09.005>
URL <http://www.sciencedirect.com/science/article/pii/S1364032116304944>
- [288] A. Moreau, F. Laurencelle, Field study of solar domestic water heaters in quebec, *Energy Procedia* 30 (2012) 1331 – 1338, 1st International Conference on Solar Heating and Cooling for Buildings and Industry (SHC 2012). doi:<http://dx.doi.org/10.1016/j.egypro.2012.11.146>
URL <http://www.sciencedirect.com/science/article/pii/S1876610212016621>
- [289] N. Suresh, B. S. Rao, Solar energy for process heating: A case study of select indian industries, *Journal of Cleaner Production* 151 (2017) 439 – 451. doi:<https://doi.org/10.1016/j.jclepro.2017.02.190>
URL <http://www.sciencedirect.com/science/article/pii/S095965261730416X>
- [290] H. Hamouchene, The ouarazate solar plant in morocco: Triumphant ‘green’capitalism and the privatization of nature.
- [291] H. Pandya, A. K. Behura, Experimental study of v-through solar water heater for tilt angle and glass transmissivity, *Energy Procedia* 109 (2017) 377 – 384, international Conference on Recent Advancement in Air Conditioning and Refrigeration, {RAAR} 2016, 10-12 November 2016, Bhubaneswar, India. doi:<https://doi.org/10.1016/j.egypro.2017.03.034>
URL <http://www.sciencedirect.com/science/article/pii/S1876610217300565>
- [292] J. A. Duffie, W. A. Beckman, *Solar engineering of thermal processes*, John Wiley & Sons, 2013.
- [293] E. M. Kleinbach, W. Beckman, S. Klein, Performance study of one-dimensional models for stratified thermal storage tanks, *Solar energy* 50 (2) (1993) 155–166.
- [294] W. Buckles, S. Klein, Analysis of solar domestic hot water heaters, *Solar Energy* 25 (5) (1980) 417–424.
- [295] X. Zhang, F. Wang, Hybrid input-output analysis for life-cycle energy consumption and carbon emissions of china’s building sector, *Building and Environment* 104 (2016) 188 – 197. doi:<http://dx.doi.org/10.1016/j.buildenv.2016.05.018>
URL <http://www.sciencedirect.com/science/article/pii/S0360132316301706>
- [296] T. Ming, W. Liu, S. Caillol, et al., Fighting global warming by climate engineering: Is the earth radiation management and the solar radiation management any option for fighting climate change?, *Renewable and Sustainable Energy Reviews* 31 (2014) 792–834.
- [297] B. Greening, A. Azapagic, Domestic solar thermal water heating: A sustainable option for the uk?, *Renewable Energy* 63 (2014) 23 – 36. doi:<https://doi.org/10.1016/j.renene.2013.07.048>
URL <http://www.sciencedirect.com/science/article/pii/S0960148113004576>
- [298] W. M. Hashim, A. T. Shomran, H. A. Jurmut, T. S. Gaaz, A. A. H. Kadhum, A. A. Al-Amiery, Case study on solar water heating for flat plate collector, *Case studies in thermal engineering* 12 (2018) 666–671.
- [299] M. Hadjiat, M. Hazmoune, S. Ouali, A. Gama, M. Yaiche, Design and analysis of a novel ics solar water heater with cpc reflectors, *Journal of Energy Storage* 16 (2018) 203–210.
- [300] J. C. Evarts, L. G. Swan, Domestic hot water consumption estimates for solar thermal system sizing, *Energy and Buildings* 58 (2013) 58 – 65. doi:<http://dx.doi.org/10.1016/j.enbuild.2012.11.020>
URL <http://www.sciencedirect.com/science/article/pii/S0378778812006238>
- [301] H. M. A. ur Rehman, F. A. Al-Sulaiman, Optimum selection of solar water heating (swh) systems based on their comparative techno-economic feasibility study for the domestic sector of saudi arabia, *Renewable and Sustainable Energy Reviews* 62 (2016) 336 – 349. doi:<http://dx.doi.org/10.1016/j.rser.2016.04.047>

- URL [//www.sciencedirect.com/science/article/pii/S1364032116300806](http://www.sciencedirect.com/science/article/pii/S1364032116300806)
- [302] L. Ayompe, A. Duffy, S. McCormack, M. Conlon, [Validated {TRNSYS} model for forced circulation solar water heating systems with flat plate and heat pipe evacuated tube collectors](#), *Applied Thermal Engineering* 31 (8–9) (2011) 1536 – 1542. doi:<http://dx.doi.org/10.1016/j.applthermaleng.2011.01.046>.
URL [//www.sciencedirect.com/science/article/pii/S1359431111000718](http://www.sciencedirect.com/science/article/pii/S1359431111000718)
- [303] Y. S. Too, G. Morrison, M. Behnia, [Performance of solar water heaters with narrow mantle heat exchangers](#), *Solar Energy* 83 (3) (2009) 350 – 362. doi:<http://dx.doi.org/10.1016/j.solener.2008.08.011>.
URL [//www.sciencedirect.com/science/article/pii/S0038092X08002119](http://www.sciencedirect.com/science/article/pii/S0038092X08002119)
- [304] S. Colle, T. Koller, [Simulation and performance analysis of a solar domestic hot water system controlled by weather forecast information](#), *Energy Procedia* 57 (2014) 2496 – 2505, 2013 {ISES} Solar World Congress. doi:<http://dx.doi.org/10.1016/j.egypro.2014.10.260>.
URL [//www.sciencedirect.com/science/article/pii/S1876610214016270](http://www.sciencedirect.com/science/article/pii/S1876610214016270)
- [305] L. Passos, J. M. Cardemil, S. Colle, [Feasibility study of using domestic solar hot water systems as alternative to reduce the electricity peak demand in brazil](#), *Energy Procedia* 57 (2014) 2487 – 2495. doi:<http://dx.doi.org/10.1016/j.egypro.2014.10.258>.
URL <http://www.sciencedirect.com/science/article/pii/S1876610214016257>
- [306] G. Martínez-Rodríguez, A. L. Fuentes-Silva, M. Picón-Núñez, *Solar thermal networks operating with evacuated-tube collectors*, *Energy* (2017).
- [307] M. Abdunnabi, K. Alakder, N. Alkishriwi, S. Abughres, [Experimental validation of forced circulation of solar water heating systems in {TRNSYS}](#), *Energy Procedia* 57 (2014) 2477 – 2486, 2013 {ISES} Solar World Congress. doi:<http://dx.doi.org/10.1016/j.egypro.2014.10.257>.
URL [//www.sciencedirect.com/science/article/pii/S1876610214016245](http://www.sciencedirect.com/science/article/pii/S1876610214016245)
- [308] Z. Zhou, L. Wang, C. Li, A. Ebert, [Performance analysis of a collective solar domestic water-heating system in the temperate zone of yunnan province, china](#), *Journal of Engineering Science and Technology Review* 9 (3) (2016) 60–65.
- [309] M. S. Buker, S. B. Riffat, [Building integrated solar thermal collectors—a review](#), *Renewable and Sustainable Energy Reviews* 51 (2015) 327–346.
- [310] A. Jamar, Z. Majid, W. Azmi, M. Norhafana, A. Razak, [A review of water heating system for solar energy applications](#), *International Communications in Heat and Mass Transfer* 76 (2016) 178–187.
- [311] K. Tanha, A. S. Fung, R. Kumar, [Performance of two domestic solar water heaters with drain water heat recovery units: Simulation and experimental investigation](#), *Applied Thermal Engineering* 90 (2015) 444 – 459. doi:<http://dx.doi.org/10.1016/j.applthermaleng.2015.07.038>.
URL [//www.sciencedirect.com/science/article/pii/S135943111500722X](http://www.sciencedirect.com/science/article/pii/S135943111500722X)
- [312] J. B. A. Lima, R. T. Prado, V. M. Taborianski, [Optimization of tank and flat-plate collector of solar water heating system for single-family households to assure economic efficiency through the {TRNSYS} program](#), *Renewable Energy* 31 (10) (2006) 1581 – 1595. doi:<http://dx.doi.org/10.1016/j.renene.2005.09.006>.
URL [//www.sciencedirect.com/science/article/pii/S0960148105002636](http://www.sciencedirect.com/science/article/pii/S0960148105002636)
- [313] M. R. Assari, H. B. Tabrizi, M. J. Movahedi, [Experimental study on destruction of thermal stratification tank in solar collector performance](#), *Journal of Energy Storage* 15 (2018) 124–132.
- [314] S. ed Din Fertahi, A. Jamil, A. Benbassou, [Review on solar thermal stratified storage tanks \(stsst\): Insight on stratification studies and efficiency indicators](#), *Solar Energy* 176 (2018) 126 – 145. doi:<https://doi.org/10.1016/j.solener.2018.10.028>.
URL <http://www.sciencedirect.com/science/article/pii/S0038092X18310077>
- [315] J. A. Alfaro-Ayala, O. A. López-Núñez, F. Gómez-Castro, J. Ramírez-Minguela, A. Uribe-Ramírez, J. Belman-Flores, S. Cano-Andrade, [Optimization of a solar collector with evacuated tubes using the simulated annealing and computational fluid dynamics](#), *Energy Conversion and Management* 166 (2018) 343–355.
- [316] C. Garnier, T. Muneer, J. Currie, [Numerical and empirical evaluation of a novel building integrated collector storage solar water heater](#), *Renewable Energy* 126 (2018) 281–295.
- [317] C. Yan, S. Wang, Z. Ma, W. Shi, [A simplified method for optimal design of solar water heating systems based on life-cycle energy analysis](#), *Renewable Energy* 74 (2015) 271 – 278. doi:<http://dx.doi.org/10.1016/j.renene.2014.08.021>.
URL [//www.sciencedirect.com/science/article/pii/S0960148114004807](http://www.sciencedirect.com/science/article/pii/S0960148114004807)
- [318] V. M. Bessa, R. T. Prado, [Reduction of carbon dioxide emissions by solar water heating systems and passive technologies in social housing](#), *Energy Policy* 83 (2015) 138–150.
- [319] T. Bouhal, Y. Agrouaz, T. El Rhafiki, T. Kousksou, Y. Zeraouli, A. Jamil, et al., [Technical assessment, economic viability and investment risk analysis of solar heating/cooling systems in residential buildings in](#)

- morocco, *Solar Energy* 170 (2018) 1043–1062.
- [320] T. Bouhal, Y. Agrouaz, A. Allouhi, T. Kousksou, A. Jamil, T. El Rhafiki, Y. Zeraoui, Impact of load profile and collector technology on the fractional savings of solar domestic water heaters under various climatic conditions, *International Journal of Hydrogen Energy* 42 (18) (2017) 13245–13258.
- [321] A. Jamil, A. Benbassou, et al., Review on solar thermal stratified storage tanks (stsst): Insight on stratification studies and efficiency indicators, *Solar Energy* 176 (2018) 126–145.
- [322] E. Bellos, C. Tzivanidis, K. A. Antonopoulos, Exergetic, energetic and financial evaluation of a solar driven absorption cooling system with various collector types, *Applied Thermal Engineering* 102 (2016) 749–759.
- [323] O. Iken, M. Dlimi, R. Agounoun, I. Kadiri, S. ed Din Fertahi, A. Zoubir, K. Sbai, Numerical investigation of energy performance and cost analysis of moroccan’s building smart walls integrating vanadium dioxide, *Solar Energy* 179 (2019) 249 – 263.
- [324] R. L. Oonk, D. E. Jones, B. E. Cole-Appel, Calculation of performance of n collectors in series from test data on a single collector, *Solar Energy* 23 (6) (1979) 535–536.
- [325] T. Kousksou, P. Bruel, G. Cherreau, V. Leoussoff, T. E. Rhafiki, [Pcm storage for solar dhw: From an unfulfilled promise to a real benefit](https://doi.org/10.1016/j.solener.2011.05.012), *Solar Energy* 85 (9) (2011) 2033 – 2040. [doi:http://dx.doi.org/10.1016/j.solener.2011.05.012](https://doi.org/10.1016/j.solener.2011.05.012).
URL <http://www.sciencedirect.com/science/article/pii/S0038092X11001927>
- [326] A. Baniassadi, M. Momen, M. Amidpour, A new method for optimization of solar heat integration and solar fraction targeting in low temperature process industries, *Energy* 90 (2015) 1674–1681.
- [327] A. Madhlopa, C. Johnstone, Model for computation of solar fraction in a single-slope solar still, *Solar Energy* 83 (6) (2009) 873–882.
- [328] A. Moià-Pol, V. Martínez-Moll, R. P. Nadal, J. M. R. Serra, [Solar thermal potential for collective systems in palma beach \(balearic island’s\)](https://doi.org/10.1016/j.egypro.2014.02.126), *Energy Procedia* 48 (2014) 1118 – 1123, proceedings of the 2nd International Conference on Solar Heating and Cooling for Buildings and Industry (SHC 2013). [doi:https://doi.org/10.1016/j.egypro.2014.02.126](https://doi.org/10.1016/j.egypro.2014.02.126).
URL <http://www.sciencedirect.com/science/article/pii/S1876610214003889>
- [329] C. Fraga, F. Mermoud, P. Hollmuller, E. Pampaloni, B. Lachal, [Large solar assisted heat pump systems in collective housing: In-situ monitoring results for summer season](https://doi.org/10.1016/j.egypro.2014.02.123), *Energy Procedia* 48 (2014) 1086 – 1095, proceedings of the 2nd International Conference on Solar Heating and Cooling for Buildings and Industry (SHC 2013). [doi:https://doi.org/10.1016/j.egypro.2014.02.123](https://doi.org/10.1016/j.egypro.2014.02.123).
URL <http://www.sciencedirect.com/science/article/pii/S1876610214003853>
- [330] A. Bertrand, A. Mastrucci, N. Schüler, R. Aggoune, F. Maréchal, [Characterisation of domestic hot water end-uses for integrated urban thermal energy assessment and optimisation](https://doi.org/10.1016/j.apenergy.2016.02.107), *Applied Energy* 186, Part 2 (2017) 152 – 166, energy and Urban Systems. [doi:https://doi.org/10.1016/j.apenergy.2016.02.107](https://doi.org/10.1016/j.apenergy.2016.02.107).
URL <http://www.sciencedirect.com/science/article/pii/S030626191630263X>
- [331] M. d. P. R. Teles, K. A. Ismail, A. Arabkoohsar, A new version of a low concentration evacuated tube solar collector: Optical and thermal investigation, *Solar Energy* 180 (2019) 324–339.
- [332] L. Zhou, Y. Wang, Q. Huang, Cfd investigation of a new flat plate collector with additional front side transparent insulation for use in cold regions, *Renewable Energy* 138 (2019) 754–763.